



UNIL | Université de Lausanne

Unicentre

CH-1015 Lausanne

<http://serval.unil.ch>

Year : 2023

THREE ESSAYS ON MACROECONOMICS OF CLIMATE CHANGE

Friedl Aleksandra

Friedl Aleksandra, 2023, THREE ESSAYS ON MACROECONOMICS OF CLIMATE CHANGE

Originally published at : Thesis, University of Lausanne

Posted at the University of Lausanne Open Archive <http://serval.unil.ch>

Document URN : urn:nbn:ch:serval-BIB_1666A3D84F820

Droits d'auteur

L'Université de Lausanne attire expressément l'attention des utilisateurs sur le fait que tous les documents publiés dans l'Archive SERVAL sont protégés par le droit d'auteur, conformément à la loi fédérale sur le droit d'auteur et les droits voisins (LDA). A ce titre, il est indispensable d'obtenir le consentement préalable de l'auteur et/ou de l'éditeur avant toute utilisation d'une oeuvre ou d'une partie d'une oeuvre ne relevant pas d'une utilisation à des fins personnelles au sens de la LDA (art. 19, al. 1 lettre a). A défaut, tout contrevenant s'expose aux sanctions prévues par cette loi. Nous déclinons toute responsabilité en la matière.

Copyright

The University of Lausanne expressly draws the attention of users to the fact that all documents published in the SERVAL Archive are protected by copyright in accordance with federal law on copyright and similar rights (LDA). Accordingly it is indispensable to obtain prior consent from the author and/or publisher before any use of a work or part of a work for purposes other than personal use within the meaning of LDA (art. 19, para. 1 letter a). Failure to do so will expose offenders to the sanctions laid down by this law. We accept no liability in this respect.



UNIL | Université de Lausanne

FACULTÉ DES HAUTES ÉTUDES COMMERCIALES
DÉPARTEMENT D'ÉCONOMIE

**THREE ESSAYS ON MACROECONOMICS OF
CLIMATE CHANGE**

THÈSE DE DOCTORAT

présentée à la

Faculté des Hautes Études Commerciales
de l'Université de Lausanne

pour l'obtention du grade de
Doctorat en Économie

par

Aleksandra FRIEDL

Directeur de thèse
Prof. Simon Scheidegger

Co-directrice de thèse
Prof. Kenza Benhima

Jury

Prof. Boris Nikolov, président
Prof. Sébastien Houde, expert interne
Prof. Christian Traeger, expert externe

LAUSANNE
2023



UNIL | Université de Lausanne

FACULTÉ DES HAUTES ÉTUDES COMMERCIALES
DÉPARTEMENT D'ÉCONOMIE

**THREE ESSAYS ON MACROECONOMICS OF
CLIMATE CHANGE**

THÈSE DE DOCTORAT

présentée à la

Faculté des Hautes Études Commerciales
de l'Université de Lausanne

pour l'obtention du grade de
Doctorat en Économie

par

Aleksandra FRIEDL

Directeur de thèse
Prof. Simon Scheidegger

Co-directrice de thèse
Prof. Kenza Benhima

Jury

Prof. Boris Nikolov, président
Prof. Sébastien Houde, expert interne
Prof. Christian Traeger, expert externe

LAUSANNE
2023

IMPRIMATUR

La Faculté des hautes études commerciales de l'Université de Lausanne autorise l'impression de la thèse de doctorat rédigée par

Aleksandra FRIEDL

intitulée

Three Essays on Macroeconomics of Climate Change

sans se prononcer sur les opinions exprimées dans cette thèse.

Lausanne, le 20.10.2023



Professeure Marianne Schmid Mast, Doyenne



Members of the Thesis Committee

Prof. Simon Scheidegger

Associate Professor of Economics, University of Lausanne

Thesis supervisor

Prof. Kenza Benhima

Professor of Economics, University of Lausanne

Thesis co-supervisor

Prof. Sébastien Houde

Associate Professor of Economics, University of Lausanne

Internal member of the thesis committee

Prof. Christian Träger

Professor of Economics, University of Oslo

External member of the thesis committee

University of Lausanne
Faculty of Business and Economics


PhD in Economics

I hereby certify that I have examined the doctoral thesis of

Aleksandra FRIEDL

and have found it to meet the requirements for a doctoral thesis.

All revisions that I or committee members
made during the doctoral colloquium
have been addressed to my entire satisfaction.

Signature: 

Date: 29.9.2023_____

Prof. Simon Scheidegger
Thesis supervisor

University of Lausanne
Faculty of Business and Economics

PhD in Economics

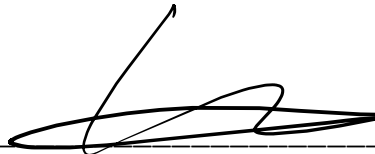
I hereby certify that I have examined the doctoral thesis of

Aleksandra FRIEDL

and have found it to meet the requirements for a doctoral thesis.

All revisions that I or committee members
made during the doctoral colloquium
have been addressed to my entire satisfaction.

Signature: _____



Date: _____

29/05/2023

Prof. Kenza Benhima
Thesis co-supervisor

University of Lausanne
Faculty of Business and Economics

PhD in Economics

I hereby certify that I have examined the doctoral thesis of

Aleksandra FRIEDL

and have found it to meet the requirements for a doctoral thesis.

All revisions that I or committee members
made during the doctoral colloquium
have been addressed to my entire satisfaction.

Signature:



Date: 27.09.2023

Prof. Sébastien HOUDE
Internal expert

University of Lausanne
Faculty of Business and Economics

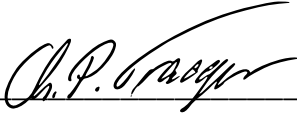
PhD in Economics

I hereby certify that I have examined the doctoral thesis of

Aleksandra FRIEDL

and have found it to meet the requirements for a doctoral thesis.

All revisions that I or committee members
made during the doctoral colloquium
have been addressed to my entire satisfaction.

Signature:  Date: 28.9.2023

Prof. Christian TRAEGER
External expert

Acknowledgments

I would like to express my deepest gratitude and appreciation to those who have contributed to the completion of my PhD journey. This dissertation would not have been possible without the support, guidance, and encouragement of many individuals.

First and foremost, I am profoundly grateful to my advisors, Professor Simon Scheidegger, and Professor Kenza Benhima. You were always there for me, generously providing me with the time, support, expertise, and mentorship throughout this research. I was truly fortunate to be guided by Simon and Kenza.

I extend my sincere thanks to the members of my doctoral committee, Professor Sébastien Houde and Professor Christian Träger, for their valuable feedback, constructive criticism, and scholarly guidance. Your expertise and diverse perspectives have enriched the quality of this dissertation.

I am deeply indebted to my co-authors, Dr. Doris Folini, Professor Felix Kübler, and Dr. Takafumi Usui, who have generously shared their knowledge and ideas, creating a stimulating intellectual environment. Our collaboration has been a source of inspiration and growth for me.

I owe a big one to my friends and colleagues, Claudia Gentile, Giacomo Mangiante, Pascal Meichtry, and Pauline Chikhani, for our countless coffees and dinners, extended Zoom calls, and long talks. I am grateful to all the PhD students from my department with whom I was fortunate to be surrounded, you are an amazing community. Special thanks are to my PhD friends from UZH and ETHZ, who shared a challenging but enjoyable first year of graduate studies with me.

Throughout this journey, my family was always there for me, supporting me through all the ups and downs. To my Mother and Father, Marina, Misha, Anton, Max, Andrey, Nelya, thank you for always being there for me and for believing in me.

Last but not least, I want to express my deepest appreciation to my husband, Ken, for his love, patience, and understanding. Your unconditional support and encouragement have been the driving force behind my perseverance.

This dissertation is a testament to the collective effort of all those who have played a role in my academic and personal development. I am profoundly grateful for your contributions and support.

Thank you all for being a part of this remarkable journey.

Lausanne, 04 Septemebr 2023

Aleksandra Friedl

Contents

List of Figures	vii
List of Tables	xiii
Introduction	1
1 The climate in climate economics	5
1.1 Introduction	6
1.2 Literature	13
1.3 A comprehensive framework to calibrate the climate in IAMs	15
1.3.1 Choice of test cases	16
1.3.2 Technical setup of test cases	16
1.3.3 Metric for performance evaluation	18
1.3.4 CMIP5 serves the purpose, no need for CMIP6	20
1.4 CDICE - re-calibrating the climate of DICE	21
1.4.1 Model equations	22
1.4.2 Atmospheric CO ₂ after 100 GtC pulse to the atmosphere	26
1.4.3 Temperature evolution upon quadrupling of CO ₂ concentration	28
1.4.4 Temperature evolution as atmospheric CO ₂ increases at 1% per year	31
1.4.5 CMIP5 historical and RCP evolution as simulated by DICE	32
1.4.6 Synthesis and lessons learned from the climate test cases	36
1.5 The social cost of carbon in partial equilibrium	38
1.5.1 Different climate calibrations and the SCC	39
1.5.2 The effect of miscalibration	41
1.6 The social cost of carbon and optimal abatement in the DICE economy	43

1.6.1	CDICE - Economic consequences of climate model uncertainty . . .	45
1.6.2	The economic consequences of miscalibrated climate	49
1.6.3	The role of discounting	52
1.7	Conclusion	55
	Appendix	58
1.A	Summary table of the models and parameters	58
1.B	Generic DICE formulation and calibration	58
1.B.2	The equations of the climate system	63
1.B.3	Economy equations	65
1.C	Sensitivity exercise: change in the exogenous forcing	67
1.D	Computational details	68
1.D.2	Mapping CDICE onto Deep Equilibrium Nets	70
1.D.3	Error Statistics	76
2	Deep Uncertainty Quantification for Stochastic Integrated Assessment	
	Models	77
2.1	Introduction	78
2.2	Literature Review	81
2.3	A Stochastic IAM with Bayesian Learning	84
2.3.1	The economic model	85
2.3.2	The climate model	87
2.3.3	Bayesian learning over the equilibrium climate sensitivity	88
2.3.4	The recursive formulation	90
2.4	Deep Uncertainty Quantification	91
2.4.1	Surrogate models for IAMs	93
2.4.2	Global sensitivity analysis in a nutshell	99
2.4.3	The deep uncertainty quantification algorithm	103
2.5	Results	105
2.5.1	Parameters for the uncertainty quantification analysis	105
2.5.2	Optimal policy	106
2.5.3	Uncertainty quantification results	108
2.6	Conclusion	112
	Appendix	114

2.A	Univariate effects on the SCC in 2100	114
2.B	Additional Model Details	115
2.C	Implementation Details	116
2.C.2	Numerical integration	123
2.C.3	Error statistics	123
2.C.4	Leave-one-out error with Gaussian processes	124
3	Green energy transition: decarbonisation of developing countries and the role of technological spillovers	127
3.1	Introduction	128
3.2	Empirical motivation	130
3.3	A brief review of the literature	133
3.4	Model	136
3.4.1	Model formulation	136
3.4.2	Parametrization	139
3.4.3	Solution method: Deep Equilibrium Nets	145
3.5	Results	145
3.5.1	Results without technological spillovers	146
3.5.2	Business-as-usual with technological spillovers	149
3.5.3	Optimal taxation and second-best taxation with technological spillovers	151
3.5.4	Welfare analysis	153
3.6	Conclusion and discussion	154
	Appendix	157
3.A	Model	157
3.A.2	Equilibrium conditions	159
3.B	Parametrisation	161
3.B.3	The climate system	162
3.B.4	Energy sector	163
3.C	Countries by income groups based on the World Bank Classification	164
	Bibliography	168

List of Figures

1.1 Illustration of CMIP5 historical and future evolution (RCP26, RCP45, RCP60, and RCP85 scenarios, shown in blue, green, yellow, and red), from 1850 to 2100, of prescribed CO2 emissions (left, in GtC per year), alternatively prescribed CO2 concentrations (middle, in ppm CO2), and the forcing derived from prescribed CO2 concentrations (right, in W/m²). The total forcing F_t (solid lines) is decomposed into forcing from CO2 (F_t^{CO2} , dashed lines) and non-CO2 forcing assumed as $F_t^{\text{EX}} = 0.3 \cdot F_t^{\text{CO2}}$ (dotted lines). 19

1.2 Fraction of an instantaneous 100 GtC pulse remaining in the atmosphere (y-axis) as a function of time (x-axis, three different time scales from left to right). Shown are benchmark data adapted from Joos et al. (2013) (black and gray lines, J13) and three calibrations against this data: CDICE (red solid), which is calibrated against the multi-model mean (MMM, black solid), and two extreme calibrations, CDICE-MESMO (red dotted) and CDICE-LOVECLIM (red dash-dotted), which essentially capture the range of benchmark models (thin gray lines). DICE-2016 (blue dashed) removes too little CO2 from the atmosphere compared to the benchmark data. Absolute values of pulse height and equilibrium masses are irrelevant in DICE’s carbon cycle model (CDICE, 5000 GtC on 1850 equilibrium masses, orange dotted), which is in contrast to findings in J13 (dashed and dotted gray lines, see their paper for details). . . 27

-
- 1.3 Parameter sensitivities (thin colored lines) of the carbon cycle, anchored at CDICE (red), illustrated at the example of an instantaneous 100 GtC pulse to the atmosphere. Shown is the fraction of the pulse remaining in the atmosphere (y-axis) as a function of time (x-axis, three different time scales from left to right). Benchmark data from Joos et al. (2013) is shown in black and gray. 28
- 1.4 Temperature response to instantaneous quadrupling of atmospheric CO₂ with respect to pre-industrial values on time scales of 20 years (left), 200 years (middle), and 1000 years (right). Parameters in CDICE (red solid) can be chosen such as to exactly reproduce the calibration target, the CMIP5 multi-model mean (black solid, G13-MMM). Also shown are two extreme ECS calibrations (solid green and light blue, CDICE-HadGEM2-ES and CDICE-GISS-E2-R). In DICE-2016 (dashed blue, 5 year time step), temperature increase is too slow compared to any CMIP5 model (thin gray lines, G13, from Geoffroy et al. (2013)). 30
- 1.5 Parameter sensitivity of the temperature equations in DICE, illustrated at the example of an instantaneous quadrupling of the CO₂ concentration with respect to pre-industrial values. Shown is warming (y-axis) as a function of time (x-axis) for different time scales (from left to right). Parameters are varied one by one with respect to the CMIP5 multi-model mean from Geoffroy et al. (2013) (black solid, G13-MMM) and its adaptation in CDICE (red solid). 30
- 1.6 Temperature response (y-axis) to transient, one percent per year, increase of the CO₂ concentration as a function of years (x-axis) from 1850 onward. The CO₂ concentration doubles within 70 years (left panel), and associated warming levels correspond, by definition, to the transient climate response (TCR) of the model. CO₂ quadruples within 140 years (right panel), and TCR roughly doubles. DICE-2016 (dashed blue), our new version CDICE (solid red), as well as its extreme scaling variants (solid cyan and green), are all compatible with CMIP5 models and their TCR (individual models and multi-model mean, solid gray and black, respectively). 32

1.7	Comparison of DICE with historical and future (years 1850 to 2100, scenarios RCP26, RCP45, RCP60, and RCP85, from top to bottom) CMIP5 data. Shown are atmospheric CO ₂ concentrations (left) as prescribed in CMIP5 (solid black, with dotted lines indicating $\pm 5\%$ and $\pm 20\%$ ranges) and as computed from CO ₂ emissions with DICE-2016 (dashed blue), CDICE (solid red), as well as CDICE-MESMO and CDICE-LOVECLIM (dotted and dash-dotted red). Also shown is temperature evolution based on prescribed CO ₂ concentrations (middle) and based on emissions (right) for DICE-2016, CDICE, and variants of CDICE.	35
1.8	SCC for different CDICE calibrations, emission scenarios, and a quadratic damage function.	40
1.9	SCC for alternative damage functions.	41
1.10	SCC for different calibrations. RCP8.5 and quadratic damage function.	42
1.11	BAU emissions (left panel) as well as growth adjusted interest rate (right panel) for different climate calibrations. Year zero on the graph corresponds to the starting year 2015.	45
1.12	This figure shows the evolution damages (left panel) and the relative SCC (right panel) over time for nine CDICE-calibrations in the business as usual case. Year zero on the graph corresponds to the starting year 2015.	47
1.13	This figure shows optimal abatement (left panel) and emissions (right panel) over time. Year zero on the graph corresponds to the starting year 2015.	48
1.14	Evolution of temperature (left panel) and SCC (right panel) with optimal abatement. Year zero on the graph corresponds to the starting year 2015.	49
1.15	Mass of carbon (left panel) and atmospheric temperature (right panel) for the CDICE and DICE-2016 calibrations. Year zero on the graph corresponds to the starting year 2015.	49
1.16	Optimal abatement in CDICE and DICE-2016. Year zero on the graph corresponds to the starting year 2015.	51
1.17	Interest rate (left panel) and SCC (right panel) under different values for ψ . Year zero on the graph corresponds to the starting year 2015.	53

1.18	Optimal abatement for different values of ψ and different climate calibrations. The left panel shows results for MMM, the middle panel for high ECS calibrations and the right panel for low ECS calibrations. Year zero on the graph corresponds to the starting year 2015.	54
1.19	Optimal temperatures for different values of ψ and different climate calibrations. The left panel shows results for MMM, the middle panel for high ECS calibrations and the right panel for low ECS calibrations. Year zero on the graph corresponds to the starting year 2015.	55
1.C1	Mass of carbon in the atmosphere (left) and temperature of the atmosphere (right) for DICE-2016, and CDICE models with different exogenous forcing evolution (DICE-2016-FEX, CDICE-FEX show the model variables under the assumption of time dependent exogenous forcings) for an optimal abatement case. Year zero on the graphs corresponds to a starting year 2015.	67
1.C2	Damages (left) and the social cost of carbon (right) for DICE-2016, and CDICE models with different exogenous forcings evolution (DICE-2016-FEX, CDICE-FEX show the model variables under the assumption of time dependent exogenous forcings) for an optimal abatement case. Year zero on the graphs corresponds to a starting year 2015.	68
2.1	The figure above depicts an FNN, where the input \mathbf{x} is a 12–dimensional vector, two hidden layers with 16 neurons each, and $\mathbf{p}(\mathbf{x})$ is a 3–dimensional output, thereby representing a stylized architecture for an IAM with 10 economic state variables, two parameters that are considered as pseudo-states, and three control variables (cf. Eq. (2.31)).	95
2.2	Emissions in deterministic case (left), with temperature shocks (middle), and with Bayesian learning (right).	106
2.3	Temperature of the atmosphere in deterministic case (left), stochastic temperature (middle), and with learning (right).	106
2.4	Abatement in deterministic case (left), stochastic temperature (middle), and with Bayesian learning (right).	107
2.5	SCC in deterministic case (left), stochastic temperature (middle), and with Bayesian learning (right).	107

2.6	Impact of the uncertain parameters on the SCC in 2020 (left), SCC in 2050 (middle), and SCC in 2100 (right) in the deterministic model.	108
2.7	Impact of the uncertain parameters on the SCC in 2020 (left), SCC in 2050 (middle), and SCC in 2100 (right) in the model with temperature shock.	109
2.8	Impact of the uncertain parameters on the SCC in 2020 (left), SCC in 2050 (middle), and SCC in 2100 (right) in the model with Bayesian learning.	109
2.9	Univariate effects on the SCC in 2020 in a deterministic model.	110
2.10	Univariate effects on the SCC in 2020 in a model with temperature shock.	111
2.11	Univariate effects on the SCC in 2020 in a model with Bayesian learning.	111
2.A1	Univariate effects on the SCC in 2100 in a deterministic model.	114
2.A2	Univariate effects on the SCC in 2100 in a model with temperature shock.	114
2.A3	Univariate effects on the SCC in 2100 in a model with Bayesian learning.	115
3.1	Cumulative CO2 emissions by income group. Source: OWID	130
3.2	Annual CO2 emissions by country income group (left) and fossil fuel share of primary energy consumption (right) for the different income groups of countries.	131
3.3	Primary energy from renewable sources (left) and renewable energy innovation (right) for the different income groups of countries.	132
3.4	Total industrial emissions	143
3.5	GDP (left) and emissions (right) for advanced and developing economies, BAU scenario, computed and actual values. Year zero on the graphs corresponds to a starting year 1990.	144
3.6	GDP (left) and emissions (right) for advanced and developing economies, BAU scenario, computed and actual values. Year zero on the graphs corresponds to a starting year 1990.	144
3.7	TFP level for the fossil fuels (left) and renewable energy (right) with and without spillovers for developing economies, BAU scenario. Year zero on the graphs corresponds to a starting year 1990.	146
3.8	Damages in advanced countries (left) and developing countries (right) under BAU and optimal taxation schemes. Year zero on the graphs corresponds to a starting year 1990.	147

3.9	Dirty energy in advanced economy (left) and developing economy (right) under BAU and optimal taxation schemes. Year zero on the graphs corresponds to a starting year 1990.	147
3.10	Clean energy in advanced economy (left) and developing economy (right) under BAU and optimal taxation schemes. Year zero on the graphs corresponds to a starting year 1990.	148
3.11	Emissions in advanced economy (left) and developing economy (right) under BAU and optimal taxation schemes. Year zero on the graphs corresponds to a starting year 1990.	148
3.12	Mass of carbon in the atmosphere (left) and temperature of the atmosphere (right) under BAU and optimal taxation schemes. Year zero on the graphs corresponds to a starting year 1990.	149
3.13	SCC in advanced region (left) and developing region (right) under optimal taxation scheme. Year zero on the graphs corresponds to a starting year 1990.	149
3.14	Dirty energy (left) and green energy (right) in developing economy. Year zero on the graphs corresponds to a starting year 1990.	150
3.15	Mass of carbon in the atmosphere (left) and temperature of the atmosphere (right). Year zero on the graphs corresponds to a starting year 1990.	151
3.16	Dirty energy in advanced (left) and developing economy (right) . Year zero on the graphs corresponds to a starting year 1990.	152
3.17	Green energy in advanced (left) and developing economy (right). Year zero on the graphs corresponds to a starting year 1990.	152
3.18	Mass of carbon in the atmosphere (left) and temperature of the atmosphere (right). Year zero on the graphs corresponds to a starting year 1990.	153

List of Tables

- 1.1 Values of free parameters in the carbon cycle, original DICE-2016 (with $\Delta_t = 5$ years) and our proposed, different calibrations of CDICE. 26
- 1.2 Values of the free parameters of the temperature equations for different versions of DICE: original DICE-2016 with $\Delta_t = 5$ years and re-calibrated (CDICE). Also given are versions mirroring CMIP5 models with extreme ECS from Geoffroy et al. (2013), which are used for comparison purposes. Note that $\lambda = F_{2XCO_2}/ECS$ is a derived quantity. 26
- 1.3 Initial conditions for the year 2015 as used in DICE-2016 and in CDICE, as well as for extreme calibrations of CDICE with respect to the carbon cycle and/or temperature. The atmospheric CO2 concentration is always 400 ppm (851 GtC). All other values result from integrating the differently calibrated CEs from 1850 to the present day using the CMIP5 setup as described in the fourth test case. 29
- 1.A1 Labelling of the models, and their respective parameterization. Note that the coefficients for the DICE-2016 model correspond to a five-year time step, whereas all other models are defined for an annual time step. 58
- 1.B2 Generic parametrization for the evolution of labor. 60
- 1.B3 Generic parametrization for the evolution of TFP. 60
- 1.B4 Generic parametrization for the carbon intensity evolution. 61
- 1.B5 Generic parametrization for the abatement cost. 62
- 1.B6 Generic parametrization for the emissions from land. 62
- 1.B7 Generic parametrization for the exogenous forcing. 63
- 1.B8 Generic parametrization for the mass of carbon. 64
- 1.B9 Generic parametrization for the temperature. 64

1.B10	Generic parametrization for the parameters of economy.	66
1.D11	Summary statistics of the loss function components along the simulation path for the optimal solution of the CDICE model. Following the literature (see, e.g., Brumm and Scheidegger (2017)), we define the maximum error as the 99.9 percent quantile of the error distribution.	76
2.1	Parameter ranges for the uncertainty quantification analysis.	105
2.B1	Annual parametrization for the Bayesian learning process.	115
2.B2	Annual parametrization for the economy.	116
2.C1	Summary statistics of the loss function components along the simulation path for the optimal solution of the stochastic model with pseudo-states.	124
3.1	Economic parameters	140
3.2	TFP parameters.	140
3.3	Energy parameters.	142
3.4	Damages parameters.	143
3.5	Welfare values expressed in percent deviation from the BAU case without spillovers	154
3.B1	Starting states	161
3.B2	Annual parametrization for labor evolution	161
3.B3	Annual parametrization for carbon intensity evolution	161
3.B4	Annual parametrization for the emissions from land.	162
3.B5	Annual parametrization for the exogenous forcing.	162
3.B6	Annual parametrization for the mass of carbon.	162
3.B7	Annual parametrization for the temperature.	162
3.B8	Energy sector initial labor share values	163
3.C9	Low income countries: economies with GNI less than \$1,086 per capita	164
3.C10	Lower-middle income countries: economies with GNI between \$1,086 and \$4,255 per capita.	165
3.C11	Upper-middle income countries: economies with GNI between \$4,256 and \$13,205 per capita	166
3.C12	High income countries: economies with GNI more than \$13,205 per capita	167

Introduction

Macroeconomics of climate change seeks to provide economic insights into how we can address the challenges posed by climate change while promoting sustainable economic growth and equity. It involves studying the complex interactions between the environment, the economy, and public policies to inform decision-making at the global, national, and local levels. To engage with these issues one may want to rely on a modeling setup that represents an interaction of the economy and climate in some form. This brings two aspects to consideration. First, to be able to explore the macroeconomic subtleties of climate change it is desirable to have a reliable and simple model of climate to work with. Second, macroeconomic models of climate change are usually high-dimensional non-linear optimization problems. To deal with these optimization problems one needs a flexible solution method that can fathom these complexities in a computationally efficient way. Having these necessary ingredients in place one can tackle a broad range of macroeconomic questions related to the climate change issues. The present thesis aims to alleviate the aforementioned difficulties as well as provide new insights into the role of the climate emulator in the economy-climate model, shed light on the uncertainty quantification in the integrated assessment models, and evaluate the role of technological spillovers in the decarbonization of developing countries.

All three chapters of the thesis employ the computational approach that is based on deep neural net algorithms to tackle non-linear dynamic-stochastic optimization problems. The impact of deep learning in many fields of life and science has been revolutionary. Global solution methods for optimization problems can also benefit from deep neural net advancements. With deep neural net-based algorithms, even previously unsolvable optimization problems with large state space and complex structures can be solved globally, creating new research opportunities in economics fields that rely on structural modeling.

Three chapters of the thesis provide various angles of the application of deep neural nets to economy-climate modeling.

The first chapter, "*The Climate in Climate Economics*", co-authored with Doris Folini, Felix Kübler, and Simon Scheidegger, proposes a transparent calibration and evaluation strategy for a climate emulator, demonstrating its importance by recalibrating the widely used DICE-2016 model. We found the functional form of the DICE-2016 emulator fit for purpose. However, we discovered miscalibration in its carbon cycle and temperature equations. We show that the recalibrated DICE-2016 model demonstrates a strongly reduced sensitivity to the discount rate and about one degree less long-term warming. We also examined the importance of the emulator calibration for the social cost of carbon. The results show a potential four-fold change in the social cost of carbon value due to model uncertainty resulting from different consistent climate calibrations.

In the second chapter, "*Deep Uncertainty Quantification for Stochastic Integrated Assessment Models*", co-authored with Felix Kübler, Simon Scheidegger, and Takafumi Usui, we quantify uncertainty in dynamic stochastic economy-climate models. We formulate a state-of-the-art stochastic integrated assessment model with Bayesian learning over the equilibrium climate sensitivity, a key climate uncertain value. We consider several uncertain model parameters, with the discount rate and risk aversion among them. The project utilizes deep learning algorithms to give the solution of the model for any possible combination of the uncertain parameters and measure the non-linear impact of each parameter on the social cost of carbon, among other quantities of interest. This method of uncertainty quantification can be considered generic for any type of problem, not only limited to the climate-economy models. Results specific to the model at hand indicate that the distribution of the impacts of uncertain parameters on the social cost of carbon changes depending on the uncertainty structure in the model. The uncertainty around equilibrium climate sensitivity on the social cost of carbon seems to be resolved with the Bayesian learning process over time.

In the third chapter, "*Green energy transition: decarbonization of developing countries and the role of technological spillovers*", I explore the role of technological spillovers and their interaction with carbon pricing in achieving decarbonization, with a particular focus on the challenges faced by developing countries. To do this, I develop a two-region integrated assessment model of the global economy and climate, which includes both fossil

fuel and renewable energy inputs and features technological spillovers in the developing economy. I solve the model using deep learning algorithms. The findings indicate that technological spillovers in developing countries contribute positively to the replacement of fossil fuels with renewable energy inputs. The study suggests that implementing carbon taxation in both advanced and developing regions, along with technological spillovers, yields the most favorable outcomes for the climate. However, the absence of carbon tax in developing countries with spillovers delivers slightly better environmental results compared to taxing both regions without taking spillovers into account. The results emphasize the importance of considering spillovers and carbon taxation when designing effective strategies to achieve environmental goals.

Chapter 1

The climate in climate economics [†]

Abstract

To analyze climate change mitigation strategies, economists rely on simplified climate models – so-called climate emulators – that provide a realistic quantitative link between CO₂ emissions and global warming at low computational costs. In this paper, we propose a generic and transparent calibration and evaluation strategy for these climate emulators that is based on freely and easily accessible state-of-the-art benchmark data from climate sciences. We demonstrate that the appropriate choice of the free model parameters can be of key relevance for the predicted social cost of carbon. The key idea we put forward is to calibrate the simplified climate models to benchmark data from comprehensive global climate models that took part in the Coupled Model Intercomparison Project, Phase 5 (CMIP5). In particular, we propose to use four different test cases that are considered pivotal in the climate science literature: two highly idealized tests to separately calibrate and evaluate the carbon cycle and temperature response, an idealized test to quantify the transient climate response, and a final test to evaluate the performance for scenarios close to those arising from economic models, and that include exogenous forcing. As a concrete example, we re-calibrate the climate part of the widely used DICE-2016, fathoming the CMIP5 uncertainty range of model responses: the multi-model mean as well as extreme, but still permissible climate sensitivities and carbon cycle responses. We demonstrate that the functional form of the climate emulator of the DICE-2016 model is fit for purpose,

[†]This chapter is co-authored with Doris Folini from the ETH Zürich, Felix Kübler from the University of Zürich, and Simon Scheidegger from the University of Lausanne.

despite its simplicity, but its carbon cycle and temperature equations are miscalibrated, leading to the conclusion that one may want to be skeptical about predictions derived from DICE-2016. We examine the importance of the calibration for the social cost of carbon in the context of a partial equilibrium setting where interest rates are exogenous, as well as the simple general equilibrium setting from DICE-2016. We find that the model uncertainty from different consistent calibrations of the climate system can change the social cost of carbon by a factor of four if one assumes a quadratic damage function. When calibrated to the multi-model mean, our model predicts similar values for the social cost of carbon as the original DICE-2016, but with a strongly reduced sensitivity to the discount rate and about one degree less long-term warming. The social cost of carbon in DICE-2016 is oversensitive to the discount rate, leading to extreme comparative statics responses to changes in preferences.

Keywords: climate change, social cost of carbon, carbon taxes, environmental policy, deep learning, integrated assessment models, DICE-2016

JEL classification: C61, E27, Q5, Q51, Q54, Q58

1.1 Introduction

Anthropogenic climate change and the associated economic damages constitute a substantial negative externality from CO₂ emissions. Economic policy can mitigate this externality and potentially lead to significant welfare gains across all economic agents (see, e.g., (L. Kotlikoff, Kubler, Polbin, & Scheidegger, 2021a, 2021b; L. J. Kotlikoff, Kubler, Polbin, & Scheidegger, 2021; W. Nordhaus, 2018)). In order to determine the optimal mitigation strategies, economists need to develop quantitative models that produce a realistic link between CO₂ emissions and global warming and that are informed by research in climate science as presented in the Intergovernmental Panel on Climate Change (IPCC)¹ reports, that is, the “state-of-the-art” in climate science.

The backbone of the IPCC reports are the Coupled Model Intercomparison Projects (CMIP5 and CMIP6; see Eyring et al. (2016); Taylor, Stouffer, and Meehl (2012)), which bundle the output from a collection of global climate models (GCMs) that run on pre-defined future scenarios, notably future greenhouse gas (GHG) concentrations. The GCMs

¹For more details on IPCC, see, e.g., <https://www.ipcc.ch>.

come essentially in two flavors: Earth System Models (ESMs), which cover biogeochemical processes like the carbon cycle and can take carbon emissions as input, and coupled Atmosphere-Ocean Global Climate Models (AOGCMs), which lack biogeochemical processes and can take only GHG concentrations as input. One fundamental challenge is that the computational costs for ESMs (and for AOGCMs) are so significant that they are not suitable for studying the two-way feedback between the Earth system and human behavior.² Therefore, economic models focusing on this feedback have to rely on a much-simplified representation of the Earth system component. Simplified and computationally cheap-to-evaluate climate models come at different levels of complexity (and computational costs) and under different names: Climate emulators (CEs), energy balance models (EBMs), simple climate models (SCMs), or ESMs of intermediate complexity (EMICs). We avoid using this differentiation throughout this paper and, somewhat loosely, just use CE or the climate model.

There is a proliferation of different CEs used in the climate-change economics literature. The most popular emulators can be found in the Dynamic Integrated Model of Climate and the Economy (DICE) (W. Nordhaus, 2018), in PAGE (Hope, 2013), as well as that in Golosov, Hassler, Krusell, and Tsyvinski (2014). Unfortunately, as Calel and Stainforth (2017) point out, *“in failing to maintain clear links to the physical science literature, the climate components of these models have become opaque to the scientific community.”* Even worse, there is no consensus in the (economics) literature about what makes a *“good”* climate model, that is, which data the model is supposed to be matched to when choosing the model’s functional forms and parameters.

We close this gap by developing a comprehensive and transparent suite of tests that aims to answer the following key questions: i) When is a particular CE used in economics fit for purpose?, and ii) Which calibration strategy should generally be applied so that the CE is in line with state-of-the-art climate science? We advocate the use of four test cases that are standard in climate science, notably in the context of CMIP (Eyring et al., 2016; Keller et al., 2018). Two of the said tests will be used for the calibration of the CE, whereas another two tests are used for evaluating the CE. For CEs as used by economists, these four tests can be regarded as comprehensive. However, the said test

²See, e.g., Danabasoglu et al. (2020), who state that the Community Earth System Model Version 2 (CESM2), one of the most popular ESMs, needs more than 3000 CPU hours to simulate one year of the global climate.

cases are typically not employed by economists to evaluate their emulators. We showcase our proposed strategy, including economic effects at an example from the seminal DICE model family: we re-calibrate one specific version – DICE-2016 (W. Nordhaus, 2018)³ – according to our battery of tests to match the output of climate science models and obtain CDICE, short for “**C**alibrated **DICE**”. In addition, we illustrate the economic importance of a proper calibration of the CE.

A key functionality of any CE is to translate anthropogenic emissions, as computed by the economic model, into a global mean temperature change. The task is typically split into two parts (see, e.g., DICE (W. Nordhaus, 2018)): a “carbon cycle” which translates anthropogenic emissions in the wake of human economic activity into changes in the atmospheric CO₂ concentration, and a temperature model which translates changes in atmospheric CO₂ concentrations into global mean temperature changes. We propose first to calibrate both parts of the CE independently, using one test case for each calibration. Each of the two test cases comes, from a climate science perspective, with a plausible range of outcomes. To capture this range, we suggest for each test case one intermediate and two extreme calibration targets, to be detailed below. This leaves us with a total of nine differently calibrated CEs, three calibrations for the carbon cycle times three calibrations for the temperature part. Finally, we advocate evaluating the performance of these differently calibrated CEs against two additional climate science benchmarks, also detailed below, that are closer to real-world applications. The four tests and the associated CMIP5-based benchmark data are well consolidated and explored in the literature.⁴

The first test we use targets the calibration of the carbon cycle. It uses a highly idealized setup; an instantaneous emission of 100 GtC to the present-day atmosphere is followed in time. The CE is calibrated such that the (steadily decreasing) fraction of emitted carbon remaining in the atmosphere aligns with benchmark data adopted from Joos et al. (2013). We choose three specific calibration targets - one intermediate and two extremes - to mirror the range of carbon cycle responses considered plausible from a climate science point of view. As an intermediate target, we use the average response of

³Below, we use the abbreviation DICE-2016 and DICE interchangeably.

⁴The CE calibrations and test cases used here are all based on CMIP5 data. Meanwhile, data from the 6th generation of the Coupled Model Intercomparison Project (CMIP6) are available, and one may wonder whether switching from the CMIP5 data to the newer CMIP6 data makes a difference. Dedicated studies comparing CMIP5 and CMIP6 simulation data suggest that this is not the case for those aspects of climate and its modeling that we are interested in here. We discuss this point in detail in Section 1.3.4 below.

all models in Joos et al. (2013); their multi-model mean (MMM).⁵ As extreme calibration targets, we use two specific models from the study by Joos et al. (2013), leaving either a very large (cf. their model “MESMO”) or small (cf. their model “LOVECLIM”) fraction of emitted carbon in the atmosphere in the long run (cf. Joos et al., 2013). In the following, to make the different calibration targets transparent where necessary, we add the name of the corresponding target model to the general name CDICE.

The second test we use targets the calibration of the temperature equations. Being highly idealized, it follows the evolution of the global mean temperature after an instantaneous quadrupling of atmospheric CO₂ concentrations with respect to pre-industrial values. The CE is calibrated to meet benchmark data anchored in CMIP5 and adopted from Geoffroy et al. (2013). The range of warming displayed by the different CMIP5 models is considered plausible from a climate science point of view, strong or weak warming are plausible limiting cases (Knutti, Rugenstein, & Hegerl, 2017). We choose three specific calibration targets again to capture this range: the MMM, as well as two models that show a rather strong (model HadGEM2-ES, Hadley Centre Global Environmental Model 2) or weak (model GISS-E2-R, Goddard Institute for Space Studies Model E) warming in the long run within CMIP5.

Any full-fledged quantitative economic treatment of climate change must take this “model uncertainty” seriously. Even in a simple representative agent framework, the attitude of the representative agent towards risk and uncertainty becomes a crucial determinant for optimal carbon policy (see, e.g., Barnett, Brock, and Hansen (2020a, 2020b)). To assess the effect of climate model uncertainty on economic models, the so-called equilibrium climate sensitivity (ECS) parameter is often varied within the range observed in CMIP5 models (see, e.g., Hassler, Krusell, and Olovsson (2018), or W. Nordhaus (2018)). The ECS measures the long-term increase in global average temperature expected to occur after an instantaneous doubling of the atmospheric CO₂ concentration; different projected warmings imply a different ECS (Geoffroy et al., 2013). While being endogenously determined in AOGCMs, the ECS is an exogenous parameter determining long-run warming in CEs. The approach of just changing the ECS parameter to sample the uncertainty range is often a useful shortcut, but it misses part of the relevant temperature dynamics. We

⁵The multi-model mean is a debated, but regularly used, benchmark quantity in climate sciences (see, e.g., Beusch, Gudmundsson, and Seneviratne (2020); Thao, Garvik, Mariethoz, and Vrac (2021), and references therein).

will show below that it makes a difference whether one changes only the ECS of the CE or, as we do, really calibrates the CE against CMIP5 model data whose ECS (high for HadGEM2-ES, low for GISS-E2-R) can then be associated with upper and lower bounds on the true costs of climate change and can also provide an average scenario (MMM) that can, perhaps, be viewed as “most likely”.

The third test evaluates the CE’s transient climate response (TCR), using the same setup as in climate science: starting in 1850 at pre-industrial levels, the atmospheric CO₂ concentration gradually increases at one percent per year until doubling after 70 years (quadrupling after 140 years). The TCR is defined as the warming after 70 years. It is not calibrated for but, rather, is an emergent property of both the CE and CMIP5 models - or any AOGCM or ESM in general. This test allows comparing the TCR of the CE with values from CMIP5. In fact, the TCR is a standard test in climate sciences and a compulsory test for any GCM to take part in CMIP (see Eyring et al. (2016)). As the test takes CO₂ concentrations as input, not emissions, it addresses only the temperature equations of the CE.

The fourth test case is closer to what integrated assessment models (IAMs) are expected to cope with in real applications: the CMIP5 simulations for the historical period and future representative concentration pathways (RCPs) for three different forcing levels (RCP26, RCP45, RCP60, RCP85).⁶ Input data are either prescribed atmospheric CO₂ concentrations or CO₂ emissions.⁷ In the latter case, the entire climate model is tested; in the former case, only its temperature equations. Within the CE, an assumption has to be made on non-CO₂ forcings, which form part of the CMIP5 data. The CE climate is evaluated against data from the CMIP5 archive.

To exemplify our calibration strategy, we apply it to the climate part of the widely used DICE-2016 model by W. Nordhaus (2018). As Dietz, van der Ploeg, Rezai, and Venmans (2021) point out, the most commonly used CEs in economics, including Nordhaus’ widely used DICE-2016 model, seem seriously flawed in that they cannot reproduce the evolution of atmospheric CO₂ and temperature for the basic test case of an instantaneous carbon

⁶The scenarios describe the results of different socioeconomic narratives that produce particular concentration profiles of greenhouse gases, aerosols, and other climatically relevant forcing agents over the 21st century. The RCP85 scenario, for instance, reflects a “no policy” narrative, in which total anthropogenic forcing reaches approximately $8.5W/m^2$ in the year 2100. Conversely, the RCP26 scenario involves aggressive decarbonization, causing radiative forcing to peak at approximately $3W/m^2$ around 2050 and to decline to approximately $2.6W/m^2$ at the end of the 21st century.

⁷Meinshausen et al. (2011), <http://www.pik-potsdam.de/~mmalte/rcps>.

pulse to the present-day atmosphere (Joos et al., 2013). Based on this one test case, which mixes the response of the carbon cycle and the temperature equations, they conclude that “*economic models of climate change are out of line with state of the art in climate science*”, and they recommend that “*the climate modules in economic models be replaced.*” While we confirm the finding by Dietz et al. (2021) that the carbon cycle of DICE-2016 leaves too much CO₂ in the atmosphere and its temperature response to a sudden increase in CO₂ concentration is too slow, our study also demonstrates that their conclusion that the climate model must be replaced is incorrect. In particular, we show that the functional form of the CE in DICE-2016 is fit for purpose and can be re-calibrated to match results from our test cases with respect to the multi-model mean as well as concerning CMIP5 extreme cases. For the carbon cycle, no perfect calibration is possible as the functional form in DICE and the benchmark data from Joos et al. (2013) are different. By contrast, the temperature equations in DICE are formally identical to those in Geoffroy et al. (2013), thus the calibration target can be matched exactly.⁸ Our study goes beyond Dietz et al. (2021) in that we present a comprehensive set of tests to ascertain transparently whether a CE is fit for purpose and, if not, we also present means to re-calibrate a CE properly on the condition that its functional form is fit for purpose.

To examine the impact of different climate calibrations on the optimal price of carbon, we first consider a very simple partial equilibrium setup where we take the path of emissions, the growth rate, and the interest rate as exogenously given. As it is standard in economic models of climate change (see, e.g., Golosov et al. (2014); W. D. Nordhaus (1979)), we assume that an aggregate damage function determines what fraction of output is destroyed as a function of the temperature. In these (deterministic) models, the optimal carbon tax equals the social cost of carbon (SCC), which can be computed as the marginal cost of carbon emissions, that is, as the sum of all future damages, discounted at the market interest rate, that results from an infinitesimal extra emission of CO₂ into the atmosphere. The ratio of growth rate and interest rate then constitutes the correct discount factor for these calculations and, as it is well documented in the literature, one of the most important determinants of the SCC. We show that for a given discount factor and emissions scenario, the model uncertainty from climate science can change the SCC

⁸The original formulation of DICE hides this similarity somewhat, as it absorbs the time step of the climate part in the coefficients of the equations. We offer a more transparent formulation where the time step is explicitly exposed, which allows us to directly use coefficients from Geoffroy et al. (2013) that are already calibrated to match the CMIP5 results.

by a factor of four if one assumes a quadratic damage function; one of the most common functional forms in the literature. This finding is (roughly) independent of discounting and emissions, but depends crucially on the functional form of the damage function. Simply adjusting the ECS in the equations of the climate emulator leads to significantly different estimates for the SCC than using our full-blown calibrations of extreme climate models. In this simple partial equilibrium setting, the incorrect calibration of the CE in DICE-2016 leads to an SCC that is oversensitive to the discount rate. This high sensitivity has important consequences for a general equilibrium setting, where the interest rates are endogenous.

In order to investigate the economic consequences of our different calibrations in a general equilibrium framework, we use the economic model from DICE-2016 together with our newly calibrated versions of “CDICE” to compute the SCC and the optimal mitigation. We find that in our re-calibrated model, when updated with respect to the MMM, the SCC and the optimal mitigation are very similar to the values found in DICE-2016 if we take the exact same economic parameters.⁹ We point out that for the BAU scenario, the temperature increases in DICE-2016 are below those predicted by our extreme calibration, that is, CDICE-HadGEM2-ES. This finding implies that the DICE-2016 predictions are within the range of what is considered plausible in climate science. However, being in the plausible range is merely caused by the fact that two different flaws in the original calibration of the temperature equations and the carbon cycle in DICE-2016 partially offset each other. In particular, the calibration gives the wrong results for the optimal economic response to climate change. In the optimal mitigation scenario, carbon taxes turn out to be too low in the sense that the temperature response of DICE-2016 now falls outside of the CMIP5 range. As a result, the model with an optimal carbon policy predicts a higher temperature than CDICE-HadGEM2-ES.

As pointed out above, the SCC in the DICE-2016 calibration is oversensitive to the discount rate. The role of the rate of time-preference of the social planner / representative agent for the SCC and optimal carbon taxes has been extensively documented and discussed in the literature (see, e.g., Barrage (2018); Hänsel and Quaas (2018)). While this parameter is obviously important for the SCC, we show that a large part of the quanti-

⁹A significant difference is that the long-run temperature in DICE-2016 is substantially higher, that is, about one degree Celsius, higher than in our calibration. This finding holds both for the business as usual (BAU) scenario without any mitigation and the optimally mitigated scenario.

tative results are driven by an incorrect calibration of the climate module in DICE-2016. Moreover, in a model with time-varying growth rates (as DICE-2016), it is not only the rate of time preference, but also the curvature of cardinal utility that determines the discount rates. We show that this implies that the DICE-2016 climate calibration does not produce reliable results for important comparative statics questions.

The remainder of the paper is organized as follows. In section 1.2, we briefly connect our paper to the related literature. In section 1.3, we detail our four test cases. Section 1.4 explains how to re-calibrate the parameters in the climate part of DICE to produce forecasts that are consistent with our test cases. Section 1.5 explores the implications of different CE calibrations for the SCC in a simple partial equilibrium model. Subsequently, in section 1.6, we use the re-calibrated DICE model, that is, CDICE, to study the role of the climate calibration in the economic model of DICE-2016. Section 1.7 concludes. In addition, for the convenience of the reader, we provide a complete specification of the different variants of the DICE model (some of which we use in our numerical experiments below) in the online Appendix 1.B, including the DICE versions from 2007, 2016, as well as the re-calibration that we suggest in this paper, that is, CDICE.

1.2 Literature

Starting with Nordhaus' seminal work on climate change (W. D. Nordhaus, 1979), a massive field of research was spawned, including Nordhaus' own development of the DICE model (see, e.g., W. Nordhaus (2013, 2018); W. D. Nordhaus (2012)). For example, Anderson, Borgonovo, Galeotti, and Roson (2014) as well as Miftakhova (2021b) conducted uncertainty quantification, whereas Cai and Lontzek (2019); Lemoine and Traeger (2014), and Lontzek, Cai, Judd, and Lenton (2015) added stochastic tipping points on top of the DICE-2007 model. Hwang, Reynès, and Tol (2017) performed learning about equilibrium climate sensitivity with fat tails, whereas Popp (2004) studied endogenous growth in the DICE framework. Wouter Botzen and van den Bergh (2012) and Michaelis and Wirths (2020) studied DICE with an alternative damage function. The fact that DICE was criticized for a flawed climate model (in particular by Dietz et al. (2021)) puts the quantitative predictions of these contributions into a questionable position and motivates our study. We show below that the climate model in DICE-2016 can be re-calibrated to perform well in our tests.

Golosov et al. (2014) develop a simple CE that is at present widely used as an alternative to the climate module of DICE (see, e.g., Hassler and Krusell (2018); Hassler, Krusell, Olovsson, and Reiter (2019); L. Kotlikoff et al. (2021b)). Due to its simplicity, the model is computationally much more tractable than DICE. However, the simplicity of this model implies that certain stylized facts of temperature change in response to CO₂ in the atmosphere cannot be captured adequately.¹⁰ This model, therefore, does not lend itself to our calibration strategy.¹¹

More directly related to our paper, there have been several important contributions about the calibration of CEs. Miftakhova, Judd, Lontzek, and Schmedders (2020) propose a general emulation method for constructing low-dimensional approximations of complex dynamic climate models and develop an emulator for MAGICC to approximate the impact of emissions on global temperature. Cai, Brock, Xepapadeas, and Judd (2019) calibrate a spatial climate system to match four RCP scenarios and historical data. Traeger (2014) and Cai, Judd, and Lontzek (2012); Cai and Lontzek (2019) re-calibrate the DICE CE from a ten-year time step (as in the DICE-2007 formulation) or five-year time step (as in the DICE-2016 formulation) to higher frequency data. In the climate-science literature, Calel and Stainforth (2017) discuss the physics of different climate models, including DICE. Thompson (2018) conducted an intercomparison study of models, including DICE to assess how they were designed from a physics point of view. Geoffroy et al. (2013) show how two-layer energy-balance models (formally identical to the temperature equations in DICE) can be used to match the results in CMIP5. Joos et al. (2013) quantify responses to emission pulses in a carbon cycle intercomparison project. Our analysis relies heavily on these two latter papers. In particular, we use Geoffroy et al. (2013)'s calibration of the temperature equation and take our carbon-cycle benchmarks from Joos et al. (2013). Our paper is closest to Dietz et al. (2021), and we compare our contributions in more detail in the following sections.

¹⁰For example, since in Golosov et al. (2014) there is only one temperature equation that links CO₂ in the atmosphere directly to the current temperature, the temperature must decrease as soon as there are net-zero emissions and CO₂ concentration in the atmosphere decreases. We will show in section 1.5.1 that the timing of warming plays an important role for the SCC.

¹¹Interestingly, Dietz et al. (2021) argue that although the model in Golosov et al. (2014) is very simple, it matches some important stylized facts that can be derived from CMIP5 data better than the original DICE-2016 calibration.

1.3 A comprehensive framework to calibrate the climate in IAMs

Naively, one would think that existing historical data suffices for calibrating and evaluating CEs used in IAMs. However, it turns out that, broadly speaking, the signal-to-noise ratio in that sort of data is simply too low for a reliable calibration of CEs with their focus on forcing from CO₂. Put differently, in observed records of annual global mean temperature, the anthropogenic signal due to CO₂ emissions comes in combination with a range of other relevant effects. The change in global mean temperature over the last 150 years is not only due to changes in CO₂. It also bears substantial imprints from other greenhouse gases, from aerosols of anthropogenic or natural origins, including volcanoes, and also from land use changes (Gambhir et al., 2017; Mengis & Matthews, 2020). Reliably disentangling the different contributions is challenging. To illustrate, Millar and Friedlingstein (2018) estimate that from 1880 to 2015, CO₂ contributed about 0.7 degrees to global warming, whereas non-CO₂ agents contributed about 0.3 degrees, with 5% to 95% uncertainty ranging from 0.5 to 1.5 degrees and -0.2 to +0.4 degrees, respectively (cf. their Figure 4). Hence, we need to base our suite of tests on historical observations, but also on the so-called third pillar of science: computational experiments.

As detailed in the introduction, the CMIP experiments are a logical choice for this purpose. We focus on CMIP5 in this paper – CMIP 6 is briefly discussed below. The range of models participating in CMIP then raises the issue that for any specific CMIP experiment (or CE test), one faces not a single benchmark, but a range of benchmarks. Given that the full range is considered plausible by climate scientists, it is important that any CE captures this model diversity in some way. In this light, a first and primary benchmark is the MMM,¹² the average of all cases reported in CMIP5. The MMM is complemented by extreme cases bracketing the CMIP5 range. Two extreme cases that bracket the plausible temperature response to CO₂ in the atmosphere in CMIP5 are the HadGEM2-ES model (strongly warming, ECS of 4.55 K) and the GISS-E2-R model (weakly warming, ECS of 2.15 K) (Geoffroy et al., 2013). Two extreme cases that bracket the amount of emitted carbon remaining in the atmosphere are MESMO and LOVECLIM, with about 55% and

¹²For a recent application of the MMM, the multi-model mean, in climate science, see, e.g., Beusch et al. (2020).

30%, respectively, of the 100 GtC test pulse mass remaining in the atmosphere after 100 years, according to Figure 1a from Joos et al. (2013).

1.3.1 Choice of test cases

The choice of the four test cases outlined in the introduction, that is, two for the calibration, and two for the evaluation of the CE, was guided by the following considerations. First, all test cases should be widely used in the relevant climate science literature and transparently documented. Thus, they can easily be reproduced and compared with published results. Second, some of the tests should be highly idealized to allow for the independent calibration of the carbon cycle and the temperature response, respectively. Third, we want some test cases to be close to the ultimately envisaged *real-world applications*, with gradual changes in CO₂ emissions, exogenous forcing, and associated temperature response. The proximity to real applications makes these tests somewhat like a gold standard, but also makes them more difficult to interpret than the highly idealized tests.

Taken together, the four test cases we propose to use may, loosely speaking, be regarded as *necessary and sufficient* to answer whether an emulator is fit for purpose. They allow the calibration and comprehensive evaluation of a CE like that in DICE, from its individual components to real application cases. To this end, it is crucial that highly idealized settings, which are frequently used as benchmarks in the literature, are augmented with closer-to-reality tests. We advocate that the same four tests may be used to examine the performance of the climate parts of other IAMs featuring a carbon cycle and a set of temperature equations. Any climate model that fits the CMIP5 data for the four test cases will likely provide a good fit for all emissions paths arising in economic modeling.

1.3.2 Technical setup of test cases

The first of four experiments in our test suite is used to calibrate the carbon cycle. Its highly idealized setup follows the temporal evolution of an instantaneous release of 100 Gt carbon (GtC) to the present-day atmosphere. The said 100 GtC roughly corresponds to ten years of present-day CO₂ emissions from fossil fuels (Le Quéré et al., 2018). The test requires two steps, which we outline here. For more detailed explanations of the test and its benchmark data, we refer to Joos et al. (2013). In a first step, the CE is used to simulate the evolution of the climate from its 1850 equilibrium to 2015, using as

input historical carbon emissions from 1850 to 2015. The simulation is then continued from 2015 onward, with annual carbon emissions being iteratively determined to keep the atmospheric CO₂ concentration constant at the value of the year 2015. These emissions are then used in a second simulation that starts in 2015, but now with an additional, instantaneous pulse of 100 GtC to the atmosphere. Changes in atmospheric CO₂ are then taken as the difference between this second and the first simulation. The test is used to calibrate the time scales and rates at which the atmospheric CO₂ concentration decays in the wake of instantaneous carbon release to the atmosphere.¹³

The second test case in our proposed framework is used to calibrate the amplitude and time scales of a given emulator's temperature response, that is, how fast and how strongly the global mean temperature warms in response to a sudden quadrupling of CO₂.¹⁴ Starting from pre-industrial equilibrium conditions, that is, in the year 1850, with atmospheric CO₂ at 285 parts per million (ppm), the atmospheric CO₂ concentration is instantaneously quadrupled, and the change in temperature as a function of time is examined. The related benchmark data is anchored in CMIP5 and adopted from Geoffroy et al. (2013).

The third test case and its benchmark data come directly from CMIP5: starting in 1850 at pre-industrial levels, the atmospheric CO₂ concentration gradually increases from 285 ppm CO₂ at one percent per year until quadrupling after 140 years. It is used to evaluate the TCR of the CE in comparison with the CMIP5 values of TCR. The test is still relatively simple, as it involves the temperature part of the CE solely, but not the carbon cycle. That is, it uses CO₂ concentrations as input, not emissions. It involves forcing only from CO₂. The change in CO₂ concentration is not an instantaneous step function, but is gradual in time. The test thus examines a situation where the temperature response time scales overlap with an additional time scale associated with the gradually increasing forcing from CO₂.

The fourth test case is close to what DICE, or some other IAM, is expected to cope with in real applications: the CMIP5 simulations for the historical period and future representative concentration pathways (RCPs) for four different forcing levels of 2.6 W/m², 4.5 W/m², 6.0 W/m², and 8.5 W/m² by 2100 (RCP26, RCP45, RCP60, RCP85). The

¹³Depending on the concrete formulation of the CE's carbon cycle, the decay of atmospheric CO₂ may result in increasing CO₂ concentrations in other carbon reservoirs, notably ocean or land.

¹⁴Note that while the test described here applies to any emulator, it will in particular target Equations (1.4) and (1.5) of the DICE-2016 model (cf. section 1.4 below).

input data consists of either prescribed atmospheric CO₂ concentrations or CO₂ emissions (Meinshausen et al., 2011, <http://www.pik-potsdam.de/~mmalte/rcps/>), as illustrated in the left and middle panel of Figure 1.1. The former case tests only the temperature response to gradually changing CO₂ concentrations. The latter case tests the full climate model of the CE, including the carbon cycle. In this test case, it is necessary to make an assumption on the non-CO₂, exogenous radiative forcing F_t^{EX} , which in the actual CMIP simulations is modeled in great detail. In the online Appendix 1.C, we show how this choice affects the quantitative results of the full model. Here, we assume $F_t^{\text{EX}} = 0.3 \cdot F_t^{\text{CO}_2}$, that is, proportional to the forcing from CO₂ alone ($F_t^{\text{CO}_2}$) and resulting in a total radiative forcing, $F_t = F_t^{\text{CO}_2} + F_t^{\text{EX}}$, which is 30% larger than from CO₂ alone (cf. section 1.4.1 below). This is in line with estimates for the radiative forcing in 2011 with respect to pre-industrial times (see, e.g., Climate Change 2014 Synthesis Report IPCC, 2014; Gambhir et al., 2017) and with estimates for the different RCPs in 2100: 26% (RCP26), 33% (RCP45), 32% (RCP60), 35% (RCP85), where the total forcing comes from the scenario and the CO₂ forcing is computed from concentrations given in Meinshausen et al. (2011); a base concentration of 285 ppm CO₂, and $F_{2\text{XCO}_2} = 3.68 \text{ W/m}^2$. An illustration of the temporal evolution of the different forcings is given in Figure 1.1, right panel. Note that estimates for the forcing from non-CO₂ GHGs by MacDougall, Eby, and Weaver (2013) (their Figure 6) show more temporal structure than F_t^{EX} . Additionally, the assumption of strict proportionality between CO₂ and non-CO₂ forcings is subject to debate in climate sciences, especially in the context of strong mitigation scenarios (see, e.g., Mengis & Matthews, 2020). Benchmark data for the evolution of atmospheric temperature is taken directly from the CMIP5 archive. The proximity to real applications makes this test difficult to interpret, yet it is a key test that CEs in economic models should pass.

1.3.3 Metric for performance evaluation

The choice of a metric to assess the calibration and subsequent evaluation of a CE is not straightforward. The basic reason lies in the design of the CE, in its reduced functional form, and the limited number of free parameters as compared to ESMs, which capture only some aspects of the benchmark cases used for calibration and evaluation. This also implies that the choice of metric may depend on the concrete form of the CE, the sim-

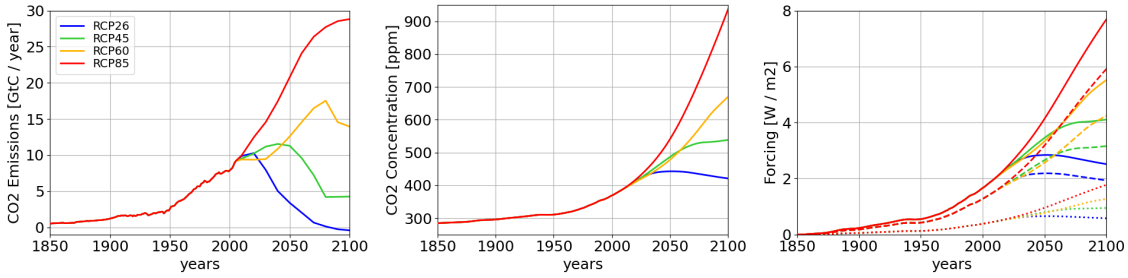


Fig. 1.1 Illustration of CMIP5 historical and future evolution (RCP26, RCP45, RCP60, and RCP85 scenarios, shown in blue, green, yellow, and red), from 1850 to 2100, of prescribed CO₂ emissions (left, in GtC per year), alternatively prescribed CO₂ concentrations (middle, in ppm CO₂), and the forcing derived from prescribed CO₂ concentrations (right, in W/m²). The total forcing F_t (solid lines) is decomposed into forcing from CO₂ ($F_t^{\text{CO}_2}$, dashed lines) and non-CO₂ forcing assumed as $F_t^{\text{EX}} = 0.3 \cdot F_t^{\text{CO}_2}$ (dotted lines).

plicity or complexity of its carbon cycle, and temperature equations. If the CE explicitly covers further elements, like, for example, methane, then not only the metric but also the benchmarks for calibration and evaluation may need adaptation.

Focusing on simple CEs, like that in DICE, one prominent difference with respect to ESMs concerns the response time scales upon perturbation: an ESM features a whole range of response time scales, whereas the CE only a few, for example, two in the case of DICE-2016. Furthermore, an ESM explicitly covers a range of forcings; the CE explicitly covers only CO₂ via its carbon cycle, while any other forcings are included in a more or less ad hoc fashion. The temperature may affect the carbon cycle in an ESM, but not in the simple CE considered here. A comprehensive discussion of why to favor any particular metric in view of these issues is beyond the scope of the present paper. Therefore, we limit ourselves to a short statement of what we did and why.

We calibrate the carbon cycle of a CE via the response to an instantaneous 100 GtC pulse to the atmosphere. The comparison is performed against benchmark data from Joos et al. (2013), using the maximum norm over a time range of 100 years after the pulse. This choice of metric favors solutions, that is, calibrations that remain close to the benchmark data at all times over a time scale of interest in an economic context. The calibration of the temperature equations does not require any metric because their functional form is identical to the benchmark data from Geoffroy et al. (2013). Therefore, we can just adopt parameter values from the benchmark data.

We evaluate a calibrated CE first with regard to TCR, and we expose the CE to the corresponding test case from climate science, where TCR is defined as the change

in global mean temperature after 70 years (and after 140 years) when the atmospheric CO₂ concentration steadily increases from 1850 onward at a rate of one percent per year. We measure the performance of the CE with respect to CMIP5 models by comparing the TCR. Finally, we evaluate the performance of the calibrated CE with regard to climate projections and historical simulation data from CMIP5. Here, we explicitly renounce using a specific metric for mainly two reasons: the CMIP5 models span a range of plausible climates, and they explicitly include non-CO₂ forcings that depend on the projection (RCP26, RCP45, or RCP85) and are included in the CE only in an ad hoc fashion. We consider the CE fit for purpose if a visual inspection shows that its climate in terms of atmospheric CO₂ concentration and the global mean temperature falls within the range of CMIP5 models.

1.3.4 CMIP5 serves the purpose, no need for CMIP6

Throughout this study, we use data from CMIP5 or studies relying on such data, notably Geoffroy et al. (2013) or Joos et al. (2013). We argue in the following that for the purpose at hand - calibration and testing of a simple CE - the CMIP5 database is sufficient; there is no need to consider the more recent CMIP6 data.

Starting with the calibration of the CE's carbon cycle, we note that the benchmark data from Joos et al. (2013) combines models that already span a rather wide range. Data from a more recent study (Jeltsch-Thömmes & Joos, 2020) examining the same test case finds a slightly faster decay of atmospheric CO₂ in the wake of the 100 GtC pulse (compare Figure 1 of both papers), yet well within the range of Joos et al. (2013). Similarly robust is the benchmark data from Geoffroy et al. (2013), used for calibrating the temperature response of the CEs. Using the same two-layer energy balance model and fitting procedure as in Geoffroy et al. (2013), but applied to 4xCO₂ data from 8 CMIP6 models, Jackson et al. (2022) find parameter values in line with Geoffroy et al. (2013), the MMM $\pm 1\sigma$ range overlap (compare Tables 3 and 4 in Geoffroy et al. (2013) with Table S2 in the supplementary material in Jackson et al. (2022)). One may worry that the larger range of the ECS reported in CMIP6, notably the higher ECS of some models (e.g. Zelinka et al., 2020), implies a too conservative ECS range in CMIP5 (bracketed here by the models GISS-E2-R and HadGEM2-ES). However, Tokarska et al. (2020) show that

the CMIP6 range is reduced considerably, becoming largely consistent again with CMIP5 if observational data is used to constrain the models.

Likewise, we see no necessity to use CMIP6 instead of CMIP5 when testing the calibrated CE against two more test cases. Warming in the ‘one percent per year atmospheric CO₂ increase’ experiment is slightly stronger in CMIP6 as compared to CMIP5, the MMM temperature across 11 models being around 10% higher after 140 years (Fredriksen, Smith, Modak, and Rugenstein (2023), Supplementary Figure S7), while the range of CMIP5 and CMIP6 models strongly overlaps. Arora et al. (2020) examine fully coupled simulations of the ‘1%/year atmospheric CO₂’ test case, finding a MMM warming after 140 years (quadrupling of atmospheric CO₂ concentration) by 4.87 Celsius in CMIP5 and 4.74 Celsius in CMIP6, that is, a difference of less than 3%.

Testing the CE against future scenarios, we note that a subset of the Shared Socioeconomic Pathways (SSPs) in CMIP6 were designed similarly to the RCPs of CMIP5 in order to provide continuity. Comparing the simulated temperature evolution for corresponding RCPs and SSPs using Reduced Complexity Models (RCMs), Nicholls et al. (2020) find that global mean temperature evolution essentially falls on top of each other (their Figure 3). Tebaldi et al. (2021) find that global mean temperature change in the CMIP5 RCPs falls within the range of corresponding SSPs in CMIP6. They elaborate on a number of reasons for the slightly wider range in CMIP6 (including differences, for example, in assumed future aerosol forcing, or methane emissions) and more generally note that CMIP5 RCPs followed a more ‘middle-of-the-road’ pollution policy path. We refer the interested reader to their original work or the paper by Fredriksen et al. (2023) for more detailed information on CMIP5 versus CMIP6. With regard to our purpose here - the calibration and testing of a simple CE - the above publications corroborate that no essential changes happened between CMIP5 and CMIP6. We take this as an argument to use the well-prepared CMIP5-based data in Joos et al. (2013) and Geoffroy et al. (2013) to calibrate a CE’s carbon cycle and temperature response, respectively. Subsequent further testing of the calibrated CE may then be done against either CMIP5 RCP or CMIP6 SSP data.

1.4 CDICE - re-calibrating the climate of DICE

So far, we put forward our suite of four test cases: one test to calibrate the carbon cycle of the CE, one test case to calibrate the temperature equation of the CE, and two test

cases to examine emerging properties of the calibrated CE, notably its performance under gradually changing conditions in terms of CO₂ and non-CO₂ forcings. We claim that, taken together, these tests are necessary and sufficient to transparently evaluate and, if needed, re-calibrate the CE of an IAM, which is used in an economic context.

In this section, we illustrate our claim with the example of the climate module of the seminal DICE-2016 model. We choose DICE-2016 as an example because it is widely used in the IAM modeling community and because it is known to be flawed (Dietz et al., 2021). We re-examine these flaws in the light of our four test cases and present an improved version, CDICE, that has the same functional form as DICE-2016 but is fully re-calibrated. We go beyond the work of Dietz et al. (2021) in three essential points: i) while Dietz et al. (2021) use one test, the 100 GtC pulse, to evaluate the CE, we stress that it is crucial to separately examine each part of the CE, carbon cycle, and temperature equations; ii) we provide corresponding test setups and show how they can be used to calibrate, and not only to examine a CE; iii) we demonstrate that even a simple CE like that in DICE is fit for purpose if properly calibrated in this way.

This section is structured as follows: First, we lay down in section 1.4.1 the fundamental building blocks of DICE's CE, its carbon cycle and temperature equations, along with the commonly used calibration of DICE-2016. Next, we demonstrate in sections 1.4.2, 1.4.3, 1.4.4, and 1.4.5 how our battery of tests can be used to systematically test and re-calibrate DICE-2016. Finally, a critical synthesis of our learnings is provided in section 1.4.6. A summary of all CDICE model parameters is given in Table 1.A1 in online Appendix 1.A.

1.4.1 Model equations

The climate model in DICE-2016 translates carbon emissions from the model's economic side into atmospheric CO₂ concentrations (i.e., the carbon cycle; cf. section 1.4.1 below) and, subsequently, into a global mean temperature change (i.e., the temperature equations; cf. section 1.4.1 below), which then feeds back into the part of the model that represents the economic side of the IAM. Thus, the carbon cycle affects temperature, but not vice versa.

The carbon cycle is a linear three-box model, where the three carbon reservoirs represent the atmosphere (AT), the upper ocean (UO), and the lower ocean (LO), with the

respective carbon masses $M = (M^{\text{AT}}, M^{\text{UO}}, M^{\text{LO}})$. Carbon can be exchanged between the atmosphere and upper ocean and between the upper and lower ocean, but not directly between the atmosphere and lower ocean. The global mean temperature is modeled via a system of two ordinary differential equations that couple two heat reservoirs, that is, the atmosphere, including the upper ocean, and the lower ocean, $T = (T^{\text{AT}}, T^{\text{LO}})$. The climate is anchored at an assumed pre-industrial equilibrium state, M_{EQ} and T_{EQ} . Climate change is quantified as deviations from this equilibrium state. In an economic context, time integration in DICE-2016 typically does not start at pre-industrial times, but at present day, for example, in the year 2015. A corresponding initial state M_{INI} and T_{INI} must be determined so as to be in line with carbon emissions since pre-industrial times and the equations of the CE (cf. section 1.4.1).

Carbon cycle

The carbon cycle model (see, e.g., Keeling, 1973) formally reads

$$M_{t+1} = (I + \Delta t \cdot B) \cdot M_t + \Delta t \cdot E_t, \quad (1.1)$$

with I being the identity matrix, Δt being the time step in years, and $M_t = (M_t^{\text{AT}}, M_t^{\text{UO}}, M_t^{\text{LO}})$ representing the carbon mass at time t in the three reservoirs. The carbon emissions per year to the atmosphere, as well as to the ocean¹⁵, are specified via E_t . The time-constant matrix B ,

$$B = \begin{pmatrix} b_{11} & b_{21} & b_{31} \\ b_{12} & b_{22} & b_{32} \\ b_{13} & b_{23} & b_{33} \end{pmatrix}, \quad (1.2)$$

describes the mass transfer among reservoirs and has units “mass fraction per time step”. Assuming that mass conservation holds, that is,

$$\sum_i b_{ji} = 0 \text{ for } j = 1, 2, 3, \quad (1.3)$$

¹⁵This is an interesting option in the context of Carbon Dioxide Removal (CDR) techniques (see, e.g., Rickels, Reith, Keller, Oschlies, & Quaas, 2018).

and that there is no direct mass transfer between AT and LO (implying that $b_{13} = b_{31} = 0$), leaves four free parameters in matrix B that are used to calibrate the carbon cycle. In DICE, the said parameters are chosen as the transfer coefficients from AT to UO (b_{12}) and from UO to LO (b_{23}), as well as the equilibrium carbon mass ratios at pre-industrial times between the reservoirs, $r_1 = M_{\text{EQ}}^{\text{AT}}/M_{\text{EQ}}^{\text{UO}}$ and $r_2 = M_{\text{EQ}}^{\text{UO}}/M_{\text{EQ}}^{\text{LO}}$. The remaining matrix entries b_{ij} are then given by $b_{11} = -b_{12}$; $b_{21} = b_{12} \cdot r_1$; $b_{22} = -b_{21} - b_{23}$; $b_{32} = b_{23} \cdot r_2$; $b_{33} = -b_{32}$. Parameter values for CDICE are given in Table 1.1. In DICE-2016, the numerical values for the free parameters are given by $M_{\text{EQ}} = (588, 360, 1720)$, $r_1 = 1.633$, $r_2 = 0.209$, as well as $b_{12} = 0.12$ and $b_{23} = 0.007$, with a time step of $\Delta t = 5$ years being hard-wired (absorbed) into the coefficients b_{ij} . To alleviate this limitation of being bound to a time step of fixed size, the b_{ij} in our formulation are specified in units of one year and are then explicitly multiplied with a time-step. The latter thus can be freely chosen, for example, as the time-step prescribed by the respective economic model.

Temperature

The two-layer energy balance model in DICE-2016 reads as

$$T_{t+1}^{\text{AT}} = T_t^{\text{AT}} + \Delta t \cdot c_1 \left(F_t - \lambda T_t^{\text{AT}} - c_3 \left(T_t^{\text{AT}} - T_t^{\text{OC}} \right) \right), \quad (1.4)$$

$$T_{t+1}^{\text{OC}} = T_t^{\text{OC}} + \Delta t \cdot c_4 \left(T_t^{\text{AT}} - T_t^{\text{OC}} \right), \quad (1.5)$$

and thus formally corresponds to that described in Geoffroy et al. (2013). T_t^{AT} and T_t^{OC} denote the temperature change with respect to pre-industrial times of the upper layer (atmosphere and upper ocean) as well as the lower layer (deep ocean), respectively, at time step t . The free parameters c_1 , c_3 , c_4 , and λ in (1.4) and (1.5) are used for calibration. From a physics perspective, they may be interpreted as a heat exchange coefficient between the upper and lower layer, $\gamma = c_3$, effective heat capacities of the upper and lower layer, $C = 1/c_1$ and $C_0 = \gamma/c_4$, and the radiative feedback parameter $\lambda = F_{2\text{XCO}_2}/T_{2\text{XCO}_2}$, that is, the ratio of the forcing from a doubling of CO₂ to the associated temperature change, that is, the ECS. Finally, F_t denotes the total radiative forcing from CO₂, $F_t^{\text{CO}_2}$, and other exogenous factors, F_t^{EX} , such as GHGs other than CO₂ and also aerosols:

$$F_t = F_{2\text{XCO}_2} \frac{\log(M_t^{\text{AT}}/M_{\text{EQ}}^{\text{AT}})}{\log(2)} + F_t^{\text{EX}}. \quad (1.6)$$

In, DICE-2016, F_t^{EX} is assumed to change linearly with time from 0.5 in the year 2015 to 1.0 in 2100. Parameter values for CDICE are given in Table 1.2. Parameter values in DICE-2016 are $c_1 = 0.1005$, $c_3 = 0.088$, $c_4 = 0.025$, and $\lambda = 3.6813/3.1 = 1.1875$, with a time step of $\Delta_t = 5$ years formally hard wired (absorbed) into c_1 and c_4 . To lift this issue, we provide, here again, a generic formulation of the temperature equations such that the time-step can be chosen freely in discrete values of one year, that is, one year, two years, and so forth.

Initialization at present day

In the context of economic models, the time integration typically does not start at pre-industrial times but rather at the present day. Corresponding initial values for the carbon and temperature reservoirs used in CDICE for 2015 are $M_{\text{INI}} = (851, 628, 1323)$ and $T_{\text{INI}} = (1.10, 0.27)$ for the MMM case (see section 1.4.5 for more details regarding the MMM and the alternative calibrations). Values for extreme calibrations of CDICE are also given in Table 1.3

These initial values should meet three criteria: the atmospheric carbon mass and temperature change should be consistent with observed changes from pre-industrial to present times, and all values should be internally consistent in that they can be obtained by integrating the CE in time from its assumed pre-industrial equilibrium to the present. Regarding the first criterion, the 851 Gt atmospheric carbon corresponds to 400 ppm CO₂, in line with measured concentrations in 2015.¹⁶ The 1.1 K change in global mean temperature since pre-industrial times corresponds to the 2015 centered 11-year average (years 2010 to 2020) observation-based value.¹⁷ We assert the third criterion by integrating the CE from its 1850 equilibrium state to the present day. We use the historical carbon emissions from CMIP5. We slightly adjust the non-CO₂ forcing, by default, at 30% of the CO₂ forcing (see section 1.3.2) to meet the warming target of 1.1 K by 2015. Such an adjustment is legitimate given that from a climate science perspective, this forcing comes with substantial uncertainty (see, e.g., Mengis & Matthews, 2020). From the internally consistent time series of M_t and T_t obtained in this way, we pick that time (year) with the desired atmospheric CO₂ concentration, for example 400 ppm, as initial conditions, M_{INI} and T_{INI} .

¹⁶<https://www.co2levels.org>.

¹⁷<http://berkeleyearth.org/global-temperature-report-for-2020>.

Model	b_{12}	b_{23}	M_{EQ}
DICE-2016, 5yr	0.12	0.007	(588, 360, 1720)
CDICE	0.054	0.0082	(607, 489, 1281)
CDICE-MESMO	0.059	0.0080	(607, 305, 865)
CDICE-LOVECLIM	0.067	0.0095	(607, 600, 1385)

Table 1.1 Values of free parameters in the carbon cycle, original DICE-2016 (with $\Delta_t = 5$ years) and our proposed, different calibrations of CDICE.

Model	c_1	c_3	c_4	ECS	F_{2XCO_2}	λ
DICE-2016, 5yr	0.1005	0.088	0.025	3.1	3.6813	1.19
CDICE	0.137	0.73	0.00689	3.25	3.45	1.06
CDICE-HadGEM2-ES	0.154	0.55	0.00671	4.55	2.95	0.65
CDICE-GISS-E2-R	0.213	1.16	0.00921	2.15	3.65	1.70

Table 1.2 Values of the free parameters of the temperature equations for different versions of DICE: original DICE-2016 with $\Delta_t = 5$ years and re-calibrated (CDICE). Also given are versions mirroring CMIP5 models with extreme ECS from Geoffroy et al. (2013), which are used for comparison purposes. Note that $\lambda = F_{2XCO_2}/ECS$ is a derived quantity.

The original initialization values used in DICE-2016 are $M_{INI} = (851, 460, 1740)$ and $T_{INI} = (0.85, 0.0068)$. The 0.85 K change in global mean temperature tends to be on the low side when compared to observation-based estimates.¹⁸

1.4.2 Atmospheric CO₂ after 100 GtC pulse to the atmosphere

To evaluate and re-calibrate the carbon cycle of DICE-2016, we use the idealized test case of an instantaneous 100 GtC pulse to the present-day atmosphere, as described in section 1.3.2 and illustrated in Figure 1.2. Compared to benchmark data from Joos et al. (2013) (black and gray lines), the known deficiency of DICE-2016 (blue dashed; see, e.g., Dietz et al. (2021)) is apparent: DICE-2016 overestimates the fraction of the pulse remaining in the atmosphere. Retaining the functional form of the carbon cycle, but re-calibrating the model against the MMM benchmark (black solid) using the maximum norm over the first 100 years after the pulse (see section 1.3.3), the new best-fit version, CDICE (red solid), performs clearly better. Full agreement between CDICE and the MMM benchmark data cannot be reached because of the different functional forms of the carbon

¹⁸<http://berkeleyearth.org/global-temperature-report-for-2020>.

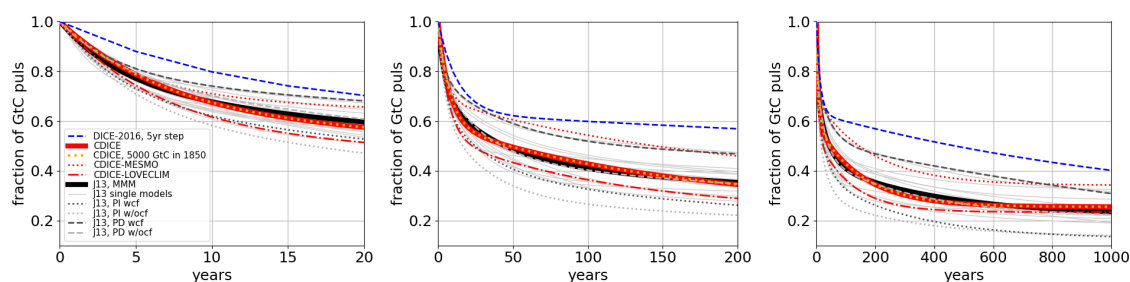


Fig. 1.2 Fraction of an instantaneous 100 GtC pulse remaining in the atmosphere (y-axis) as a function of time (x-axis, three different time scales from left to right). Shown are benchmark data adapted from Joos et al. (2013) (black and gray lines, J13) and three calibrations against this data: CDICE (red solid), which is calibrated against the multi-model mean (MMM, black solid), and two extreme calibrations, CDICE-MESMO (red dotted) and CDICE-LOVECLIM (red dash-dotted), which essentially capture the range of benchmark models (thin gray lines). DICE-2016 (blue dashed) removes too little CO₂ from the atmosphere compared to the benchmark data. Absolute values of pulse height and equilibrium masses are irrelevant in DICE’s carbon cycle model (CDICE, 5000 GtC on 1850 equilibrium masses, orange dotted), which is in contrast to findings in J13 (dashed and dotted gray lines, see their paper for details).

cycle.¹⁹ Extreme calibrations against MESMO and LOVECLIM (CDICE-MESMO, red dotted, and CDICE-LOVECLIM, dash-dotted) are also shown. They are representative of scientifically plausible, but extreme, carbon cycles that remove CO₂ very efficiently (or inefficiently) from the atmosphere, and which we use later on in our economic analysis.

Figure 1.2 also shows the functional limitation of the carbon cycle model in CDICE (or DICE in general). The fraction of the carbon pulse remaining in the atmosphere is sensitive to neither the pulse height nor the equilibrium state. The 100 GtC test case (red solid line) shows the same decay as a 5000 GtC pulse to pre-industrial equilibrium (orange dashed line). This is in contrast with informed expectations (see, e.g., Joos et al., 2013): the pulse should decay more slowly if it is larger, if it is applied to present day instead of pre-industrial conditions, or if climate feedback processes are taken into account (dashed and dotted gray lines, PI and PD indicating pre-industrial and present day, respectively, adapted from Joos et al. (2013)).

The test case used here is further suited to examine sensitivities to the parameter values of the carbon cycle (colored lines) in Figure 1.3, anchored at CDICE (see Table 1.2). As expected, the transfer coefficient b_{12} between the atmosphere and the upper ocean has the largest effect on short time scales. On intermediate time scales, up to about 50 years,

¹⁹The benchmark data in Joos et al. (2013) has three characteristic decay time scales, whereas DICE with its three carbon reservoirs has only two.

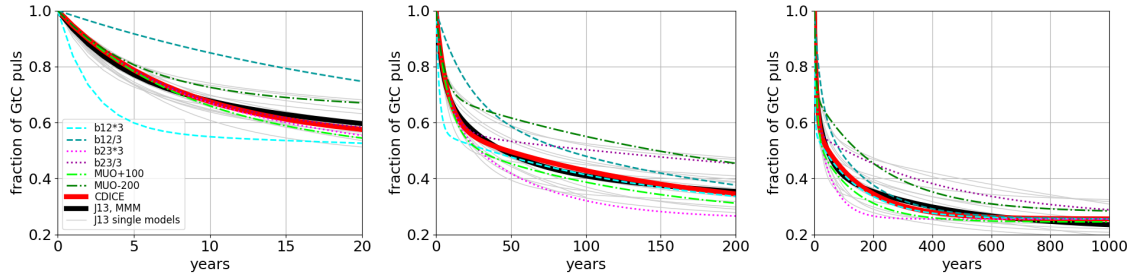


Fig. 1.3 Parameter sensitivities (thin colored lines) of the carbon cycle, anchored at CDICE (red), illustrated at the example of an instantaneous 100 GtC pulse to the atmosphere. Shown is the fraction of the pulse remaining in the atmosphere (y-axis) as a function of time (x-axis, three different time scales from left to right). Benchmark data from Joos et al. (2013) is shown in black and gray.

assumptions about the equilibrium masses in the upper and lower ocean start to matter. The effect of the transfer coefficient b_{23} starts to have a clear effect only later on. The long-term evolution is equally dependent on b_{23} and the equilibrium masses in the upper and lower ocean.

In this context, the eigenvalues (EV) of matrix B are of interest, as they relate to the decay or the half-life time scales ($\tau = \Delta_t \cdot \ln(0.5) / \ln(EV)$) of an instantaneous perturbation (carbon emission). One EV equals 1 and corresponds to the equilibrium solution. The other two EVs are $(1 + g \pm h)/2$, with $g = 1 - b_{12} \cdot (1 + r_1) - b_{23} \cdot (1 + r_2)$ and $h = ((1 - g)^2 - 4f)^{1/2}$, where $f = b_{12} \cdot b_{23} \cdot (1 + r_2(1 + r_1))$. Associated numerical values for DICE-2016 are 0.6796 and 0.9959, corresponding to half-life times of 9 and 851 years. For our CDICE calibration, we arrive at EVs of 0.8742 and 0.9933, corresponding to half-life times of 5 and 102 years. This highlights the difference between our carbon-cycle calibration and that in DICE-2016.

1.4.3 Temperature evolution upon quadrupling of CO2 concentration

Our second test case, namely the temperature response to an instantaneous quadrupling of the atmospheric CO2 concentration (cf. section 1.3.2), allows for an evaluation and re-calibration of the temperature equations of the CE under consideration. In principle, a metric would again be needed for this purpose (see section 1.3.3). However, as CDICE (or DICE in general) and the benchmark data from Geoffroy et al. (2013) share the same functional form (cf. section 1.4.1), a re-calibration is trivial: we simply adopt the parameter values already fitted to the CMIP5 data by Geoffroy et al. (2013). Specifically,

Model	M_{INI}	T_{INI}
DICE-2016, 5yr	(851, 460, 1740)	(0.85, 0.0068)
CDICE	(851, 628, 1323)	(1.10, 0.27)
CDICE-HadGEM2-ES	(851, 628, 1323)	(1.10, 0.27)
CDICE-GISS-E2-R	(851, 628, 1323)	(1.10, 0.27)
CDICE-MESMO	(851, 403, 894)	(1.10, 0.27)
CDICE-LOVECLIM	(850, 770, 1444)	(1.10, 0.27)
CDICE-HadGEM2-ES-MESMO	(851, 403, 894)	(1.10, 0.27)
CDICE-HadGEM2-ES-LOVECLIM	(850, 770, 1444)	(1.10, 0.27)
CDICE-GISS-E2-R-MESMO	(851, 403, 894)	(1.10, 0.27)
CDICE-GISS-E2-R-LOVECLIM	(850, 770, 1444)	(1.10, 0.27)

Table 1.3 Initial conditions for the year 2015 as used in DICE-2016 and in CDICE, as well as for extreme calibrations of CDICE with respect to the carbon cycle and/or temperature. The atmospheric CO₂ concentration is always 400 ppm (851 GtC). All other values result from integrating the differently calibrated CEs from 1850 to the present day using the CMIP5 setup as described in the fourth test case.

we obtain CDICE using their fit to the multi-model mean and two extreme models, that is, CDICE-HadGEM2-ES and CDICE-GISS-E2-R. As explained above, these extreme cases play an important role in our economic analysis below (cf. sections 1.5 and 1.6). Table 1.2 summarizes the relevant coefficients for these alternative calibrations.

The test confirms previous findings that DICE-2016 warms too slowly compared to any CMIP5 model (dashed blue versus solid gray lines in Figure 1.4). All the CMIP5 models (solid gray lines) agree that warming occurs rapidly. Meanwhile, their level of warming differs by a factor of roughly two, in line with their differing ECS, given in Table 1.2. The overly slow warming in DICE-2016 finds confirmation via formal expressions for the characteristic fast and slow response time scales associated with Equations (1.4) and (1.5) (see Geoffroy et al., 2013, their Table 1), which yield numerical values of 4 and 249 years for the CMIP5 multi-model mean in Geoffroy et al. (2013), but 40 and 219 years for DICE-2016.

The test discussed here is further suited to shed some light on the role of the different parameter values in the temperature equations of CDICE, as illustrated in Figure 1.5. How quickly the temperature responds to an increase in atmospheric CO₂ is mainly governed by the heat capacity of the upper ocean via the parameter c_1 (left panel, yellow and brown dashed lines), which, in turn, does not affect the mid- and long-term absolute warming (beyond roughly 20 years, middle and right panel). As expected, the very long-

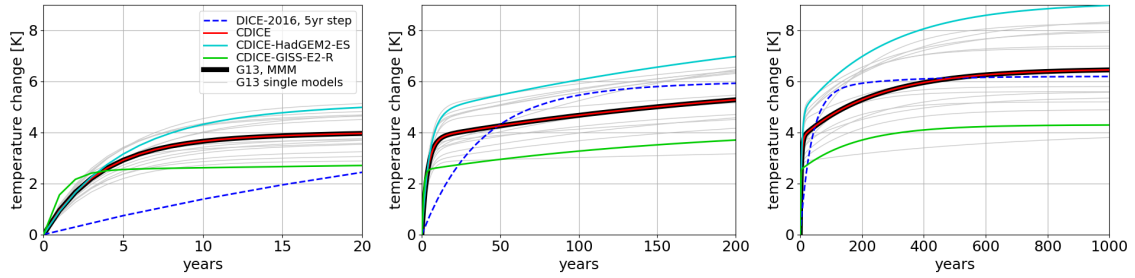


Fig. 1.4 Temperature response to instantaneous quadrupling of atmospheric CO₂ with respect to pre-industrial values on time scales of 20 years (left), 200 years (middle), and 1000 years (right). Parameters in CDICE (red solid) can be chosen such as to exactly reproduce the calibration target, the CMIP5 multi-model mean (black solid, G13-MMM). Also shown are two extreme ECS calibrations (solid green and light blue, CDICE-HadGEM2-ES and CDICE-GISS-E2-R). In DICE-2016 (dashed blue, 5 year time step), temperature increase is too slow compared to any CMIP5 model (thin gray lines, G13, from Geoffroy et al. (2013)).

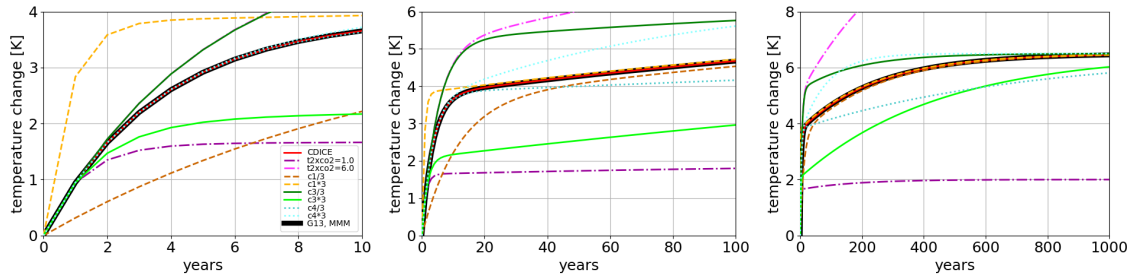


Fig. 1.5 Parameter sensitivity of the temperature equations in DICE, illustrated at the example of an instantaneous quadrupling of the CO₂ concentration with respect to pre-industrial values. Shown is warming (y-axis) as a function of time (x-axis) for different time scales (from left to right). Parameters are varied one by one with respect to the CMIP5 multi-model mean from Geoffroy et al. (2013) (black solid, G13-MMM) and its adaptation in CDICE (red solid).

term warming is set by the ECS (right panel, pink and violet dash-dotted lines). The track toward long term equilibrium across intermediate time scales and levels of warming depends on the energy exchange between the upper and lower ocean, via the choice of c_3 (solid green lines, after roughly four years), and on the heat capacity of the deep ocean, entering in the form of c_4 (cyan dotted lines, after roughly 20 years).

In summary, the test case demonstrates that the temperature equations in DICE-2016 can be re-calibrated to reach general agreement with corresponding results from CMIP5. Specific CMIP5 models or the multi-model mean as given in Geoffroy et al. (2013) can be recovered precisely by appropriate parameter choice.

1.4.4 Temperature evolution as atmospheric CO₂ increases at 1% per year

The purpose of the third test is to evaluate a CE's TCR. In contrast, the first two test cases primarily aim at calibrating a CE. The TCR is of interest as a measure of how the (model) climate responds to steadily changing conditions. From the point of view of a CE, one may also say that the TCR examines the CE's performance upon a series of perturbations; not a single one as in the tests used for calibration of the CE. Although still highly idealized, this test is thus closer to reality. Consequently, TCR is often considered a better measure to evaluate the performance of a climate model than ECS, which assumes the climate system to have equilibrated. A reasonable TCR is a necessary condition for any CE but, as we shall see, not a sufficient one.

Of the test results shown in Figure 1.6, two aspects deserve highlighting. First, all variants of DICE (shown in different color coding) are compatible with the CMIP5 data (black and gray lines). The temperature evolution of DICE-2016 (blue dashed lines) now lies within the range of CMIP5 models (solid gray lines). However, the warming is still slightly slower than the CMIP5 multi-model mean (black solid) during the first few decades. CDICE (solid red) warms slightly faster than the CMIP5 multi-model mean. Variants of CDICE with extreme ECS (green and cyan lines, see Table 1.2 for parameters) indeed bracket the individual CMIP5 models. Second, the transient warming of the models remains clearly below their ECS, even after the quadrupling of CO₂ after 140 years. The TCR of the models is between 1.3 K and 2.3 K across CMIP5 models (gray lines in Figure 1.6). Associated values for ECS are roughly 50% to 100% larger, ranging between 2.05 K and 4.55 K (see Table 1.2). Upon the quadrupling of CO₂ after 140 years, ECS still exceeds the transient temperature change by about 40% to 70%.

Contrasting the above findings with those from Sect. 1.4.3 demonstrates that the model performance is highly sensitive to the concrete test. In particular, the striking under-performance of DICE-2016 in the idealized CO₂ quadrupling test case is hardly detectable if CO₂ increases gradually at a rate of one percent per year instead. The decent performance in terms of TCR may seem to come as a relief given the ample amount of existing literature using DICE-2016. This impression is, however, deceptive, as will be further elaborated on in section 1.6.

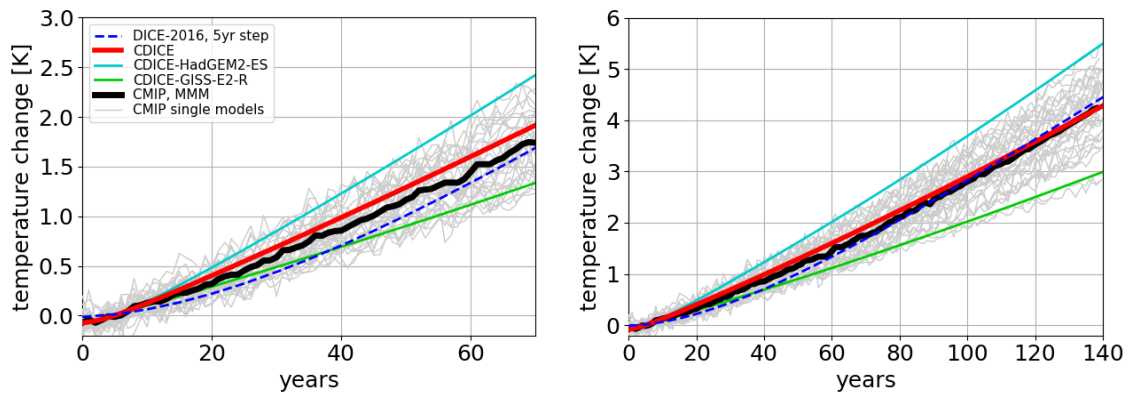


Fig. 1.6 Temperature response (y-axis) to transient, one percent per year, increase of the CO₂ concentration as a function of years (x-axis) from 1850 onward. The CO₂ concentration doubles within 70 years (left panel), and associated warming levels correspond, by definition, to the transient climate response (TCR) of the model. CO₂ quadruples within 140 years (right panel), and TCR roughly doubles. DICE-2016 (dashed blue), our new version CDICE (solid red), as well as its extreme scaling variants (solid cyan and green), are all compatible with CMIP5 models and their TCR (individual models and multi-model mean, solid gray and black, respectively).

1.4.5 CMIP5 historical and RCP evolution as simulated by DICE

Our fourth test was chosen to be as close as possible to real applications, that is, a necessary gold standard test any CE should pass: the CMIP5 simulations for historical and future representative concentration pathways (RCP26, RCP45, RCP60, and RCP85, from top to bottom in Figure 1.7). Compared to the other three tests, this test features some additional hurdles. First, the entire CE is examined, that is, the carbon cycle combined with the temperature equations. Second, strong mitigation scenarios are considered that test a CE's ability to capture a regime transition from, basically, emission-dominated to response-dominated. Third, non-CO₂ forcings must be taken into account. They form part of the CMIP5 simulations and the real world alike and thus must be incorporated and examined in the context of any CE. To facilitate the interpretation of results, we separately examine in Figure 1.7 CO₂ concentrations due to changing carbon emissions (left column, performance of carbon cycle), the temperature in response to changing CO₂ concentrations (middle column, performance of temperature equations), and finally, temperature as a function of carbon emissions (right column, performance of full CE).

The CMIP5 data (gray and black lines in Figure 1.7) provide a benchmark range: depending on the model, warming by 2100 is between 1 K and 2.5 K for RCP26 and between

3 K and over 6 K for RCP85. The range exists, although the models feed on prescribed concentrations, not emissions. A subset of CMIP5 models recomputed the RCP85 scenario based on prescribed emissions. By 2100, their CO₂ concentrations lie in a range from 800 ppm to 1150ppm, or within about 20% of the CMIP5 prescribed value of 935 ppm, and warming ranges roughly from 2.7 K to 6.5K (Figure 12.36 in the Intergovernmental Panel on Climate Change & Intergovernmental Panel on Climate Change, 2015). The episodic cooling apparent in Figure 1.7, which is due to significant volcanic eruptions such as Mt. Pinatubo in 1991, is a reminder that the temperature evolution in CMIP5 encapsulates a whole range of forcings. The decreasing CO₂ concentrations and temperatures in RCP26 are of particular interest as they allow us to benchmark the CE in the context of mitigation scenarios.

Looking at the carbon cycle (left column in Figure 1.7), we find that CO₂ concentrations modeled by the DICE family are mostly within 20% of those prescribed by CMIP5 (black dotted lines), thus within the range of emission-based CMIP5 simulations (see above). Concentrations are always highest for DICE-2016, followed by CDICE-MESMO, CDICE, and CDICE-LOVECLIM, in line with calibration (CDICE family) and evaluation (DICE-2016) against the 100 GtC pulse test (see section 1.4.2). Looking at the different scenarios, the strong mitigation scenario RCP26 has concentrations prescribed in CMIP5 (black solid) that are lower than in any model of the DICE family. The situation changes as one moves to RCP45 and RCP85, where towards the end of the century (the year 2100), concentrations in CDICE are even lower than those prescribed in CMIP5. The behavior may indicate a dependence of the carbon cycle on the scenario (strong mitigation versus continued strong emission) either on the side of the DICE model family or on the side of CMIP5. A dedicated analysis is beyond the scope of the present paper.

Turning to the temperature response to CO₂ concentrations as prescribed in CMIP5 (middle column), the curves for the different versions of CDICE echo corresponding calibrations (see section 1.4.3). In particular, CDICE (red solid) falls on top of the CMIP5 multi-model mean (black solid) independent of the RCP scenario considered. This is remarkable in several respects. The temperature equations in CDICE were calibrated against one perturbation (instantaneous quadrupling of CO₂), whereas CO₂ keeps constantly changing here. The temperature evolution is well captured even in RCP26 after 2050, when CO₂ concentrations decrease again. Finally, the data by Geoffroy et al. (2013),

used to calibrate CDICE, incorporates only a subset of CMIP5 models.²⁰ DICE-2016 (blue dashed line) features relatively high temperatures under strong mitigation (RCP26) and rather low temperatures in the strong forcing RCP85 scenario. One reason could be that the slow temperature response of DICE-2016 to an instantaneous increase in CO₂ concentrations turns into a lagging response upon gradually changing CO₂. Another reason could be the non-CO₂ forcing (see Section 1.4.1), which may be too strong in the RCP26 scenario, but too weak in the RCP85 scenario. For CDICE, the (assumed) non-CO₂ forcing (dotted orange line) contributes around 0.5 to 1-degree warming by 2100.

The performance of the entire CE (Figure 1.7, right column) encapsulates the features just described. Some combinations of the independently calibrated carbon cycle and temperature equations fall outside the range of CMIP5 models (thin gray lines). For example, CDICE-HadGEM2-ES-MESMO and CDICE-HadGEM2-ES are too warm in RCP26, whereas CDICE-GISS-E2-R-LOVECLIME tends to be on the cool side in RCP85. The relative importance of the carbon cycle and temperature response depends on the forcing scenario. Upon strong forcing, like RCP85, temperatures differ mainly because of the different ECS calibrations (cyan, red, and green curves). In contrast, the calibration of the carbon cycle plays a minor role (dotted, solid, and dash-dotted curves). For RCP26, CEs that combine high ECS with efficient removal of carbon emissions (CDICE-HadGEM2-ES-LOVECLIM, cyan dash-dotted) have a similar temperature evolution as CEs combining inefficient carbon removal with an intermediate ECS (CDICE-MESMO, red dotted). In section 1.6, we examine the degree to which this degeneracy persists within an economic context.

In summary, CDICE falls within CMIP5 models for all future scenarios. This is not the case for some variants of CDICE that combine extreme calibrations of the carbon cycle and temperature equations. DICE-2016 performs better for the strong forcing scenario RCP85 than for the strong mitigation scenario RCP26. Concrete assumptions about the non-CO₂ forcing term, notably its strength, are demonstrated to matter for global mean temperature change.

²⁰Only a subset of all CMIP5 data was available when Geoffroy et al. (2013) performed their analysis.

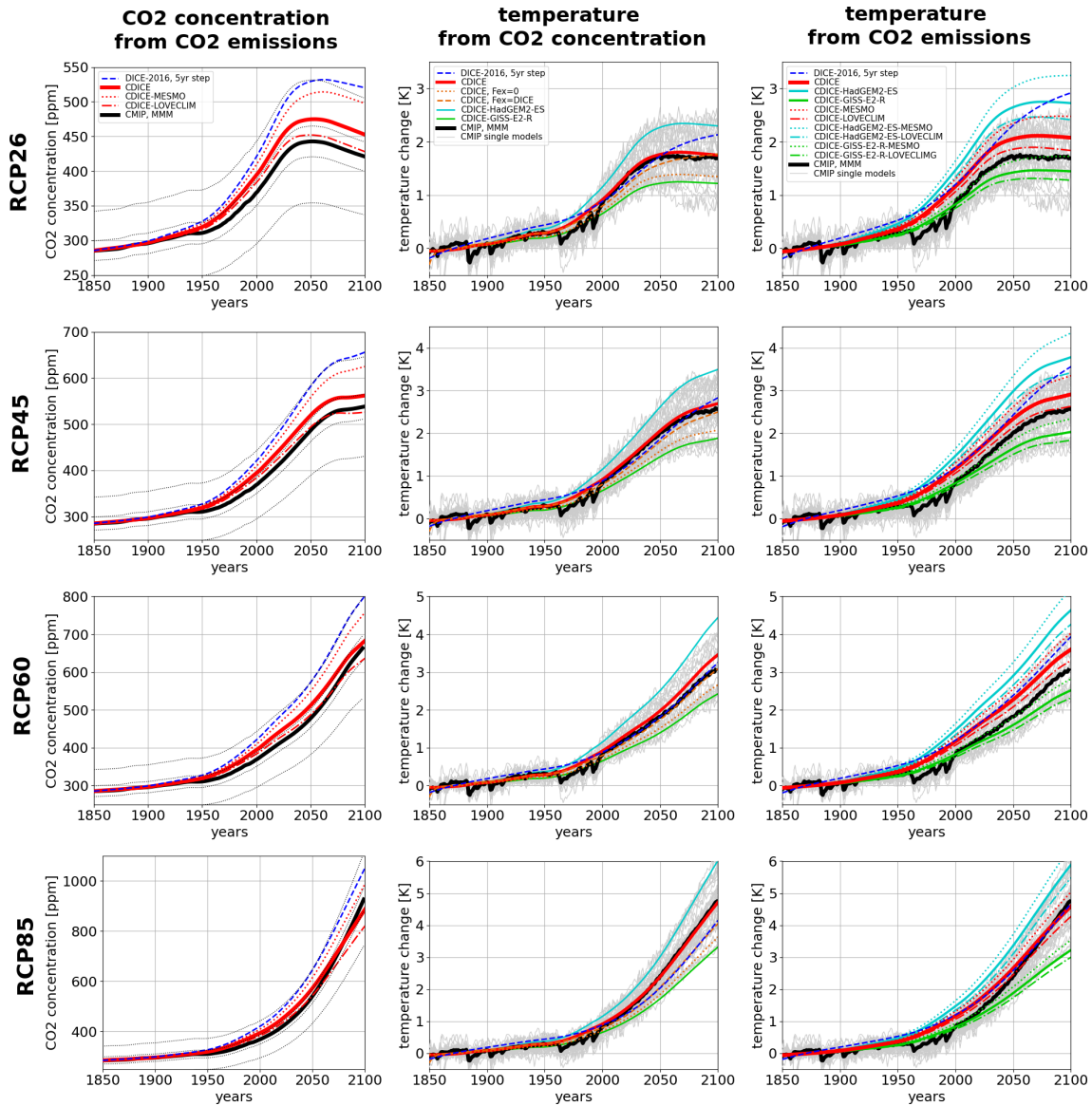


Fig. 1.7 Comparison of DICE with historical and future (years 1850 to 2100, scenarios RCP26, RCP45, RCP60, and RCP85, from top to bottom) CMIP5 data. Shown are atmospheric CO2 concentrations (left) as prescribed in CMIP5 (solid black, with dotted lines indicating $\pm 5\%$ and $\pm 20\%$ ranges) and as computed from CO2 emissions with DICE-2016 (dashed blue), CDICE (solid red), as well as CDICE-MESMO and CDICE-LOVECLIM (dotted and dash-dotted red). Also shown is temperature evolution based on prescribed CO2 concentrations (middle) and based on emissions (right) for DICE-2016, CDICE, and variants of CDICE.

1.4.6 Synthesis and lessons learned from the climate test cases

The results presented in this section show that it is important to independently calibrate the two basic building blocks of any CE, that is, the carbon cycle and the temperature equations. In this paper, we provide two corresponding, highly idealized test cases that are based on published data from CMIP5. We advocate that the calibrated CE should, subsequently, be exposed to two additional tests: one to quantify the CE's transient climate response and the other to evaluate the CE's performance for realistic future scenarios, under strong forcing as well as under strong mitigation. Associated tests are described that rely only on publicly accessible data from CMIP5. We illustrated that DICE-2016, although failing both calibration tests, passes the two additional tests, possibly due to compensating errors. Additionally, we demonstrated that the functional form of the DICE family is fit for purpose: a re-calibrated version, CDICE, passes all four tests.

The CMIP5 test cases highlight the existence of a target range for both the carbon cycle and the temperature equations. Full-fledged ESMs do not agree on global mean temperature change, even if this change is only due to prescribed gradual changes in atmospheric CO₂ concentration, as in the one percent per year CO₂ increase test case. Variants of CDICE using calibrations for the temperature response that are extreme yet in line with CMIP5 have been shown to bracket the range of CMIP5 models for all four RCPs examined. We advocate exploiting this bracketing behavior in the context of economic studies as a measure of the uncertainty arising from the climate part. The same applies with regard to the carbon cycle. We caution, however, that combining extreme calibrations for both the carbon cycle and the temperature equations may result in an overly extreme climate of the CE.

Non-CO₂ forcings have been shown to play a prominent role and, as such, constitute another source of uncertainty for any CE. Their assumed linear increase with time in DICE-2016 has the advantage of being simple. Climate literature rather advocates that non-CO₂ forcings amount to about one-third of the forcing from CO₂ (cf. section 1.3.2); the form adopted in CDICE. It is not obvious whether any of the two forms is clearly superior with regard to the envisaged applications; studying the interplay of climate, society, economy, and technology. Net-zero targets, mitigation scenarios, or scenarios presenting even more heavy use of fossil fuels may affect the mix of non-CO₂ forcing agents and associated lifetimes. A more detailed description of such developments is not desirable as it would

necessitate including non-CO₂ agents, reservoirs, and processes, thereby violating the deliberately simple approach to climate taken in DICE. Retaining a simple form, but testing for associated sensitivities, seems a more promising avenue.

Focusing again on CO₂-forcings alone, the temperature part of CDICE has been shown to perform very well with respect to any benchmark data for prescribed CO₂ concentrations. Working with carbon emissions has turned out to be more challenging. It is difficult for CDICE to reproduce both high emission and mitigation scenarios, like RCP85 and RCP26 (cf. Figure 1.7, left column) equally well. The point is relevant given that DICE should be applicable to a broad range of socio-economic scenarios, from fossil fuel dominated to mitigation and net-zero emissions. We speculate that the issue is rooted at least in part in the availability of only two time scales (of 5 and 102 years, see section 1.4.1) related to the three reservoir carbon cycle.

A reservoir-based carbon cycle model has the advantage that the total amount of carbon is preserved. In particular, carbon leaving the atmospheric reservoir is still present in another reservoir, notably the ocean, in the case of DICE. From there, it may continue to play a role for the climate system at some point in time. This capability of a reservoir-based approach is especially interesting with regard to strong mitigation scenarios, where the amount of carbon currently being stored in the (upper) ocean is likely to affect the carbon uptake capability of the ocean as emissions decline (Ridge & McKinley, 2021). For the same reason, it seems questionable whether even simpler climate models without any reservoirs - an example of such a model could be the approximately linear relationship between cumulative carbon emissions and global mean temperature - would be able to properly cope with strong mitigation scenarios.

In summary, the emission-based global mean temperature evolution from 1850 to 2100 as modeled by either DICE-2016 or CDICE lies, despite the models' simple functional form, well within the range of CMIP5 results for most RCPs. For DICE-2016, this finding is noteworthy as the model, in contrast to CDICE, clearly fails more idealized tests (instantaneous quadrupling of CO₂ and 100 GtC pulse). Moreover, it is deceiving, as compensating errors play an important role in DICE-2016. Noteworthy also is the challenge posed to either DICE-2016 or CDICE by the strong mitigation scenario RCP2.6: CDICE struggles, and DICE-2016 clearly fails and clearly warms far too much towards 2100. As

already noted by Traeger (2014), such strong mitigation scenarios excessively challenge the models' functional form.

1.5 The social cost of carbon in partial equilibrium

In standard economic models, climate change is treated as an externality, and, going back all the way to the work of Pigou (1920), it is well known that Pareto efficiency can be restored by adding the marginal value of the externality to the market price of carbon. To reach this goal, IAMs compute the net present value of all future damages caused by the emission of an additional unit of carbon at some date t . The effect of these extra emissions on damages depends on the calibration of the damage function and the path of emissions. Computing the net present value of the damages requires knowledge of all future interest rates. A change in the market price of carbon will change the path of emissions and of interest rates. Consequently, one has to impose an economic model with many assumptions to obtain an accurate estimate of the SCC. However, one can gain important insights by examining the future path of damages caused by a pulse of emissions for a given RCP emissions scenario. One can then assume constant interest and growth rates and make general statements about the SCC. As we will show in section 1.5.1 below, in the BAU case of the DICE-2016 model, the effects of the climate model on emissions and the interest rates are indeed tiny (of course, the effects on optimal abatement and mitigated emissions are very large). The social cost of carbon is defined for each date t . As it turns out, if one assumes constant interest rates, the SCC relative to output is relatively constant across the next 50 years, and we, therefore, focus on the somewhat arbitrary date 2020 for reporting the SCC in this section.

In this, and the subsequent section 1.6, we assume that exogenous forcing, F_t^{EX} , changes linearly with time from 0.5 in the year 2015 to 1.0 in 2100, that is, as specified in DICE-2016 (cf. equation (1.6)). This measure allows us to compare the impact of our CDICE calibration with DICE-2016 consistently. However, to be fully in line with state-of-the-art climate science, it might be better to assume $F_t^{\text{EX}} = 0.3 \cdot F_t^{\text{CO2}}$ (see, e.g., Climate Change 2014 Synthesis Report IPCC, 2014; Gambhir et al., 2017). In the online Appendix 1.C, we show how such change in the full model affects our quantitative results.

Following the majority of the economic literature on climate change, we assume that the temperature influences the economic activity via a damage function $\Omega(\cdot)$ that multi-

plies total output $Y_t^{\text{Gross}}(\cdot)$ at time t . Given a constant interest rate r , and a constant growth rate of output, g , the present value of damages at some future date t is given by $\left(\frac{1+g}{1+r}\right)^t \Omega(T_{AT,t})$. In this section, we take $\frac{1+r}{1+g}$ as given, and refer to it simply as the “g-adjusted interest rate”. Note that output growth can come from population growth as well as total factor productivity (TFP) growth, and it is likely not to be constant over the next 300 years. Real risk-free rates and returns to capital certainly vary over the business cycle, but also might change in the long term (see, e.g., Bauer and Rudebusch (2021)).

The damage functions used in DICE-2016, but also in Hänsel et al. (2020) and Howard and Sterner (2017) among others, all assume the following quadratic functional form:

$$\Omega(T_{AT,t}) = \psi_2 \cdot (T_{AT,t})^2. \quad (1.7)$$

Since, in this section, we only consider the SCC relative to the CDICE calibration (both the temperature equations as well as the carbon cycle calibrated to the MMM), the value of the parameter ψ_2 is irrelevant. Of course, ψ_2 matters for the absolute value of the SCC and for optimal abatement, but not for ratios of the SCC for different calibrations. However, as we show, the functional form is very important, and higher-order terms (as, for instance, discussed in Weitzman (2012a)) can make a significant difference in the effect of climate model uncertainty on the SCC.

1.5.1 Different climate calibrations and the SCC

Figure 1.8 displays the SCC under two different RCP emission scenarios, that is, RCP8.5 with very high emissions and RCP2.6 with very low emissions, and four different calibrations of our CE. In all the cases in the Figure, the social cost of carbon is relative to the CDICE MMM social cost of carbon for RCP2.6. We consider the MMM for both the temperature equations and the carbon cycle (denoted by CDICE). Furthermore, we also look at HadGEM2-ES and GISS-E2-R as alternative temperature calibrations, as well as MESMO as an alternative carbon-cycle calibration. As we vary the growth-adjusted interest rate from 0.5 percent to 4 percent, the SCC for the RCP 2.6 scenario with the basic CDICE model (both temperature equation and carbon cycle calibrated to the MMM) is always normalized to one. All models considered in this Figure are a calibration of CDICE; for simplicity, the term CDICE is often omitted in the legends in Figures 1.8 and 1.9.

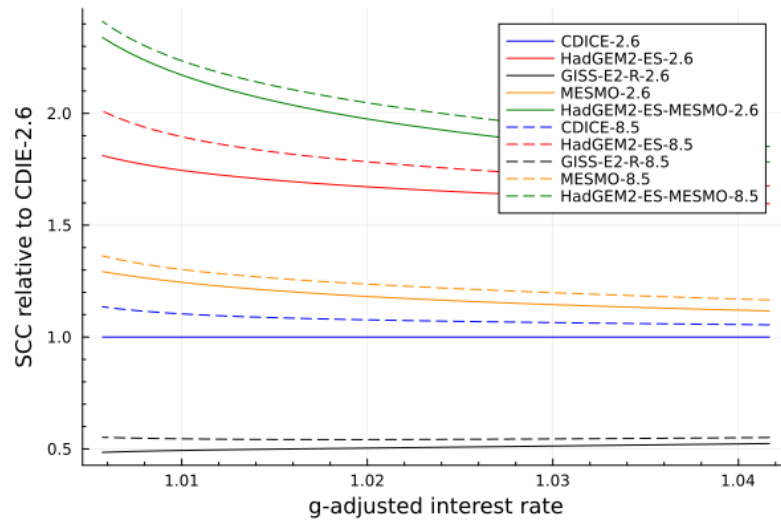


Fig. 1.8 SCC for different CDICE calibrations, emission scenarios, and a quadratic damage function.

There are four key takeaways from this stylized exercise. First, model uncertainty for the temperature equation can lead to three to five times higher SCC for very pessimistic scenarios as opposed to the most optimistic scenario. Second, the effect of an extreme carbon cycle is much smaller compared to the temperature block (it increases the SCC by about 20 percent relative to the MMM), but the combined effect of a pessimistic carbon cycle and a pessimistic temperature scenario can be very large. Third, the relative uncertainty introduced by climate model uncertainty does not change very much with discounting, at least for g-adjusted interest rates above 2 percent. Fourth, the SCC does not change very much with an alternative to the emissions scenario. It is uniformly higher when the emissions are very large, but relative to the effect of the climate model uncertainty and the discount factor, the changes are small.

It is important to note that the last two observations depend crucially on the assumption that damages are quadratic (cf. equation (1.7)). Typically, for any strictly convex cost function, one would expect that marginal costs increase in quantity and that, therefore, the SCC is substantially higher for RCP8.5 than for RCP2.6. However, the marginal costs of emissions also include the non-linear effects of emissions on the temperature. The concavity in the forcing equation (1.6) counters the convexity of damages, and thus, the overall shape of the cost function is an unknown a priori.

This point is further illustrated in Figure 1.9, where we show the analog of Figure 1.8 for a linear damage function (left panel) as well as a cubic damage function of the form $\Omega(T_{AT,t}) = \psi_3 \cdot (T_{AT,t})^3$ (right panel).

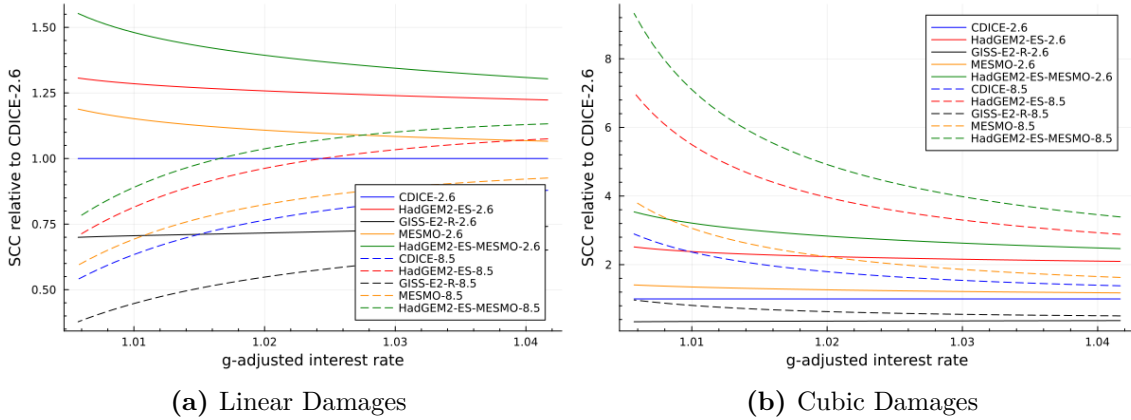


Fig. 1.9 SCC for alternative damage functions.

For linear damages, the marginal costs decrease in emissions. For high-emission scenarios, the SCC is lower than for low-emission scenarios. The overall effect of climate model uncertainty is significantly smaller than in the quadratic cost case. For the cubic damages, on the other hand, marginal costs clearly increase. For high-emission scenarios, the SCC is much higher. The effect of model uncertainty, in this case, is huge. Depending on the assumed interest rate, the SCC for the most pessimistic climate scenario can be almost eight times the SCC for the most optimistic scenario.

1.5.2 The effect of miscalibration

How important are the exact details of our calibration for the SCC? What happens, for instance, if, instead of using the CDICE-HadGem2-ES calibration, we just change the ECS-parameter in Equation (1.4) to 2.15 or to 4.55 without changing any other parameters? How does the SCC for the original DICE-2016 calibration differ from the SCC in our calibration? Figure 1.10 shows how the SCC changes with various calibrations of the CE. We focus here on the RCP 8.5 scenario with quadratic damages and compute the SCC at $t=5$ (the year 2020) relative to the CDICE calibration.

Figure 1.10 shows the SCC for CDICE-HadGEM2-ES and CDICE-GISS-E2-R as alternative temperature calibrations and compares them to simply setting the ECS to the associated values (4.55 in CDICE-HadGEM2-ES and 2.15 in CDICE-GISS-E2-R), but

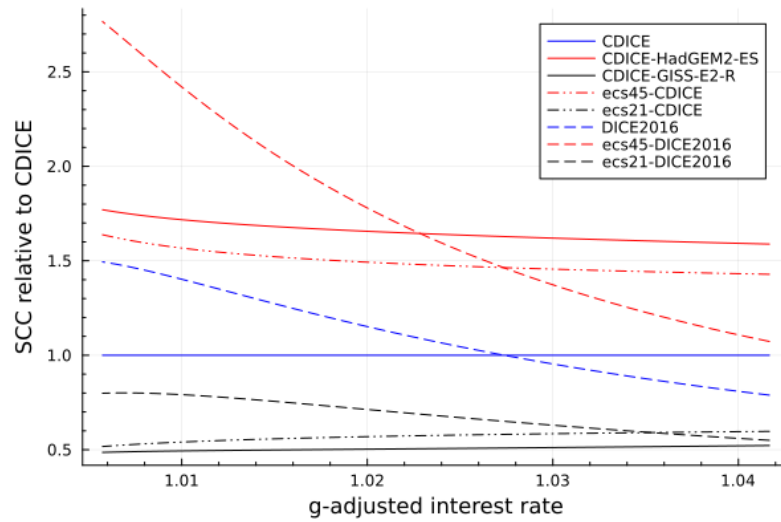


Fig. 1.10 SCC for different calibrations. RCP8.5 and quadratic damage function.

leaving the CDICE calibration unchanged otherwise (cf. the dot-dashed lines labeled 'ecs45-CDICE' and 'ecs21-CDICE'). This is how uncertainty about the ECS is typically treated in economic models of climate change (see, e.g., W. Nordhaus (2018) or Hassler and Krusell (2018)). We observe that even within the CDICE calibration, just changing the ECS is not a very good proxy for the extreme warming scenarios in CMIP5. In particular, the SCC for an ECS of 2.15 is about 15 percent too large relative to GISS-E2-R, and the SCC for an ECS of 4.55 is about 10 percent too small relative to CDICE-HadGEM2-ES. This indicates that for a quantitative treatment of climate model uncertainty, it is not sufficient to simply vary the ECS parameter in the CE. As explained above, the ECS is not a free parameter in Earth System models, but emerges as one characteristic of simulated climate change describing the very long-run behavior of temperature. For the social cost of carbon, this very long run is largely irrelevant, and the speed of warming is often more important. Modeling the climate uncertainty by simply varying the ECS parameters in the climate emulator incorrectly reduces the uncertainty about the SCC by a significant amount.

Figure 1.10 also shows the ECS for the DICE-2016 calibration, the MMM, as well as calibrations with an ECS of 2.15 and with 4.55. The differences with respect to CDICE are apparent: For intermediate values of the discount factor (say 0.97 or so), the SCC for CDICE and DICE-2016 are very similar, both for the MMM and for the calibrations with ECS of 2.15 and 4.55, respectively. In the case of a discount factor of 0.96, DICE-2016

underestimates the SCC substantially and is about 20 percent lower than for CDICE. For high values of this parameter, DICE-2016 produces much higher values for the SCC, for a value of 0.99, about 30 percent larger than CDICE.

1.6 The social cost of carbon and optimal abatement in the DICE economy

In this section, we present the optimal solutions for the adjusted DICE-2016 model, which features both the calibration of the economic part as presented in DICE-2016 (W. Nordhaus, 2018) merged with the re-calibrated CDICE climate part (cf. section 1.4). We will, in the following, also refer to this complete IAM as CDICE. A comprehensive summary of the complete calibration of CDICE is available in the online Appendix 1.B. We will refer to the original calibration of the DICE model as DICE-2016.²¹

The key non-climate part of the DICE-2016 model consists of a single, infinitely lived, representative consumer and a single firm. As it is standard in economics the equilibrium allocation can be described as the solution to a planner's problem (see, e.g., Golosov et al. (2014) for more details, and L. Kotlikoff et al. (2021a) for a critique of this approach). The planner / representative agent maximizes a time-separable utility function over (per capita) consumption $(\frac{C_t}{L_t})_{t=0}^{\infty}$ with a constant intertemporal elasticity of substitution (IES), $\psi > 0$, and a time preference parameter, $0 < \beta < 1$.²² The optimal value, V_0 is given by the following expression:

$$V_0 = \max_{\{C_t, \mu_t\}_{t=0}^{\infty}} \sum_{t=0}^{\infty} \beta^t \frac{\left(\frac{C_t}{L_t}\right)^{1-1/\psi} - 1}{1 - 1/\psi} L_t \quad (1.8)$$

$$\text{s.t. } K_{t+1} = (1 - \Theta(\mu_t) - \Omega(T_{AT,t})) K_t^\alpha (A_t L_t)^{1-\alpha} + (1 - \delta)K_t - C_t \quad (1.9)$$

$$\text{Eq. (1.1), Eq. (1.4), Eq. (1.5)}$$

$$0 \leq K_{t+1} \quad (1.10)$$

$$0 \leq \mu_t \leq 1 \quad (1.11)$$

$$\text{where } E_t = \sigma_t Y_t^{\text{Gross}} (1 - \mu_t) + E_t^{\text{Land}}. \quad (1.12)$$

²¹Note that the calibration for the original DICE-2016 stems from the publicly available GAMS code specification. For details, see <http://www.econ.yale.edu/~nordhaus/homepage/homepage/DICE2016R-091916ap.gms>.

²²In the online Appendix 1.B, we list all exogenous variables, equations, and parameters of DICE-2016 and CDICE.

The CO2 emissions, denoted by E_t , consist of non-industrial emissions, E_t^{Land} , as well as industrial emissions that are modeled as a fraction of output, $\sigma_t Y_t^{\text{Gross}}$, with σ_t being emission intensity and $\mu_t \geq 0$ being mitigation. Output is produced in a Cobb-Douglas technology with capital, K_t , and labor, L_t . Mitigation is costly and decreases output at a rate $\Theta(\mu_t)$. Higher temperatures decrease output at a damage $\Omega(T_t^{\text{AT}})$. For a detailed specification and parametrization of all the equations including exogenous variables and damages, please refer to the online Appendix 1.B.

First, the planner solves the maximization problem stated above without understanding that higher mitigation μ_t leads to lower damages from a temperature increase. In the BAU scenario, she only chooses an investment path, and mitigation is set to zero. Then, she solves the problem optimally by choosing mitigation as well as an investment path. In both cases, the SCC is the marginal cost of atmospheric carbon in terms of the numeraire good. Following the literature (see, e.g., Traeger (2014) and Cai and Lontzek (2019)), we can write the SCC as the planner's marginal rate of substitution between the atmospheric carbon concentration and the capital stock. Thus, we have:²³

$$SCC_t = -\frac{\partial V_t / \partial M_{\text{AT},t}}{\partial V_t / \partial K_t}. \quad (1.13)$$

The optimal carbon tax (CT_t) is the tax that equates the private and the social cost of carbon. W. Nordhaus (2018), among others, defines the optimal carbon tax as a function of mitigation μ_t . The social planner chooses the mitigation μ_t , which is equivalent to choosing the carbon tax in units [USD/tC]²⁴, that is,

$$CT_t = \frac{\theta_{1,t} \theta_2 \mu_t^{\theta_2 - 1}}{\sigma_t}, \quad (1.14)$$

where $\theta_{1,t}$ is the abatement cost, and σ_t is emission intensity.²⁵ By definition, the SCC is equal to the optimal carbon tax if $\mu_t < 1$.

²³We mention here for the sake of accuracy that in DICE-2016, the cost of backstop is given in 2010 thousand USD per ton of CO2 in 2015, whereas the mass of carbon in the atmosphere is measured in tons of carbon. Thus to make the social cost of carbon formula numerically correct with respect to units of measurement, one needs to adjust it by a factor of 3.66, which is a conversion rate between carbon and CO2. The SCC is measured in 2010-US dollars per ton of carbon.

²⁴One needs to multiply the carbon intensity σ_t in the denominator by 1000 because we define the carbon intensity in the units of 1000 GtC.

²⁵A detailed description of all parameters and exogenous parameters of the model can be found in the online Appendix 1.B.

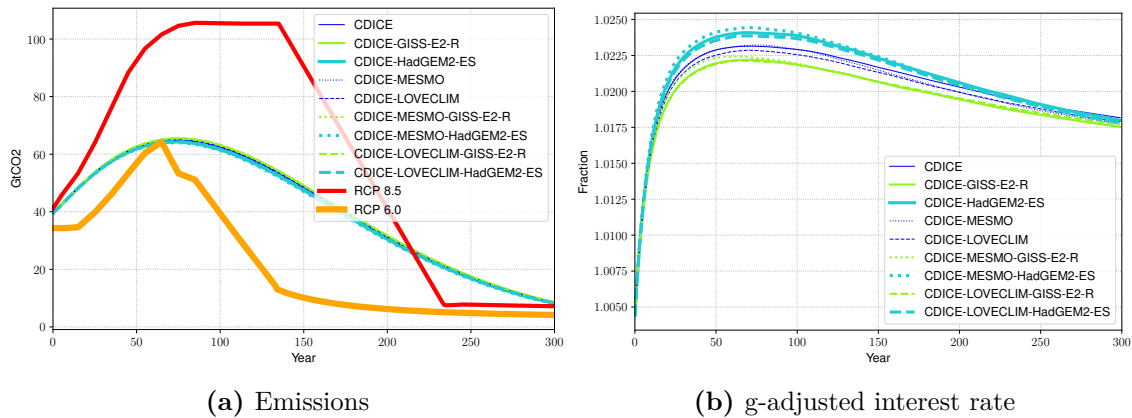


Fig. 1.11 BAU emissions (left panel) as well as growth adjusted interest rate (right panel) for different climate calibrations. Year zero on the graph corresponds to the starting year 2015.

In the following, we first consider the CDICE model under different CMIP5 calibrations for the carbon cycle and the temperature equation. This is to illustrate that different reasonable calibrations for the CE can have large effects on the optimal abatement. Second, we compare CDICE to DICE-2016 to show some economic consequences of the incorrect calibration in DICE-2016. We do so in two steps. First, we compare the predictions of the two calibrations with the exact economic calibration from DICE-2016. Second, we also investigate the effects of differences in the IES-parameter ψ , which can have large effects on future g-adjusted interest rates.

1.6.1 CDICE - Economic consequences of climate model uncertainty

We consider the economic model of DICE-2016 combined with our nine different reasonable calibrations for carbon-cycle and temperature equations. We explore the economic consequences of the large uncertainty in our climate model.²⁶

We take as a starting date ($t=0$) the year 2015. In addition, the initial conditions are listed in Table 1.3.

We start our analysis by examining the predictions of the model in a scenario without mitigation. The first observation is that in this framework, the emissions are not sensitive to the climate calibration used. Figure 1.11a shows the path of emissions for our nine

²⁶All results we report in the following were obtained by using “Deep Equilibrium Nets” by Azinovic, Gaegauf, and Scheidegger (2022), a method for computing global solutions to high-dimensional dynamic economic models. Additional implementation details, as well as the level of accuracy for our computations, are provided in the online Appendix 1.D.

versions of CDICE and compares it to the emissions in RCP 8.5 and RCP 6. The assumed climate parameters have an effect on BAU emissions via differences in damages (higher temperatures imply higher damages that, in turn, imply less carbon emissions in this model), but the effect is quantitatively insignificant. One reason for this behavior is that the damages only become large once emissions have started to decline substantially. The fraction by which emissions are reduced by these damages might be significant, but the absolute value of the reduction is small. Figure 1.11a also shows that the emissions from DICE-16 lie somewhere between RCP6 and RCP8.5. The lessons from our detailed analysis of these emission scenarios above should also carry over to the DICE-2016 BAU emissions.

Figure 1.11b shows that the path of the growth-adjusted interest rate is also more or less the same across different climate calibrations. There is some variation that can be explained by differences in future damages that translate into differences in the interest rate. Higher expected future damages imply a lower capital stock and a (slightly) higher interest rate today. The variation over time, which is much more substantial, is mostly explained by the assumption in DICE-2016 that TFP growth, as well as population growth, flattens over time. The DICE-2016 calibration starts with an initial population growth of 1.4 percent and an initial TFP growth of 2.25 percent, with population growth declining fast over the next 50-100 years and TFP growth declining substantially slower. The way the time-varying growth rates translate into the time-varying interest rate depends crucially on the preferences of the representative agent. We will return to this issue in section 1.6.3 below. Note for now that the initial g-adjusted interest rate is close to zero, whereas after 50 years, it is around 2 percent, and then finally converges to 1.5 percent in the very long run.

Figure 1.12 shows the effect of different climate calibrations on damages as a percentage of GDP and the SCC as a percentage of GDP. As is to be expected from our discussions in section 1.5.1 above, our three different calibrations for the carbon cycle imply three vastly different predictions for CO₂ concentrations. Across different temperature equations, for a fixed carbon cycle, this then results in 9 vastly different paths for temperature. As already pointed out in section 1.5.1 above, the effects of the carbon cycle calibration on temperatures and damages are not nearly as large as the effect of the calibrations of the temperature equation, and the combination of an extreme carbon cycle and an extreme temperature equations yields extreme damages. This is true both

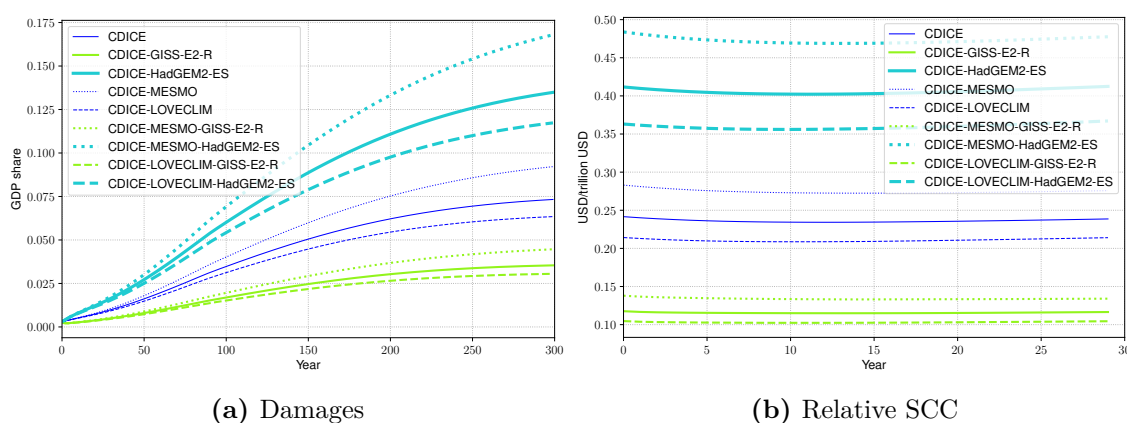


Fig. 1.12 This figure shows the evolution damages (left panel) and the relative SCC (right panel) over time for nine CDICE-calibrations in the business as usual case. Year zero on the graph corresponds to the starting year 2015.

for CDICE-MESMO-HadGEM2-ES as well as for CDICE-LOVECLIM-GISS-E2-R. The range of plausible damages in 300 years goes from around three percent of GDP to over 17.5 percent of GDP; almost a factor of six. As expected this has a very large effect on optimal abatement. The relative SCC depicted over the next 50 years in Figure 1.12b is fully consistent with our results in section 1.5.1 above. In this section, we discussed only the SCC at a fixed date $t = 5$, whereas we examine it here over the next 30 periods. The SCC initially falls over time, and this effect is caused by the stark rise in the g-adjusted interest rate discussed above. After that, it stays relatively flat, and the relative SCC between the different temperature calibrations is similar to that described in section 1.5.1 above.

The large differences in damages and the SCC across calibrations imply large differences in the optimal solution. We now assume that the social planner optimally chooses mitigation, μ_t , in the optimization-problem (1.8). Figure 1.13a shows the optimal abatement choices for the nine different climate calibrations. Differences in the social cost of carbon translate mechanically into differences in optimal abatement via Equation (1.14) above. Since the exogenous parameters in (1.14) are time-varying, optimal mitigation is time-varying. The differences in optimal mitigation between the different climate calibrations are huge over the next 80 years; about a factor of three. By definition, differences in abatement lead to differences in emissions. Figure 1.13b shows BAU emissions for our 9 cases compared to the emission scenarios in RCP 2.6 and in RCP 4.5. It is interesting to note that in all cases, optimal emissions remain far above RCP 2.6 emissions. This is a

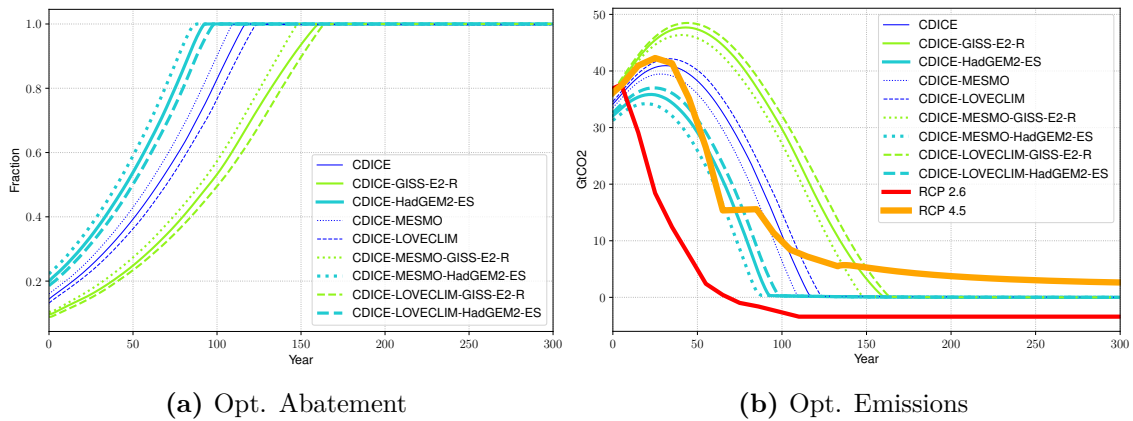


Fig. 1.13 This figure shows optimal abatement (left panel) and emissions (right panel) over time. Year zero on the graph corresponds to the starting year 2015.

consequence of the specification of the damage function in DICE-2016, which we use here, and the fact that the model does not allow for carbon removal, which becomes an active part of future policy in RCP 2.6. Emissions in the MMM case closely mirror optimal emissions in RCP 4.5.

The fact that optimal emissions stay far above RCP2.6, which is the strong-mitigation scenario from IPCC, readily implies that the optimal temperature rises far above the Paris limit. Figure 1.14a shows that in the MMM calibration, temperature rises (relative to preindustrial levels) by 3 degrees Kelvin and stays at that level for hundreds of years. In our most pessimistic climate calibration, the optimal temperature rises by over 4 degrees. As pointed out before, this depends crucially on the choice of the damage function, which we take directly from DICE-2016 for comparison purposes. As W. D. Nordhaus (2008) points out, “*the economic impact of climate change ... is the thorniest issue in climate-change economics*”. See Hänsel et al. (2020) or Carleton et al. (2020) for more realistic treatments of damages.

Naturally, the choice of the damage function leads to relatively low SCC in levels. Figure 1.14b depicts the social cost of carbon in dollars over the next 50 years. Note that it increases only because of GDP growth. The relative SCC is almost identical to that in the BAU case depicted in Figure 1.12b above. Recall that the optimal tax on carbon is equal to the SCC. Thus, the model’s optimal tax lies, for the MMM case, slightly below what is typically discussed for economic policy purposes.

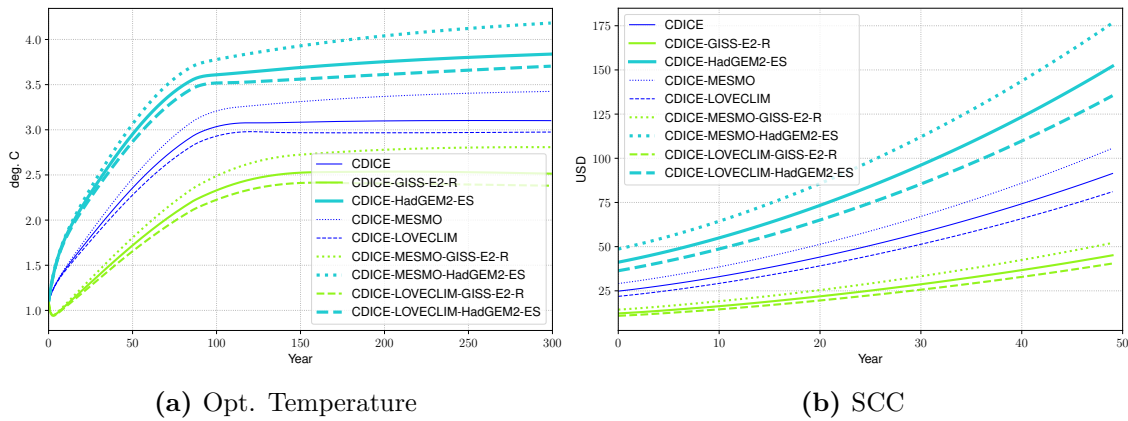
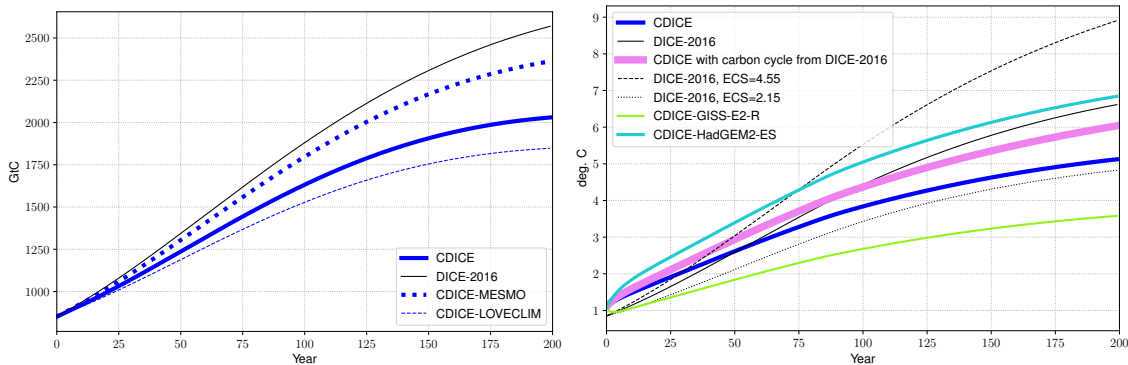


Fig. 1.14 Evolution of temperature (left panel) and SCC (right panel) with optimal abatement. Year zero on the graph corresponds to the starting year 2015.



(a) Mass of carbon in the atmosphere, BAU case **(b)** Temperature of the atmosphere, BAU case

Fig. 1.15 Mass of carbon (left panel) and atmospheric temperature (right panel) for the CDICE and DICE-2016 calibrations. Year zero on the graph corresponds to the starting year 2015.

1.6.2 The economic consequences of miscalibrated climate

As pointed out above, the calibration of the climate part of DICE-2016 has two serious flaws. Both the temperature equations and the carbon cycle are miscalibrated. As mentioned in Section 1.4.2, the carbon cycle in DICE-2016 overstates the fraction of CO₂ emissions that end up in the atmosphere relative to the MMM in Joos et al. (2013) and the extreme CDICE-MESMO case. We can confirm this by inspecting the BAU results. Compared to all three carbon calibrations in CDICE, DICE-2016 predicts way too much carbon in the atmosphere (cf. Figure 1.15a). In fact, the amount of carbon in the atmosphere is larger than for the CDICE-MESMO calibration (which corresponds to the extreme case in (Joos et al., 2013)) at any point in time.

The effect is less pronounced if one considers the overall temperature response. In addition to a mistake in the carbon cycle, the DICE-2016 calibration also makes a mistake in the temperature equation. As Figure 1.15b illustrates, in the short run (for the first 50 years or so), CDICE predicts more warming than the DICE-2016, despite the fact that there is far less CO₂ in the atmosphere. Even for an ECS of 4.5, DICE-2016 initially warms slower than the CDICE MMM calibration. The combined effect of temperature- and carbon-cycle miscalibration is crucial here; if one takes the CDICE MMM temperature equations together with the DICE-2016 carbon cycle, the temperature evolution is comparable to DICE-2016. The most notable difference is the initially overly slow warming in the DICE-2016 temperature equations.

Note that in the very long run, the dynamic system, defined by equations (1.1), (1.4) and (1.5), that governs climate in our simple model will converge to a new steady-state after all emissions are zero. In this steady-state, relative masses of carbon are given by the vector $M_{EQ} / \sum_{l=1}^3 M_{EQ,l}$ and it can be easily seen that the fraction of emitted CO₂ that remains in the atmosphere is about 0.26 for our CDICE calibration and about 0.22 for DICE-2016. The long-run effect on temperature is determined by the ECS, which is chosen to be 3.25 in CDICE and 3.1 in DICE-2016. Overall, the very long-run behavior of the two calibrations will be similar, with more warming in CDICE than in DICE-2016. Nevertheless, the miscalibration in DICE-2016 implies a consistently higher mass of carbon in the atmosphere over the next 500 years and a higher temperature after about 100 years. The important lesson is that parameters that determine the very long run of the climate system are more or less irrelevant to temperature over the next 300 years and, therefore, for the SCC that determines optimal policy today.

So far, we are repeating statements that we already made in section 1.4 above. The crucial question is what the implications of this miscalibration are for the optimal policy. Figure 1.16a depicts the optimal levels of abatement for the different calibrations. Abatement is presented as a share of industrial emissions that are mitigated. Hence, its numerical values are bound to the interval $[0, 1]$, where 0 corresponds to the absence of any abatement, whereas 1 implies using the full mitigation capacities. The figure shows that the DICE-2016 calibrations imply a little more optimal abatement than the respective CDICE calibrations. The differences are so small because initial warming lies below the CDICE case and, with discounting, this is important for abatement over the next

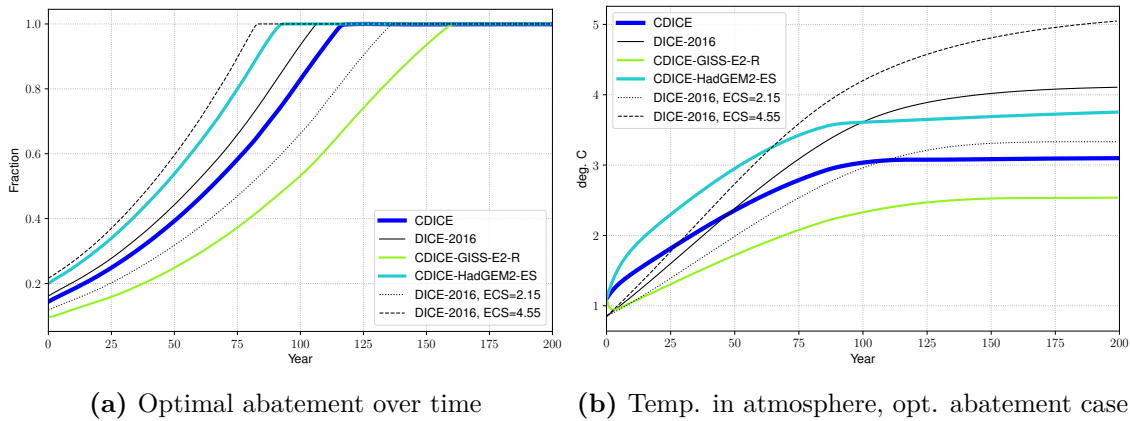


Fig. 1.16 Optimal abatement in CDICE and DICE-2016. Year zero on the graph corresponds to the starting year 2015.

decade. This finding again highlights the relevance of both parts of the climate model, of the carbon cycle and the temperature response, and of caution against the potential for compensating errors.

From this figure, one might be tempted to argue that for policy recommendations it does not make much of a difference whether one uses the CDICE calibration or the DICE-2016 calibration. However, it makes a large difference for optimal temperature as Figure 1.16b demonstrates. The DICE-2016 (with the ECS of 3.1) atmospheric temperature is now outside of the CMIP5 range. It can be seen that after about 90 years, the black line (corresponding to DICE-2016) crosses the predicted temperature under the optimal mitigation in DICE-2016, and it is above the temperature predicted by the extreme climate sensitivity scenario CDICE-HadGEM2-ES. In the BAU scenario, DICE-2016 falls well within the CMIP5 range, whereas in the economic model with mitigation, this is no longer the case. This issue arises because, in the BAU scenario, DICE-2016 is ‘helped’ by offsetting errors in the climate equations and the carbon cycle. In the case of optimal mitigation, the flaw in the carbon cycle dominates and leads to so little mitigation that the temperature rises by more than 4 degrees. This is already implicit in the BAU SCC. Despite the fact that DICE-2016 leads to much larger damages and much higher temperatures than CDICE, the SCC is almost identical. This implies (to first order) the same optimal carbon tax for CDICE and DICE-2016, resulting in far higher temperatures in DICE-2016.

Although long-run temperatures differ so much, the reason why abatement and the SCC are comparable between CDICE and DICE-2016 is simply that these temperature

differences only become significant in 75 years and, as shown in Figure 1.11b, the g-adjusted interest rate is relatively high at that point in time. The damages that occur are heavily discounted. If one takes a different perspective and, instead of maximizing the utility of a social planner, restricts long-run warming to lie below 2 degrees Kelvin, the differences between the two climate-model calibrations become starker. In fact, for the DICE-2016 calibration, it is impossible to keep the temperature below 2 degrees. Full abatement that reduces industrial emissions to zero does not suffice to keep global warming below 2 degrees. This is very different in CDICE, where putting an immediate stop to industrial emissions will keep warming below 1.7 degrees. Somewhat more realistically, if one considers the RCP 2.6 emissions profile (that includes carbon removal), DICE-2016 warms by more than 2.5 degrees (as can already be seen in Figure 1.7 above) and stays above 2.3 degrees beyond 2300 while CDICE warms by 2.1 degrees, but warming is below 1.8 degrees by 2300.

Clearly, discounting is crucial for the small differences in abatement between the two calibrations. The interest rate is endogenous, as it depends on consumption growth, but also on the preferences of the representative agent.

1.6.3 The role of discounting

There is a large literature (see, e.g., Hänsel and Quaas (2018); N. H. Stern (2007)) about the “right” discount rate for the social planner, that is, about the correct value of the parameter $\beta = \frac{1}{1+\rho}$ in the planner’s utility function. It is sometimes argued that this parameter can be pinned down by the observed average rates of return to capital (or interest rates). In a growth economy, this is not quite correct as the curvature of the planner’s felicity function, ψ , and the time preference β are not jointly identified from average interest rates. The fact that in DICE-2016, the SCC is so sensitive to the growth-adjusted interest rate (documented in section 1.5 above) implies that changing these two preference parameters simultaneously while keeping average interest rates fixed has large effects on the SCC and on optimal abatement in the DICE-2016 calibration. For simplicity, we take the baseline per-capita consumption growth rate to be 2 percent, which gives an interest rate of 4 percent in the DICE-2016 calibration (the long-run average growth rate in DICE-2016 is assumed to be zero, so we pick the 2 percent somewhat arbitrary to be consistent with the historical average and common long-run assumptions).

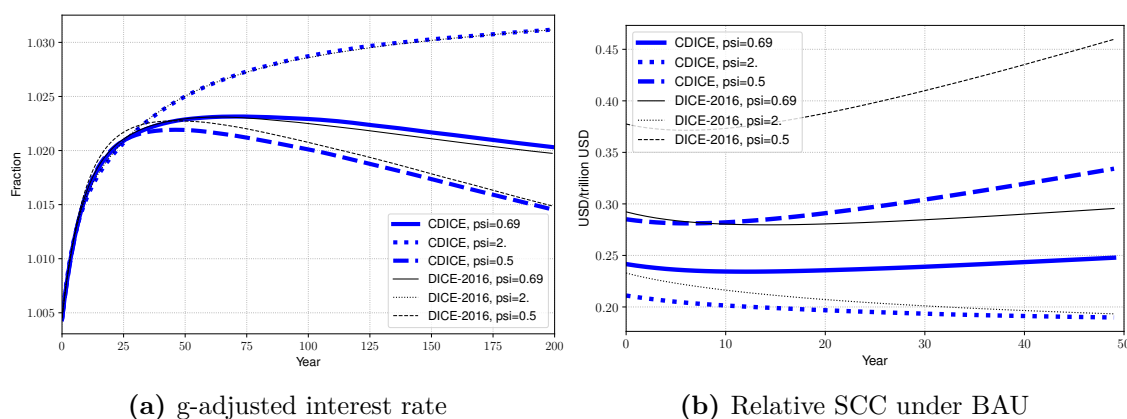


Fig. 1.17 Interest rate (left panel) and SCC (right panel) under different values for ψ . Year zero on the graph corresponds to the starting year 2015.

Figure 1.17a shows the paths of growth adjusted interest rate for different values of the IES, ψ , in the business as usual case. G-adjusted interest rates are quite similar for the first 40 years, but there is significant divergence in the long run. After 200 years the difference in g-adjusted interest rates between $\psi = 0.5$ and $\psi = 2$ is almost a factor of 2. As Figure 1.17b shows, this naturally translates into a large difference in the social cost of carbon across different specifications of the IES. The figure shows the SCC relative to output. The absolute SCC increases over time in all cases because of output growth. Because of the incorrect timing in the climate calibration of DICE-2016, the effect of the parameter ψ on interest rates is amplified, and the differences in the SCC between low and high ψ are larger than 50 percent. While a value of $\psi = 2$ might be considered an unrealistically high value of the IES, $\psi = 0.5$ is certainly well within the range of the IES which is typically assumed.²⁷

For the $\psi = 0.5$ case, the relative social cost of carbon initially decreases slightly and then strongly increases over time. This is obviously caused by the fact that g-adjusted interest rates decrease over time. In contrast, for a high value of the IES, $\psi = 2$, g-adjusted interest rates start decreasing significantly in about 40 years, leading to decreases in the SCC over time.

These differences in the BAU SCC obviously imply large differences in optimal policies. Figure 1.18 shows optimal abatement for the three values of ψ , comparing the DICE-2016 calibration to CDICE. The three panels in the figure show different ECS calibrations for

²⁷There are large differences in the IES typically assumed in the macro-literature (one or larger) to those typically found in household studies. There it is found that the IES varies significantly across households, ranging from 0.3 to 1. See, e.g., Calvet, Campbell, Gomes, and Sodini (2021).

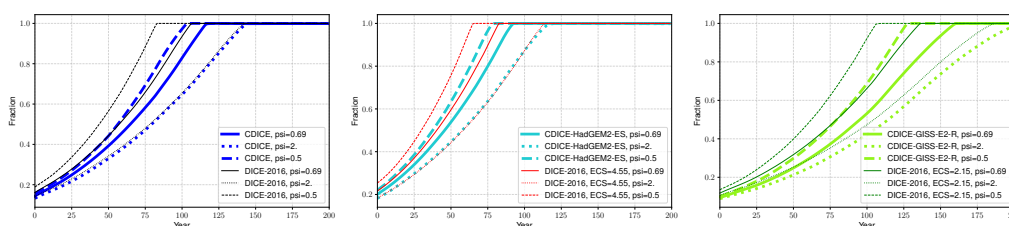


Fig. 1.18 Optimal abatement for different values of ψ and different climate calibrations. The left panel shows results for MMM, the middle panel for high ECS calibrations and the right panel for low ECS calibrations. Year zero on the graph corresponds to the starting year 2015.

DICE-2016 and HadGEM2-ES and GISS-E2-R for CDICE. Differences in abatement are very large between the different ψ -cases. In particular, in DICE-2016, for large ψ , the use of carbon is extended by about 50 years relative to the low IES case. This is true independently of the assumption on the ECS. Since the timing in the DICE-2016 calibration is wrong, the effects of future lower interest rates are much more pronounced than for CDICE. In fact, for a high value of ψ (higher future interest rates), the optimal policy in CDICE and DICE-2016 are quite similar; the differences become large as expected future interest rates become small. The range of plausible values for ψ adds another model uncertainty to economic models of climate change, and it turns out that the miscalibration in DICE-2016 amplifies the effect. In more interesting models with uncertainty and Epstein-Zin utility (see, e.g., Cai and Lontzek (2019)), the use of the DICE-2016 climate calibration is likely to lead to serious problems.

As above, optimal long-run temperatures in DICE-2016 are far above the values in CDICE. Now there is an even larger spread caused by different values for ψ . Figure 1.19 shows future temperature under optimal abatement for different values of ψ and for the three different specifications of ECS. For the case of a high ECS, the optimal warming under DICE-2016 is now quite dramatic if one assumes a high value of ψ . In 200 years, optimal warming is almost 6 degrees; far above anything considered acceptable by most climate scientists. Even for the MMM calibration, a high ψ implies warming by more than 4.5 degrees. For this high IES case, warming prescribed by DICE-2016 falls significantly out of the CMIP5 range.

Future interest rates and growth rates matter a lot for optimal mitigation and optimal interest rates. Even if one settles on a path for TFP growth, different reasonable preference specifications lead to large differences in interest rates. The fact that the DICE-2016

calibration of the climate emulator contains two flaws (discussed in detail above) implies an unrealistically large sensitivity to discounting, and differences in future interest rates translate into an unrealistically large difference in the SCC.

The results presented here clearly highlight the need for reliable climate calibrations and show the advantages of our approach. The fact that DICE-2016 lies within the range of CMIP5 predictions in some cases does not ensure that it can be used as a reliable tool within a calibrated economic model.

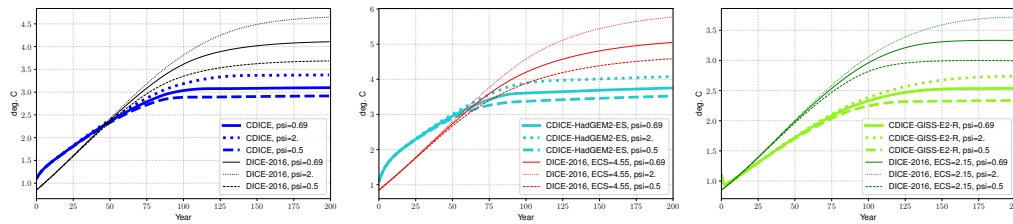


Fig. 1.19 Optimal temperatures for different values of ψ and different climate calibrations. The left panel shows results for MMM, the middle panel for high ECS calibrations and the right panel for low ECS calibrations. Year zero on the graph corresponds to the starting year 2015.

1.7 Conclusion

IAMs provide a quantitative framework that takes into account economic and environmental stocks and flows as well as their interaction and which allows researchers to investigate climate change and possible mitigation pathways (Hassler, Krusell, & Smith, 2016b). IAMs differ very much in terms of structure, complexity, level of detail, and possible solution methods (Flamos, 2019; Hare, Brecha, & Schaeffer, 2018; Weyant, 2017). Models like the one by Clarke et al. (2009) have very rich climate representation, whereas Bosetti, Eni, Mattei, Massetti, and Tavoni (2007) provide a detailed economic model. Other models provide a detailed representation of the energy sector. Models like Golosov et al. (2014); Hambel, Kraft, and Schwartz (2021); Hassler and Krusell (2018); W. Nordhaus (2018); Traeger (2019) have a more parsimonious structure and exhibit a higher level of aggregation, but allow for monetary estimates both for the cost of curbing climate change and for the economic benefits that it brings, which is a necessary feature from a policy-making perspective. Having a very detailed model with the possibility of a cost-benefit analysis would be the preferable option. However, computational costs for such kinds of models

are extremely high. Thus, there is a strong demand for IAMs, on the one hand, for capturing and reflecting relevant processes both in the economy and climate. On the other hand, IAMs are necessary for quantitative estimation (uncertainty, risks, tipping points, endogenous growth), so they should be parsimonious enough to have reasonable computational complexity. The perfect candidate to satisfy both requirements could be the DICE model (W. Nordhaus, 2018). However, it has been strongly criticized by climate scientists and recently by economists for representing climate not in accordance with the recent climate science advancements (Dietz et al., 2021).

Our paper's three main contributions are as follows. First, we develop a series of tests to evaluate the quality of CEs used in economic modeling. These tests include one test that is similar to Dietz et al. (2021), but overall they are more comprehensive in that they specifically test both, the temperature equations and the carbon cycle of CEs.

Second, we update the parsimonious climate representation of climate in DICE with a new calibration of coefficients that aligns it with the CMIP5 benchmark, making the DICE model both simple and transparent yet making it realistically represent climate. The functional form of the climate part in DICE is retained. This allows authors who have the climate module of DICE "hard-wired" in their economic model to obtain more reliable results by simply changing parameters.

Third, we explain that, although the DICE-2016 predictions in a BAU scenario fall within the range of CMIP5, this is caused by two compensating errors in the calibration. We demonstrate that mitigation scenarios are highly sensitive to such compensating errors between the carbon cycle and the temperature response of the model. We advocate that this result is generic and not specific to DICE-2016 and that the proposed battery of tests enables the identification of such issues in climate models used in climate economics. Regarding DICE-2016, our conclusion is similar to that in Dietz et al. (2021); the calibration of DICE-2016 is not suited for reliable policy analysis.

An important aspect for the calibration and testing of a CE, is what physics is covered by either the test data or the functional form of the CE - as, for example, the box-model formulation used here or an impulse response function (IRF) formulation frequently seen in the literature. This is a vast question that may easily fill a paper of its own, but it is useful to point out a few aspects that come to mind in the context of the present study. We first note that a box model, as used here for the carbon cycle, preserves the total carbon mass

in the system, apart from carbon added to the system via human activity. A corollary is that such a box description ‘knows’ when its reservoirs (boxes) are out of (pre-industrial) equilibrium, factoring in any resulting associated fluxes among reservoirs automatically. This is in contrast to IRF approaches, as used, for example, in Joos et al. (2013), where the temporal evolution of a perturbation to a reservoir (as a carbon emission pulse to the atmosphere) is described as a function of time but without taking into account where the part of the perturbation leaving that reservoir (e.g., the atmosphere) goes. Consequently, an IRF formulation cannot be aware of whether or how strongly out of equilibrium different reservoirs (atmosphere, ocean, land, etc.) are. Coefficients in either formulation, box, or IRF, can be made aware (calibrated) such as to take into account feedbacks affecting the exchange among reservoirs (e.g., Sterner and Johansson (2017) for box models, or Joos et al. (2001) for IRFs). On the side of the carbon cycle, such feedbacks include carbon concentration and carbon-climate feedback, that is, carbon fluxes among reservoirs are sensitive to changes in atmospheric carbon concentration or global mean temperature that have already occurred relative to pre-industrial times (see, e.g., Arora et al. (2013, 2020)). Other effects present in the full climate system are more difficult to capture via simple climate emulators. An example here is feedback due to two-dimensional patterns of ocean surface temperature (see, e.g., Andrews et al. (2022)). By design, such feedbacks are beyond the scope of simple zero-dimensional CEs as the one studied here. Nevertheless, such simple CEs are of obvious interest for economic applications.

Appendix

1.A Summary table of the models and parameters

Name	b_{12}	b_{23}	$M_{AT,UO,LO}^{EQ}$	$M_{AT,UO,LO}^{INI}$	c_1	c_3	c_4	f_{2xco2}	t_{2xco2}	$T_{AT,OC}^{INI}$
CDICE (MMM-MMM)	0.054	0.0082	(607, 489, 1281)	(851, 628, 1323)	0.137	0.73	0.00689	3.45	3.25	(1.1, 0.27)
CDICE-HadGEM2-ES	0.054	0.0082	(607, 489, 1281)	(851, 628, 1323)	0.154	0.55	0.00671	2.95	4.55	(1.1, 0.27)
CDICE-GISS-E2-R	0.054	0.0082	(607, 489, 1281)	(851, 628, 1323)	0.213	1.16	0.00921	3.65	2.15	(1.1, 0.27)
CDICE-MESMO	0.059	0.008	(607, 305, 865)	(851, 403, 894)	0.137	0.73	0.00689	3.45	3.25	(1.1, 0.27)
CDICE-LOVECLIM	0.067	0.0095	(607, 600, 1385)	(850, 770, 1444)	0.137	0.73	0.00689	3.45	3.25	(1.1, 0.27)
CDICE-MESMO-HadGEM2-ES	0.059	0.008	(607, 305, 865)	(851, 403, 894)	0.154	0.55	0.00671	2.95	4.55	(1.1, 0.27)
CDICE-MESMO-GISS-E2-R	0.059	0.008	(607, 305, 865)	(851, 403, 894)	0.213	1.16	0.00921	3.65	2.15	(1.1, 0.27)
CDICE-LOVECLIM-HadGEM2-ES	0.067	0.0095	(607, 600, 1385)	(850, 770, 1444)	0.154	0.55	0.00671	2.95	4.55	(1.1, 0.27)
CDICE-LOVECLIM-GISS-E2-R	0.067	0.0095	(607, 600, 1385)	(850, 770, 1444)	0.213	1.16	0.00921	3.65	2.15	(1.1, 0.27)
DICE-2016	0.12	0.007	(588, 360, 1720)	(851, 460, 1740)	0.1005	0.088	0.025	3.6813	3.1	(0.85, 0.0068)

Table 1.A1 Labelling of the models, and their respective parameterization. Note that the coefficients for the DICE-2016 model correspond to a five-year time step, whereas all other models are defined for an annual time step.

1.B Generic DICE formulation and calibration

In section 1.6, we laid out the DICE model as a whole, that is, we specified the dynamic optimization problem that we solve with a calibration of parameters that are either given by DICE-2016 or by variants of our CDICE. We call this dynamic problem, specified by Eqs. (1.8) to (1.12), the generic formulation of the DICE model in terms of its formal structure. The generic formulation allows for an easy switch in parameters between different versions of the DICE model (DICE-2007, DICE-2016) as well as a switch to the CDICE parametrization.²⁸ The functional forms of DICE-2007 and DICE-2016 are slightly different; however, they do not provide a critical difference in the results. This fact is especially relevant for the laws of motion of exogenous parameters in both models because of the differences in time steps (DICE-2007 operates with a ten-year time step, and DICE-2016 operates with a five-year time step), differences in units of measurement for emissions (GtC in DICE-2007 versus GtCO₂ in DICE-2016) and other minor divergences. We believe that it is important to have a unified specification for the DICE model, which

²⁸Note that in the online Appendix Section 1.B, we also include DICE-2007, for completeness, as there is a vast number of research papers and policy studies that have used this formulation of the DICE model.

in turn allows a broader group of researchers to consider updating their parametrization of the model with respect to our proposed CDICE.

Another feature of the generic specification of the DICE model is that we explicitly allow for the time step. The time step enters all relevant equations as the multiplication factor Δ_t with respect to the annual baseline calibration for all the parameters. This applies both for the main equations of the model specified in Sections 1.B.2 and 1.B.3 and for exogenously specified parameters of the model in Section 1.B.1.

This online Appendix is organized as follows. We present the generic equations and calibration for all the exogenous parameters of the DICE-2007 (reads Value 2007 in the tables with parameters), DICE-2016 (reads Value 2016), and CDICE first. Then we provide core equations of the model corresponding to the mass of carbon evolution, temperature evolution, and economic growth with calibrations corresponding to DICE-2007, DICE-2016, and CDICE. When necessary, we provide a detailed comment on how the functional forms of certain equations were changed to be the same in the generic formulation and, at the same time, equivalent to the initial formulation of DICE-2007 and DICE-2016 (for example, the law of motion for TFP).

1.B.1 Exogenous variables

We start by introducing the law of motion for exogenous variables that are time dependent. The law of motion for labor is given in Eq. (1.B.1) along with labor growth presented in Eq. (1.B.2):

$$L_t = L_0 + (L_\infty - L_0) \left(1 - \exp(-\Delta_t \delta^L t) \right), \quad (1.B.1)$$

$$g_t^L = \frac{\frac{dL_t}{dt}}{L_t} = \frac{\Delta_t \delta^L}{\frac{L_\infty}{L_\infty - L_0} \exp(\Delta_t \delta^L t) - 1}. \quad (1.B.2)$$

The numerical values of the parameters for the world population and its growth rate given in Table 1.B2:

Calibrated parameter	Symbol	Value 2007	Value 2016/CDICE
Annual rate of convergence	δ^L	0.035	0.0268
World population at starting year [millions]	L_0	6514	7403
Asymptotic world population [millions]	L_∞	8600	11500
Time step of a model	Δ_t	10	5/1

Table 1.B2 Generic parametrization for the evolution of labor.

The total factor productivity evolves according to the equation Eq. (1.B.3) with its growth rate following Eq. (1.B.4):

$$A_t = A_0 \exp\left(\frac{\Delta_t g_0^A (1 - \exp(-\Delta_t \delta^A t))}{\Delta_t \delta^A}\right). \quad (1.B.3)$$

$$g_t^A = \frac{dA_t}{A_t} = \Delta_t g_0^A \exp(-\Delta_t \delta^A t). \quad (1.B.4)$$

The respective parameters of the total factor productivity evolution and TFP growth rate are given in Table 1.B3:

Calibrated parameter	Symbol	Value 2007	Value 2016/CDICE
Initial growth rate for TFP per year	g_0^A	0.01314	0.0217
Decline rate of TFP growth per year	δ^A	0.001	0.005
Initial level of TFP	A_0	0.0058	0.010295
Time step of a model	Δ_t	10	5/1

Table 1.B3 Generic parametrization for the evolution of TFP.

The carbon intensity, defined in Eq. (1.B.5) for DICE-2007 and in Eq. (1.B.6), characterizes how much anthropogenic carbon inflows the climate system due to production activity:

$$\sigma_t = \sigma_0 \exp\left(\frac{\Delta_t g_0^\sigma (1 - \exp(-\Delta_t \delta^\sigma t))}{\Delta_t \delta^\sigma}\right). \quad (1.B.5)$$

The carbon intensity in DICE-2016 is given by:

$$\sigma_t = \sigma_0 \exp\left(\frac{\Delta_t g_0^\sigma}{\log(1 + \Delta_t \delta^\sigma)} \left((1 + \Delta_t \delta^\sigma)^t - 1\right)\right). \quad (1.B.6)$$

The parametrization for carbon intensity processes is given by Table 1.B4:

Calibrated parameter	Symbol	Value 2007	Value 2016/CDICE
Initial growth of carbon intensity per year	g_0^σ	-0.0073	-0.0152
Decline rate of decarbonization per year	δ^σ	0.003	0.001
Initial carbon intensity (1000GtC)	σ_0	0.00013418	0.00009556
Time step	Δ_t	10	5/1

Table 1.B4 Generic parametrization for the carbon intensity evolution.

DICE-2016 uses a backstop technology capable of mitigating the full amount of industrial emissions that enter the atmosphere. The cost of backstop technology is assumed to be initially high but could be reduced over time, which is reflected in the definition of the coefficient of the abatement cost function $\theta_{1,t}$ as defined in Eq. (1.B.7) for DICE-2007 and Eq. (1.B.8) for DICE-2016.²⁹

The abatement cost in DICE-2007 is given by:

$$\theta_{1,t} = \frac{p_0^{\text{back}}(1 + \exp(-g^{\text{back}}t))1000\sigma_t}{\theta_2}. \quad (1.B.7)$$

The abatement cost in DICE-2016 is given by:

$$\theta_{1,t} = \frac{p_0^{\text{back}} \exp(-g^{\text{back}}t) 1000 \cdot c_{2\text{co}2} \cdot \sigma_t}{\theta_2}. \quad (1.B.8)$$

The parameters for the abatement cost are presented in Table 1.B5:

²⁹The scale parameter 1000 in the equations (1.B.7) and (1.B.8) reflects the fact that we use a 1000 GtC unit of measurement; the parameter $c_{2\text{co}2}$ transforms carbon intensity measured in GtC into GtCO₂, as the backstop price in DICE-2016 is given for GtCO₂ instead of GtC.

Calibrated parameter	Symbol	Value 2007	Value 2016/CDICE
Cost of backstop 2005 thUSD per tC 2005	p_0^{back}	0.585	-
Cost of backstop 2010 thUSD per tCO2 2015	p_0^{back}	-	0.55
Initial cost decline backstop cost per year	g^{back}	0.005	0.005
Exponent of control cost function	θ_2	2.8	2.6
Transformation coefficient from C to CO2	c2co2	-	3.666

Table 1.B5 Generic parametrization for the abatement cost.

The non-industrial emissions from land use and deforestation decline over time according to Eq. (1.B.9), with parameters are presented in Table 1.B6:

$$E_{\text{Land},t} = E_{\text{Land},0} \exp(-\Delta_t \delta^{\text{Land}} t). \quad (1.B.9)$$

Calibrated parameter	Symbol	Value 2007	Value 2016/CDICE
Emissions from land 2005 (1000GtC per year)	$E_{\text{Land},0}$	0.0011	-
Emissions from land 2015 (1000GtC per year)	$E_{\text{Land},0}$	-	0.000709
Decline rate of land emissions (per year)	δ^{Land}	0.01	0.023
Time step	Δ_t	10	5/1

Table 1.B6 Generic parametrization for the emissions from land.

The exogenous radiative forcings that result from non-CO2 GHG are described in Eq. (1.B.10):

$$F_t^{\text{EX}} = F_0^{\text{EX}} + \frac{1}{T/\Delta_t} (F_1^{\text{EX}} - F_0^{\text{EX}}) \min(t, T/\Delta_t). \quad (1.B.10)$$

The parameters of the exogenous radiative forcings are given in Table 1.B7:

Calibrated parameter	Symbol	Value 2007	Value 2016/CDICE
2000 forcings of non-CO2 GHG (Wm-2)	F_0^{EX}	-0.06	-
2015 forcings of non-CO2 GHG (Wm-2)	F_0^{EX}	-	0.5
2100 forcings of non-CO2 GHG (Wm-2)	F_1^{EX}	0.3	1.0
Number of years before 2100	T	100	85
Time step	Δ_t	10	5/1

Table 1.B7 Generic parametrization for the exogenous forcing.

1.B.2 The equations of the climate system

The laws of motion for the mass of carbon in the atmosphere are presented in the main body of the text with Eq. (1.1). The temperature equations are given in Eqs. (1.4) and (1.5). However, we believe it can be helpful to provide the full description of the equations above together with their parametrization that can be used to relate DICE-2007 to DICE-2016 and CDICE.

The evolution for the mass of carbon in all three reservoirs is given by the Eqs. (1.B.11) to (1.B.13), carbon emissions are determined with the Eq. (1.B.14):

$$M_{t+1}^{AT} = (1 - \Delta_t b_{12}) M_t^{AT} + \Delta_t b_{12} \frac{M_{EQ}^{AT}}{M_{EQ}^{UO}} M_t^{UO} + \Delta_t E_t, \quad (1.B.11)$$

$$M_{t+1}^{UO} = \Delta_t b_{12} M_t^{AT} + (1 - \Delta_t b_{12} \frac{M_{EQ}^{AT}}{M_{EQ}^{UO}} - \Delta_t b_{23}) M_t^{UO} + \Delta_t b_{23} \frac{M_{EQ}^{UO}}{M_{EQ}^{LO}} M_t^{LO}, \quad (1.B.12)$$

$$M_{t+1}^{LO} = \Delta_t b_{23} M_t^{UO} + (1 - \Delta_t b_{23} \frac{M_{EQ}^{UO}}{M_{EQ}^{LO}}) M_t^{LO}, \quad (1.B.13)$$

$$E_t = \sigma_t Y_t^{\text{Gross}} (1 - \mu_t) + E_t^{\text{Land}}. \quad (1.B.14)$$

$$(1.B.15)$$

The parameters for the laws of motion for the masses of carbon, as well as the starting values and equilibrium values, are given in Table 1.B8.

Calibrated parameter	Symbol	2007	2016	CDICE
Carbon cycle, annual value	b_{12}	0.0189288	0.024	0.054
Carbon cycle, annual value	b_{23}	0.005	0.0014	0.0082
Time step	Δ_t	10	5	1
Eq. concentration in atmosphere (1000GtC)	M_{EQ}^{AT}	0.587473	0.588	0.607
Eq. concentration in upper strata (1000GtC)	M_{EQ}^{UO}	1.143894	0.360	0.489
Eq. concentration in lower strata (1000GtC)	M_{EQ}^{LO}	18.340	1.720	1.281
Concentration in atmosphere 2015 (1000GtC)	M_{INI}^{AT}	0.8089	0.851	0.851
Concentration in upper strata 2015 (1000GtC)	M_{INI}^{UO}	1.255	0.460	0.628
Concentration in lower strata 2015 (1000GtC)	M_{INI}^{LO}	18.365	1.740	1.323

Table 1.B8 Generic parametrization for the mass of carbon.

The temperature evolution is determined by Eqs. (1.B.16) to (1.B.18) with parameters and starting values given in Table 1.B9:

$$T_{t+1}^{AT} = T_t^{AT} + \Delta_t c_1 F_t - \Delta_t c_1 \frac{F_{2XCO_2}}{T_{2XCO_2}} T_t^{AT} - \Delta_t c_1 c_3 (T_t^{AT} - T_t^{OC}), \quad (1.B.16)$$

$$T_{t+1}^{OC} = T_t^{OC} + \Delta_t c_4 (T_t^{AT} - T_t^{OC}), \quad (1.B.17)$$

$$F_t = F_{2XCO_2} \frac{\log(M_t^{AT}/M_{base}^{AT})}{\log(2)} + F_t^{EX}. \quad (1.B.18)$$

Calibrated parameter	Symbol	2007	2016	CDICE
Temperature coefficient, annual value	c_1	0.022	0.0201	0.137
Temperature coefficient, annual value	c_3	0.3	0.088	0.73
Temperature coefficient, annual value	c_4	0.01	0.005	0.00689
Forcings of equilibrium CO2 doubling (Wm-2)	F_{2XCO_2}	3.8	3.6813	3.45
Eq temperature impact (°C per doubling CO2)	T_{2XCO_2}	3.0	3.1	3.25
Eq concentration in atmosphere (1000GtC)	M_{base}^{AT}	0.5964	0.588	0.607
Atmospheric temp change (°C) from 1850	T_0^{AT}	0.7307	0.85	1.1
Lower stratum temp change (°C) from 1850	T_0^{OC}	0.0068	0.0068	0.27
Time step	Δ_t	10	5	1

Table 1.B9 Generic parametrization for the temperature.

1.B.3 Economy equations

The capital evolution and gross output in both models, DICE-2007 and DICE-2016, are given by:

$$K_{t+1} = (1 - \delta^K)^{\Delta_t} K_t + \Delta_t I_t, \quad (1.B.19)$$

$$Y_t^{\text{Gross}} = (A_t L_t)^{1-\alpha} K_t^\alpha. \quad (1.B.20)$$

The functional forms of damages differ in DICE-2007 and DICE-2016. In DICE-2007, damages, abatement costs, output net of damages, and output net of damages and abatement costs are given by:

$$\Omega_t = \frac{1}{1 + \psi_1 T_t^{\text{AT}} + \psi_2 (T_t^{\text{AT}})^2}, \quad (1.B.21)$$

$$\Theta_t = \theta_{1,t} \mu_t^{\theta_2}, \quad (1.B.22)$$

$$Y_t^{\text{Net}} = Y_t^{\text{Gross}} \cdot \Omega_t = \frac{Y_t^{\text{Gross}}}{1 + \psi_1 T_t^{\text{AT}} + \psi_2 (T_t^{\text{AT}})^2}, \quad (1.B.23)$$

$$Y_t = Y_t^{\text{Gross}} \cdot \Omega_t \cdot (1 - \Lambda_t) = \frac{Y_t^{\text{Gross}} (1 - \theta_{1,t} \mu_t^{\theta_2})}{1 + \psi_1 T_t^{\text{AT}} + \psi_2 (T_t^{\text{AT}})^2}. \quad (1.B.24)$$

$$(1.B.25)$$

The same variables for DICE-2016 are given by the following equations:

$$\Omega_t = \psi_1 T_t^{\text{AT}} + \psi_2 (T_t^{\text{AT}})^2, \quad (1.B.26)$$

$$\Theta_t = \theta_{1,t} \mu_t^{\theta_2}, \quad (1.B.27)$$

$$Y_t^{\text{Net}} = Y_t^{\text{Gross}} \cdot (1 - \Omega_t) = Y_t^{\text{Gross}} (1 - \psi_1 T_t^{\text{AT}} - \psi_2 (T_t^{\text{AT}})^2), \quad (1.B.28)$$

$$Y_t = Y_t^{\text{Gross}} \cdot (1 - \Lambda_t - \Omega_t) = Y_t^{\text{Gross}} (1 - \theta_{1,t} \mu_t^{\theta_2} - \psi_1 T_t^{\text{AT}} - \psi_2 (T_t^{\text{AT}})^2). \quad (1.B.29)$$

$$(1.B.30)$$

Consumption in both DICE-2007 and DICE-2016 models is given by:

$$C_t = Y_t - I_t. \quad (1.B.31)$$

However, the utility function in DICE-2007 differs slightly from the utility used in DICE-2016. Utility in DICE-2007 is the following:

$$U_t = \sum_{t=0}^T \beta^t \cdot \Delta_t \cdot \frac{\left(\frac{C_t}{L_t}\right)^{1-1/\psi} - 1}{1 - 1/\psi} L_t. \quad (1.B.32)$$

And utility in DICE-2016 is given by:

$$U_t = \sum_{t=0}^T \beta^t \cdot \Delta_t \cdot \frac{\left(\frac{C_t}{L_t}\right)^{1-1/\psi} - 1}{1 - 1/\psi} L_t. \quad (1.B.33)$$

The discount rate in both DICE-2007 and DICE-2016 models is the same and determined as:

$$\beta = \frac{1}{(1 + \rho)^{\Delta_t}}. \quad (1.B.34)$$

The parameters for the economic part of DICE-2007 and DICE-2016 are given in Table 1.B10.

Calibrated parameter	Symbol	Value 2007	Value 2016/CDICE
Capital annual depreciation rate	δ^K	0.1	0.1
Elasticity of capital	α	0.3	0.3
Damage parameter	ψ_1	0.0	0.0
Damage quadratic parameter	ψ_2	0.0028388	0.00236
Exponent of control cost function	θ_2	2.8	2.6
Risk aversion	ψ	0.5	0.69
Time preferences	ρ	0.015	0.015
Initial capital (trillions USD 2015)	K_0	-	223.
Initial capital (trillions USD 2005)	K_0	137.	-
Time step	Δ_t	10	5/1

Table 1.B10 Generic parametrization for the parameters of economy.

1.C Sensitivity exercise: change in the exogenous forcing

In section 1.4.5 we used an alternative evolution equation for exogenous forcings, namely

$$F^{\text{EX}} = 0.3 \cdot F_t^{\text{CO}_2}. \quad (1.C.35)$$

This specification was adopted instead of Eq. (1.B.10) that was used in DICE-2016. As was shown in Figure 1.7, this switch from the original DICE-2016 exogenous forcings can make quite a difference in the temperature evolution. However, when computing the simulation results in section 1.6, we used the original exogenous forcings equation Eq. (1.B.10) to remain consistent with the DICE-2016 model and to focus on analyzing the influence of the re-calibrated climate part on policies, which was the goal of the section. Therefore, in this section of the online Appendix, we want to investigate the consequences of implementing time-dependent exogenous forcings that differ for the DICE-2016 and CDICE models.

Below we present some solution results for the optimization problem Eq. (1.8) when the agent chooses optimal investment and mitigation paths. Furthermore, we compare DICE-2016 and CDICE with original and alternative exogenous forcings. Overall changing exogenous forcings does not make much of a difference for the modeling results. However, there are a couple of interesting observations that are worth mentioning.

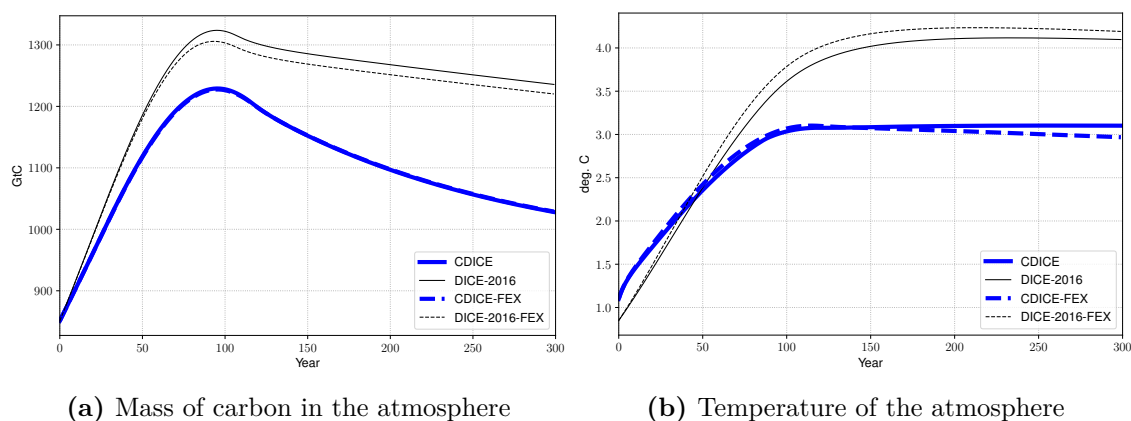


Fig. 1.C1 Mass of carbon in the atmosphere (left) and temperature of the atmosphere (right) for DICE-2016, and CDICE models with different exogenous forcing evolution (DICE-2016-FEX, CDICE-FEX show the model variables under the assumption of time dependent exogenous forcings) for an optimal abatement case. Year zero on the graphs corresponds to a starting year 2015.

From Figure 1.C1 we see that change in the exogenous forcings does not affect the CDICE model much but has some effect on DICE-2016. In DICE-2016 exogenous forcings being time-dependent results in a lower mass of carbon in the atmosphere than in DICE-2016 with the original forcings. However, it leads to an even higher temperature increase. The reason for this increased sensitivity of DICE-2016 is the same as for its excessive sensitivity to the discount rate. The carbon cycle and temperature equations are not in balance. Thus they overreact in transmitting changes in the inputs of the model towards outputs.

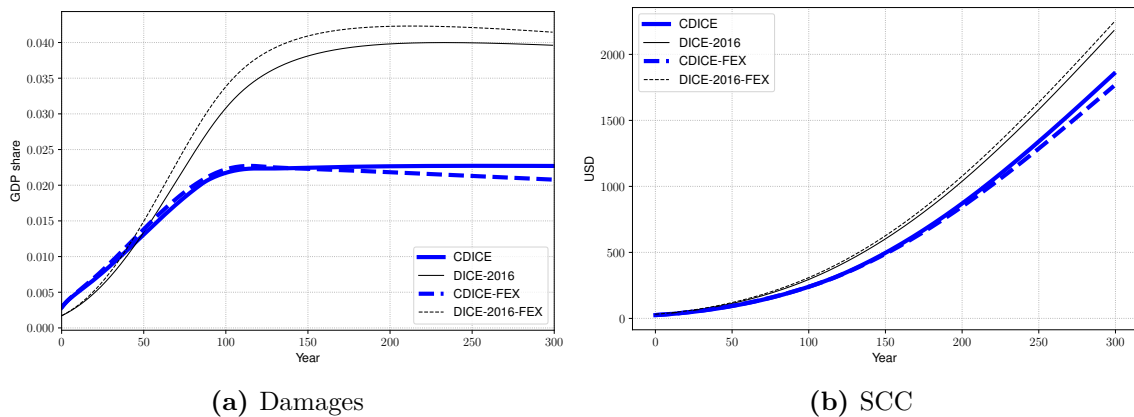


Fig. 1.C2 Damages (left) and the social cost of carbon (right) for DICE-2016, and CDICE models with different exogenous forcings evolution (DICE-2016-FEX, CDICE-FEX show the model variables under the assumption of time dependent exogenous forcings) for an optimal abatement case. Year zero on the graphs corresponds to a starting year 2015.

Figure 1.C2 reports damages and the social cost of carbon for models under consideration. Both variables are coherently in line with the expectations that one might get analyzing temperature equations. DICE-2016 with time-dependent forcings predicts more damages and thus a higher social cost of carbon. For CDICE, both damages and the social cost of carbon remain roughly the same, with CDICE variables being slightly lower for alternative exogenous forcing formulation.

1.D Computational details

In this online Appendix, we briefly outline how we numerically solve the re-calibrated DICE-2016 model (cf. Section 1.6) by applying “Deep Equilibrium Nets”(DEQNs) (Azinovic et al., 2022). To do so, we proceed in two steps. First, we summarize in Section 1.D.1 the DEQN solution technique in the most general form. Second, we detail in Section 1.D.2

how the CDICE model can be cast in a form amenable to DEQNs. Section 1.D.3 finally reports detailed error statistics for our benchmark CDICE model. For further implementation details, we refer the reader to the repository hosted under the following URL: https://github.com/ClimateChangeEcon/Climate_in_Climate_Economics and which contains all replication codes.

1.D.1 Deep Equilibrium Nets in a Nutshell

From an abstract perspective, the DEQN algorithm is a simulation-based solution method using deep neural networks³⁰ to compute an approximation of the *optimal policy function* $\mathbf{p} : X \rightarrow Y \subset \mathbb{R}^K$ to a dynamic model under the assumption that the underlying economy can be characterized via discrete-time first-order equilibrium conditions, that is,

$$\mathbf{G}(\mathbf{x}, \mathbf{p}) = \mathbf{0} \quad \forall \mathbf{x} \in X, \quad (1.D.36)$$

Intuitively, DEQNs work as follows: An unknown policy function is approximated with a neural network, that is, $\mathbf{p}(\mathbf{x}) \approx \mathcal{N}_\nu(\mathbf{x})$, and where the ν 's are ex-ante unknown coefficients of the neural network that have to be determined based on some suitable loss function measuring the quality of a given approximation at a given state of the economy.

The DEQN algorithm is started by randomly initializing the ν 's (Glorot & Bengio, 2010), that is, an arbitrary guess for the ex-ante unknown approximate policy function. Next, we simulate a sequence of $N_{\text{path length}}$ states. Starting from some given state \mathbf{x}_t , the next state \mathbf{x}_{t+1} is a result of the policies encoded by the neural network, $\mathcal{N}_\nu(\mathbf{x})$, and remaining model-implied dynamics.

If we knew the (approximate) policy function satisfying the equilibrium conditions, expression (1.D.36) would hold along a simulated path. However, since the neural network is initialized with random coefficients, $\mathbf{G}(\mathbf{x}_t, \mathcal{N}_\nu(\mathbf{x}_t)) \neq \mathbf{0}$ along the simulated path of length $N_{\text{path length}}$. This fact is now leveraged to improve the quality of the guessed policy function. Specifically, DEQNs use the error in the equilibrium conditions as a loss function, that is,

$$\ell_\nu := \frac{1}{N_{\text{path length}}} \sum_{\mathbf{x}_t \text{ on sim. path}} \sum_{m=1}^{N_{eq}} (G_m(\mathbf{x}_t, \mathcal{N}_\nu(\mathbf{x}_t)))^2, \quad (1.D.37)$$

³⁰See, e.g., Goodfellow, Bengio, and Courville (2016) for a textbook treatment of neural networks.

where $G_m(\mathbf{x}_t, \mathcal{N}_\nu(\mathbf{x}_t))$ represent all the N_{eq} first-order equilibrium conditions of a given model. Expression (1.D.37) can now be used to update the parameters of the network with any variant of gradient descent,³¹ namely,

$$\nu'_k = \nu_k - \alpha^{\text{learn}} \frac{\partial \ell(\boldsymbol{\nu})}{\partial \nu_k}, \quad (1.D.38)$$

where ν'_k represents the updated k -th parameter of the neural network, that is, $\mathcal{N}_\nu = \mathcal{N}_{\nu'}$, and where $\alpha^{\text{learn}} \in \mathbb{R}$ denotes the so-called learning rate. The updated neural network-based representation of the policy is subsequently used to simulate a sequence of length $N_{\text{path length}}$ steps, along which the loss function is recorded, and the latter is again used to update the network parameters. This iterative procedure is pursued until $\ell_\nu < \epsilon \in \mathbb{R}$, that is, until an approximate equilibrium policy, has been found.

In summary, the DEQN algorithm consists of four building blocks: i) deep neural networks for approximating the equilibrium policies; ii) a suitable loss function measuring the quality of a given approximation at a given state of the economy; iii) an updating mechanism to improve the quality of the approximation; and iv) a sampling method for choosing states for updating and evaluating of the approximation quality. We next outline each of these components for clarity in the context of CDICE.

1.D.2 Mapping CDICE onto Deep Equilibrium Nets

In this online Appendix, we introduce a formal way of mapping CDICE, but more broadly speaking, non-stationary models, onto the neural network-based DEQN solution framework. To ensure the replicability of our procedure, we next thoroughly list every mathematical manipulation that is required.

We begin by stating the CDICE model (cf. the online Appendix 1.B for the detailed calibration), that is,

$$\max_{\{C_t, \mu_t\}_{t=0}^{\infty}} \sum_{t=0}^{\infty} \beta^t \frac{\left(\frac{C_t}{L_t}\right)^{1-1/\psi} - 1}{1 - 1/\psi} L_t \quad (1.D.39)$$

$$\text{s.t. } K_{t+1} = (1 - \Omega(T_{AT,t}) - \Theta(\mu_t)) K_t^\alpha (A_t L_t)^{1-\alpha} + (1 - \delta)K_t - C_t \quad (\lambda_t) \quad (1.D.40)$$

³¹In our practical applications, we use ‘‘Adam’’ (Kingma & Ba, 2014).

$$M_{t+1}^{\text{AT}} = (1 - b_{12}) M_t^{\text{AT}} + b_{12} \frac{M_{\text{EQ}}^{\text{AT}}}{M_{\text{EQ}}^{\text{UO}}} M_t^{\text{UO}} + \sigma_t (1 - \mu_t) K_t^\alpha (A_t L_t)^{1-\alpha} + E_t^{\text{Land}} \quad (\nu_t^{\text{AT}}) \quad (1.D.41)$$

$$M_{t+1}^{\text{UO}} = b_{12} M_t^{\text{AT}} + \left(1 - b_{12} \frac{M_{\text{EQ}}^{\text{AT}}}{M_{\text{EQ}}^{\text{UO}}} - b_{23}\right) M_t^{\text{UO}} + b_{23} \frac{M_{\text{EQ}}^{\text{UO}}}{M_{\text{EQ}}^{\text{LO}}} M_t^{\text{LO}} \quad (\nu_t^{\text{UO}}) \quad (1.D.42)$$

$$M_{t+1}^{\text{LO}} = b_{23} M_t^{\text{UO}} + \left(1 - b_{23} \frac{M_{\text{EQ}}^{\text{UO}}}{M_{\text{EQ}}^{\text{LO}}}\right) M_t^{\text{LO}} \quad (\nu_t^{\text{LO}}) \quad (1.D.43)$$

$$T_{t+1}^{\text{AT}} = T_t^{\text{AT}} + c_1 \left(F_{2\text{XCO}_2} \frac{\log(M_t^{\text{AT}}/M_{\text{base}}^{\text{AT}})}{\log(2)} + F_t^{\text{EX}} \right) - c_1 \frac{F_{2\text{XCO}_2}}{T_{2\text{XCO}_2}} T_t^{\text{AT}} - c_1 c_3 (T_t^{\text{AT}} - T_t^{\text{OC}}) \quad (\eta_t^{\text{AT}}) \quad (1.D.44)$$

$$T_{t+1}^{\text{OC}} = T_t^{\text{OC}} + c_4 (T_t^{\text{AT}} - T_t^{\text{OC}}) \quad (\eta_t^{\text{OC}}) \quad (1.D.45)$$

$$0 \leq \mu_t \leq 1 \quad (\lambda_t^\mu), \quad (1.D.46)$$

where the Lagrange and KKT multipliers we will employ below have been added in parentheses for completeness.

The state of the economy at time t is given by

$$\mathbf{x}_t \in \mathbb{R}^6 := (k_t, M_t^{\text{AT}}, M_t^{\text{UO}}, M_t^{\text{LO}}, T_t^{\text{AT}}, T_t^{\text{OC}}, t)^T. \quad (1.D.47)$$

Note that we take time t as an exogenous state to account for the non-stationary nature of the IAM, whereas all other states are endogenously determined. Furthermore, to ensure computational tractability, we follow Traeger (2014) and map the unbounded physical time $t \in [0, \infty)$ via the strictly monotonic transformation

$$\tau = 1 - \exp(-\vartheta t). \quad (1.D.48)$$

into the unit interval, $\tau \in (0, 1]$.³² To scale back from the auxiliary time τ to the physical time, the inverse transformation of equation (1.D.48) can be applied, that is,

$$t = -\frac{\ln(1 - \tau)}{\vartheta}. \quad (1.D.49)$$

³²An alternative way to deal with transitory dynamics is to use so-called “shooting methods” (see, e.g., Arellano, Bai, and Mihalache (2020), and references therein).

Next, we re-scale consumption and capital as

$$c_t := \frac{C_t}{A_t L_t}, k_t := \frac{K_t}{A_t L_t}. \quad (1.D.50)$$

The following normalization of the Lagrangian and the KKT multipliers helps to stabilize the solution process, that is:

$$\begin{aligned} \hat{\lambda}_t &:= \frac{\lambda_t}{A_t^{1-\frac{1}{\psi}} L_t}, \hat{\lambda}_t^\mu := \frac{\lambda_t^\mu}{A_t^{1-\frac{1}{\psi}} L_t}, \hat{\nu}_t^{\text{AT}} := \frac{\nu_t^{\text{AT}}}{A_t^{1-\frac{1}{\psi}} L_t}, \hat{\nu}_t^{\text{UO}} := \frac{\nu_t^{\text{UO}}}{A_t^{1-\frac{1}{\psi}} L_t}, \hat{\nu}_t^{\text{LO}} := \frac{\nu_t^{\text{LO}}}{A_t^{1-\frac{1}{\psi}} L_t}, \\ \hat{\eta}_t^{\text{AT}} &:= \frac{\eta_t^{\text{AT}}}{A_t^{1-\frac{1}{\psi}} L_t}, \hat{\eta}_t^{\text{OC}} := \frac{\eta_t^{\text{OC}}}{A_t^{1-\frac{1}{\psi}} L_t}. \end{aligned} \quad (1.D.51)$$

Furthermore, we introduce a quantity called the “effective discount factor”,

$$\hat{\beta}_t := \exp\left(-\rho + \left(1 - \frac{1}{\psi}\right) g_t^A + g_t^L\right). \quad (1.D.52)$$

The policy function \mathbf{p} we intend to approximate with the aid of deep neural networks is given by

$$\mathcal{N}_\nu(\mathbf{x}_t) \in \mathbb{R}^9 := \left(k_{t+1}, \mu_t, \hat{\lambda}_t, \hat{\lambda}_t^\mu, \hat{\nu}_t^{\text{AT}}, \hat{\nu}_t^{\text{UO}}, \hat{\nu}_t^{\text{LO}}, \hat{\eta}_t^{\text{AT}}, \hat{\eta}_t^{\text{OC}}\right). \quad (1.D.53)$$

and consists of the choice variables (k_{t+1}, μ_t) ³³ as well as the Lagrange and KKT multipliers.

Next, we derive the first-order conditions in order to form a loss function for the CDICE model that is suitable for DEQNs (cf. equation (1.D.37)). To do so, we start by formulating the Lagrangian of the model, which reads,

$$\begin{aligned} \mathcal{L} = \sum_{t=0}^{\infty} \hat{\beta}_t & \left[\frac{c_t^{1-1/\psi} - A_t^{1/\psi-1}}{1 - 1/\psi} \right. \\ & + \hat{\lambda}_t \left\{ (1 - \Omega(T_{\text{AT},t}) - \Theta(\mu_t)) k_t^\alpha + (1 - \delta) k_t - c_t - \exp(g_t^A + g_t^L) k_{t+1} \right\} \\ & + \hat{\lambda}_t^\mu \{1 - \mu_t\} \\ & \left. + \hat{\nu}_t^{\text{AT}} \left\{ (1 - b_{12}) M_t^{\text{AT}} + b_{12} \frac{M_{\text{EQ}}^{\text{AT}}}{M_{\text{EQ}}^{\text{UO}}} M_t^{\text{UO}} + \sigma_t (1 - \mu_t) A_t L_t k_t^\alpha + E_t^{\text{Land}} - M_{t+1}^{\text{AT}} \right\} \right] \end{aligned}$$

³³In our computations, we follow the literature and employ k_{t+1} instead of c_t as a choice variable, as it allows for a simpler update of the state variable k_t . Nevertheless, we still keep the first-order conditions with respect to k_{t+1} and c_t . In practical applications, the performance of neural networks can, as in our case, often benefit from redundant information (see, e.g., Azinovic et al. (2022) for more details).

$$\begin{aligned}
& + \hat{\nu}_t^{\text{UO}} \left\{ b_{12} M_t^{\text{AT}} + \left(1 - b_{12} \frac{M_{\text{EQ}}^{\text{AT}}}{M_{\text{EQ}}^{\text{UO}}} - b_{23} \right) M_t^{\text{UO}} + b_{23} \frac{M_{\text{EQ}}^{\text{UO}}}{M_{\text{EQ}}^{\text{LO}}} M_t^{\text{LO}} - M_{t+1}^{\text{UO}} \right\} \\
& + \hat{\nu}_t^{\text{LO}} \left\{ b_{23} M_t^{\text{UO}} + \left(1 - b_{23} \frac{M_{\text{EQ}}^{\text{UO}}}{M_{\text{EQ}}^{\text{LO}}} \right) M_t^{\text{LO}} - M_{t+1}^{\text{LO}} \right\} \\
& + \hat{\eta}_t^{\text{AT}} \left\{ T_t^{\text{AT}} + c_1 \left(F_{2\text{XCO}_2} \frac{\log(M_t^{\text{AT}}/M_{\text{base}}^{\text{AT}})}{\log(2)} + F_t^{\text{EX}} \right) - c_1 \frac{F_{2\text{XCO}_2}}{T_{2\text{XCO}_2}} T_t^{\text{AT}} \right. \\
& - c_1 c_3 \left(T_t^{\text{AT}} - T_t^{\text{OC}} \right) - T_{t+1}^{\text{AT}} \\
& \left. + \hat{\eta}_t^{\text{OC}} \left\{ T_t^{\text{OC}} + c_4 \left(T_t^{\text{AT}} - T_t^{\text{OC}} \right) - T_{t+1}^{\text{OC}} \right\} \right\} \quad (1.D.54)
\end{aligned}$$

The Lagrangian is now used to compute the first-order conditions, that is,

$$\begin{aligned}
\frac{\partial \mathcal{L}}{\partial k_{t+1}} = 0 & \Leftrightarrow \exp(g_t^A + g_t^L) \hat{\lambda}_t - \hat{\beta}_t \left[\hat{\lambda}_{t+1} \left((1 - \Omega(T_{\text{AT},t+1}) - \Theta(\mu_t)) \alpha k_{t+1}^{\alpha-1} + (1 - \delta) \right) \right. \\
& \left. + \hat{\nu}_{t+1}^{\text{AT}} \sigma_{t+1} (1 - \mu_{t+1}) A_{t+1} L_{t+1} \alpha k_{t+1}^{\alpha-1} \right] = 0 \quad (1.D.55)
\end{aligned}$$

$$\frac{\partial \mathcal{L}}{\partial c_t} = 0 \Leftrightarrow c_t^{-1/\psi} A_t^{1-1/\psi} L_t - \hat{\lambda}_t = 0 \quad (1.D.56)$$

$$\frac{\partial \mathcal{L}}{\partial \mu_t} = 0 \Leftrightarrow \hat{\lambda}_t \Theta'(\mu_t) k_t^\alpha + \lambda_t^\mu + \hat{\nu}_t^{\text{AT}} \sigma_t A_t L_t k_t^\alpha = 0 \quad (1.D.57)$$

$$\begin{aligned}
\frac{\partial \mathcal{L}}{\partial M_{\text{AT},t+1}} = 0 & \Leftrightarrow \hat{\nu}_t^{\text{AT}} - \hat{\beta}_t \left[\hat{\nu}_{t+1}^{\text{AT}} (1 - b_{12}) + \hat{\nu}_{t+1}^{\text{UO}} b_{12} + \hat{\eta}_{t+1}^{\text{AT}} c_1 F_{2\text{XCO}_2} \frac{1}{\ln 2 M_{\text{AT},t+1}} \right] = 0 \\
& (1.D.58)
\end{aligned}$$

$$\begin{aligned}
\frac{\partial \mathcal{L}}{\partial M_{\text{UO},t+1}} = 0 & \Leftrightarrow \hat{\nu}_t^{\text{UO}} - \hat{\beta}_t \left[\hat{\nu}_{t+1}^{\text{AT}} b_{12} \frac{M_{\text{EQ}}^{\text{AT}}}{M_{\text{EQ}}^{\text{UO}}} + \hat{\nu}_{t+1}^{\text{UO}} \left(1 - b_{12} \frac{M_{\text{EQ}}^{\text{AT}}}{M_{\text{EQ}}^{\text{UO}}} - b_{23} \right) + \hat{\nu}_{t+1}^{\text{LO}} b_{23} \right] = 0 \\
& (1.D.59)
\end{aligned}$$

$$\frac{\partial \mathcal{L}}{\partial M_{\text{LO},t+1}} = 0 \Leftrightarrow \hat{\nu}_t^{\text{LO}} - \hat{\beta}_t \left[\hat{\nu}_{t+1}^{\text{UO}} b_{23} \frac{M_{\text{EQ}}^{\text{UO}}}{M_{\text{EQ}}^{\text{LO}}} + \hat{\nu}_{t+1}^{\text{LO}} \left(1 - b_{23} \frac{M_{\text{EQ}}^{\text{UO}}}{M_{\text{EQ}}^{\text{LO}}} \right) \right] = 0 \quad (1.D.60)$$

$$\begin{aligned}
\frac{\partial \mathcal{L}}{\partial T_{\text{AT},t+1}} = 0 & \Leftrightarrow \hat{\eta}_t^{\text{AT}} - \hat{\beta}_t \left[-\lambda_{t+1} \Omega'(T_{\text{AT},t+1}) k_{t+1}^\alpha + \hat{\eta}_{t+1}^{\text{AT}} \left(1 - c_1 \frac{F_{2\text{XCO}_2}}{T_{2\text{XCO}_2}} - c_1 c_3 \right) + \hat{\eta}_{t+1}^{\text{OC}} c_4 \right] = 0 \\
& (1.D.61)
\end{aligned}$$

$$\begin{aligned}
\frac{\partial \mathcal{L}}{\partial T_{\text{OC},t+1}} = 0 & \Leftrightarrow \hat{\eta}_t^{\text{OC}} - \hat{\beta}_t \left[\hat{\eta}_{t+1}^{\text{AT}} c_1 c_3 + \hat{\eta}_{t+1}^{\text{OC}} (1 - c_4) \right] = 0 \\
& (1.D.62)
\end{aligned}$$

$$\begin{aligned}
\frac{\partial \mathcal{L}}{\partial \hat{\lambda}_t} = 0 & \Leftrightarrow (1 - \Omega(T_{\text{AT},t}) - \Theta(\mu_t)) k_t^\alpha + (1 - \delta) k_t - c_t - \exp(g_t^A + g_t^L) k_{t+1} = 0 \\
& (1.D.63)
\end{aligned}$$

$$\begin{aligned}
\frac{\partial \mathcal{L}}{\partial \hat{\nu}_t^{\text{AT}}} = 0 & \Leftrightarrow (1 - b_{12}) M_t^{\text{AT}} + b_{12} \frac{M_{\text{EQ}}^{\text{AT}}}{M_{\text{EQ}}^{\text{UO}}} M_t^{\text{UO}} + \sigma_t (1 - \mu_t) A_t L_t k_t^\alpha + E_t^{\text{Land}} - M_{t+1}^{\text{AT}} = 0 \\
& (1.D.64)
\end{aligned}$$

$$\frac{\partial \mathcal{L}}{\partial \hat{\nu}_t^{\text{UO}}} = 0 \Leftrightarrow b_{12} M_t^{\text{AT}} + \left(1 - b_{12} \frac{M_{\text{EQ}}^{\text{AT}}}{M_{\text{EQ}}^{\text{UO}}} - b_{23} \right) M_t^{\text{UO}} + b_{23} \frac{M_{\text{EQ}}^{\text{UO}}}{M_{\text{EQ}}^{\text{LO}}} M_t^{\text{LO}} - M_{t+1}^{\text{UO}} = 0 \quad (1.D.65)$$

$$\frac{\partial \mathcal{L}}{\partial \hat{\nu}_t^{\text{LO}}} = 0 \Leftrightarrow b_{23} M_t^{\text{UO}} + \left(1 - b_{23} \frac{M_{\text{EQ}}^{\text{UO}}}{M_{\text{EQ}}^{\text{LO}}} \right) M_t^{\text{LO}} - M_{t+1}^{\text{LO}} = 0 \quad (1.D.66)$$

$$\begin{aligned} \frac{\partial \mathcal{L}}{\partial \hat{\eta}_t^{\text{AT}}} = 0 \Leftrightarrow T_t^{\text{AT}} + c_1 \left(F_{2\text{XCO}_2} \frac{\log(M_t^{\text{AT}}/M_{\text{base}}^{\text{AT}})}{\log(2)} + F_t^{\text{EX}} \right) - c_1 \frac{F_{2\text{XCO}_2}}{T_{2\text{XCO}_2}} T_t^{\text{AT}} - \\ c_1 c_3 \left(T_t^{\text{AT}} - T_t^{\text{OC}} \right) - T_{t+1}^{\text{AT}} = 0 \end{aligned} \quad (1.D.67)$$

$$\frac{\partial \mathcal{L}}{\partial \hat{\eta}_t^{\text{OC}}} = 0 \Leftrightarrow T_t^{\text{OC}} + c_4 \left(T_t^{\text{AT}} - T_t^{\text{OC}} \right) - T_{t+1}^{\text{OC}} = 0, \quad (1.D.68)$$

as well as the KKT condition, that is,

$$1 - \mu_t \geq 0 \quad \perp \quad \hat{\lambda}_t^\mu \geq 0. \quad (1.D.69)$$

In our practical applications, though, we replace the KKT condition Eq. (1.D.69) above with the Fischer-Burmeister function (see, e.g., Maliar, Maliar, and Winant (2021), and references therein), that is,

$$\Psi^{\text{FB}} \left(\hat{\lambda}_t^\mu, 1 - \mu_t \right) = \hat{\lambda}_t^\mu + (1 - \mu_t) - \sqrt{\left(\hat{\lambda}_t^\mu \right)^2 + (1 - \mu_t)^2}, \quad (1.D.70)$$

where we replaced $\hat{\lambda}_t^\mu$ such that

$$\hat{\lambda}_t^\mu := -\hat{\lambda}_t \Theta'(\mu_t) k_t^\alpha - \hat{\nu}_t^{\text{AT}} \sigma_t A_t L_t k_t^\alpha \quad (1.D.71)$$

holds. We also use expression (1.D.56) to replace consumption c_t in the budget constraint (1.D.63).

One feature that appears when working with first-order conditions of an IAM is the need to compute them not only with respect to the economic choice variables such as μ_t and c_t , but also with respect to the climate variables, despite the fact that they are not choice variables. The reason for this is that one needs to assess the marginal effects of the change in choice variables that propagate through the climate system. Those effects cannot be computed analytically here, which is why we need Lagrange multipliers associated with every single climate equation (cf. expressions (1.D.41)-(1.D.45)) to estimate the shadow price of a marginal change in a respective constraint.

Using all the above definitions, the eight individual components that enter the loss function amendable for the DEQN algorithm read as

$$l_1 := \exp\left(g_t^A + g_t^L\right) \hat{\lambda}_t - \hat{\beta} \left[\hat{\lambda}_{t+1} \left((1 - \Omega(T_{AT,t+1}) - \Theta(\mu_t)) \alpha k_{t+1}^{\alpha-1} + (1 - \delta) \right) + \hat{\nu}_{t+1}^{AT} (1 - \mu_{t+1}) \sigma_{t+1} A_{t+1} L_{t+1} \alpha k_{t+1}^{\alpha-1} \right] = 0 \quad (1.D.72)$$

$$l_2 := (1 - \Omega(T_{AT,t}) - \Theta(\mu_t)) k_t^\alpha + (1 - \delta) k_t - c_t - \exp\left(g_t^A + g_t^L\right) k_{t+1} = 0 \quad (1.D.73)$$

$$l_3 := \hat{\nu}_t^{AT} - \beta \left[\hat{\nu}_{t+1}^{AT} (1 - b_{12}) + \hat{\nu}_{t+1}^{UO} b_{12} + \hat{\eta}_{t+1}^{AT} c_1 F_{2XCO2} \frac{1}{\ln 2 M_{AT,t+1}} \right] = 0 \quad (1.D.74)$$

$$l_4 := \hat{\nu}_t^{UO} - \beta \left[\hat{\nu}_{t+1}^{AT} b_{12} \frac{M_{EQ}^{AT}}{M_{EQ}^{UO}} + \hat{\nu}_{t+1}^{UO} \left(1 - b_{12} \frac{M_{EQ}^{AT}}{M_{EQ}^{UO}} - b_{23} \right) + \hat{\nu}_{t+1}^{LO} b_{23} \right] = 0 \quad (1.D.75)$$

$$l_5 := \hat{\nu}_t^{LO} - \beta \left[\hat{\nu}_{t+1}^{UO} b_{23} \frac{M_{EQ}^{UO}}{M_{EQ}^{LO}} + \hat{\nu}_{t+1}^{LO} \left(1 - b_{23} \frac{M_{EQ}^{UO}}{M_{EQ}^{LO}} \right) \right] = 0 \quad (1.D.76)$$

$$l_6 := \hat{\eta}_t^{AT} - \beta \left[-\hat{\lambda}_{t+1} \Omega'(T_{AT,t+1}) k_{t+1}^\alpha + \hat{\eta}_{t+1}^{AT} (1 - c_1 \frac{F_{2XCO2}}{T_{2xco2}} - c_1 c_3) + \hat{\eta}_{t+1}^{OC} c_4 \right] = 0 \quad (1.D.77)$$

$$l_7 := \hat{\eta}_t^{OC} - \beta \left[\hat{\eta}_{t+1}^{AT} c_1 c_3 + \hat{\eta}_{t+1}^{OC} (1 - c_4) \right] = 0 \quad (1.D.78)$$

$$l_8 := \hat{\lambda}_t^\mu + (1 - \mu_t) - \sqrt{(\hat{\lambda}_t^\mu)^2 + (1 - \mu_t)^2} = 0, \quad (1.D.79)$$

and result in the total loss function given by

$$\ell_\nu := \frac{1}{N_{\text{path length}} \sum_{\mathbf{x}_t \text{ on sim. path}} \sum_{m=1}^{N_{eq}=8} (l_m(\mathbf{x}_t, \mathcal{N}_\nu(\mathbf{x}_t)))^2}. \quad (1.D.80)$$

The final ingredient we need for the DEQN algorithm is the evolution of the state \mathbf{x}_t one period forward such that the loss function (1.D.80) can be evaluated along a simulated path. In CDICE, \mathbf{x}_{t+1} is given by

$$\mathbf{x}_{t+1} = \left(k_{t+1}, M_{t+1}^{AT}, M_{t+1}^{UO}, M_{t+1}^{LO}, T_{t+1}^{AT}, T_{t+1}^{OC}, t + 1 \right)^T, \quad (1.D.81)$$

where k_{t+1} is updated as a choice variable from the policy function Eq. (1.D.53) and the climate variables M_{t+1}^{AT} , M_{t+1}^{UO} , M_{t+1}^{LO} , T_{t+1}^{AT} , and T_{t+1}^{OC} can be updated via equations (1.D.64)-(1.D.68), whereas time t is simply incremented by one unit.

1.D.3 Error Statistics

Table 1.D11 provides detailed error statistics for the benchmark CDICE model at convergence (cf. all the normalized expressions (1.D.72) - (1.D.79) that contribute to the loss function (1.D.80)). All other models presented in the article reach a similar level of accuracy.

Stats.	l_1	l_2	l_3	l_4	l_5	l_6	l_7	l_8
mean	$1.13e-04$	$5.32e-04$	$2.29e-04$	$3.76e-04$	$1.15e-04$	$1.82e-05$	$3.07e-05$	$5.04e-04$
std	$6.35e-05$	$1.23e-04$	$1.15e-04$	$7.75e-05$	$6.31e-05$	$1.49e-05$	$2.42e-05$	$3.17e-04$
min	$1.19e-07$	$1.90e-05$	$5.36e-07$	$5.39e-05$	$1.18e-05$	$5.96e-08$	$< 1.0e-8$	$< 1.0e-8$
0.1%	$1.19e-07$	$1.91e-05$	$5.36e-07$	$5.39e-05$	$1.18e-05$	$5.96e-08$	$< 1.0e-8$	$< 1.0e-8$
25%	$5.82e-05$	$4.28e-04$	$1.37e-04$	$3.23e-04$	$6.71e-05$	$8.15e-06$	$1.09e-05$	$1.89e-04$
50%	$1.15e-04$	$5.28e-04$	$2.58e-04$	$3.62e-04$	$9.70e-05$	$1.33e-05$	$2.60e-05$	$5.06e-04$
75%	$1.70e-04$	$6.34e-04$	$3.16e-04$	$4.11e-04$	$1.58e-04$	$2.32e-05$	$4.71e-05$	$7.83e-04$
max.	$3.26e-04$	$9.83e-04$	$5.36e-04$	$7.40e-04$	$3.13e-04$	$8.54e-05$	$1.26e-04$	$1.30e-03$

Table 1.D11 Summary statistics of the loss function components along the simulation path for the optimal solution of the CDICE model. Following the literature (see, e.g., Brumm and Scheidegger (2017)), we define the maximum error as the 99.9 percent quantile of the error distribution.

Chapter 2

Deep Uncertainty Quantification for Stochastic Integrated Assessment Models[†]

Abstract

Integrated assessment models (IAMs) are essential tools in climate economics for guiding policy decisions and risk management. However, the reliability of IAMs is contingent upon assumptions about parameters and functional forms and the results are subject to significant uncertainty. To address these concerns, the current study presents a two-fold approach. Firstly, a stochastic IAM with Bayesian learning is constructed to address the uncertainty arising from the equilibrium climate sensitivity (ECS) in economy-climate models. Secondly, a computationally efficient framework is developed to solve the stochastic IAM while quantifying its parametric uncertainty using deep learning techniques. The proposed method is applicable beyond IAMs, offering insights into a variety of economic models.

This study contributes to enhancing the understanding of uncertainty in climate economics, offering a novel framework for addressing parameter uncertainty in complex economic models.

[†]This chapter is co-authored with Felix Kübler from the University of Zürich, Simon Scheidegger from the University of Lausanne, and Takafumi Usui from the University of Zürich.

Keywords: Climate policy, Epstein-Zin preferences, Deep learning, Uncertainty quantification, Gaussian processes

JEL classification: C61, C63, D58, H23, Q54, Q58

2.1 Introduction

In climate economics, integrated assessment models (IAMs) are crucial for making informed policy decisions and managing risks. However, as with any other economic model, their performance and results are dependent on sometimes restrictive assumptions about the parameters and functional forms. This can make one skeptical about their predictions. (Pindyck, 2013, 2017) claimed that certain inputs of IAMs - namely functional forms, e.g. damage function, and parameter values, e.g. preferences, climate sensitivity values - are arbitrary. Based on this (Pindyck, 2013, p. 860) warned against using the IAMs in general since IAMs "*have crucial flaws that make them close to useless as tools for policy analysis*". Rather than considering model uncertainty and parametric uncertainty as fatal limitations to the applicability of the whole class of the models, we address the issue by (i) building a stochastic IAM with Bayesian learning about the equilibrium climate sensitivity to study the most significant source of uncertainty in economy-climate models (ii) developing a unified computationally efficient framework for solving this stochastic IAM and quantifying its parametric uncertainty using the deep learning based solution method.

We depart from the stochastic version of the seminal DICE model (W. D. Nordhaus, 2017) with Epstein-Zin preferences (Epstein and Zin (1989) as presented in Jensen and Traeger (2014) and make certain changes to it. First, we adopt the re-calibrated climate module developed in Folini, Friedl, Kubler, and Scheidegger (2023). This way the climate dynamics match the most comprehensive global climate models that participated in the Coupled Model Intercomparison Project, Phase 5 (CMIP5). Second, equilibrium climate sensitivity (ECS), which is another iconic number in climate science (Knutti et al., 2017), is known to take enormous uncertainty, and the probability distribution of climate sensitivity exhibits fat-tailed, potentially causing catastrophic outcomes for the economy (Allen & Frame, 2007; Roe & Baker, 2007; Zaliapin & Ghil, 2010). We assume that the social planner in the model can update her belief on ECS following the Bayes rule, and we demonstrate that she effectively reduces uncertainty in climate sensitivity over time.

To perform the parametric uncertainty quantification we select two types of uncertainty: economic uncertainty and climate uncertainty. To study economic parametric uncertainty we select the pure rate of time preference, (see W. D. Nordhaus (2008) and N. Stern (2008)), intertemporal elasticity of substitution (IES), and relative risk aversion. To address the climate uncertainty we take the initial values of the prior distribution of the ECS and parameter affecting severity of damages. We propagate parametric uncertainty *globally* on the social cost of carbon. Global sensitivity analysis identifies non-linearities when mapping from input parameters to model outcomes considering interactions among input parameters, which are largely underestimated in conventional *local* or 'one-at-a-time' sensitivity analyses. Specifically, we employ Shapley values in addition to Sobol' indices and univariate effects, which are typically used in the recent economic literature see, among others, Harenberg, Marelli, Sudret, and Winschel (2019). By examining these metrics, we attribute the overall model variance to each input parameter, prioritize which parameter(s) shall be investigated, and in which direction each parameter affects the model outcomes.

To globally solve the model outlined above together with the uncertain parameters presents a formidable computational challenge. The problem has nine state variables, two sources of stochastic shocks, and six uncertain parameters. The high number of states in the problem implies the presence of the curse of dimensionality Bellman (1961). Strong non-linearities in the functional forms that come from the interaction of climate and economy together with the stochastic shocks make the problem impossible to solve by the traditional numerical methods for global optimisation. To address these issues we employ deep equilibrium nets (DEQN) - deep-learning based global solution method (Azinovic et al., 2022).¹ We leverage the fact that the stochastic gradient descent, the optimization routine we employed to train the neural net, can ameliorate the curse of dimensionality. Being able to efficiently handle the curse of dimensionality problem in the case of high-dimensional state spaces, we add the uncertain parameters as additional and continuous pseudo-states (Scheidegger & Billionis, 2019). This approach circumvents potential difficulties found in the literature, which limit the applications of global sensitivity analysis only to a deterministic case, for instance, see Miftakhova (2021a), or a simple stochastic model, for instance, see Harenberg et al. (2019). Our approximated policy functions

¹Kelly and Kolstad (1999) and Kelly and Kolstad (2001) interpolate the value function by the neural net.

globally support all possible realizations of model parameters in a single run instead of resolving the same model for varying model parameters. The parametric uncertainty is propagated by repeatedly simulating the model with the approximated policy functions from the first part at randomly drawn parameter vectors. In the literature, the sampling is typically done via Monte Carlo simulations, but due to the slow convergence properties of Monte Carlo, a very large number of sampling is necessary. Moreover, one model simulation requires a non-negligible computation cost, which makes global sensitivity analysis of large-scale models even infeasible. To overcome these, we interpolate mapping from input parameters to model outcomes using a Gaussian process-based surrogate model (Iooss & Prieur, 2019; Marrel, Iooss, Laurent, & Roustant, 2009). By deploying the surrogate model, we compute the Shapley values, the Sobol' indices, and the univariate effects with high accuracy but at a negligible computational cost. Finally, the application of the proposed numerical method is not limited to dynamic stochastic IAM. Rather, we use IAM as a showcase, and our method would be highly applicable to any economic model. We perform the uncertainty quantification analysis on the stochastic model with Bayesian learning over the ECS to evaluate the impact of the uncertain parameters on the value of the social cost of carbon (SCC) in the years 2020, 2050, and 2100. The Shapley and Sobol' indices show that for the SCC in 2020, the most contributing parameters are the initial belief of the social planner about the ECS value and the pure rate of time preferences. The IES has less of an impact and the variance of the initial belief about the ECS does not play any significant role in explaining the variance of the SCC in 2020. With the time uncertainty about the ECS resolves due to the learning. The value of the SCC becomes more robust towards the initial belief about the ECS. The impact of the pure rate of time preferences also diminishes with time. At the same time, the IES gains its importance in explaining the variance of the SCC, dominating all other uncertain parameters for the SCC value in 2100. The univariate effects - they indicate the direction of the impact of the uncertain parameters on the SCC - all show the expected direction of the influence, except the IES. Different from the literature studying the impact of the IES on the SCC in case of the TFP shock Jensen and Traeger (2014), Cai and Lontzek (2019), we find that with the IES increasing the SCC is decreasing. A significant difference of our model from the studies mentioned above, is that our model includes temperature shocks but no TFP shock. We believe that TFP shock and temperature shock may affect decision-making

under uncertainty differently, however this remains a future avenue for the research. The remainder of this article is organized as follows. In Section 2.2, we provide a brief review of the related literature. Next, we outline in Section 2.3 a stochastic IAM as a benchmark we intend to study. Section 2.4 introduces our generic uncertainty quantification framework and discusses its computational advantages relative to other existing methods. Section 2.5 presents an application of our proposed method. Section 2.6 finally concludes.

2.2 Literature Review

This paper is related to four key strands of the literature: i) research focusing on stochastic IAMs, ii) studies investigating the uncertain ECS, such as through Bayesian learning, iii) parametric UQ in IAMs, and iv) global solution methods based on machine learning.²

First, our paper contributes to a fast-growing body of literature on endogenizing economic and climate uncertainty in the IAMs to study, among other quantities, the SCC. Various studies (see, e.g., Golosov et al. (2014); Traeger (2019)) solve stochastic IAMs analytically and offer closed-form representations of the SCC but it comes at the expense of strong assumptions on the carbon cycle and other functional forms that enter the model. Other work that tackles IAMs with uncertainty while trying to maintain numerical tractability by introducing various assumptions consists of Traeger (2014), which implements a state-reduced and annually calibrated recursive dynamic programming version of the canonical DICE-2007 model (W. D. Nordhaus, 2008), (Crost & Traeger, 2013, 2014) to study uncertainty in the damage function, long-run growth risk is studies in (Jensen & Traeger, 2014), and climate tipping points (Lemoine & Traeger, 2014, 2016). Other work is based on deterministic finite-horizon models, which investigates the implications of uncertainty by Monte-Carlo sampling in the parameter space (see, e.g., Ackerman, Stanton, and Bueno (2010); Anthoff, Tol, and Yohe (2009); Gillingham et al. (2018); W. Nordhaus (2018)). One of the disadvantages of this approach is that “...*this first-order approximation to stochastic analysis does not model a decision maker’s optimal response to uncertainty.*” as Jensen and Traeger (2014) point out. In a series of papers, the team of authors (Cai & Lontzek, 2019; Lontzek et al., 2015; Lontzek & Narita, 2011), (Cai, Judd, Lenton, Lontzek, & Narita, 2015; Cai, Lenton, & Lontzek, 2016; Lontzek, Narita, & Wilms, 2016) examine the social cost of carbon under long-run growth risk and irreversible climate tipping,

²Hassler, Krusell, and Smith (2016a) provide an excellent general introduction and review on IAMs.

dropping many analytical simplifications and resorting to high-performance computing. McInerney, Lempert, and Keller (2012) explore the robust strategies of the climate policies and Barnett et al. (2020a) continue on the topic of robust decision-making in climate policies by studying ambiguity. Barnett (2023) applies an asset pricing approach to assess uncertainty related to climate change impact, and van der Ploeg (2021) take uncertainty into account, deriving the risk-adjusted discount rate. The work presented here differs from previous studies in that we introduce a deep-learning-based method to solve stochastic IAMs of unprecedented complexity without the need to analytically simplify IAMs in a restrictive way or tap high-performance computing systems.

Second, our work is related to studies examining the interplay of uncertainty in the ECS (Knutti et al., 2017) and the economy. Kelly and Kolstad (1999), subsequently followed for instance by Leach (2007), Jensen and Traeger (2013), Kelly and Tan (2015), Fitzpatrick and Kelly (2017), and Hwang et al. (2017), developed a dynamic stochastic IAM in a recursive formulation and considered Bayesian learning to update a posterior distribution of the equilibrium climate sensitivity parameter, which is unknown to the social planner. The literature found that the social planner with Bayesian learning resolves fat-tailed uncertainty in the equilibrium climate sensitivity in the long run. We build on the aforementioned literature of the Bayesian learning over the ECS and combine it with the disentangled Epstein-Zin preferences to capture the risk preferences and intertemporal consumption decisions under the long-run risk.

Third, our work contributes to studies that examine parametric uncertainty in IAMs.³ Parametric uncertainty is often evaluated by averaging over a large number of deterministic Monte-Carlo simulation runs, where input parameters are drawn from relevant distributions for each simulation (Ackerman et al., 2010; W. D. Nordhaus, 2008). Saltelli and D’Hombres (2010) criticize these Monte-Carlo analyses, as they follow the so-called *one-at-a-time* (OAT) principle and can be highly misleading, failing to offer reliable policy recommendations (Crost & Traeger, 2013). In our work presented below, we propagate and quantify the parametric uncertainty when computing the SCC using a global sensitivity analysis (GSA) method (see, e.g., (Smith, 2014) for a review). Anderson et al.

³Other sources of uncertainty, which we do not pursue in this paper but have been studied in the literature, include model misspecification and ambiguity (see, e.g. Barnett et al. (2020b); Zhao, Basu, Lontzek, and Schmedders (0)). Other sources of uncertainty encompass climate tipping points (Lenton et al., 2008), the damage function, and the transition to green technology. Weitzman (2012b), for instance, introduced a tipping point to the standard Nordhaus damage function, which raises damages dramatically for temperature increases beyond a given level.

(2014) and Butler, Reed, Fisher-Vanden, Keller, and Wagener (2014) are early examples where GSA is applied to the canonical DICE model based on a large number of Monte-Carlo samples. More recently, Miftakhova (2021a) constructed surrogate models⁴ of the deterministic DICE model using the polynomial chaos expansion method and analyzed the GSA of the SCC on various input parameters.⁵ In the GSA literature, the so-called Sobol' indices are standard metrics to measure the importance of some input parameters to overall model outcome uncertainty. An alternative, important metric in the context of UQ is the Shapley value. Owen (2014) adopted the idea of the Shapley value from the literature of cooperative game theory and demonstrated that the Shapley values intuitively attribute the overall variance of the model to some input variables but not necessarily to be matched to the Sobol' indices. Song, Nelson, and Staum (2016) proposed an efficient numerical routine to avoid traversing all permutations of input variables in estimating the Shapley values, and Iooss and Prieur (2019) efficiently sped up the numerical estimation of the Shapley values by replacing the true model with a Gaussian process-based surrogate model. Scheidegger and Billionis (2019) intrusively added the uncertain parameters as pseudo-state variables and solved the model globally for all possible realizations of the uncertain parameters in a single model evaluation. When enlarging the number of state variables, one has to overcome the curse of dimensionality (Bellman, 1961), which the authors addressed by applying the active subspace method (see also Constantine (2015); Kubler and Scheidegger (2023), and references therein). The current study enhances the existing body of knowledge by presenting novel, machine-learning-oriented techniques that capitalize on contemporary concepts originating from deep neural networks, Gaussian process regression, and the surrogate modeling approach. These methods are employed to conduct Global Sensitivity Analysis (GSA) within extensive Integrated Assessment Models (IAMs) in a resource-efficient manner. To the best of our comprehension, this work represents the pioneering endeavor to investigate Sobol' indices, Shapley values, and univariate effects within stochastic IAMs, while incorporating Bayesian learning regarding the Equilibrium Climate Sensitivity (ECS).

⁴A surrogate model is a high-precision approximation of an otherwise expensive-to-evaluate model, such as a high-dimensional, nonlinear, and non-stationary IAM. For more details on the applications of surrogate models in economics and finance, see, e.g., Chen, Didisheim, and Scheidegger (2021); Scheidegger and Billionis (2019), and references therein.

⁵Harenberg et al. (2019) is the first example in economics to present GSA based on a polynomial chaos expansion of a standard real-business-cycle model.

Finally, our work relates to the emerging but fast-growing literature on machine learning-based solution methods in dynamic economic models (see, e.g., Duarte (2018); Ebrahimi Kahou, Fernández-Villaverde, Perla, and Sood (2021); Fernández-Villaverde, Nuño, Sorg-Langhans, and Vogler (2020); Maliar et al. (2021); Renner and Scheidegger (2018); Villa and Valaitis (2019)). The numerical solution to stochastic IAMs is often achieved by applying traditional, grid-based value-function iteration (see, e.g., Cai and Judd (2014); Cai and Lontzek (2019), and references therein). However, while highly successful in small to mid-scale models, such methods are strongly limited when the model complexity increases, and consequently often needs to resort to high-performane computers. In our work presented below, we solve for the functional rational expectations equilibrium (Spear, 1988) of the IAM by adopting the so-called “deep equilibrium net” algorithm (Azinovic et al., 2022; Folini et al., 2023) to the context of stochastic, nonstationary IAMs. To the best of our knowledge, we are the first to implement a deep learning-based solution method to solve a high-dimensional and stochastic IAM with Bayesian learning about the equilibrium climate sensitivity parameter and to propagate parametric uncertainty using a Gaussian process-based surrogate model when estimating the social cost of carbon in a computationally efficient fashion, guaranteeing affordable numerical precision, as all our numerical results are computed on a laptop. This methodological contribution will enable the IAM community to tackle much richer models without the need of using hundreds of thousands of CPU hours of compute time on a supercomputer to solve a single model specification.

2.3 A Stochastic IAM with Bayesian Learning

This section posits a discrete-time stochastic IAM with Bayesian learning about the uncertain equilibrium climate sensitivity. Our model combines a stochastic representative agent framework with Epstein-Zin-Weil preferences (Epstein & Zin, 1989; Weil, 1989), a climate emulator⁶ that follows the specification of Folini et al. (2023), and stochastic tipping points modeled similarly to L. Kotlikoff et al. (2021b).

We proceed with the following four steps: First, in Section 2.3.1, we provide a brief summary of the economic building blocks of the model. Second, in Section 2.3.2, we

⁶To analyze climate change mitigation strategies, economists rely on simplified climate models – so-called climate emulators – that provide a realistic quantitative link between CO2 emissions and global warming at low computational costs.

outline the climate externality. Third, Section 2.3.3 describes our approach to modeling the learning process concerning the climate equilibrium sensitivity. Finally, in Section 2.3.4, we present the recursive formulation of our model. In addition, a comprehensive summary of the complete model calibration is available in Section 2.B.

2.3.1 The economic model

The economic side of our IAM is a growth model where production produces greenhouse gas emissions, and productivity is affected by the state of the climate. Following the spirit of W. D. Nordhaus (2017), we describe our economy using a Ramsey growth model in a social planner formulation. Within this economic setup, the model assumes a single, infinitely-lived representative agent.

We adopt the Epstein-Zin (-Weil) preferences (Epstein & Zin, 1989; Weil, 1989) to address the critical aspects of risk preferences and intertemporal consumption decisions in long-run climate policy discussions (see, e.g., Cai and Lontzek (2019); Crost and Traeger (2013), and references therein). The social welfare function U_t is recursively defined as follows:

$$U_t = \left[(1 - \beta) \frac{(C_t/L_t)^{1-1/\psi}}{1 - 1/\psi} L_t + e^{-\rho} \mathbb{E}_t \left[U_{t+1}^{1-\gamma} \right]^{\frac{1-1/\psi}{1-\gamma}} \right]^{\frac{1}{1-1/\psi}}, \quad (2.1)$$

where time t is discrete and measured in years, C_t represents consumption, and L_t denotes an exogenous population path adopted from W. D. Nordhaus (2017). In addition, ρ denotes the pure rate of time preference, ψ measures the intertemporal elasticity of substitution, γ represents the Arrow-Pratt risk aversion parameter, and $\mathbb{E}_t[\cdot]$ denotes the expectation operator conditional on time t .

The gross output Y_t^{Gross} in the economy is described by a standard Cobb-Douglas production function with labor-augmenting technological progress, that is,

$$Y_t^{\text{Gross}} = K_t^\alpha (A_t L_t)^{1-\alpha}, \quad (2.2)$$

where α elasticity of substitution of capital, and A_t is a deterministic trend (cf. Section 2.B). There is an externality to the production in the form of industrial carbon

emissions, $E_{\text{Ind},t}$, that reads as

$$E_{\text{Ind},t} = \sigma_t(1 - \mu_t)Y_t^{\text{Gross}}. \quad (2.3)$$

Through the emission flow, the economic side of our IAM affects the climate module (cf. Section 2.3.2 below). We follow W. D. Nordhaus (2017) and assume that the emissions produced are proportional to the final output, and scaled with an exogenous emission intensity σ_t . In our model, the emissions can be abated, that is, reduced, at a rate $\mu_t \in [0, 1]$. A zero abatement rate corresponds to the business-as-usual (BAU) case, whereas a value of $\mu = 1$, abatement corresponds to full mitigation.⁷ As W. D. Nordhaus (2017), we assume that abatement is costly for the social planner and depends on the abatement rate with the following functional form:

$$\Theta_t(\mu_t) = \theta_{1,t}\mu_t^{\theta_2}. \quad (2.4)$$

In Eq. (2.4), $\theta_{1,t}$ is an exogenous process for the abatement cost evolution, and θ_2 is a parameter of the abatement cost function (see Section 2.B for more details).

The unabated emissions enter the climate system and will ultimately lead to an increase in the temperature $T_{\text{AT},t}$ of the atmosphere (cf. Section 2.3.2). A rise in the atmospheric temperature triggers damages that, in turn, will affect the final output. In our modeling set-up, we employ the type of damage functions commonly used in the IAM literature. The damage function denoted by $\Omega_t(T_{\text{AT},t})$ is quadratic damage by W. D. Nordhaus (2017):

$$\Omega_t(T_{\text{AT},t}) = \frac{1}{1 + \pi_1 T_{\text{AT},t} + \pi_2 T_{\text{AT},t}^2}. \quad (2.5)$$

The abatement costs and the damages jointly reduce the gross output of the economy. Thus the budget constraint reads as follows:

$$(1 - \Theta_t(\mu_t))\Omega_t(T_{\text{AT},t})Y_t^{\text{Gross}} - C_t - I_t = 0. \quad (2.6)$$

⁷Note that in this augmented Ramsey model with a climate externality, the abatement rate is a choice variable for the social planner in addition to the standard choice of investment.

2.3.2 The climate model

In our modeling setup, we employ a climate emulator following the specification of Folini et al. (2023). This emulator is built on W. D. Nordhaus (2017) and comprises two fundamental building blocks: i) three stacked carbon reservoirs, i.e., boxes, that represent the global carbon cycle and ii) a two-layer energy balance model.

There are two sources of emissions that enter the simple carbon cycle: industrial emissions $E_{\text{Ind},t}$, as defined in Eq. (2.3), which are related to the economic activity of the representative agent, and exogenous emissions $E_{\text{Land},t}$. Their sum $E_t = E_{\text{Ind},t} + E_{\text{Land},t}$ constitutes the total emission flow entering the carbon cycle.

The three carbon reservoirs are represented by a three-dimensional vector $\mathbb{M}_t = (M_{\text{AT},t}, M_{\text{UO},t}, M_{\text{LO},t})$, where the entries represent the mass of carbon in the atmosphere (AT), upper ocean (UO) and lower ocean (LO) respectively. The concentration of carbon in those three boxes evolves according to a diffusion process described by the following expression:

$$\mathbb{M}_{t+1} = B\mathbb{M}_{t+1} + E_t, \quad (2.7)$$

where A is given by

$$B = \begin{pmatrix} 1 - b_{12} & b_{21} & 0 \\ b_{12} & 1 - b_{21} - b_{23} & b_{32} \\ 0 & b_{23} & 1 - b_{32} \end{pmatrix}. \quad (2.8)$$

The diffusion coefficients $b_{12}, b_{21}, b_{23}, b_{32}$ that we will employ in our computations are based on the calibration by Folini et al. (2023).

The baseline energy balance system—which we will have to slightly modify in Section 2.3.3—comprises two layers: the temperature of the atmosphere, $T_{\text{AT},t+1}$ (representing the atmosphere and upper ocean), and the temperature of the deep ocean, $T_{\text{OC},t}$, which are described by the following equations:

$$T_{\text{AT},t+1} = \left(1 - c_1 c_3 - c_1 \frac{F_{2\text{xco}_2}}{\Delta T_{\text{AT},\times 2}} \right) T_{\text{AT},t} + c_1 c_3 T_{\text{OC},t} + c_1 \left(F_{2\text{xco}_2} \log_2 \left(\frac{M_{\text{AT},t}}{M_{\text{AT}}^*} \right) + F_{\text{EX},t} \right) \quad (2.9)$$

$$T_{\text{OC},t+1} = c_4 T_{\text{AT},t} + (1 - c_4) T_{\text{OC},t}. \quad (2.10)$$

$F_{2\times\text{CO}_2}$ denotes the forcing of equilibrium CO2 doubling, $\Delta T_{\text{AT},\times 2}$ is the ECS, M_{AT}^* stands for the equilibrium mass of carbon in the atmosphere, $F_{\text{EX},t}$ represents exogenous radiative forcing, and c_1, c_3, c_4 are temperature-related parameters. All values, except the ECS, are calibrated according to Folini et al. (2023). A detailed discussion about the ECS follows in Section 2.3.3. More details on the calibration of our climate model are given in Section 2.B.

2.3.3 Bayesian learning over the equilibrium climate sensitivity

The climate response in the form of the atmospheric temperature increase to the emissions (cf. Section 2.3.2) is subject to uncertainty in many ways. However, the ECS is presumably the most controversial number determining how severe climate change will be in the long run (Knutti et al., 2017), as arguments between Roe and Baker (2007) and Zaliapin and Ghil (2010) in the climate science community illustrate. Therefore, in order to take state-of-the-art climate science seriously in our IAM, Eq. (2.9) has to be modified appropriately.

Empirical observations, as well as studies based on energy-balance models and global climate models, suggest that the probability density function of the ECS is most likely to peak in the region $[2.0^\circ\text{C}, 4.5^\circ\text{C}]$, but exhibits a highly skewed and fat-tailed distribution (Roe & Baker, 2007). The latter authors, among others, pointed out that the ECS, $T_{\text{AT},\times 2}$, relates to the following feedback process:

$$T_{\text{AT},\times 2} = \frac{T_{\text{AT},\times 2}^0}{1 - f}, \quad (2.11)$$

where f denotes the so-called climate feedback parameter, and $T_{\text{AT},\times 2}^0$ is a reference climate sensitivity parameter, and which is known to the social planner. Climate feedback consists of the climate processes (such as clouds, precipitation, forest greening, etc.) which can either magnify or lessen the effect of climate forcings. The climate feedback parameter determines the actual amplitude of the climatic response to the climate forcings (IPCC (2021)). If the absolute value of the feedback parameter is small, the warming will be weaker and if it is big, the warming will be more intense. The true value of the climate feedback parameter is not known with certainty. Thus, the uncertainty in the equilibrium climate sensitivity $T_{\text{AT},\times 2}$ can be represented as the uncertainty in the climate feedback parameter f . Following Roe and Baker (2007), we assume that f follows a Gaussian distribution. By substituting Eq. (2.11) into Eq. (2.9), we obtain

$$T_{\text{AT},t+1} = \left(c_1 \frac{F_{2\text{xco}_2}}{\Delta T_{\text{AT},\text{x}_2}^0} f + 1 - c_1 c_3 - c_1 \frac{F_{2\text{xco}_2}}{\Delta T_{\text{AT},\text{x}_2}^0} \right) T_{\text{AT},t} + c_1 c_3 T_{\text{OC},t} + c_1 \left(F_{2\text{xco}_2} \log_2 \left(\frac{M_{\text{AT},t}}{M_{\text{AT}}^*} \right) + F_{\text{EX},t} \right) + \tilde{\epsilon}_{T,t+1}, \quad (2.12)$$

where the uncertainty about the ECS is now modeled indirectly via f . Following the literature, we introduce the Gaussian distributed shock $\tilde{\epsilon}_{T,t+1} \sim \mathcal{N}(0, S_{\epsilon_T})$, which the social planner cannot observe.

Following a seminar strand of literature on Bayesian learning (see, e.g., Fitzpatrick and Kelly (2017); Hwang et al. (2017); Kelly and Kolstad (1999); Kelly and Tan (2015); Leach (2007); Webster, Jakobovits, and Norton (2008)), we update the social planner's belief on the climate feedback parameter, not the ECS parameter, which is uncertain to the social planner. The social planner subjectively assumes his belief on the climate feedback parameter in period t , \tilde{f}_{t+1} , when solving the dynamic programming problem.

As Roe and Baker (2007) suggest,⁸ we assume that his prior belief on \tilde{f}_{t+1} follows a Gaussian distribution with mean $\mu_{f,t}$ and variance $S_{f,t}$. We also assume that the distribution is truncated from below at $\underline{f} = 0.45$ and from above at $\bar{f} = 0.85$. This means that $\tilde{f}_{t+1} \sim \mathcal{N}(\mu_{f,t}, S_{f,t}, \underline{f}, \bar{f})$ ⁹, and leads to an enhanced expression for the evolution of the atmospheric temperature, that is,

$$T_{\text{AT},t+1} = \left(c_1 \frac{F_{2\text{xco}_2}}{\Delta T_{\text{AT},\text{x}_2}^0} \tilde{f}_{t+1} + 1 - c_1 c_3 - c_1 \frac{F_{2\text{xco}_2}}{\Delta T_{\text{AT},\text{x}_2}^0} \right) T_{\text{AT},t} + c_1 c_3 T_{\text{OC},t} + c_1 \left(F_{2\text{xco}_2} \log_2 \left(\frac{M_{\text{AT},t}}{M_{\text{AT}}^*} \right) + F_{\text{EX},t} \right) + \tilde{\epsilon}_{T,t+1}. \quad (2.13)$$

In period t , we denote the prior probability function of the social planner's belief of the climate feedback parameter, which follows the Gaussian distribution with mean μ_t^f and variance $S_{f,t}$, as $p(f)$. Given the prior $p(f)$, the planner observes the atmospheric temperature change and the likelihood function of which is also given as a Gaussian $p(T_{\text{AT}} | f)$. By applying Bayes' rule, the posterior probability function of the climate feedback param-

⁸We take initial values for the prior mean, and prior variance as in Roe and Baker (2007). With this, we need to take a value of a reference climate sensitivity $\Delta T_{\text{AT},\text{x}_2}^0 = 1.2^\circ\text{C}$. This value, together with the starting value of the prior mean to a large extent, corresponds to our baseline calibration of the ratio between radiative forcing that is $F_{2\text{xco}_2} = 3.45\text{W}/\text{m}^2$ and equilibrium climate sensitivity that is $\Delta T_{\text{AT},\text{x}_2} = 3.25^\circ\text{C}$.

⁹The details of numerical integration of the truncated normal distribution are presented in Section 2.C.2.

eter given the observation T_{AT} is also Gaussian distributed, and reads as:

$$p(f | T_{AT}) \propto p(T_{AT} | f) \times p(f) \quad (2.14)$$

Following Kelly and Tan (2015), we rewrite the two stochastic components in Eq. (2.13) as

$$\begin{aligned} & \left(1 - c_1 c_3 - c_1 \frac{F_{2\text{xco2}}}{\Delta T_{AT, \times 2}^0}\right) T_{AT,t} + c_1 c_3 T_{OC,t} + c_1 \left(F_{2\text{xco2}} \log_2 \left(\frac{M_{AT,t-1}}{M_{AT}^*}\right) + F_{EX,t}\right) \\ & + \varphi_{1C} \tilde{f}_{t+1} T_{AT,t} + \tilde{\epsilon}_{T,t+1} - T_{AT,t+1} = 0, \end{aligned} \quad (2.15)$$

where $\varphi_{1C} = c_1 \frac{F_{2\text{xco2}}}{\Delta T_{AT, \times 2}^0}$, and where $\tilde{f}_{t+1} \sim \mathcal{N}(\mu_{f,t}, S_{f,t}, \underline{f}, \bar{f})$, $\tilde{\epsilon}_{T,t+1} \sim \mathcal{N}(0, S_{\epsilon_T})$. Finally, by applying DeGroot (1970, p. 167, Theorem 1), we can analytically compute the posterior mean and the variance, that is,

$$\mu_{f,t+1} = \frac{S_{\epsilon_T} \mu_{f,t} + \varphi_{1C} T_{AT,t} \left(\varphi_{1C} T_{AT,t} \tilde{f}_{t+1} + \tilde{\epsilon}_{T,t+1}\right) S_{f,t}}{S_{\epsilon_T} + (\varphi_{1C} T_{AT,t})^2 S_{f,t}} \quad (2.16)$$

$$S_{f,t+1} = \frac{S_{\epsilon_T} S_{f,t}}{S_{\epsilon_T} + (\varphi_{1C} T_{AT,t})^2 S_{f,t}}. \quad (2.17)$$

2.3.4 The recursive formulation

After having put all building blocks in place in Sections 2.3.1 to 2.3.3, we now present the recursive formulation of our IAM with Bayesian learning about the ECS. The social planner chooses consumption C_t , investment K_{t+1} and mitigation $\mu_t \in [0, 1]$ to solve

$$V(\mathbf{X}_t)^{1-1/\psi} = \max_{C_t, K_{t+1}, \mu_t} \left\{ \left(\frac{C_t}{L_t}\right)^{1-1/\psi} L_t + e^{-\rho} \mathbb{E}_t \left[V(\mathbf{X}_{t+1})^{1-\gamma} \right]^{\frac{1-1/\psi}{1-\gamma}} \right\} \quad (2.18)$$

$$\text{s.t.} \quad (1 - \Theta(\mu_t)) \Omega_t (T_{AT,t}) K_t^\alpha (A_t L_t)^{1-\alpha} - C_t - I_t = 0 \quad (2.19)$$

$$(1 - \delta) K_t + I_t - K_{t+1} = 0 \quad (2.20)$$

$$1 - \mu_t \geq 0 \quad (2.21)$$

$$(1 - b_{12}) M_{AT,t} + b_{21} M_{UO,t} + (1 - \mu_t) \sigma_t K_t^\alpha (A_t L_t)^{1-\alpha} + E_{Land,t} - M_{AT,t+1} = 0 \quad (2.22)$$

$$b_{12} M_{AT,t} + (1 - b_{21} - b_{23}) M_{UO,t} + b_{32} M_{LO,t} - M_{UO,t+1} = 0 \quad (2.23)$$

$$b_{23} M_{UO,t} + (1 - b_{32}) M_{LO,t} - M_{LO,t+1} = 0 \quad (2.24)$$

$$(1 - c_1 c_3 - \varphi_{1C}) T_{AT,t} + c_1 c_3 T_{OC,t} + c_1 \left(F_{2\text{xco}_2} \log_2 \left(\frac{M_{AT,t}}{M_{AT}^*} \right) + F_{EX,t} \right) + \varphi_{1C} \tilde{f}_{t+1} T_{AT,t} + \tilde{\epsilon}_{T,t+1} - T_{AT,t+1} = 0 \quad (2.25)$$

$$c_4 T_{AT,t} + (1 - c_4) T_{OC,t} - T_{OC,t+1} = 0 \quad (2.26)$$

$$\frac{S_{\epsilon_T} \mu_{f,t} + \varphi_{1C} T_{AT,t} (\varphi_{1C} T_{AT,t} \tilde{f}_{t+1} + \tilde{\epsilon}_{T,t+1}) S_{f,t}}{S_{\epsilon_T} + (\varphi_{1C} T_{AT,t})^2 S_{f,t}} - \mu_{f,t+1} = 0 \quad (2.27)$$

$$\frac{S_{\epsilon_T} S_{f,t}}{S_{\epsilon_T} + (\varphi_{1C} T_{AT,t})^2 S_{f,t}} - S_{f,t+1} = 0 \quad (2.28)$$

$$\tilde{f}_{t+1} \sim \mathcal{N}(\mu_{f,t}, S_{f,t}, \underline{f}, \bar{f}), \tilde{\epsilon}_{T,t+1} \sim \mathcal{N}(0, S_{\epsilon_T}) \quad (2.29)$$

$$\Omega_t(T_{AT,t}) = \frac{1}{1 + \pi_1 T_{AT,t} + \pi_2 T_{AT,t}^2} \quad (2.30)$$

where the Bellman equation, given by Eq. (2.18) is subject to the budget constraint (2.19), the occasionally binding upper bound on mitigation variable μ_t , the three laws of motion of the carbon concentration in the atmosphere (2.22), in the upper ocean (2.23) and in the lower ocean (2.24), the two laws of motion of the atmospheric temperature (2.25) and the ocean temperature (2.26), the Bayesian updates of the ECS, and the stochastic motion of the damage coefficients.

In Eq. (2.18), the the state of the model is given by $\mathbf{X}_t = (K_t, \mathbf{\Gamma}_t, \mathbf{S}_t, t; \boldsymbol{\vartheta})$, where $\mathbf{\Gamma}_t = (M_{AT,t}, M_{UO,t}, M_{LO,t}, T_{AT,t}, T_{OC,t})$ denote the climate variables, $\mathbf{S}_t = (\mu_{f,t}, S_{f,t})$ the mean and variance of the agent's beliefs, whereas t abbreviates the state variable that handles time. Finally, $\boldsymbol{\vartheta}$ is a collection of N uncertain parameters $\boldsymbol{\vartheta} = (\vartheta_1, \dots, \vartheta_N)$, which we consider pseudo state variables (Scheidegger & Bilonis, 2019), and over which the planner, in contrast to the other stochastic variables, does not compute expectations. Thus, the total dimensionality d of the IAM, therefore, is given by:

$$d = |K_t| + |\mathbf{\Gamma}_t| + |\mathbf{S}_t| + |t| + |\boldsymbol{\vartheta}| = 1 + 5 + 2 + 1 + N = 9 + N. \quad (2.31)$$

2.4 Deep Uncertainty Quantification

This section introduces our computational framework called "Deep Uncertainty Quantification" (Deep UQ), which can effectively solve non-stationary high-dimensional dynamic stochastic climate economy models and perform uncertainty quantification (UQ) at neg-

ligible computational costs.¹⁰ An important task in UQ, and the one we are concerned with in this paper, is to measure the relative importance of the various parameter inputs to quantities of interest, such as the SCC. Importance can be quantified via the effects of changing those inputs at random. This leads to a global sensitivity analysis (Saltelli et al., 2008), in which statistical methods based on an analysis of variance decomposition measure variable importance. However, the measures traditionally used in the literature, that is, Sobol’ indices, univariate effects, and Shapley values (see, e.g., Owen (2014) and Song et al. (2016), and references therein) typically require thousands, if not tens of thousands of model solutions to obtain convergent statistics (Harenberg et al., 2019). Thus, such an approach is a significant roadblock for performing UQ on stochastic IAMs, where a single model solution can take more than 100k CPU hours (Cai & Lontzek, 2019). Consequently, the previous literature on UQ in IAMs has typically been limited to local perturbations of solutions to stochastic models or to global sensitivity analysis in non-stochastic settings (see, e.g., Anderson et al. (2014), Butler et al. (2014) and Miftakhova (2021a), and references therein).

We now introduce a two-step approach for performing global sensitivity analysis in IAMs to alleviate the abovementioned challenges. First, we adopt a generic, deep learning-based algorithm for solving stochastic IAMs globally¹¹ as a function of the endogenous and exogenous state variables as well as their parameters at once in a single model solution (cf. Section 2.3.4). Such a “deep surrogate” – a high-precision approximation of an IAM based on deep neural networks,¹² speeds up the model evaluations required to perform UQ by orders of magnitudes and thus allows for various compute-intensive applications, as the respective tasks now simplify to interpolation tasks on the pre-computed optimal policies—which are now functions of the state variables and parameters—rather than solving an entire model for a fixed set of parameters. Second, we propose constructing a second, cheap-to-evaluate surrogate model for the quantities of interests (QoIs), such as SCC, to perform global sensitivity analysis by using the former neural network surrogate of the IAM as an input. For computational tractability, we propose to use Gaussian Process

¹⁰For a textbook treatment of UQ, see, e.g., Saltelli et al. (2008), and references therein.

¹¹A *global solution* adheres to the model equilibrium conditions throughout the entire state space, that is, the computational domain. In contrast, a *local solution* is only concerned with the local approximation around a point, typically the deterministic steady state of the model, as discussed, e.g., in Eftekhari and Scheidegger (2022).

¹²For a thorough introduction to deep surrogates in economics and finance, see, e.g., Chen et al. (2021), and references therein.

Regression (GPR) as the surrogate modeling technique to approximate QoIs as a function of the model parameters.¹³

In what follows, we introduce our Deep UQ methodology in three steps. First, we outline in Section 2.4.1 how “Deep Equilibrium Nets” can be adapted to compute global solutions to (non-stationary) stochastic IAM model as a function of its economic states and parameters (Section 2.4.1), and how the resulting optimal policies can subsequently be used to construct cheap-to-evaluate surrogate models for derived quantities of interest, such as the SCC, by using GPR (Section 2.4.1). Section 2.4.2 introduces the global sensitivity measures we intend to study in the context of our IAM. Section 2.4.3 finally presents the Deep UQ algorithm formally. Additional implementation details are found in Section 2.C.

2.4.1 Surrogate models for IAMs

Deep equilibrium nets

There are substantial computational bottlenecks in solving the type of IAMs detailed in Section 2.3 as a function of endogenous and exogenous states as well as parameters in a single model evaluation globally because of i) the presence of random shocks, ii) a high-dimensional state space, iii) strong non-linearities in the optimal policies (introduced, for instance, by the presence of highly non-linear damage functions (see, e.g., Cai and Lontzek (2019), and references therein), iv) irregular, that is, non-hypercubic geometries of the set of states visited along a simulation, and v) non-stationarity. In the presence of these five features, the curse of dimensionality (Bellman, 1961) imposes a considerable roadblock. While some methods can handle a subset of i) - v), most fail at matching all five requirements. Currently, and to the best of our knowledge, the only numerically tractable method that jointly addresses all five features relies on deep neural networks. Therefore, Section 2.4.1 will briefly summarize the general idea of DEQN, thereby adopting the notation of Azinovic et al. (2022); Folini et al. (2023).

¹³In this study, we deliberately construct the surrogate models using two different function approximators. As a rule of thumb, one should use a surrogate model based on deep neural networks when dealing with large datasets that require learning complex nonlinear relationships. For example, in the context of solving our stochastic, nonlinear IAMs, we generate billions of observations in the solution process to train our neural network. Hence, we apply neural networks. Conversely, surrogate models based on GPs are appropriate when dealing with small datasets or when interpretability is a priority over predictive accuracy. Consequently, since in our concrete case, the SCC and other QoIs are based on relatively expensive simulations based on the model solution, we apply GPs in the latter case.

The DEQN algorithm is a simulation-based solution method using deep neural networks to compute an approximation of the *optimal policy function* $\mathbf{p} : X \rightarrow Y \subset \mathbb{R}^M$ to a dynamic model under the assumption that the underlying economy can be characterized via discrete-time first-order equilibrium conditions, that is,

$$\mathbf{G}(\mathbf{x}, \mathbf{p}) = \mathbf{0} \quad \forall \mathbf{x} \in X \subset \mathbb{R}^d. \quad (2.32)$$

Intuitively, DEQNs work as follows: An unknown policy function is approximated with a neural network, that is, $\mathbf{p}(\mathbf{x}) \approx \mathcal{N}_\nu(\mathbf{x})$, and where the ν 's are ex-ante unknown coefficients of the neural network that have to be determined based on some suitable loss function measuring the quality of a given approximation at a given state of the economy.

Although there are several different types of deep neural networks, we use in this paper the so-called densely-connected feedforward neural networks (FNN).¹⁴ Following the literature, we define an L -layer FNN as a function $\mathcal{NN}^L(\mathbf{x}) : \mathbb{R}^{d_{\text{input}}} \rightarrow \mathbb{R}^{d_{\text{output}}}$ and say that there are $L - 1$ hidden layers such that the ℓ -th layer has N_ℓ neurons. In our concrete case, $K = N_0 = d_{\text{in}}$ and $M = N_L = d_{\text{output}}$.¹⁵ Furthermore, for each $1 \leq \ell \leq L$, we define a so-called weight matrix $\mathbf{W}^\ell \in \mathbb{R}^{N_\ell \times N_{\ell-1}}$ and bias vector $\mathbf{b}^\ell \in \mathbb{R}^{N_\ell}$. Then, letting $A^\ell(\mathbf{x}) = \mathbf{W}^\ell \mathbf{x} + \mathbf{b}^\ell$ be the affine transformation in the ℓ -th layer, for some non-linear activation function $\sigma(\cdot)$ such as relu, swish, or selu, an FNN is given by

$$\mathbf{p}(\mathbf{x}) \approx \mathcal{N}_\nu(\mathbf{x}) = \mathcal{NN}^L(\mathbf{x}) = A^L \circ \sigma_{L-1} \circ A^{L-1} \circ \dots \circ \sigma_1 \circ A^1(\mathbf{x}). \quad (2.33)$$

In Figure 2.1, we illustrate a simple FNN with two hidden layers. The selection of hyper-parameters $\{L, \{N_l\}_{l=1}^L, \{\sigma_l(\cdot)\}_{l=1}^L\}$ is known as the architecture selection. Approaches to determine these hyper-parameters include using prior experience, manual, random, or grid search, as well as more complex methods such as Bayesian optimization (see, e.g., Bergstra, Bardenet, Bengio, and Kégl (2011)).

The DEQN algorithm to determine $\mathbf{p}(\mathbf{x})$ is started by randomly initializing the ν 's (Glorot & Bengio, 2010), that is, an arbitrary guess for the ex-ante unknown approximate policy

¹⁴Neural networks are universal function approximators (Hornik, Stinchcombe, & White, 1989), can resolve highly non-linear features, and can handle a large amount of high-dimensional input data. See, e.g., Goodfellow et al. (2016) for an excellent introduction to deep learning.

¹⁵Recall that in our model, we $d_{\text{in}} = d = 10 + N$ input dimensions (cf. Eq. (2.31)). Furthermore, $d_{\text{output}} = 3$, as we have our model has three choice variables, that is, choices consumption, investment, and mitigation (cf. Section 2.3.4).

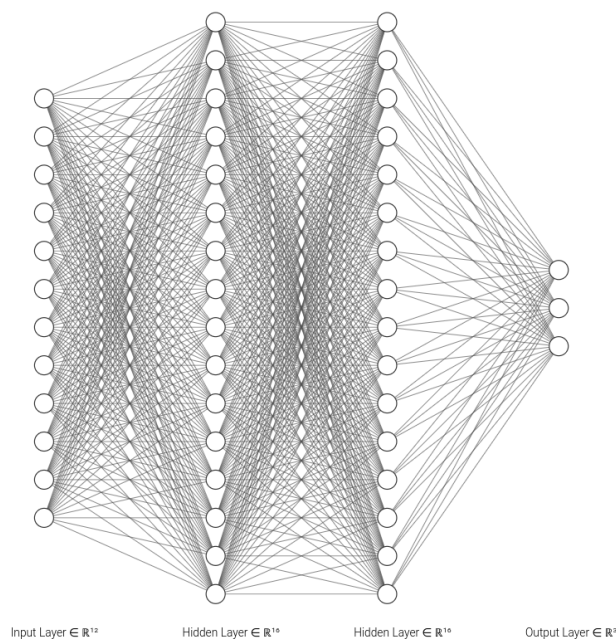


Fig. 2.1 The figure above depicts an FNN, where the input \mathbf{x} is a 12–dimensional vector, two hidden layers with 16 neurons each, and $\mathbf{p}(\mathbf{x})$ is a 3–dimensional output, thereby representing a stylized architecture for an IAM with 10 economic state variables, two parameters that are considered as pseudo-states, and three control variables (cf. Eq. (2.31)).

function. Next, we simulate a sequence of $N_{\text{path length}}$ states. Starting from some given state \mathbf{x}_t , the next state \mathbf{x}_{t+1} is a result of the policies encoded by the neural network, $\mathcal{N}_\nu(\mathbf{x})$, and remaining, model-implied dynamics.

If we knew the (approximate) policy function satisfying the equilibrium conditions, Eq. (2.32) would hold along a simulated path. However, since the neural network is initialized with random coefficients, $\mathbf{G}(\mathbf{x}_t, \mathcal{N}_\nu(\mathbf{x}_t)) \neq \mathbf{0}$ along the simulated path of length $N_{\text{path length}}$. This fact is now leveraged to improve the quality of the guessed policy function. Specifically, DEQNs use a loss function as the error in the equilibrium conditions, that is,

$$\ell_\nu := \frac{1}{N_{\text{path length}}} \sum_{\mathbf{x}_t \text{ on sim. path}} \sum_{m=1}^{N_{eq}} (G_m(\mathbf{x}_t, \mathcal{N}_\nu(\mathbf{x}_t)))^2, \quad (2.34)$$

where $G_m(\mathbf{x}_t, \mathcal{N}_\nu(\mathbf{x}_t))$ represent all the N_{eq} first-order equilibrium conditions of a given model, that is, $\mathbf{G}(\mathbf{x}_t, \mathcal{N}_\nu(\mathbf{x}_t)) = \sum_{m=1}^{N_{eq}} (G_m(\mathbf{x}_t, \mathcal{N}_\nu(\mathbf{x}_t)))$. Expression (2.34) can now be

used to update the weights of the network with any variant of gradient descent,¹⁶ namely,

$$\nu'_k = \nu_k - \alpha^{\text{learn}} \frac{\partial \ell(\boldsymbol{\nu})}{\partial \nu_k}, \quad (2.35)$$

where ν'_k represents the updated k -th weight of the neural network, and where $\alpha^{\text{learn}} \in \mathbb{R}$ denotes the so-called learning rate. The updated neural network-based representation of the policy is subsequently used to simulate a sequence of length $N_{\text{path length}}$ steps, along which the loss function is recorded, and the latter is again used to update the network parameters. This iterative procedure is pursued until $\ell_{\boldsymbol{\nu}} < \epsilon \in \mathbb{R}$, that is, an approximate equilibrium policy, has been found.

In summary, the DEQN algorithm consists of four building blocks: i) deep neural networks for approximating the equilibrium policies; ii) a suitable loss function measuring the quality of a given approximation at a given state of the economy; iii) an updating mechanism to improve the quality of the approximation; and iv) a sampling method for choosing states for updating and evaluating of the approximation quality. In Section 2.C.1, the step-by-step procedure for mapping stochastic and non-stationary climate economic models in general, and our model in particular, onto the neural network-based DEQN solution framework is provided.

Gaussian process surrogate models for global sensitivity analysis

We now briefly introduce the Gaussian process regression (GPR), a probabilistic approach for modeling a regression problem¹⁷ that we will use below to construct surrogates for approximating and interpolating quantities of interest (QoIs), such as the SCC, as a function of the model input parameters, to enable the swift computation of global sensitivity measures such as the Sobol' indices, the univariate effects and the Shapley values (cf. Section 2.4.2 below).

GPR assumes that the underlying function is a sample from a Gaussian process (GP). The latter is defined by a mean function, $m(x)$, and a covariance function, $k(x, x')$. For a regression problem, we are given a set of n input-output pairs, $\mathcal{D} = \{x_i, y_i\}_{i=1}^n = [X, y]$, where $x_i \in \mathbb{R}^d$, $y_i \in \mathbb{R}$, $X \in \mathbb{R}^{n \times d}$ and $y \in \mathbb{R}^{n \times 1}$, and to which the literature also

¹⁶In our practical applications, we use "Adam" (Kingma & Ba, 2014).

¹⁷See, e.g., Rasmussen and Williams (2005), for a textbook treatment.

refers to as “training dataset” or “experimental design”.¹⁸ The goal is to “learn”, that is, approximate a function $f(x)$ that maps inputs to outputs. In GPR, one often assumes that the output y is generated by a noisy evaluation of the function $f(x)$, i.e., $y = f(x) + \epsilon$, where $\epsilon \sim \mathcal{N}(0, \sigma_\epsilon^2)$, as it renders the computations numerically more stable (see, e.g., Murphy (2012); Rasmussen and Williams (2005)).

The prior distribution over functions is given by a GP, that is, $f(x) \sim \mathcal{GP}(m(x), k(x, x'))$. In practical applications, the mean function, $m(x)$, is often set to a constant value, e.g., zero. The covariance function, $k(x, x')$, defines the correlation between two arbitrary inputs x and x' . The exact choice of the kernel within an application depends on how the modeler encodes prior knowledge about the function(s) to be approximated, such as differentiability and periodicity. In our work below, we use the Matérn 5/2 kernel, which is given by:

$$k(x, x') = \sigma_f^2 \left(1 + \frac{\sqrt{5}r}{\rho} + \frac{5r^2}{3\rho^2} \right) \exp \left(-\frac{\sqrt{5}r}{\rho} \right), \quad (2.36)$$

where σ_f^2 denotes the variance parameter, and ρ represents the length scale parameter. The distance r between x and x' can be calculated using a suitable metric, such as the Euclidean distance.¹⁹

Given the input-output pairs in \mathcal{D} , we can compute the posterior distribution over functions using Bayes’ rule, that is,

$$p(f_* | x_*, \mathcal{D}) = \mathcal{N}(\mu_*, \sigma_*^2), \quad (2.37)$$

where x_* is an arbitrary point from the computational domain (also referred to as “test input”), f_* is the corresponding output, and μ_* and σ_*^2 are the mean and variance of the predictive distribution. They can be computed as:

$$\mu_*(x_*) = k(x_*, X)[K(X, X) + \sigma_\epsilon^2 I]^{-1} y, \quad (2.38)$$

$$\sigma_*^2(x_*) = k(x_*, x_*) - k(x_*, X)[K(X, X) + \sigma_\epsilon^2 I]^{-1} k(X, x_*), \quad (2.39)$$

¹⁸Below, the input vector x_i will be given by the vector of parameters of dimensionality N (cf. Eq. (2.31)), whereas corresponding observations y_i will represent the QoIs.

¹⁹Note that the hyperparameters of the covariance function are typically estimated by maximizing the likelihood (Rasmussen & Williams, 2005). For more details on kernels, see, e.g., Murphy (2022, Ch. 18.2).

where $K(X, X')$ is the matrix of pairwise covariances between inputs in X and X' . Moreover, I is an identity matrix, and σ_ϵ is the assumed noise level of observations, that is, the variance of ϵ . Thus, the interpolation value of a function at a location x_* is given by $f(x_*) = \mu_*$. For more details on GPs, see, e.g., Renner and Scheidegger (2018), and references therein.

Below, we require cheap-to-evaluate GP surrogates for one particular QoI as a function of the model input parameters that is relevant to the climate policy and for which we intend to perform global sensitive analysis at any given point in time. The SCC is defined as the marginal cost of atmospheric carbon in terms of the numeraire good. Following the literature (see, e.g., Traeger (2014)), we define SCC as the marginal rate of substitution between atmospheric carbon concentration of a 1000 Gt of carbon where $c2co2$ represents carbon to CO2 transformation coefficient²⁰ and the normalized capital stock, that is,

$$SCC_t = \frac{-(\partial V_t / \partial M_{AT,t}) / c2co2}{\partial V_t / \partial K_t} = \frac{-(\partial v_t / \partial M_{AT,t}) / c2co2}{\partial v_t / \partial k_t} A_t L_t. \quad (2.40)$$

To enable a comparison to related studies, we focus below on the SCC in the year 2100, a date commonly used in the literature (see, e.g., Cai and Lontzek (2019)), that is,

$$y_{SCC} = \mathbb{E}[SCC_{2100}]. \quad (2.41)$$

To construct the GP surrogates of the QoI mentioned above as a function of the model input parameters $\boldsymbol{\vartheta}$, we proceed as follows:²¹ We generate a training set $\mathcal{D}_s = \{\boldsymbol{\vartheta}_i, y_i\}_{i=1}^n = [\Theta_s, y_s]$ consisting of n sample vectors $\boldsymbol{\vartheta}_i \in \mathbb{R}^N$ from a joint (uniform) distribution of the uncertain model parameters (cf. Section 2.3.4), whereas $y_i \in \mathbb{R}$ corresponds to the QoI at a given combination of parameters and can be generated at essentially zero computational costs by interpolating on the DEQN surrogate of the pre-computed IAM solution (cf. Eq. (2.33)).

Next, we fit a GP model to the training data set \mathcal{D}_s . We use the predictive mean, $\mu_*(\boldsymbol{\vartheta})$, of the respective GP model that we denote by $\mathcal{M}_{GP|\Theta_s, y_s}$, as the interpolation value

²⁰The stock of carbon in the carbon cycle is measured in 1000 Gt of carbon; however, the backstop cost as in W. D. Nordhaus (2017) is measured in 1000 Gt of CO₂ emissions; thus, to obtain a correct value for the SCC, we need to transform a value measured in carbon into CO₂ by the transformation coefficient $c2co2 = 3.666$.

²¹In Section 2.4.1, we generally introduce the GPR that is trained on a set of n input-output pairs, which is $\mathcal{D} = \{x_i, y_i\}_{i=1}^n = [X, y]$. Hereafter we focus more on our specific case where the mode input parameters are denoted by $\boldsymbol{\vartheta}_i$, not x_i and define the n input-output pairs $\mathcal{D}_s = \{\boldsymbol{\vartheta}_i, y_i\}_{i=1}^n = [\Theta_s, y_s]$.

for the respective QoI, that is, y_{SCC} .²² Evaluating $\mu_*(\cdot)$ numerically is extremely fast, as the algorithmic complexity is linearly in the size n of the training data set (cf. Eq. (2.38)). Thus, global sensitivity analysis of very rich specified models (cf. Section 2.4.2) now becomes numerically tractable. More details regarding the accuracy of GP surrogate models are provided in Section 2.C.4.

2.4.2 Global sensitivity analysis in a nutshell

In this section, we present a formal introduction to surrogate-based global sensitivity analysis.

Some definitions

We commence our discussion on GSA by introducing essential notation, following the notation set forth by Harenberg et al. (2019); Sudret (2008). Let us define a (true) mathematical model $\mathcal{M}(\cdot)$ that maps

$$\boldsymbol{\vartheta} \in \mathcal{D}_{\boldsymbol{\vartheta}} \subset \mathbb{R}^N \rightarrow Y = \mathcal{M}(\boldsymbol{\vartheta}) \in \mathbb{R}, \quad (2.42)$$

where Y is a QoI²³ that is, a random endogenous outcome of the computational model $\mathcal{M}(\cdot)$, where $\boldsymbol{\vartheta} = (\vartheta_1, \dots, \vartheta_N)$ is the random vector of N input parameters, where each of which is characterized by a probability density function (PDF) $f_{\vartheta_i}, i = 1, \dots, N$, and where the joint density $f_{\boldsymbol{\vartheta}}$ is defined over a probabilistic space (see, e.g., Jaynes (1957, 1982)). The corresponding ex-ante unknown distribution of the endogenous output Y is inferred by evaluating the model on a large sample of parameter values drawn from the specified distribution $f_{\boldsymbol{\vartheta}}$, a technique that is termed *uncertainty propagation* (see, e.g., Sudret (2008) and references therein). Based on this distribution, we next look at three particular types of metrics that are typically studied in UQ, namely, Sobol' indices (Section 2.4.2), univariate effects (Section 2.4.2), and Shapley values (Section 2.4.2).

²²Note that the GP surrogate is redundant when a QoI is not a derived quantity from the optimal policies such as μ_t . In contrast, where a QoI relies on simulations such as the SCC, constructing a GP-based surrogate can reduce the computational burden substantially since next to evaluating the exact formula of the SCC at n points to train a GP, everywhere else in the parameter space, the respective quantity can be retrieved by evaluating the surrogate model.

²³Recall that in our case, we consider the SCC as a function of the model parameters at a given point in time (cf. Eq. (2.40)).

Sobol' indices

Variance-based GSA methods discriminate among all the model's parameters according to their contribution to the variance of its output. In our concrete case, we intend to study which (combinations of) parameters drive the QoI's volatility by applying Sobol's decomposition (Sobol, 2001). Given a square-integrable function $\nu(\cdot)$ over the N -dimensional unit hypercube $\Omega_N \subset \mathbb{R}^N$, Sobol's decomposition is given by²⁴

$$\nu(\boldsymbol{\vartheta}) = \nu_0 + \sum_{i=1}^N \nu_i(\vartheta_i) + \sum_{1 \leq i < j \leq N} \nu_{i,j}(\vartheta_i, \vartheta_j) + \cdots + \nu_{1,2,\dots,N}(\vartheta_1, \vartheta_2, \dots, \vartheta_N), \quad (2.43)$$

where the components of the expansion are given by $\nu_0 = \mathbb{E}[\nu(\boldsymbol{\vartheta})]$, $\nu_i(\vartheta_i) = \mathbb{E}[\nu(\boldsymbol{\vartheta}) \mid \vartheta_i] - \nu_0$, $\nu_{ij}(\vartheta_i, \vartheta_j) = \mathbb{E}[\nu(\boldsymbol{\vartheta}) \mid \vartheta_i, \vartheta_j] - \nu_0 - \nu_i(\vartheta_i) - \nu_j(\vartheta_j)$, and so forth.²⁵ Furthermore, $\mathbb{E}[\cdot]$ is the expectation operator, and $\mathbb{E}[\nu(\boldsymbol{\vartheta}) \mid \vartheta_i]$ is the expectation of the function $\nu(\boldsymbol{\vartheta})$ conditional on its input ϑ_i .

It is common practice in the UQ literature to apply the Sobol expansion given by Eq. (2.43) to decompose the variance of a given QoI,

$$\text{Var}[Y] = \mathbb{E}[(\mathcal{M}(\boldsymbol{\vartheta}) - \mathbb{E}[\mathcal{M}(\boldsymbol{\vartheta})])^2], \quad (2.44)$$

into its partial variances, that is,

$$\text{Var}[Y] = \sum_{i=1}^N \text{Var}[\mathcal{M}_i(\vartheta_i)] + \sum_{1 \leq i < j \leq N} \text{Var}[\mathcal{M}_{ij}(\vartheta_i, \vartheta_j)] + \cdots + \text{Var}[\mathcal{M}_{\mathcal{K}}(\boldsymbol{\vartheta})], \quad (2.45)$$

where $\text{Var}[\mathcal{M}_{\mathbf{u}}(\boldsymbol{\vartheta}_{\mathbf{u}})]$ denotes the partial variances for any subset of parameter indices $\mathbf{u} \subset 1, \dots, N$, and $\mathcal{K} = \{1, \dots, N\}$ is a full set of uncertain parameters. A natural extension to the relative shares of partial variances in the total variance leads to the well-known sensitivity measures, i.e., Sobol' indices (Sobol, 2001). For any subset of parameters' indices \mathbf{u} , the Sobol' index is defined as

$$S_{\mathbf{u}} = \frac{\text{Var}[\mathcal{M}_{\mathbf{u}}(\boldsymbol{\vartheta}_{\mathbf{u}})]}{\text{Var}[Y]}. \quad (2.46)$$

²⁴Note that expression Eq. (2.43) is unique if the components of the expansion are orthogonal.

²⁵Sobol's decomposition is closely related to a function approximation technique called "high-dimension model representation" (see, e.g., Ma and Zabaras (2010), Eftekhari and Scheidegger (2022); Eftekhari, Scheidegger, and Schenk (2017), and references therein).

The Sobol’ indices given by Eq. (2.46) are indicators used in the variance-based sensitivity analysis (Sobol, 2001). In practical terms, Sobol’ indices quantify which uncertain parameters and non-linear interactions among uncertain parameters primarily contribute to the variances of model outcomes. In other words, one can *screen* uncertain parameters to decrease overall model variance by investigating the Sobol’ indices. In our work below, we particularly look at the first-order Sobol’ index when we set $\mathbf{u} = \{i\}$ in Eq. (2.46), that is,

$$S_i = \frac{\text{Var}[\mathcal{M}_i(\vartheta_i)]}{\text{Var}[Y]}. \quad (2.47)$$

In our numerical examples below, we follow Marrel et al. (2009); Oakley and O’Hagan (2004) and use the predictive mean of the fitted GP surrogate model $\mathcal{M}_{GP|\vartheta_s, y_s}$ instead of the “true” $\mathcal{M}(\cdot)$ to enable a swift computation of the first-order Sobol’ indices defined in Eq. (2.47).²⁶

Univariate effects

From the aforementioned variance decomposition, we do not obtain any information as to which direction a QoI moves when the uncertain parameters deviate from their benchmark values. To this end, GSA is also concerned with computing univariate effects (Younes et al., 2013). Formally, a univariate effect represents the model’s conditional expectation given its parameter ϑ_i , that is,

$$\mathcal{U}(\vartheta_i) = \mathbb{E}[\mathcal{M}(\vartheta|\vartheta_i)]. \quad (2.48)$$

As we discussed in Section 2.4.2, we replace the true “true” $\mathcal{M}(\cdot)$ again by the GP surrogate model $\mathcal{M}_{GP|\vartheta_s, y_s}$, and evaluate the model outputs by using the posterior mean of the GP.

Shapley value

An essential task in UQ is to attribute the uncertainty of the overall outcome of the model to various input parameters. In the field of GSA, the Sobol’ indices have been widely

²⁶Next to GPs, polynomial chaos expansions is also commonly used in the literature to construct surrogate models for the swift computation of Sobol’ indices (see, e.g., Harenberg et al. (2019); Sudret (2008)).

adopted for variance decomposition (Harenberg et al., 2019; Saltelli et al., 2008). On the other hand, the economic literature, especially in cooperative game theory, has studied a similar problem and developed a solution concept known as the Shapley value (Shapley, 1953; Winter, 2002). The key idea behind the Shapley value is to determine a fair way to attribute the value created by a team effort to each team member. Based on this insight, Owen (2014) introduced a global sensitivity measure that is based on the Shapley value, and shows that the Shapley value is a compelling choice for identifying how much model variance can be attributed to the uncertainty in input parameters.

Following Owen (2014); Song et al. (2016) and our previously introduced notation we define a Shapley value for the i -th uncertain parameter as:

$$Sh_i = \sum_{\mathbf{u} \subseteq \mathcal{K} \setminus i} \frac{(N - |\mathbf{u}| - 1)! |\mathbf{u}|!}{N!} \left(\text{Var} [\mathcal{M}_{\mathbf{u} \cup \{i\}}(\boldsymbol{\vartheta}_{\mathbf{u} \cup \{i\}})] - \text{Var} [\mathcal{M}_{\mathbf{u}}(\boldsymbol{\vartheta}_{\mathbf{u}})] \right), \quad (2.49)$$

where $N = |\mathcal{K}|$ is the size of the whole set and $|\mathbf{u}|$ is the size of subset \mathbf{u} . We also define $\text{Var} [\mathcal{M}_{\emptyset}(\boldsymbol{\vartheta}_{\emptyset})] = 0$. Eq. (2.49) measures the incremental cost when including parameter i in set \mathbf{u} averaged over all sets $\mathbf{u} \subseteq \mathcal{K} \setminus i$. Owen (2014) proposes to choose

$$\text{Var} [\mathcal{M}_{\mathbf{u}}(\boldsymbol{\vartheta}_{\mathbf{u}})] = \text{Var}_{\mathbf{u}} \left[\mathbb{E}_{\mathcal{K} \setminus \mathbf{u}} [Y | \boldsymbol{\vartheta}_{\mathbf{u}}] \right], \quad (2.50)$$

with which one can measure a similar effect as the one of the first-order Sobol' indices. Another functional form of the cost function used in the literature is given by the following expression:

$$\text{Var} [\mathcal{M}_{\mathbf{u}}(\boldsymbol{\vartheta}_{\mathbf{u}})] = \mathbb{E}_{\mathcal{K} \setminus \mathbf{u}} \left[\text{Var}_{\mathbf{u}} \left[Y | \boldsymbol{\vartheta}_{\mathcal{K} \setminus \mathbf{u}} \right] \right]. \quad (2.51)$$

Song et al. (2016) prove that the Shapley values using either the cost function in Eq. (2.50) or Eq. (2.51) are equivalent. Furthermore, when numerically estimating the Shapley value, Sun, Apley, and Staum (2011) pointed out that the Monte Carlo estimation of the inner expectation operator in Eq. (2.50) requires a sufficiently large number of model evaluations and could be highly biased. On the other hand, the estimation in Eq. (2.51) is unbiased for all sample sizes. Consequently, we use Eq. (2.51) in all our computations.

When the number of uncertain parameters N , as in our case, is reasonably "small", one typically uses the "exact" method by Song et al. (2016). The latter involves traversing

$N!$ permuted sets. To enhance the efficiency of the Monte Carlo sampling required for precise evaluation of the expectation and variance operators, we again employ the GP-based surrogate model, thereby replacing the original model; that is, we utilize the predictive mean of the posterior for this purpose.²⁷

2.4.3 The deep uncertainty quantification algorithm

After having discussed the ingredients to our “Deep UQ” methodology in Section 2.4.1 and Section 2.4.2, we now present code listing Section 2.4.3 the complete algorithm. It consists of two fundamental building blocks. First, the DEQN is used to solve the IAM as a function of all endogenous, exogenous, and pseudo-state variables in a single solution step. The resulting neural network-based surrogate model then serves as an input to construct Gaussian Process (GP) surrogates for QoI metrics, such as the SCC. Subsequently, UQ can be performed on these GP surrogates to assess and analyze the uncertainty in the model predictions.

²⁷See Iooss and Prieur (2019) for more technical details.

Algorithm 1 Deep UQ algorithm

Part 1: Deep equilibrium nets

Approximate policy functions $p(x_t)$ using DEQN parametrized by the coefficients ν , where $x_t \equiv [K_t, \Gamma_t, \mathbf{X}_t, t; \vartheta]$.

Input:

Neural network architecture and hyper-parameters, simulation length T (length of an episode), α^{learn} (learning rate), x_0 (initial states). Upper and lower bound of the pseudo states $\vartheta \in [\underline{\vartheta}, \bar{\vartheta}]$.

Output:

The neural network's trained parameters ν^* , such that the policy function $p(x_t) \approx \mathcal{NN}(x_t)$ minimizes the loss function, i.e., the system of the first-order equilibrium conditions.

while $\ell_\nu > \epsilon$ do

$x_0^i \leftarrow x_0$ ▷ Initialize the states at time 0

$\mathcal{D}_{\text{train}}^i \leftarrow \{x_0, x_1^i, x_2^i, \dots, x_T^i\}$ ▷ Generate training data based on the previous policy $p^{i-1}(x_t)$

Evaluate a loss function

$$\ell_\nu := \frac{1}{N_{\text{path length}}} \sum_{x_t \text{ on sim.}} \sum_{m=1}^{N_{\text{eq}}} (G_m(x_t, \mathcal{NN}(x_t)))^2$$

for $k \in \{1, 2, \dots, \text{len}(\nu)\}$ do

▷ Perform stochastic gradient descent

$$\nu'_k = \nu_k - \alpha^{\text{learn}} \frac{\partial \ell(\nu)}{\partial \nu_k}$$

end for

$i \leftarrow i + 1$

▷ Go to the next episode $i + 1$

end while

return $\nu^* \leftarrow \nu^i$

▷ Optimal policy at convergence: $p^*(x_t) \approx \mathcal{NN}(x_t)$

Part 2: Uncertainty quantification based on GP surrogate models

Uncertainty quantification using the predictive mean of the GP surrogate model $\mathcal{M}_{\text{GP}|\Theta_s, y_s}$.

Input:

$p^*(x_t)$ (optimal policy functions), n (size of training set for the GPs), and y (QoI, e.g., the SCC).

Output:

S_i (the first-order Sobol' indices), U_i (the univariate effects) and Sh_i (the Shapley values) for the uncertain parameter ϑ_i .

while $\epsilon_{\text{GP}|\Theta_s, y_s}^{\text{LOO}} \geq \epsilon_{\text{GP}}^{\text{LOO}}$ do ▷ Criterion to ensure high-quality GP surrogate model (cf. Appendix B.3)

for $j \in \{1, \dots, n\}$ do ▷ Generate a training set \mathcal{D}_s for the GP

$y_j = \mathcal{M}(\vartheta_j)$ ▷ Compute the QoI for a given combination of parameters ϑ_j by using $p^*(x_t)$

end for

Fit the GP model $\mathcal{M}_{\text{GP}|\Theta_s, y_s}$ to \mathcal{D}_s

Compute the leave-one-out error $\epsilon_{\text{GP}|\Theta_s, y_s}^{\text{LOO}}$

$n \leftarrow n + 1$

▷ Increase the size of the training set if necessary

end while

return $\mathcal{M}_{\text{GP}|\Theta_s, y_s}$ ▷ Accurate GP surrogate model; used to replace true model $\mathcal{M}(\cdot)$ in UQ tasks

for $i \in \{1, \dots, N\}$ do

▷ UQ for each uncertain parameter ϑ_i

Compute the Sobol' indices S_i (cf. Eq. (47)).

Compute the univariate effects \mathcal{U}_i (cf. Eq. (48)).

Compute the Shapley values Sh_i following (cf. Eq. (49)).

return S_i, \mathcal{U}_i and Sh_i

end for

2.5 Results

This section reports the illustrative results. First, we describe the parameter choices for the uncertainty quantification. Second, we briefly present the optimal policy results for three types of models: the fully deterministic model, the model with the temperature shock and the one with the Bayesian learning over the equilibrium climate sensitivity - our benchmark model. Third, we complete the section with discussing the results of the uncertainty quantification with respect to the benchmark model and outlining the further research steps.

2.5.1 Parameters for the uncertainty quantification analysis

We subjectively select uncertain parameters ϑ as summarized in Table 2.1. We introduce three uncertain parameters from the economic module and three from the climate module. From the economic module we include the pure rate of time preferences ρ , the Arrow-Patt relative risk aversion γ and the intertemporal elasticity of substitution ψ that characterize the Epstein-Zin preferences.

From the climate module we include the initial values of the prior mean $\mu_{f,0}$ and variance $S_{f,0}$ of the Bayesian learning process over equilibrium climate sensitivity. We as well include damage parameter π_2 that is a part of quadratic damage function.

As there is no apriori knowledge available on the distribution of each uncertain parameter ϑ_i , in line with Harenberg et al. (2019), we assume a uniform distribution with a lower $\underline{\vartheta}_i$ and upper bound $\bar{\vartheta}_i$, and each parameter ϑ_i is statistically independent, as reported in Table 2.1. $\vartheta_i \in [\underline{\vartheta}_i, \bar{\vartheta}_i]$ shall be plausible yet still arbitrary selected to include common values in the literature.

Table 2.1 Parameter ranges for the uncertainty quantification analysis.

Parameter	ϑ_i^0	$\underline{\vartheta}_i$	$\bar{\vartheta}_i$	Source etc.
ρ	0.015	0.01	0.02	N. Stern (2008)
γ	10	2.5	12.5	Jensen and Traeger (2014) and Cai and Lontzek (2019)
ψ	1.5	1.2	2.0	Jensen and Traeger (2014) and Cai and Lontzek (2019)
π_2	0.00236	0.002	0.008	W. D. Nordhaus (2017) and Weitzman (2012b)
$\mu_{f,0}$	0.65	0.45	0.73	Roe and Baker (2007) and Folini et al. (2023)
$S_{f,0}$	0.0169	0.01	0.04	Roe and Baker (2007)

2.5.2 Optimal policy

In this section, we present and briefly discuss the optimal policy results for the deterministic model, a model with the temperature shock without learning, and a model with Bayesian learning over the ECS. In the Figure 2.2 we see that optimal emissions are the highest for the case with learning and the lowest for the deterministic case. The intuition behind this result is that to quicker learn the ECS the agent needs to emit more carbon in the beginning.

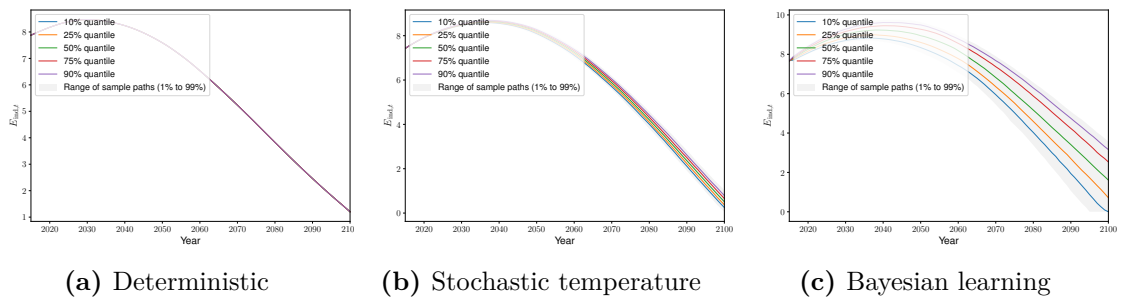


Fig. 2.2 Emissions in deterministic case (left), with temperature shocks (middle), and with Bayesian learning (right).

The mean of atmospheric temperature increase in the Figure 2.3 is approximately the same in all the cases and comprises $2.4 - 2.5^\circ\text{C}$. The variance of the temperature increase is observed to be the highest in the case of learning, as the model features two types of shocks, one to the climate feedback parameter and one to the temperature itself.

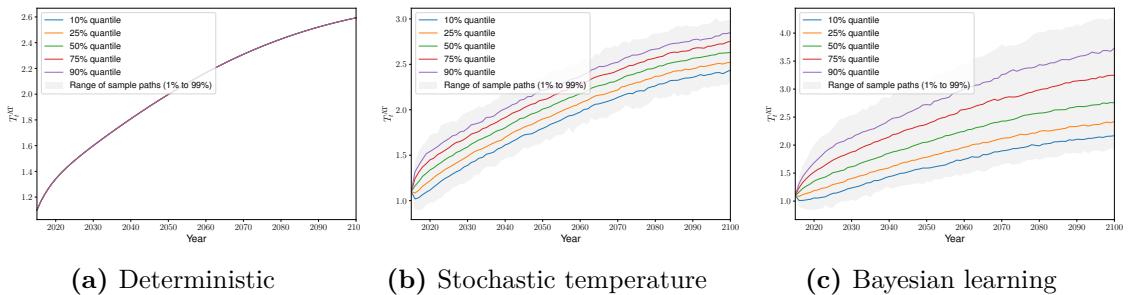


Fig. 2.3 Temperature of the atmosphere in deterministic case (left), stochastic temperature (middle), and with learning (right).

Abatement level in Figure 2.4 as well as the value of the social cost of carbon in Figure 2.5 are the lowest for the deterministic case, with more abatement in place in case

of a stochastic temperature and also in case of learning. This reveals the precautionary motive of the agent, to increase abatement in case of uncertainty.

The abatement rate as well as the SCC in the case of stochastic temperature are slightly higher than in the case of learning. This happens because in the case of learning the agent's precautionary motive to increase abatement in response to uncertainty is counteracted by the gains of more emissions, which help the agent to learn quicker and resolve uncertainty quicker.

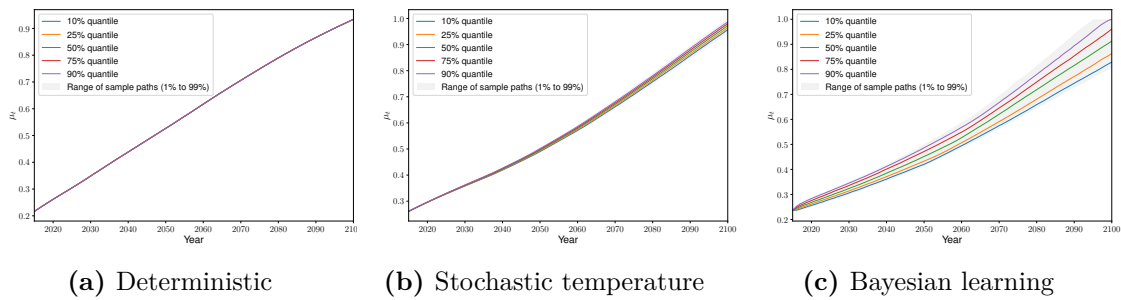


Fig. 2.4 Abatement in deterministic case (left), stochastic temperature (middle), and with Bayesian learning (right).

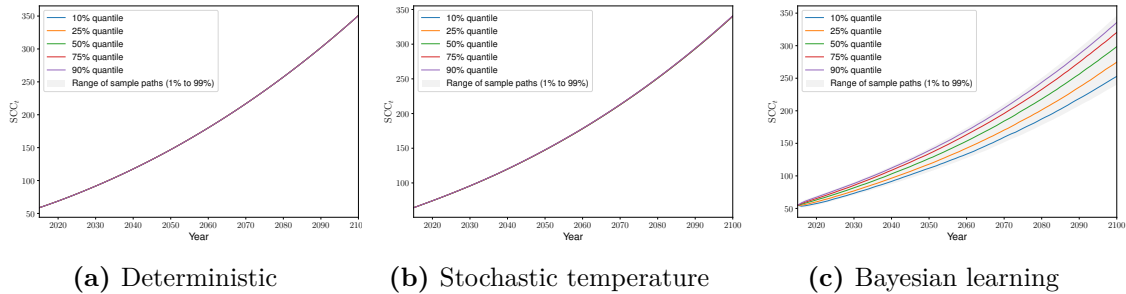


Fig. 2.5 SCC in deterministic case (left), stochastic temperature (middle), and with Bayesian learning (right).

Overall the results found from a comparison of three types of models correspond to the findings in the literature for example Kelly and Tan (2015) and Hwang et al. (2017). However, our results are different from Jensen and Traeger (2013). They find that first, there is no change in mitigation and a slight increase in emissions in the stochastic temperature case in comparison to the deterministic case. Second, they also find that there is more mitigation under the Bayesian learning case in comparison to the stochastic temperature case. The differences in results can be potentially explained by the fact that Jensen and Traeger (2013) did not use the disentangled Epstein-Zin preferences and also the variance

of the stochastic temperature shock in their model is almost two orders of magnitude higher than in our model.

2.5.3 Uncertainty quantification results

The set of figures Figures 2.6 to 2.8 presents the value of Shapley indices (in blue) and Sobol' indices (in green) for the impact of uncertain parameters on the value of the SCC in the years 2020, 2050, and 2100. Both indices measure the contribution of the variance of uncertain parameters to the variance of the quantity of interest, in our case the value of the SCC.

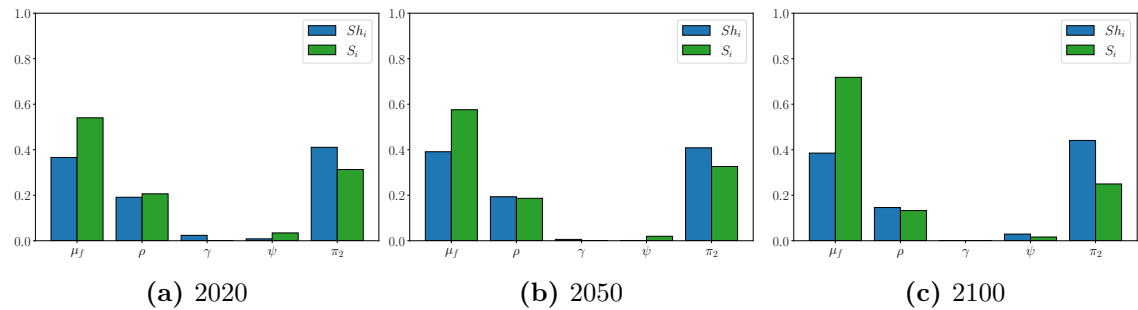


Fig. 2.6 Impact of the uncertain parameters on the SCC in 2020 (left), SCC in 2050 (middle), and SCC in 2100 (right) in the deterministic model.

In the fully deterministic case (Figure 2.6) ECS contributes the most to the variance of the SCC together with the damage parameter. Over time the influence of the ECS on the variance of the SCC remains constant with a slight tendency to get higher, and the impact of the damages remains constant with a modest leaning to lower values. The same diminishing over time pattern can be observed in the pure rate of time preferences contribution. These impacts are related, as damages are reflected in the social cost of carbon through the discount rate. With time the contribution of the discount rate on the SCC variance drops, so the damages follow the same pattern. Neither the intertemporal elasticity of substitution (IES) nor the relative risk aversion parameters matter for the social cost of carbon, which is predictable, as in the deterministic case Epstein-Zin preferences collapse into the standard CRRA preferences.

In the case of the model with the temperature shock, the IES starts to play a significant role in the variance of the SCC. The damage parameter remains important as in the deterministic case but with less of an impact. Interestingly enough, in the case of the temperature shock, there is no observed impact of the ECS on the variance of the SCC. It

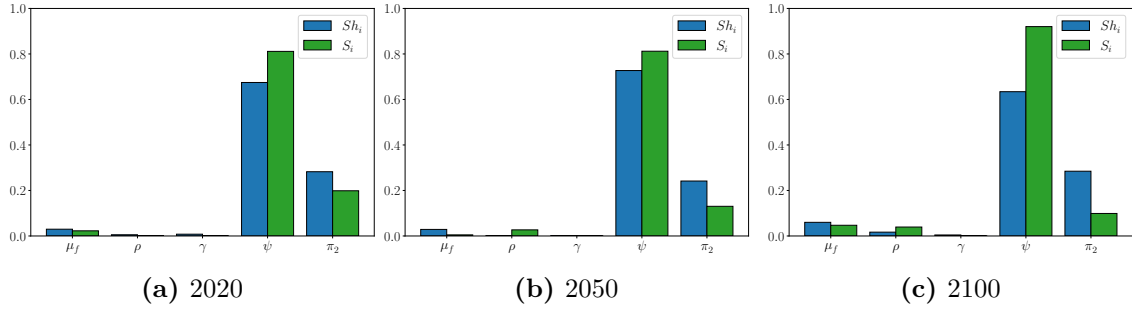


Fig. 2.7 Impact of the uncertain parameters on the SCC in 2020 (left), SCC in 2050 (middle), and SCC in 2100 (right) in the model with temperature shock.

appears that uncertainty related to the climatic factor is not reflected in the variance of the SCC in the presence of internalized temperature uncertainty. At the same time, the impact of the IES by far dominates the contribution of the other uncertain parameters on the variance of the SCC. The value of consumption smoothing preferences alone explains around eighty percent of the SCC variance. All the impacts remain rather constant with time.

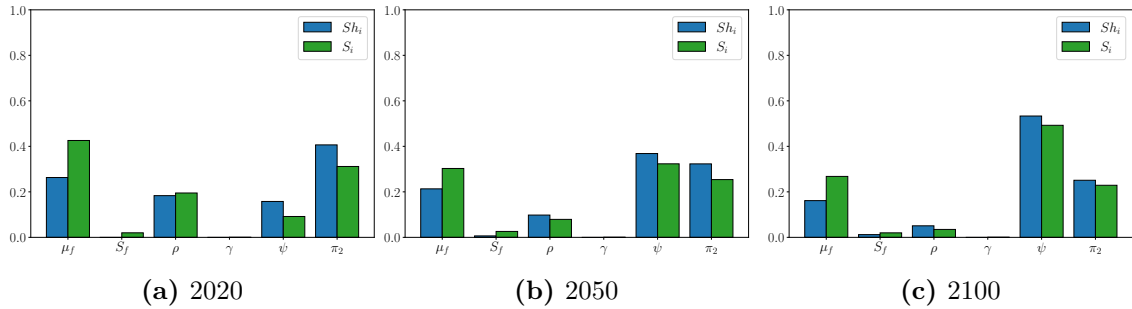


Fig. 2.8 Impact of the uncertain parameters on the SCC in 2020 (left), SCC in 2050 (middle), and SCC in 2100 (right) in the model with Bayesian learning.

The impact of uncertain parameters in the variance of the SCC in the case of learning about the ECS seems to be the middle case between deterministic and pure stochastic temperature case.

First, we can observe that the uncertainty around the prior mean of the climate feedback parameter $\mu_{f,0}$ does get resolved with the learning over time. This is an effect of learning, that we did not observe in the deterministic case. The contribution of the prior mean in the SCC variance decreases by 1.5 times in 2100 in comparison to the year 2020. Second, the impact of the damage uncertainty as well as the pure rate of time preferences is also diminishing over time. This reminds us in some way of the deterministic case results.

Third, we observe the increase in the contribution of the IES on the SCC variance over time which resembles the temperature shock case. The SCC value in 2100 becomes robust to other uncertain parameters and the only parameter that still contributes to the SCC variability is the desire to smooth consumption over time. These results can be interpreted as follows. By the year 2100, the major part of the uncertainty that could be resolved was already resolved due to learning. The remaining uncertainty, as in the case of the pure temperature shock, is manifested through the sensitivity of the SCC to the IES. In a way, by the year 2100, the impact of the uncertain parameters in the case of learning becomes closer to the case of pure temperature shock. Finally, the prior variance of the climate feedback parameter, as well as relative risk aversion, does not have any effect on the variance of the SCC in the learning case.

The Figures 2.9 to 2.11 present the univariate effects of the uncertain parameters on the value of the SCC²⁸. The univariate effects depict the direction of the influence of the uncertain parameters on the absolute value of the SCC. For most of the parameters, the directions of the impacts correspond to the economic intuition behind it: the SCC grows in the prior mean of the feedback parameter and damages; the SCC decreases in the pure rate of time preferences; the SCC does not change in relative risk aversion and the prior variance of the climate feedback parameter.

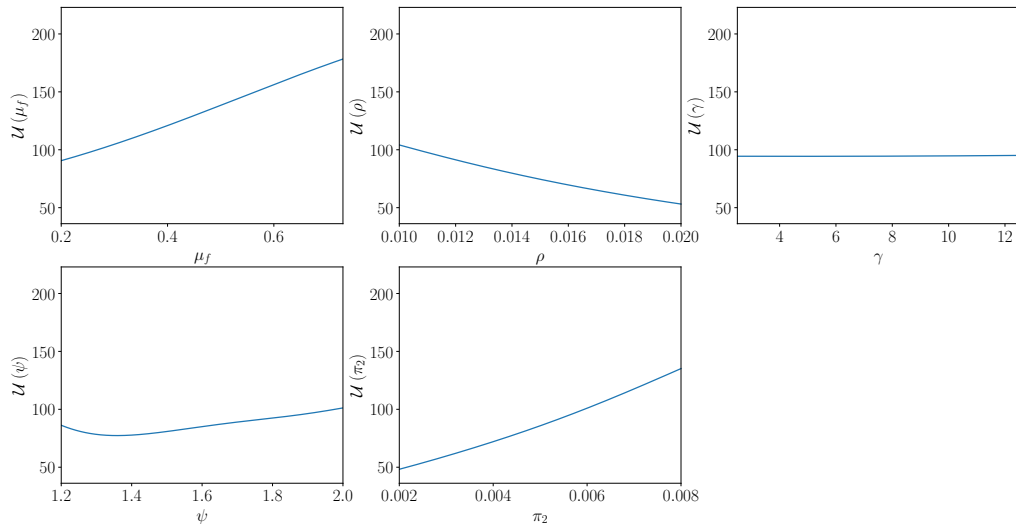


Fig. 2.9 Univariate effects on the SCC in 2020 in a deterministic model.

²⁸The univariate effects for the SCC values in the year 2100 can be found in Section 2.A

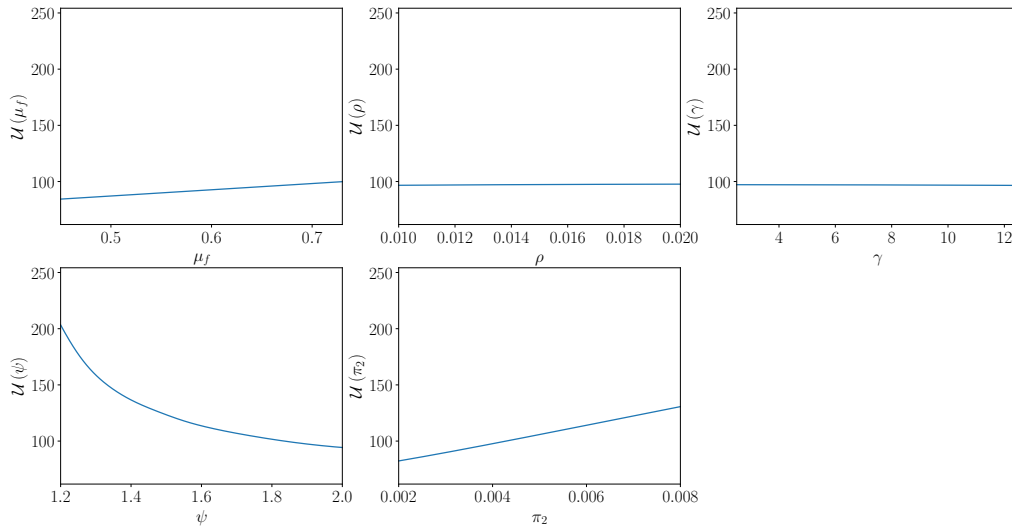


Fig. 2.10 Univariate effects on the SCC in 2020 in a model with temperature shock.

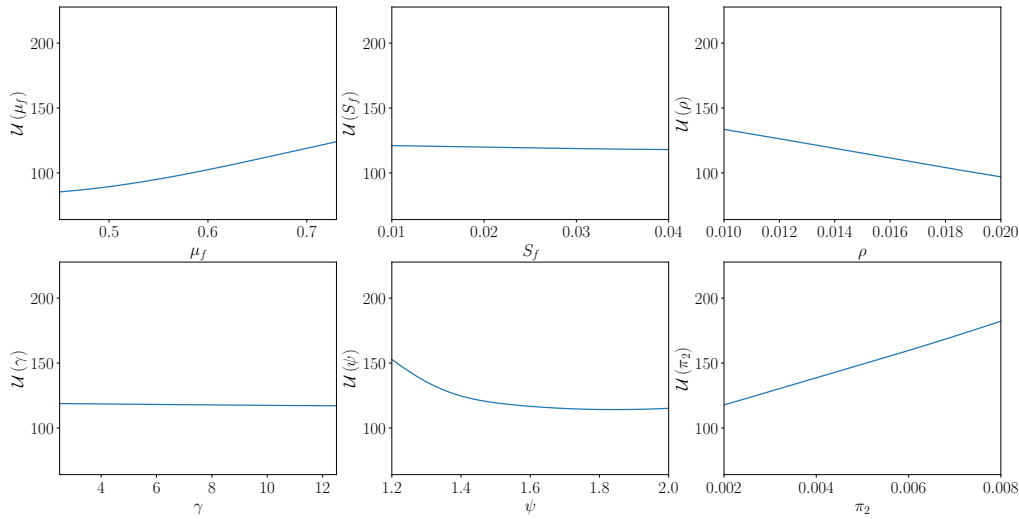


Fig. 2.11 Univariate effects on the SCC in 2020 in a model with Bayesian learning.

The only parameter that impacts the SCC in a non-obvious way is the IES. In the deterministic case, the SCC seems to increase with the increase in IES which is in line with the results for the deterministic case reported by Jensen and Traeger (2014). However, in stochastic cases (both pure temperature shock and learning) SCC decreases in case of an increase in the IES (decrease in desire to smooth consumption).

This finding is different from the results reported in Jensen and Traeger (2014) and Cai and Lontzek (2019), which document the increase in the SCC in response to the increase in IES. However, there is an important distinction between our model and the models in the studies mentioned above. Specifically, in our model we include the temperature

shocks, while in the aforementioned studies, the TFP shock is considered. It can be that TFP shock and temperature shock affect decision-making under uncertainty differently. A possible explanation can be as follows. Positive TFP shock has a counteracting first-order impact on the economy: on the one hand, it gives output, on the other hand, it is related to more emissions and consequently more damages. Positive temperature shock has a one-direction first-order impact on the economy: emissions stay the same, but the net output is reduced. In both cases of shocks, the agent increases investments in capital for a precautionary motive as a response to uncertainty. In the case of TFP shock, additional investment into mitigation helps to gain more from 'good' TFP shock. This way the effect of positive TFP on the emission rise is being addressed by higher mitigation. In case of temperature shock, additional investment into abatement does not seem to pay off in terms of the possible gains; the precautionary motive alone may be too small to justify more abatement efforts due to little consumption smoothing desire. However, this is just one possible explanation to the results observed and it requires further research to understand and quantify potential differences in the decision-making under uncertainty coming from the different sources.

2.6 Conclusion

Uncertainty in IAMs comes from several sources: modeling uncertainty, uncertainty around the evolution of the economy and climate, and parametric uncertainty. In the present research, we quantify parametric uncertainty of the stochastic IAM that explicitly features (i) the main source of the climatic uncertainty, which is ECS, and (ii) the possibility of the social planner to uncover the ECS through Bayesian learning. To tackle our problem we develop a new methodological approach. We implement a deep learning-based solution method to solve a high-dimensional and stochastic IAM with Bayesian learning about the ECS parameter and propagate parametric uncertainty using a Gaussian process-based surrogate model when estimating the social cost of carbon in a computationally efficient fashion. We find that indeed the Bayesian learning process contributes to the reduction of the impact of the uncertain prior of the ECS on the value of the SCC. Naturally, the impact of the uncertain pure rate of time preferences and damages also decreases with time. At the same time, the importance of the IES to the SCC increases with the SCC decreasing in response to an increase in IES. This finding is different from the previous literature

studying the impact of the IES on the SCC. In the case of the TFP shock Jensen and Traeger (2014), Cai and Lontzek (2019) find that with IES increasing the SCC is increasing as well. A significant difference in our model from the studies mentioned above is that our model includes temperature shocks but no TFP shock. We believe, that TFP shock and temperature shock may affect decision-making under uncertainty differently however, this is subject to further research. The comprehensive computationally efficient methodology for the uncertainty quantification analysis presented in this paper allows us to investigate further the subtle underlying economic mechanisms under the decision-making response to uncertainty. This forms the future area of research.

Appendix

2.A Univariate effects on the SCC in 2100

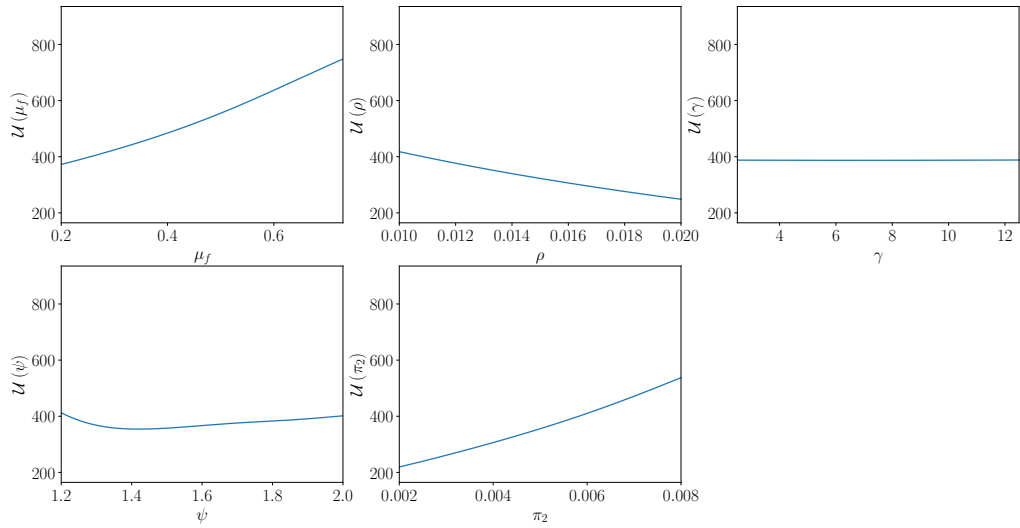


Fig. 2.A1 Univariate effects on the SCC in 2100 in a deterministic model.

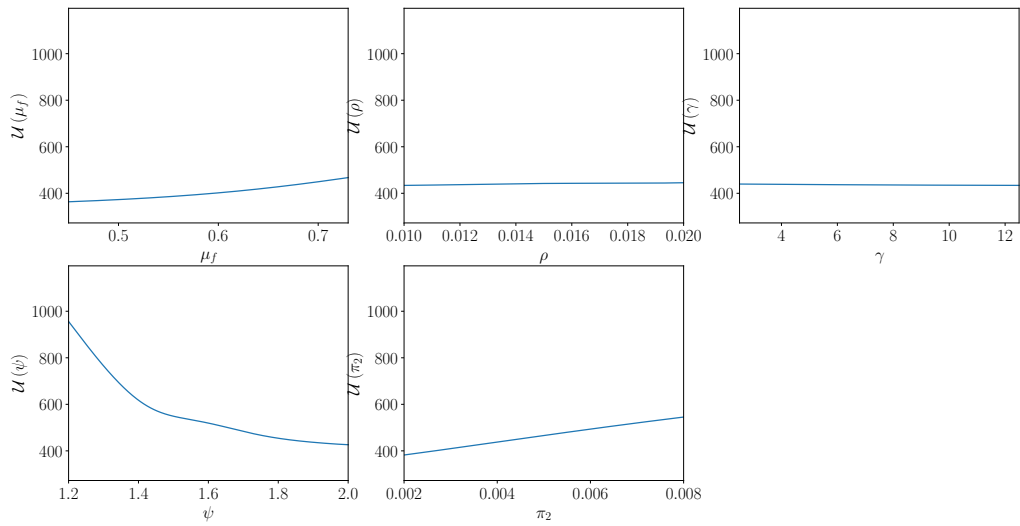


Fig. 2.A2 Univariate effects on the SCC in 2100 in a model with temperature shock.

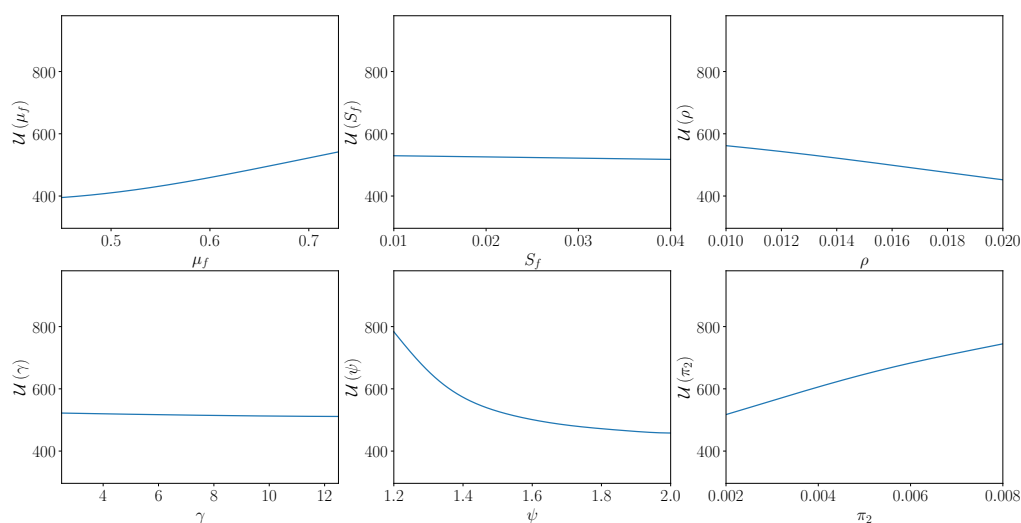


Fig. 2.A3 Univariate effects on the SCC in 2100 in a model with Bayesian learning.

2.B Additional Model Details

The complete parametrization of the model as well as full specification of the functional forms of the model can be found in the Section 1.B. The model in the Chapter 2 differs from the model in the Chapter 1 in two main ways. First, the model in the Chapter 2 features the Bayesian learning around the equilibrium climate sensitivity. The parameters and starting values of Bayesian learning are given in Table 2.B1:

Calibrated parameter	Symbol	Value
Initial prior mean	$\mu_{f,0}$	0.65
Initial prior variance	$S_{f,0}$	0.0169
Upper bound for a climate feedback parameters	\bar{f}	0.85
Lower bound for a climate feedback parameters	\underline{f}	0.45
Reference temperature impact ($^{\circ}\text{C}$ per doubling CO_2)	$\Delta T_{\text{ATX2}}^{\circ}$	1.2
Variance of temperature shock	$S_{\epsilon T}$	0.01

Table 2.B1 Annual parametrization for the Bayesian learning process.

Second, the preferences are not in CRRA form but expressed in Epstein-Zin form. The parameters specific for the Epstein-Zin preferences are given in the Table 2.B2.

Calibrated parameter	Symbol	Value
Intertemporal elasticity of substitution	ψ	1.5
Risk aversion	γ	10.

Table 2.B2 Annual parametrization for the economy.

2.C Implementation Details

In this section, we discuss some practical points when an IAM is mapped to the DEQN solution method.

2.C.1 Deep equilibrium nets for stochastic IAMs

In this Appendix, we provide a detailed procedure for mapping a stochastic, nonlinear, and non-stationary IAM onto the DEQN solution framework. The original problem, as introduced in Section 2.3.4 (cf. Eqs. (2.18) to (2.30)), requires some modifications to leverage the capabilities of the DEQN.

Recall that the state of the economy at time t is given by

$$\mathbf{X}_t \in \mathbb{R}^{9+N} := \left(K_t, M_t^{\text{AT}}, M_t^{\text{UO}}, M_t^{\text{LO}}, T_t^{\text{AT}}, T_t^{\text{OC}}, \mu_{f,t}, S_{f,t}, t, \boldsymbol{\vartheta} \right)^T \quad (2.C.1)$$

, where, next to the endogenous and exogenous state variables, we consider N uncertain parameters as pseudo-state variables.

Following, for instance Folini et al. (2023), we consider time t as an exogenous state to account for the non-stationary nature of the IAM, whereas all the other states except the pseudo-states $\boldsymbol{\vartheta}$ are endogenously determined. Furthermore, to ensure computational tractability, we follow Traeger (2014) and map the unbounded physical time $t \in [0, \infty)$ via the strictly monotonic transformation,

$$\tau = 1 - \exp(-\zeta t), \quad (2.C.2)$$

into the unit interval $\tau \in (0, 1]$. To scale back from the artificial time τ to the physical time, the inverse transformation of equation (2.C.2) can be applied, that is,

$$t = -\frac{\ln(1 - \tau)}{\varsigma}. \quad (2.C.3)$$

It is known that the dynamic programming problem presented in Section 2.3.4 would be computationally inefficient and unstable, mainly due to the capital stock that evolves significantly over time. Following Traeger (2014) among others, we normalize economic variables, capital stock, consumption, and investment, as well as the value function in the effective labor units, that is,

$$c_t := \frac{C_t}{A_t L_t}, k_t := \frac{K_t}{A_t L_t}, i_t := \frac{I_t}{A_t L_t}, v_t := \frac{V_t}{A_t L_t^{\frac{1}{1-1/\psi}}}, \quad (2.C.4)$$

where A_t represents a deterministic TFP growth trend and L_t is the global population (or labor).

Furthermore, we introduce a quantity called the effective, or growth-adjusted, discount factor,

$$\hat{\beta}_t := \exp\left(-\rho + \left(1 - \frac{1}{\psi}\right)g_t^A + g_t^L\right). \quad (2.C.5)$$

Using Eq. (2.C.4), we transform the original dynamic programming problem.

Furthermore, we also apply Eqs. (2.16) and (2.17) and also leverage the fact that $\tilde{f}_{t+1} = \mu_{f,t} + \sqrt{S_{f,t}}\epsilon^f$, where $\epsilon^f \sim \mathcal{N}(0, 1, \underline{\epsilon}^f, \overline{\epsilon}^f)$, $\underline{\epsilon}^f = \frac{f - \mu_{f,t}}{\sqrt{S_{f,t}}}$, $\overline{\epsilon}^f = \frac{\bar{f} - \mu_{f,t}}{\sqrt{S_{f,t}}}$. For simplicity we replace $\tilde{\epsilon}_{T,t+1}$ from Eqs. (2.16) and (2.17) with by the short-hand notation ϵ^T . The laws of motion for posterior mean and posterior variance can be expressed as:

$$\mu_{f,t+1} = \mu_{f,t} + \frac{\sqrt{S_{f,t}}S_{f,t}(\varphi_{1C}T_{AT,t})^2}{S_{\epsilon^T} + (\varphi_{1C}T_{AT,t})^2 S_{f,t}}\epsilon^f + \frac{\varphi_{1C}T_{AT,t}S_{f,t}}{S_{\epsilon^T} + (\varphi_{1C}T_{AT,t})^2 S_{f,t}}\epsilon^T, \quad (2.C.6)$$

$$S_{f,t+1} = \frac{S_{\epsilon^T}S_{f,t}}{S_{\epsilon^T} + (\varphi_{1C}T_{AT,t})^2 S_{f,t}}, \quad (2.C.7)$$

where $\epsilon^f \sim \mathcal{N}(0, 1, \underline{\epsilon}^f, \overline{\epsilon}^f)$, $\underline{\epsilon}^f = \frac{f - \mu_{f,t}}{\sqrt{S_{f,t}}}$, $\overline{\epsilon}^f = \frac{\bar{f} - \mu_{f,t}}{\sqrt{S_{f,t}}}$ and $\epsilon^T \sim \mathcal{N}(0, S_{\epsilon^T})$.

The normalized problem reads as follows:

$$v(\mathbf{x}_t)^{1-1/\psi} = \max_{k_{t+1}, c_t, \mu_t} \left\{ c_t^{1-1/\psi} + \beta_t \mathbb{E}_t \left[v(\mathbf{x}_{t+1})^{1-\gamma} \right]^{\frac{1-1/\psi}{1-\gamma}} \right\} \quad (2.C.8)$$

$$\text{s.t.} \quad (1 - \Theta(\mu_t)) \Omega(T_{\text{AT},t}) k_t^\alpha - c_t - i_t = 0 \quad (\lambda_t) \quad (2.C.9)$$

$$(1 - \delta) k_t + i_t - \exp(g_t^A + g_t^L) k_{t+1} = 0 \quad (\nu_t^K) \quad (2.C.10)$$

$$1 - \mu_t \geq 0 \quad \perp \quad \lambda_t^\mu \geq 0 \quad (2.C.11)$$

$$(1 - b_{12}) M_{\text{AT},t} + b_{21} M_{\text{UO},t} + (1 - \mu_t) \sigma_t A_t L_t k_t^\alpha + E_{\text{Land},t} - M_{\text{AT},t+1} = 0 \quad (\nu_t^{\text{AT}}) \quad (2.C.12)$$

$$b_{12} M_{\text{AT},t} + (1 - b_{21} - b_{23}) M_{\text{UO},t} + b_{32} M_{\text{LO},t} - M_{\text{UO},t+1} = 0 \quad (\nu_t^{\text{UO}}) \quad (2.C.13)$$

$$b_{23} M_{\text{UO},t} + (1 - b_{32}) M_{\text{LO},t} - M_{\text{LO},t+1} = 0 \quad (\nu_t^{\text{LO}}) \quad (2.C.14)$$

$$(1 - c_1 c_3 - \varphi_{1C}) T_{\text{AT},t} + c_1 c_3 T_{\text{OC},t} + c_1 \left(F_{2\text{xco2}} \log_2 \left(\frac{M_{\text{AT},t}}{M_{\text{AT}}^*} \right) + F_{\text{EX},t} \right) \\ + \varphi_{1C} T_{\text{AT},t} \mu_{f,t} + \varphi_{1C} T_{\text{AT},t} \sqrt{S_{f,t}} \epsilon^f + \epsilon^T - T_{\text{AT},t+1} = 0 \quad (\eta_{t+1}^{\text{AT}}), \quad (2.C.15)$$

$$\text{where } \epsilon^f \sim \mathcal{N}(0, 1, \underline{\epsilon}^f, \overline{\epsilon}^f), \epsilon^T \sim \mathcal{N}(0, S_{\epsilon^T})$$

$$c_4 T_{\text{AT},t} + (1 - c_4) T_{\text{OC},t} - T_{\text{OC},t+1} = 0 \quad (\eta_t^{\text{OC}}) \quad (2.C.16)$$

$$\mu_{f,t} + \frac{\sqrt{S_{f,t}} S_{f,t} (\varphi_{1C} T_{\text{AT},t})^2}{S_{\epsilon^T} + (\varphi_{1C} T_{\text{AT},t})^2 S_{f,t}} \epsilon^f + \frac{\varphi_{1C} T_{\text{AT},t} S_{f,t}}{S_{\epsilon^T} + (\varphi_{1C} T_{\text{AT},t})^2 S_{f,t}} \epsilon^T - \mu_{f,t+1} = 0 \quad (\lambda_{t+1}^{\mu_f})$$

$$\text{where } \epsilon^f \sim \mathcal{N}(0, 1, \underline{\epsilon}^f, \overline{\epsilon}^f), \epsilon^T \sim \mathcal{N}(0, S_{\epsilon^T}) \quad (2.C.17)$$

$$\frac{S_{\epsilon^T} S_{f,t}}{S_{\epsilon^T} + (\varphi_{1C} T_{\text{AT},t})^2 S_{f,t}} - S_{f,t+1} = 0 \quad (\lambda_t^{S_f}) \quad (2.C.18)$$

where the Lagrange multipliers we will employ below have been added in parentheses for completeness. In Eq. (2.C.11), the symbol \perp indicates complementary slackness. Note also that the Lagrangian multipliers η_{t+1}^{AT} in Eq. (2.C.15) and $\lambda_{t+1}^{\mu_f}$ in Eq. (2.C.17) are stochastic due to the uncertain shocks ϵ^f, ϵ^T .

The policy function \mathbf{p} we intend to approximate with the aid of deep neural networks is given by

$$\mathcal{N}_\nu(\mathbf{x}_t) \in \mathbb{R}^{14} := \left(c_t, i_t, v_t, \mu_t, \lambda_t, \eta_t^K, \lambda_t^\mu, \nu_t^{\text{AT}}, \nu_t^{\text{UO}}, \nu_t^{\text{LO}}, \eta_{t+1}^{\text{AT}} \eta_t^{\text{OC}}, \lambda_{t+1}^{\mu_f}, \lambda_t^{S_f} \right), \quad (2.C.19)$$

and consists of the choice variables (c_t, i_t, μ_t) ²⁹ as well as the Lagrange and KKT multipliers.

²⁹We keep the first-order conditions with respect to k_{t+1} and i_t . In practical applications, the performance of neural networks can, as in our case, often benefit from redundant information (see, e.g., Azinovic et al. (2022) for more details).

Next, we derive the first-order conditions to form a loss function for the IAM model that is suitable for DEQNs (cf. Eq. (2.34)).

We derive the following first-order conditions in effective labor units.

$$\frac{\partial v_t}{\partial k_{t+1}} = \left(1 - \frac{1}{\psi}\right) \beta_t \mathbb{E}_t \left[v_{t+1}^{1-\gamma} \right]^{\frac{\gamma-1/\psi}{1-\gamma}} \mathbb{E}_t \left[v_{t+1}^{-\gamma} v_{k,t+1} \right] - \lambda_t \exp \left(g_t^A + g_t^L \right) = 0 \quad (2.C.20)$$

$$\frac{\partial v_t}{\partial c_t} = \left(1 - \frac{1}{\psi}\right) c_t^{-\frac{1}{\psi}} - \lambda_t = 0 \quad (2.C.21)$$

$$\frac{\partial v_t}{\partial \mu_t} = \lambda_t \Theta'(\mu_t) \Omega_t(T_{AT,t}) k_t^\alpha + \lambda_t^\mu + \nu_t^{AT} \sigma_t A_t L_t k_t^\alpha = 0 \quad (2.C.22)$$

$$\frac{\partial v_t}{\partial M_{AT,t+1}} = \left(1 - \frac{1}{\psi}\right) \beta_t \mathbb{E}_t \left[v_{t+1}^{1-\gamma} \right]^{\frac{\gamma-1/\psi}{1-\gamma}} \mathbb{E}_t \left[v_{t+1}^{-\gamma} v_{M_{AT},t+1} \right] - \nu_t^{AT} = 0 \quad (2.C.23)$$

$$\frac{\partial v_t}{\partial M_{UO,t+1}} = \left(1 - \frac{1}{\psi}\right) \beta_t \mathbb{E}_t \left[v_{t+1}^{1-\gamma} \right]^{\frac{\gamma-1/\psi}{1-\gamma}} \mathbb{E}_t \left[v_{t+1}^{-\gamma} v_{M_{UO},t+1} \right] - \nu_t^{UO} = 0 \quad (2.C.24)$$

$$\frac{\partial v_t}{\partial M_{LO,t+1}} = \left(1 - \frac{1}{\psi}\right) \beta_t \mathbb{E}_t \left[v_{t+1}^{1-\gamma} \right]^{\frac{\gamma-1/\psi}{1-\gamma}} \mathbb{E}_t \left[v_{t+1}^{-\gamma} v_{M_{LO},t+1} \right] - \nu_t^{LO} = 0 \quad (2.C.25)$$

$$\begin{aligned} \frac{\partial v_t}{\partial T_{AT,t+1}} &= \left(1 - \frac{1}{\psi}\right) \beta_t \mathbb{E}_t \left[v_{t+1}^{1-\gamma} \right]^{\frac{\gamma-1/\psi}{1-\gamma}} \mathbb{E}_t \left[v_{t+1}^{-\gamma} v_{T_{AT},t+1} \right] \\ &- \int_{-\infty}^{+\infty} \int_{\underline{\epsilon^f}}^{\overline{\epsilon^f}} \eta_{t+1}^{AT}(\epsilon^f, \epsilon^T) \text{pdf}(\epsilon^f) d\epsilon^f \text{pdf}(\epsilon^T) d\epsilon^T = 0 \end{aligned} \quad (2.C.26)$$

$$\frac{\partial v_t}{\partial T_{OC,t+1}} = \left(1 - \frac{1}{\psi}\right) \beta_t \mathbb{E}_t \left[v_{t+1}^{1-\gamma} \right]^{\frac{\gamma-1/\psi}{1-\gamma}} \mathbb{E}_t \left[v_{t+1}^{-\gamma} v_{T_{OC},t+1} \right] - \eta_t^{OC} = 0 \quad (2.C.27)$$

$$\begin{aligned} \frac{\partial v_t}{\partial \mu_{f,t+1}} &= \left(1 - \frac{1}{\psi}\right) \beta_t \mathbb{E}_t \left[v_{t+1}^{1-\gamma} \right]^{\frac{\gamma-1/\psi}{1-\gamma}} \mathbb{E}_t \left[v_{t+1}^{-\gamma} v_{\mu_f,t+1} \right] \\ &- \int_{-\infty}^{+\infty} \int_{\underline{\epsilon^f}}^{\overline{\epsilon^f}} \lambda_{t+1}^{\mu_f}(\epsilon^f, \epsilon^T) \text{pdf}(\epsilon^f) d\epsilon^f \text{pdf}(\epsilon^T) d\epsilon^T = 0 \end{aligned} \quad (2.C.28)$$

$$\frac{\partial v_t}{\partial S_{f,t+1}} = \left(1 - \frac{1}{\psi}\right) \beta_t \mathbb{E}_t \left[v_{t+1}^{1-\gamma} \right]^{\frac{\gamma-1/\psi}{1-\gamma}} \mathbb{E}_t \left[v_{t+1}^{-\gamma} v_{S_f,t+1} \right] - \lambda_t^{S_f} = 0 \quad (2.C.29)$$

At the equilibrium, the following envelop theorem conditions hold

$$\begin{aligned} v_{k,t} &= \frac{\partial v_t}{\partial k_t} = \lambda_t \frac{\partial k_{t+1}}{\partial k_t} + \nu_t^{AT} \frac{\partial M_{AT,t+1}}{\partial k_t} \\ &\Leftrightarrow \left(1 - \frac{1}{\psi}\right) v_t^{-1/\psi} v_{k,t} = \lambda_t \left\{ (1 - \Theta(\mu_t)) \Omega(T_{AT,t}) \alpha k_t^{\alpha-1} + (1 - \delta) \right\} \\ &+ \nu_t^{AT} (1 - \mu_t) \sigma_t A_t L_t \alpha k_t^{\alpha-1} \end{aligned} \quad (2.C.30)$$

$$\begin{aligned} v_{M_{AT},t} &= \frac{\partial v_t}{\partial M_{AT,t}} = \nu_t^{AT} \frac{\partial M_{AT,t+1}}{\partial M_{AT,t}} + \nu_t^{UO} \frac{\partial M_{UO,t+1}}{\partial M_{AT,t}} + \eta_{t+1}^{AT} \frac{\partial T_{AT,t+1}}{\partial M_{AT,t}} \\ &\Leftrightarrow \left(1 - \frac{1}{\psi}\right) v_t^{-1/\psi} v_{M_{AT},t} = \nu_t^{AT} (1 - b_{12}) + \nu_t^{UO} b_{12} + \\ &c_1 F_{2\text{xc}o2} \frac{1}{\log 2M_{AT,t}} \int_{-\infty}^{+\infty} \int_{\underline{\epsilon^f}}^{\overline{\epsilon^f}} \eta_{t+1}^{AT}(\epsilon^f, \epsilon^T) \text{pdf}(\epsilon^f) d\epsilon^f \text{pdf}(\epsilon^T) d\epsilon^T \end{aligned} \quad (2.C.31)$$

$$\begin{aligned}
v_{M_{\text{UO},t}} &= \frac{\partial v_t}{\partial M_{\text{UO},t}} = \nu_t^{\text{AT}} \frac{\partial M_{\text{AT},t+1}}{\partial M_{\text{UO},t}} + \nu_t^{\text{UO}} \frac{\partial M_{\text{UO},t+1}}{\partial M_{\text{UO},t}} + \nu_t^{\text{LO}} \frac{\partial M_{\text{LO},t+1}}{\partial M_{\text{UO},t}} \\
&\Leftrightarrow \left(1 - \frac{1}{\psi}\right) v_t^{-1/\psi} v_{M_{\text{UO},t}} = \nu_t^{\text{AT}} b_{21} + \nu_t^{\text{UO}} (1 - b_{21} - b_{23}) + \nu_t^{\text{LO}} b_{23}
\end{aligned} \tag{2.C.32}$$

$$\begin{aligned}
v_{M_{\text{LO},t}} &= \frac{\partial v_t}{\partial M_{\text{LO},t}} = \nu_t^{\text{UO}} \frac{\partial M_{\text{UO},t+1}}{\partial M_{\text{LO},t}} + \nu_t^{\text{LO}} \frac{\partial M_{\text{LO},t+1}}{\partial M_{\text{LO},t}} \\
&\Leftrightarrow \left(1 - \frac{1}{\psi}\right) v_t^{-1/\psi} v_{M_{\text{LO},t}} = \nu_t^{\text{UO}} b_{32} + \nu_t^{\text{LO}} (1 - b_{32})
\end{aligned} \tag{2.C.33}$$

$$\begin{aligned}
v_{T_{\text{AT},t}} &= \frac{\partial v_t}{\partial T_{\text{AT},t}} = \lambda_t \frac{\partial k_{t+1}}{\partial T_{\text{AT},t}} + \eta_{t+1}^{\text{AT}} \frac{\partial T_{\text{AT},t+1}}{\partial T_{\text{AT},t}} + \eta_t^{\text{OC}} \frac{\partial T_{\text{OC},t+1}}{\partial T_{\text{AT},t}} + \lambda_{t+1}^{\mu_f} \frac{\partial \mu_{f,t+1}}{\partial T_{\text{AT},t}} + \lambda_t^{S_f} \frac{\partial S_{f,t+1}}{\partial T_{\text{AT},t}} \\
&\Leftrightarrow \left(1 - \frac{1}{\psi}\right) v_t^{-1/\psi} v_{T_{\text{AT},t}} = \lambda_t (1 - \Theta(\mu_t)) \Omega'(T_{\text{AT},t}) k_t^\alpha \\
&\quad + \int_{-\infty}^{+\infty} \int_{\underline{\epsilon^f}}^{\bar{\epsilon^f}} \eta_{t+1}^{\text{AT}}(\epsilon^f, \epsilon^T) \left((1 - c_1 c_3 - \varphi_{1C}) + \varphi_{1C} \mu_{f,t} + \varphi_{1C} \sqrt{S_{f,t} \epsilon^f} \right) \text{pdf}(\epsilon^f) d\epsilon^f \text{pdf}(\epsilon^T) d\epsilon^T \\
&\quad + \eta_t^{\text{OC}} c_4 + \\
&\quad \int_{-\infty}^{+\infty} \int_{\underline{\epsilon^f}}^{\bar{\epsilon^f}} \lambda_{t+1}^{\mu_f}(\epsilon^f, \epsilon^T) \frac{2S_{f,t}^{3/2} \varphi_{1C}^2 T_{\text{AT},t} S_{\epsilon^T} \epsilon^f + \varphi_{1C} S_{f,t} S_{\epsilon^T} \epsilon^T - \varphi_{1C}^3 T_{\text{AT},t}^2 S_{f,t}^2 \epsilon^T}{\left(S_{\epsilon^T} + (\varphi_{1C} T_{\text{AT},t})^2 S_{f,t}\right)^2} \text{pdf}(\epsilon^f) d\epsilon^f \text{pdf}(\epsilon^T) d\epsilon^T \\
&\quad - \lambda_t^{S_f} \frac{2S_{\epsilon^T} \varphi_{1C}^2 T_{\text{AT},t} S_{f,t}^2}{\left(S_{\epsilon^T} + (\varphi_{1C} T_{\text{AT},t})^2 S_{f,t}\right)^2}
\end{aligned} \tag{2.C.34}$$

$$\begin{aligned}
v_{T_{\text{OC},t}} &= \frac{\partial v_t}{\partial T_{\text{OC},t}} = \eta_{t+1}^{\text{AT}} \frac{\partial T_{\text{AT},t+1}}{\partial T_{\text{OC},t}} + \eta_t^{\text{OC}} \frac{\partial T_{\text{OC},t+1}}{\partial T_{\text{OC},t}} \\
&\Leftrightarrow \left(1 - \frac{1}{\psi}\right) v_t^{-1/\psi} v_{T_{\text{OC},t}} = c_1 c_3 \int_{-\infty}^{+\infty} \int_{\underline{\epsilon^f}}^{\bar{\epsilon^f}} \eta_{t+1}^{\text{AT}}(\epsilon^f, \epsilon^T) \text{pdf}(\epsilon^f) d\epsilon^f \text{pdf}(\epsilon^T) d\epsilon^T + \eta_t^{\text{OC}} (1 - c_4)
\end{aligned} \tag{2.C.35}$$

$$\begin{aligned}
v_{\mu_{f,t}} &= \frac{\partial v_t}{\partial \mu_{f,t}} = \eta_{t+1}^{\text{AT}} \frac{\partial T_{\text{AT},t+1}}{\partial \mu_{f,t}} + \lambda_{t+1}^{\mu_f} \frac{\partial \mu_{f,t+1}}{\partial \mu_{f,t}} \\
&\Leftrightarrow \left(1 - \frac{1}{\psi}\right) v_t^{-1/\psi} v_{\mu_{f,t}} = \varphi_{1C} T_{\text{AT},t} \int_{-\infty}^{+\infty} \int_{\underline{\epsilon^f}}^{\bar{\epsilon^f}} \eta_{t+1}^{\text{AT}}(\epsilon^f, \epsilon^T) \text{pdf}(\epsilon^f) d\epsilon^f \text{pdf}(\epsilon^T) d\epsilon^T + \\
&\quad \int_{-\infty}^{+\infty} \int_{\underline{\epsilon^f}}^{\bar{\epsilon^f}} \lambda_{t+1}^{\mu_f}(\epsilon^f, \epsilon^T) \text{pdf}(\epsilon^f) d\epsilon^f \text{pdf}(\epsilon^T) d\epsilon^T
\end{aligned} \tag{2.C.36}$$

$$\begin{aligned}
v_{S_{f,t}} &= \frac{\partial v_t}{\partial S_{f,t}} = \eta_{t+1}^{\text{AT}} \frac{\partial T_{\text{AT},t+1}}{\partial S_{f,t}} + \lambda_{t+1}^{\mu_f} \frac{\partial \mu_{f,t+1}}{\partial S_{f,t}} + \lambda_t^{S_f} \frac{\partial S_{f,t+1}}{\partial S_{f,t}} \\
&\Leftrightarrow \left(1 - \frac{1}{\psi}\right) v_t^{-1/\psi} v_{S_{f,t}} = \int_{-\infty}^{+\infty} \int_{\underline{\epsilon^f}}^{\bar{\epsilon^f}} \eta_{t+1}^{\text{AT}}(\epsilon^f, \epsilon^T) \frac{1}{2} \varphi_{1C} T_{\text{AT},t} S_{f,t}^{-1/2} \epsilon^f \text{pdf}(\epsilon^f) d\epsilon^f \text{pdf}(\epsilon^T) d\epsilon^T \\
&\quad + \int_{-\infty}^{+\infty} \int_{\underline{\epsilon^f}}^{\bar{\epsilon^f}} \lambda_{t+1}^{\mu_f}(\epsilon^f, \epsilon^T) \\
&\quad \frac{\frac{3}{2} (\varphi_{1C} T_{\text{AT},t})^2 \epsilon^f S_{\epsilon^T} + \frac{1}{2} S_{f,t} (\varphi_{1C} T_{\text{AT},t})^4 \epsilon^f + \varphi_{1C} T_{\text{AT},t} S_{\epsilon^T} \epsilon^T}{\left(S_{\epsilon^T} + (\varphi_{1C} T_{\text{AT},t})^2 S_{f,t}\right)^2} \text{pdf}(\epsilon^f) d\epsilon^f \text{pdf}(\epsilon^T) d\epsilon^T
\end{aligned}$$

$$+ \lambda_t^{S_f} \frac{S_{\epsilon^T}^2}{\left(S_{\epsilon^T} + (\varphi_{1C} T_{AT,t})^2 S_{f,t}\right)^2} \quad (2.C.37)$$

Finally, the following optimality condition holds:

$$v_t^{1-1/\psi} = c_t^{1-1/\psi} + \beta_t \mathbb{E}_t \left[v_{t+1}^{1-\gamma} \right]^{\frac{1-1/\psi}{1-\gamma}}, \quad (2.C.38)$$

as well as budget constraint, that is,

$$(1 - \Theta(\mu_t)) \Omega(T_{AT,t}) k_t^\alpha - c_t - i_t = 0. \quad (2.C.39)$$

We replace the KKT condition in Eq. (2.C.11) with the Fischer-Burmeister function (see, e.g., Maliar et al. (2021), and references therein) and directly embed it in the system of non-linear equilibrium conditions:

$$\Psi^{\text{FB}}(\lambda_t^\mu, 1 - \mu_t) = \lambda_t^\mu + (1 - \mu_t) - \sqrt{\lambda_t^{\mu^2} + (1 - \mu_t)^2}, \quad (2.C.40)$$

where from Eq. (2.C.22), we define λ_t^μ such that

$$\lambda_t^\mu \equiv -\lambda_t \Theta'(\mu_t) \Omega(T_{AT,t}) k_t^\alpha - \nu_t^{\text{AT}} \sigma_t A_t L_t k_t^\alpha. \quad (2.C.41)$$

One feature one faces with working with first-order conditions of an IAM is that one needs to compute them not only with respect to the economic choice variables such as μ_t and c_t , but also with respect to the climate variables, even though they are not choice variables. The reason for this is that one needs to assess the marginal effects of the change in choice variables that propagates through the climate system. Those effects cannot be computed analytically here, which is why we need Lagrange multipliers associated with every single climate equation (cf. Eqs. (2.C.23) to (2.C.27)) to estimate the shadow price of a marginal change in a respective constraint.

Using all the above definitions, the eleven individual components that enter the loss function amendable for the DEQN algorithm read as

$$l_1 := c_t^{1-1/\psi} + \beta_t \mathbb{E}_t \left[v_{t+1}^{1-\gamma} \right]^{\frac{1-1/\psi}{1-\gamma}} - v_t^{1-1/\psi} \quad (2.C.42)$$

$$l_2 := (1 - \Theta(\mu_t)) \Omega(T_{AT,t}) k_t^\alpha - c_t - i_t \quad (2.C.43)$$

$$l_3 := \lambda_t^\mu + (1 - \mu_t) - \sqrt{\lambda_t^{\mu^2} + (1 - \mu_t)^2} \quad (2.C.44)$$

$$l_4 := \lambda_t \exp(g_t^A + g_t^L) - \left(1 - \frac{1}{\psi}\right) \beta_t \mathbb{E}_t \left[v_{t+1}^{1-\gamma} \right]^{\frac{\gamma-1/\psi}{1-\gamma}} \mathbb{E}_t \left[v_{t+1}^{-\gamma} v_{k,t+1} \right] \quad (2.C.45)$$

$$l_5 := \nu_t^{\text{AT}} - \left(1 - \frac{1}{\psi}\right) \beta_t \mathbb{E}_t \left[v_{t+1}^{1-\gamma} \right]^{\frac{\gamma-1/\psi}{1-\gamma}} \mathbb{E}_t \left[v_{t+1}^{-\gamma} v_{M_{\text{AT}},t+1} \right] \quad (2.C.46)$$

$$l_6 := \nu_t^{\text{UO}} - \left(1 - \frac{1}{\psi}\right) \beta_t \mathbb{E}_t \left[v_{t+1}^{1-\gamma} \right]^{\frac{\gamma-1/\psi}{1-\gamma}} \mathbb{E}_t \left[v_{t+1}^{-\gamma} v_{M_{\text{UO}},t+1} \right] \quad (2.C.47)$$

$$l_7 := \nu_t^{\text{LO}} - \left(1 - \frac{1}{\psi}\right) \beta_t \mathbb{E}_t \left[v_{t+1}^{1-\gamma} \right]^{\frac{\gamma-1/\psi}{1-\gamma}} \mathbb{E}_t \left[v_{t+1}^{-\gamma} v_{M_{\text{LO}},t+1} \right] \quad (2.C.48)$$

$$l_8 := \int_{-\infty}^{+\infty} \int_{\underline{\epsilon^f}}^{\overline{\epsilon^f}} \eta_{t+1}^{\text{AT}}(\epsilon^f, \epsilon^T) \text{pdf}(\epsilon^f) d\epsilon^f \text{pdf}(\epsilon^T) d\epsilon^T \\ - \left(1 - \frac{1}{\psi}\right) \beta_t \mathbb{E}_t \left[v_{t+1}^{1-\gamma} \right]^{\frac{\gamma-1/\psi}{1-\gamma}} \mathbb{E}_t \left[v_{t+1}^{-\gamma} v_{T_{\text{AT}},t+1} \right] \quad (2.C.49)$$

$$l_9 := \eta_t^{\text{OC}} - \left(1 - \frac{1}{\psi}\right) \beta_t \mathbb{E}_t \left[v_{t+1}^{1-\gamma} \right]^{\frac{\gamma-1/\psi}{1-\gamma}} \mathbb{E}_t \left[v_{t+1}^{-\gamma} v_{T_{\text{OC}},t+1} \right] \quad (2.C.50)$$

$$l_{10} := \int_{-\infty}^{+\infty} \int_{\underline{\epsilon^f}}^{\overline{\epsilon^f}} \lambda_{t+1}^{\mu_f}(\epsilon^f, \epsilon^T) \text{pdf}(\epsilon^f) d\epsilon^f \text{pdf}(\epsilon^T) d\epsilon^T \\ - \left(1 - \frac{1}{\psi}\right) \beta_t \mathbb{E}_t \left[v_{t+1}^{1-\gamma} \right]^{\frac{\gamma-1/\psi}{1-\gamma}} \mathbb{E}_t \left[v_{t+1}^{-\gamma} v_{\mu_f,t+1} \right] \quad (2.C.51)$$

$$l_{11} := \lambda_t^{S_f} - \left(1 - \frac{1}{\psi}\right) \beta_t \mathbb{E}_t \left[v_{t+1}^{1-\gamma} \right]^{\frac{\gamma-1/\psi}{1-\gamma}} \mathbb{E}_t \left[v_{t+1}^{-\gamma} v_{S_f,t+1} \right] \quad (2.C.52)$$

and result in the total loss function given by

$$\ell_\nu := \frac{1}{N_{\text{path length}}} \sum_{\mathbf{x}_t \text{ on sim. path}} \sum_{m=1}^{N_{\text{eq}}=11} (l_m(\mathbf{x}_t, \mathcal{N}_\nu(\mathbf{x}_t)))^2. \quad (2.C.53)$$

The final ingredient we need for the DEQN algorithm is the evolution of the state \mathbf{x}_t one period forward such that the loss function (2.C.53) can be evaluated along a simulated path. In our application, \mathbf{x}_{t+1} is given by

$$\mathbf{x}_{t+1} = \left(k_{t+1}, M_{t+1}^{\text{AT}}, M_{t+1}^{\text{UO}}, M_{t+1}^{\text{LO}}, T_{t+1}^{\text{AT}}, T_{t+1}^{\text{OC}}, \mu_{f,t+1}, S_{f,t+1}, t+1, \boldsymbol{\vartheta} \right)^T, \quad (2.C.54)$$

where k_{t+1} is updated through the law of motion using a choice variable from the policy function Eq. (2.C.19) and the climate variables $M_{t+1}^{\text{AT}}, M_{t+1}^{\text{UO}}, M_{t+1}^{\text{LO}}, T_{t+1}^{\text{AT}}$, and T_{t+1}^{OC} can be updated via Eqs. (2.C.12) to (2.C.18), whereas time t is simply incremented by one unit, and the pseudo-states $\boldsymbol{\vartheta}$ are re-sampled from their distribution at every iteration step.

2.C.2 Numerical integration

For reasons of numerical tractability, we replace $\tilde{f}_{t+1} = \mu_{f,t} + \sqrt{S_{f,t}}\epsilon^f$, where $\epsilon^f \sim \mathcal{N}\left(0, 1, \underline{\epsilon^f}, \overline{\epsilon^f}\right)$, $\underline{\epsilon^f} = \frac{f - \mu_{f,t}}{\sqrt{S_{f,t}}}$, $\overline{\epsilon^f} = \frac{\bar{f} - \mu_{f,t}}{\sqrt{S_{f,t}}}$. We replace $\tilde{\epsilon}_{T,t+1}$ from Eqs. (2.16) and (2.17) with the short-hand notation ϵ^T . Taking these notational changes into account, we have to approximate the following integral numerically:

$$\int_{-\infty}^{+\infty} \int_{\underline{\epsilon^f}}^{\overline{\epsilon^f}} \left(\varphi_{1C} T_{AT,t} \sqrt{S_{f,t}} \epsilon^f + \epsilon^T \right) \text{pdf}(\epsilon^f) d\epsilon^f \text{pdf}(\epsilon^T) d\epsilon^T \quad (2.C.55)$$

where $\text{pdf}(\epsilon^f) = \frac{K}{\sqrt{2\pi}} \exp\left(-\frac{(\epsilon^f)^2}{2}\right)$, $K = \left(\text{cdf}(\overline{\epsilon^f}) - \text{cdf}(\underline{\epsilon^f})\right)^{-1}$, and $\text{pdf}(\epsilon^T) = \frac{1}{\sqrt{2\pi S_{\epsilon^T}}} \exp\left(-\frac{(\epsilon^T)^2}{2S_{\epsilon^T}}\right)$.

To apply Gauss-Hermite quadrature, we need to make a change of notation by replacing:

$$x = \frac{\epsilon^T}{\sqrt{2S_{\epsilon^T}}} \Rightarrow \epsilon^T = \sqrt{2S_{\epsilon^T}} x. \quad (2.C.56)$$

Thus we get:

$$\int_{-\infty}^{+\infty} \int_{\underline{\epsilon^f}}^{\overline{\epsilon^f}} \left(\varphi_{1C} T_{AT,t} \sqrt{S_{f,t}} \epsilon^f + \sqrt{2S_{\epsilon^T}} x \right) \frac{K}{\sqrt{2\pi}} \exp\left(-\frac{(\epsilon^f)^2}{2}\right) d\epsilon^f \frac{1}{\sqrt{\pi}} \exp(-x^2) dx. \quad (2.C.57)$$

With the change of variables necessary for the Gauss-Legendre quadrature, we get:

$$\sum_{i=1}^n \frac{w_i}{\sqrt{\pi}} \sum_{j=1}^m v_j \left(\varphi_{1C} T_{AT,t} \sqrt{S_{f,t}} \left(y_j \frac{\overline{\epsilon^f} - \underline{\epsilon^f}}{2} + \frac{\overline{\epsilon^f} + \underline{\epsilon^f}}{2} \right) + \sqrt{2S_{\epsilon^T}} x_i \right) \frac{\overline{\epsilon^f} - \underline{\epsilon^f}}{2} \frac{K}{\sqrt{2\pi}} \exp\left(-\frac{\left(y_j \frac{\overline{\epsilon^f} - \underline{\epsilon^f}}{2} + \frac{\overline{\epsilon^f} + \underline{\epsilon^f}}{2} \right)^2}{2}\right) \quad (2.C.58)$$

where w_i are Gauss-Hermite weights, x_i - Gauss-Hermite nodes, v_j are Gauss-Legendre weights, y_j - Gauss-Legendre nodes.

2.C.3 Error statistics

Table 2.C1 provides detailed error statistics for the model with learning and pseudo-states at convergence. All other models presented in the article reach a similar level of accuracy.

Stats.	l_1	l_2	l_3	l_4	l_5	l_6	l_7	l_8	l_9	l_{10}	l_{11}
mean	$7.43e-4$	$3.00e-3$	$7.48e-5$	$6.06e-3$	$6.69e-4$	$4.54e-4$	$2.92e-4$	$1.44e-3$	$2.55e-3$	$9.88e-4$	$3.78e-4$
std	$1.05e-3$	$6.19e-3$	$2.34e-1$	$1.04e-2$	$7.18e-4$	$5.34e-4$	$5.02e-4$	$1.34e-3$	$4.76e-3$	$1.90e-3$	$5.18e-4$
min	$< 1.e-9$	$< 1.e-9$	$< 1.e-9$	$< 1.e-9$	$< 1.e-9$	$< 1.e-9$	$< 1.e-9$	$1.86e-9$	$< 1.e-9$	$< 1.e-9$	$< 1.e-9$
0.1%	$7.15e-7$	$1.07e-6$	$< 1.e-9$	$1.84e-6$	$5.96e-7$	$4.76e-7$	$2.68e-7$	$1.00e-6$	$1.39e-6$	$9.53e-7$	$3.27e-7$
25%	$1.84e-4$	$2.99e-4$	$< 1.e-9$	$5.14e-4$	$1.70e-4$	$1.27e-4$	$7.01e-5$	$2.77e-4$	$3.66e-4$	$2.52e-4$	$8.68e-5$
50%	$4.18e-4$	$9.15e-4$	$2.3e-10$	$1.67e-3$	$4.21e-4$	$2.95e-4$	$1.58e-4$	$6.78e-4$	$9.55e-4$	$5.97e-4$	$2.02e-4$
75%	$8.81e-4$	$3.08e-3$	$1.86e-9$	$5.99e-3$	$9.18e-4$	$6.02e-4$	$3.20e-4$	$1.43e-3$	$2.69e-3$	$1.28e-3$	$4.39e-4$
99.9%	$1.12e-2$	$6.75e-2$	$2.20e-3$	$7.00e-2$	$4.81e-3$	$5.51e-3$	$6.17e-3$	$9.10e-3$	$4.77e-2$	$1.02e-2$	$4.33e-3$
max	$4.03e-2$	$1.464e-1$	$5.03e-3$	$1.08e-1$	$2.36e-2$	$2.42e-2$	$1.31e-2$	$1.35e-2$	$9.37e-2$	$6.34e-2$	$1.51e-2$

Table 2.C1 Summary statistics of the loss function components along the simulation path for the optimal solution of the stochastic model with pseudo-states.

2.C.4 Leave-one-out error with Gaussian processes

The selection of the number of sample points n contained in the training set \mathcal{D} is a trade-off between accuracy and efficiency: our design philosophy is to minimize n but still guarantee the accuracy of the surrogate model predictions based GP in a computationally affordable way.

One common choice in the UQ literature to strike a balance between these two opposing factors, although primarily discussed with polynomial chaos expansions (see, e.g., Blatman and Sudret (2010); Harenberg et al. (2019); Le Gratiet, Marelli, and Sudret (2017)), is to use the *leave-one-out* (LOO) error estimator. Recall that, as in Eq. (2.42), we have a computational model $\mathcal{M}(\cdot)$ that maps an input vector x_i to a scalar output y_i . We repeatedly evaluate Eq. (2.42) n times to obtain a training dataset $\mathcal{D} = \{x_i, y_i\}_{i=1}^n = [X, y]$. Then, we fit the GP interpolation of the original model $\mathcal{M}(\cdot)$, denoted as $\mathcal{M}_{\text{GP}|X,y}(\cdot)$, as discussed in Section 2.4.1. To measure the LOO error, we first construct a GP surrogate model $\mathcal{M}_{\text{GP}|X_{-i},y_{-i}}$ on experimental design points $X_{-i} \equiv X \setminus x_i = \{x_1, \dots, x_{i-1}, x_{i+1}, \dots, x_n\}$, and estimate the error Δ_i on the excluded point x_i between the outcome from the true model and the prediction from the GP model, that is,

$$\Delta_i \equiv \mathcal{M}(x_i) - \mathcal{M}_{\text{GP}|X_{-i},y_{-i}}(x_i) \quad (2.C.59)$$

Next, we compute the sum of Δ_i over i and define the LOO error, that is,

$$\epsilon_{\text{LOO}}^{\text{GP}} \equiv \frac{1}{n} \sum_{i=1}^n \Delta_i^2 = \frac{1}{N} \sum_{i=1}^n \left(\mathcal{M}(x_i) - \mathcal{M}_{\text{GP}|X_{-i},y_{-i}}(x_i) \right)^2. \quad (2.C.60)$$

In our numerical applications below, we choose the size of the training set n for the GP surrogate such that we achieve $\epsilon_{\text{LOO}}^{\text{GP}} \leq 10^{-2}$, which guarantees the required high accuracy of the GP surrogate for our QoIs, obtained at moderate computational costs. If a given initial n is insufficient, we systematically increase the size of the training set, e.g., by applying Bayesian active learning (see, e.g., Renner and Scheidegger (2018), and references therein).

Chapter 3

Green energy transition: decarbonisation of developing countries and the role of technological spillovers

Abstract

The green energy transition is necessary within the next few decades to mitigate climate change. In the paper, I explore the effectiveness of carbon pricing and the role of technological spillovers in achieving decarbonization, with a particular focus on the challenges faced by developing countries. I develop a two-region integrated assessment model that incorporates fossil fuel and renewable energy sources to investigate the quantitative impact of spillovers on decarbonization in developing countries. The findings indicate that technological spillovers in developing countries contribute to the replacement of fossil fuels with renewable energy inputs. The study suggests that implementing carbon taxation in both advanced and developing regions, along with technological spillovers, yields the most favorable outcomes for the climate. However, the absence of carbon tax in developing countries with spillovers still delivers slightly better environmental results compared to taxing both regions without spillovers. The results emphasize the importance of considering spillovers and carbon taxation when designing effective policies to achieve environmental goals.

Keywords: Green energy transition, developing countries, carbon justice, integrated assessment model, social cost of carbon

JEL classification: C61, C69, E17, E27, O00, O13, O44, Q50

3.1 Introduction

The green energy transition is necessary within the next few decades to mitigate climate change. In simple terms, first, there should be some form of carbon pricing to internalize the climate externality. In its turn, increasing the relative price of fossil fuels leads to a higher demand for renewable energy sources. Second, more demand incentivizes innovation in renewable technologies with subsequent further increase in their productivity. These processes create the green energy transition leading to the decarbonization of the energy inputs.

This decarbonization mechanism seems to be working for the advanced countries¹. Many advanced countries have some form of carbon pricing in place e.g. carbon tax, cap and trade etc.; a significant reduction in prices for renewable energy sources is observed together with the rise in the share of renewable energy in primary energy consumption (Känzig and Konradt (2023)). Application of the same decarbonization mechanism to the developing countries does not seem to be straightforward for two reasons. First, carbon pricing in developing countries is controversial due to concerns about carbon justice. Second, as economic growth literature Aghion and Howitt (1997) points out, developing countries are not innovating, but rather adopting already existing technology to catch up to the technological frontier through global technological spillovers.

Difficulties with carbon pricing together with the key role of technological spillovers for growth in developing countries create two counteracting forces. On the one hand, in the absence of carbon pricing in developing countries, there is no economic incentive for them to switch from fossil fuels to renewable energy sources. On the other hand, in the case of decarbonization in advanced countries, renewable energy sources are becoming more prevalent and generating more spillovers, substituting for fossil fuel technologies in developing countries even without carbon pricing. Given that developing countries do

¹The term "advanced countries" refers to the high-income (HI) and upper-middle-income (UMI) countries. The term "developing countries" refers to the low-income (LI) and lower-middle-income (LMI) countries from the World Bank country classification by income level. The list of the countries in each income group can be found in the Section 3.C.

not have well-established energy infrastructure that relies on fossil fuels, they may have a chance for an easy transition to renewable energy for sustaining growth as discussed in Fay et al. (2015).

This motivates the research questions of the present paper. It investigates the role and the quantitative impact of technological spillovers on decarbonization in developing countries. Specifically, it aims to determine (i) whether a "renewable energy path" can be established in the presence of spillovers without carbon taxation and (ii) whether a "fossil fuel path" could emerge if there are high spillovers in fossil fuels.

To address these questions I develop a two-region integrated assessment model of the global economy and climate with two energy sources, specifically fossil fuel and green energy. The setup incorporates advanced and developing economies, with an advanced economy featuring exogenous growth in energy inputs and a developing economy relying on technological spillovers for the growth in both energy inputs.

The model introduced in this paper follows the spirit of DICE model as in W. D. Nordhaus (2017), but also relies on Golosov et al. (2014) and Dietz and Venmans (2019) in terms of the economic block of the integrated assessment model (IAM) and on Folini et al. (2023) in terms of the climate block. The first novelty of the model presented in the paper comes from coupling fossil fuels and renewable energy sources in the economy with the three-reservoir carbon cycle and with two-reservoir temperatures in the climate emulator. The second novelty is that the model explicitly features developing economies and technological spillovers in energy. To solve the model I rely on a novel deep learning algorithm for global solutions suggested by Azinovic et al. (2022). This method is especially suitable for large-scale highly non-linear dynamic optimization problems and this paper is the first one to apply it to the multi-region integrated assessment models which make up for the third, computational, novelty of the paper.

The main finding of the paper is that the presence of technological spillovers in developing countries leads to faster growth of renewable energy and slower growth of fossil fuels resulting in the higher share of renewable energy input in the energy mix. This result highlights the positive impact of spillovers on decarbonization efforts. Additionally, the study suggests that implementing carbon taxation in both advanced and developing regions in conjunction with technological spillovers still yields the most favorable outcomes for the climate. However, it is worth noting that the absence of carbon tax in developing

countries with spillovers still delivers slightly better environmental results compared to taxation of both regions without spillovers.

These results emphasize the importance of considering both spillovers and carbon taxation in designing effective strategies for achieving environmental goals. They motivate further work in extending the model presented below with endogenous growth and endogenous spillover rates to understand how advanced economies can influence the decarbonization process in developing countries through technological spillovers.

The remainder of the paper is organized as follows. Section 3.2 presents some stylized empirical evidence that motivates the research, Section 3.3 provides a brief literature overview on the topic, Section 3.4 outlines the model, parametrization, and the solution method employed, Section 3.5 presents the findings of the paper and Section 3.6 concludes.

3.2 Empirical motivation

Throughout history, economically advanced countries have been the main contributors to climate change being responsible for almost 90% of cumulative carbon emissions (see Figure 3.1).

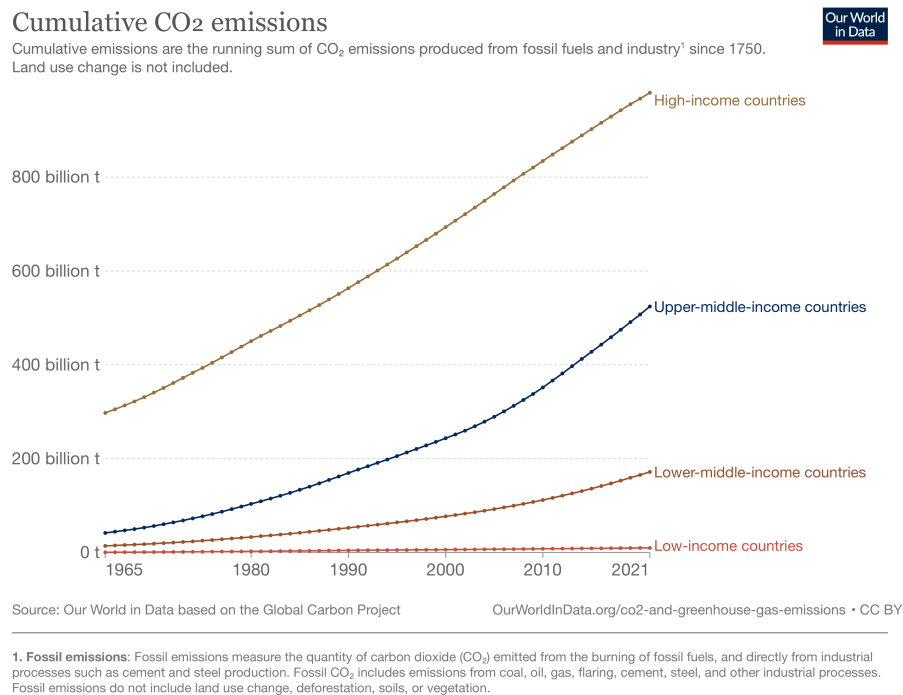
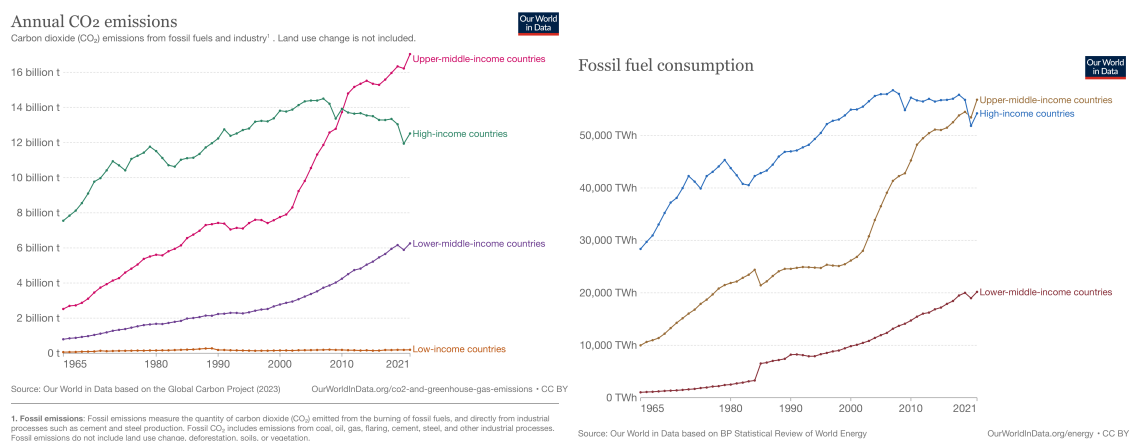


Fig. 3.1 Cumulative CO₂ emissions by income group. Source: OWID

Thus, they have been at the forefront of discussions on decarbonization and green energy transition. As a result of these efforts, a number of the advanced countries have some form of carbon initiative implemented or in progress and there is evidence of the green energy transition process happening in these countries.

Developing countries being accountable for the remaining 10% in cumulative carbon emissions (see Figure 3.1) may not seem to be a priority in discussions regarding immediate decarbonization efforts at least for two reasons. First, their current emissions account only for less than 20% of annual global emissions (Figure 3.2a), making them incapable of playing a decisive role in the world's decarbonization. Second, the climate justice principle claims that advanced countries, which benefited the most from carbon emissions during the industrialization process, have a greater responsibility to mitigate climate change. According to this principle, it is considered unfair to demand developing countries equal participation in decarbonization and green energy transition. Indeed, this reflects in the empirical evidence on the adoption of decarbonization measures by developing countries. Among fifty-four LMI countries, only two of them (Indonesia and Ukraine) have already implemented some form of the carbon tax, with eight other countries considering carbon pricing measures. LI countries do not have any decarbonization initiatives in place or under consideration.

At the same time, according to the data from 1965 to 2021, fossil fuels comprise more than 90% of the current energy mix and its consumption in developing countries has been growing at an average rate of 6% per year (Figure 3.2b).



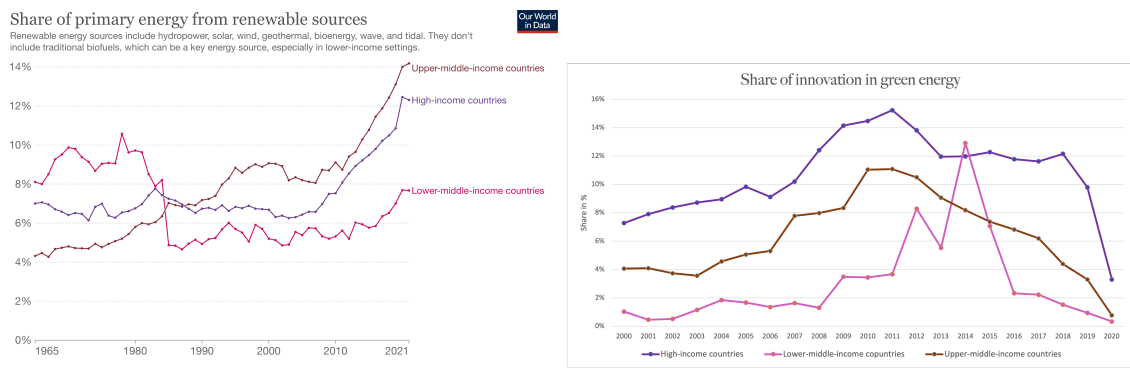
(a) Annual CO₂ emissions. Source: OWID

(b) Fossil fuel consumption. Source: OWID

Fig. 3.2 Annual CO₂ emissions by country income group (left) and fossil fuel share of primary energy consumption (right) for the different income groups of countries.

If this growth rate persists, they could reach the current level of fossil fuel usage in high-income countries by the year 2050. This potential future amount of fossil fuel consumption coupled with the lack of decarbonization measures in developing countries becomes significant for the climate change mitigation perspectives. It brings us to the question of decarbonization and green energy transition possibilities available for developing countries.

One view on the decarbonization of developing countries can be by applying the same mechanism as for the advanced countries: internalizing climate externality by carbon pricing which creates more demand for renewable energy and incentivizes innovation in green technology ultimately leading to the green energy transition. However, the assumption about the possibility of innovation in developing countries seems to be unreasonable. The growth literature suggests that developing countries up to a certain stage of development do not innovate, they are involved in the activity of imitating the technological frontier (Aghion and Howitt (1997)). In line with this growth literature narrative, in the Figure 3.3 I depict the share of the primary energy from renewable energy sources that are used by different income groups of countries (Figure 3.3a) and the share of innovation in the green energy among the total innovation (Figure 3.3b).



(a) Primary energy from renewable sources. Source: OWID
 (b) Renewable energy innovation. Author's elaboration based on the data from WIPO, IRENA, OWID.

Fig. 3.3 Primary energy from renewable sources (left) and renewable energy innovation (right) for the different income groups of countries.

Lower-middle-income countries tend to increase their renewable energy usage however, their innovation rate in terms of patenting activity is the lowest among all the income groups. This indirectly suggests that the clean technologies in lower-income countries are

the result of technological imitation. Thus, relying on the mechanism that involves carbon pricing to unleash the process of green energy transition does not seem a viable option for developing countries. On the one hand, carbon pricing may still seem necessary in developing countries to steer the imitation process in the right direction. On the other hand, if developing countries by imitation follow the technological portfolio of the advanced countries, the switch to clean technologies may happen just by the nature of the technology imitation process. These competing ideas pose the motivation for the present research. Specifically, I would like to quantitatively investigate the role of technological imitation in the decarbonization of developing countries and its interaction with carbon pricing.

Technological imitation is a process in which the developing (recipient) country is involved in the activity of acquiring an existing technological frontier and adapting it to the local realities. The frontier technology may be transferred in a regulated way, through the rights to use the patented technology, or in an unregulated way, through other forms of technological diffusion. The frontier technology cannot be perfectly acquired immediately and takes time to fully diffuse in the world. All the transfer and diffusion processes (regulated and unregulated) that make the imitation process possible for developing countries I call technological spillovers.² As an example of the technological spillover one can think of the solar photovoltaic (PV) technology. The technology was developed in the middle of the 20th century in the advanced economies, then intensively commercialized by China at the beginning of the 21st century, and is now being ramped up significantly in developing countries. It is hard to credibly track how this diffusion of technology was happening, probably via all forms of diffusion. For the sake of simplicity in this paper, I call this process technology spillovers.

3.3 A brief review of the literature

This paper is mainly related to the three strands of the literature. First, it follows the tradition of carbon pricing literature based on the economy-climate modeling pioneered

²I depart here from the definition of Grossman and Helpman (1993):

'By technological spillovers, we mean that (1) firms can acquire information created by others without paying for that information in a market transaction and (2) the creators (or current owners) of the information have no effective recourse, under prevailing laws, if other firms utilize information so acquired.'

in a way, that as technology spillovers I understand any processes of technological diffusion, with or without market transactions involved in acquiring the information.

by W. D. Nordhaus (1997). Second, it complements the increasing number of papers on integrated assessment modeling with a heterogeneity of regions in the spirit of Hassler, Krusell, Olovsson, and Reiter (2020). Third, it closely follows the literature on endogenous growth and technological spillovers within integrated assessment set-ups as in Barrett (2021).

The main purpose of the integrated assessment modeling is to quantify the welfare-maximizing carbon price that is necessary for climate change mitigation. Pioneering research of this cost-benefit analysis was done by W. D. Nordhaus (1997). His modeling framework, although criticized, evolved with time as in W. D. Nordhaus (2017) and became a cornerstone for further research of single-agent models including analytical set-ups like Golosov et al. (2014) and Traeger (2019).

However, single-agent integrated assessment models suggest universal carbon policies that are hard to implement in all countries due to the lack of agreement. This gives a rise to the multiple-agent modeling framework. This literature was pioneered by W. D. Nordhaus and Boyer (2000), with his famous RICE model which was later transformed by Hassler and Krusell (2012) into a stochastic general equilibrium version. A number of other integrated assessment models with multiple agents were developed, such as FUND (the most recent version of the model is used in Waldhoff, Anthoff, Rose, and Tol (2014)), REMIND ³, WITCH (Bosetti et al. (2007)) among others. These models were trying to address the issue of cooperation in global climate mitigation. Further, W. A. Brock, Engström, Grass, and Xepapadeas (2013), W. Brock, Cai, Judd, and Xepapadeas (2018) discuss the transfers and how to set a carbon policy optimally across countries with differences in income level and production possibilities. In a similar vein, Hillebrand and Hillebrand (2019) present a dynamic general equilibrium model with a heterogeneous region structure. Krusell and Smith Jr (2018) analyze gains and losses from climate change around the world and L. J. Kotlikoff et al. (2021) add inter-generational perspective to the discussion. The main take-away of this strand of the literature is that an optimal climate policy in the presence of regional heterogeneity consists of an emissions tax and a transfer policy.

A parallel strand of the literature was dedicated to single-agent models that feature endogenous technological change in the energy sector. The major contribution was done

³The full model description can be found on the f Potsdam Institute for Climate Impact Research

by Acemoglu, Aghion, Bursztyn, and Hemous (2012), showing that the carbon tax should induce innovation in green technologies due to market size and price effects. Fried and Lagakos (2023) empirically evaluates the quantitative impact of these channels and confirms that a carbon tax induces large changes in innovation.

These two last strands of literature merge in Hassler et al. (2019), where a multi-regional set-up with endogenous technological change is analyzed. Continuing with this framework, Hassler et al. (2020) discuss second-best cases for carbon mitigation policies and Hassler and Krusell (2018) study the consequences of a carbon tax for oil-consuming and oil-producing regions. Barrett (2021) builds on top of these models adding a technological spillovers process for energy technology proliferation. This set-up with multiple heterogeneous regions directed technical change and technological spillovers is an important step forward. However, a possible limitation of this framework is the assumption that all the regions have equal possibilities to innovate. This assumption does not seem plausible as developing countries usually do not innovate in the energy sector and rather catch up with some lag to the current productivity frontier that is set by advanced economies Aghion and Howitt (1997). Thus it is reasonable to assume that there is no endogenous growth in energy source possible in developing countries, and the only source of growth for them is through imitation. This setup was investigated in (Acemoglu, Aghion, & Hémous, 2014). The authors analytically show that the first-best solution requires coordination between Northern and Southern regions, however, it is also possible to avoid a climate disaster only with the mitigation efforts of the Northern countries. This paper provides a significant insight into the innovation and imitation dynamics between regions. However, an analytical solution of the model required significant simplifications of the climate as well and the paper does not provide a quantitative evaluation of the process. A very detailed quantitative model that deals with multiple regions and addresses the innovation and imitation dynamics between the regions is the WITCH model ⁴. It includes exogenously determined energy innovation processes and their spillovers to the countries that imitate rather than innovate. However, the innovation and technological spillover processes in WITCH are not the central focus of attention and they lack tractability.

The present paper addresses the issue of decarbonization in a two-region world with a simple quantitative framework that separates innovation activity and technological

⁴The current vintage of the model can be found here

spillovers in heterogeneously developed countries. The model explicitly features advanced and developing regions as in Acemoglu et al. (2014) but delivers quantitative results. It provides a tractable framework that allows to study of the technology spillover counterfactual to the baseline case in which the regions rely on their innovation processes. The framework also includes a rather detailed climate-emulator that is in agreement with CMIP5.

3.4 Model

3.4.1 Model formulation

Economy

The model builds on W. Nordhaus (2018), Golosov et al. (2014), Hassler et al. (2019), and Barrett (2021). The world is populated with two regions $i \in \{A, D\}$: advanced economy (A) and developing economy (D). No trade happens in the model and there are no other international markets.

Both regions have a representative consumer with identical preferences where C_t^i is the stream of consumption for region i and the world total labor evolves according to the exogenous process $L_t = L_0 + (L_\infty - L_0) \left(1 - \exp(-\delta L t)\right)$ with the population in an advanced economy and developing economy summing up to the total labor force $L_t^A + L_t^D = L_t$. The welfare of the region i can be presented as:

$$V_t^i = \sum_{t=0}^{\infty} \phi_t^i \frac{(C_t^i/L_t^i)^{1-1/\psi}}{1 - 1/\psi} L_t^i \quad (3.1)$$

where ϕ_t^i is a dynamic Negishi weight of the economy defined as in Denning and Emmerling (2017), Cai et al. (2019):

$$\phi_t^i = \frac{(C_t^i)^{1/\psi}}{\sum_{i \in \{A, D\}} (C_t^i)^{1/\psi}}. \quad (3.2)$$

Advanced and developing economy use an aggregate production function for the final good as follows:

$$Y_t^i = (K_t^i)^\alpha \left(A_t^i (1 - \pi_t^i - \xi_t^i) L_t^i\right)^{1-\alpha-\nu} (E_t^i)^\nu \quad (3.3)$$

where A_t^i is the total factor productivity that grows exogenously as $A_t^i = A_0^i (1 + g^A)^t$ at the same rate g^A for both regions, K_t^i is the capital, and E_t^i is the energy input into production, π_t^i and ξ_t^i are labor shares that are used in energy production. The final good is assumed to be a numeraire.

Energy is produced in advanced and developing economies by a representative firm with the following production aggregator over two available sources of energy $E_t^{i,dt}$ - dirty energy and $E_t^{i,cl}$ - green energy:

$$E_t^i = \left(\kappa_{dt}^i \left(E_t^{i,dt} \right)^{\rho_{CES}} + \kappa_{cl}^i \left(E_t^{i,cl} \right)^{\rho_{CES}} \right)^{1/\rho_{CES}} \quad (3.4)$$

where $\kappa_{dt}^i + \kappa_{cl}^i = 1$. Dirty and green energy is produced via fuel-specific production technologies $A_{dt,t}^i$ and $A_{cl,t}^i$ respectively which are linear in labor that goes into production as in Golosov et al. (2014):

$$E_{t,dt}^i = A_{dt,0}^i \left(1 + g_{dt}^i \right)^t \pi_t^i L_t^i \quad (3.5)$$

$$E_{t,cl}^i = A_{cl,0}^i \left(1 + g_{cl}^i \right)^t \xi_t^i L_t^i. \quad (3.6)$$

The growth rate of the technological progress in the dirty and green energy sources is given exogenously and differs between the regions in the baseline formulation of the model.

In the modeling set-up that features technological spillovers, there is a possibility for developing regions to benefit from the production technology from the advanced region. The technological spillovers process is a simplification of one from Barrett (2021) and states:

$$A_{dt,t+1}^D = A_{dt,0}^D + \varsigma (A_{dt,t}^A - A_{dt,0}^A) \quad (3.7)$$

$$A_{cl,t+1}^D = A_{cl,0}^D + \varsigma (A_{cl,t}^A - A_{cl,0}^A). \quad (3.8)$$

where ς is the intensity of spillovers that is assumed to be the same for both fuels at the baseline. The idea behind this spillover definition is straightforward. The developing economy starts in period zero with the initial level of the TFP in the respective energy sector. In period one the upgrade on the TFP level of the advanced economy net of its initial level is being transmitted to the developing country. Spillover intensity ς determines

how much of the TFP progress in the advanced country goes in the developing country. Spillover intensity is assumed to be less than one, meaning that there is no full transmission of the TFP progress from the advanced country in one given year. Transmitting the TFP progress of the advanced economy net of the initial level is based on the assumption that the developing region never catches up with the technological level in the advanced region. More discussion on the no catch-up assumption for the developing countries is provided in Sections 3.4.2 and 3.6.

Climate externality

The climate module in the integrated assessment model under consideration consists of three reservoir carbon cycle $M = (M_t^{\text{AT}}, M_t^{\text{UO}}, M_t^{\text{LO}})$ and two reservoir energy balance $T = (T_t^{\text{AT}}, T_t^{\text{OC}})$. The model takes the functional forms of climate part from W. D. Nordhaus (2017), and calibration from Folini et al. (2023).

$$M_{t+1}^{\text{AT}} = (1 - b_{12}) M_t^{\text{AT}} + b_{12} \frac{M_{\text{EQ}}^{\text{AT}}}{M_{\text{EQ}}^{\text{UO}}} M_t^{\text{UO}} + E_t^f \quad (3.9)$$

$$M_{t+1}^{\text{UO}} = b_{12} M_t^{\text{AT}} + \left(1 - b_{12} \frac{M_{\text{EQ}}^{\text{AT}}}{M_{\text{EQ}}^{\text{UO}}} - b_{23}\right) M_t^{\text{UO}} + b_{23} \frac{M_{\text{EQ}}^{\text{UO}}}{M_{\text{EQ}}^{\text{LO}}} M_t^{\text{LO}} \quad (3.10)$$

$$M_{t+1}^{\text{LO}} = b_{23} M_t^{\text{UO}} + \left(1 - b_{23} \frac{M_{\text{EQ}}^{\text{UO}}}{M_{\text{EQ}}^{\text{LO}}}\right) M_t^{\text{LO}} \quad (3.11)$$

$$T_{t+1}^{\text{AT}} = T_t^{\text{AT}} + c_1 F_t - c_1 \frac{F_{2\text{xco2}}}{T_{2\text{xco2}}} T_t^{\text{AT}} - c_1 c_3 (T_t^{\text{AT}} - T_t^{\text{OC}}) \quad (3.12)$$

$$T_{t+1}^{\text{OC}} = T_t^{\text{OC}} + c_4 (T_t^{\text{AT}} - T_t^{\text{OC}}) \quad (3.13)$$

where $M_{\text{EQ}} = (M_{\text{EQ}}^{\text{AT}}, M_{\text{EQ}}^{\text{UO}}, M_{\text{EQ}}^{\text{LO}})$ are equilibrium carbon masses in preindustrial times, E_t emissions, and F_t is exogenous radiative forcing process. Coefficients b_{12}, b_{23} in carbon cycle and c_1, c_3, c_4 in energy balance describe diffusion processes in the reservoirs, $F_{2\text{xco2}}$ is forcings of equilibrium CO2 doubling and $T_{2\text{xco2}}$ is equilibrium temperature impact.

Emissions from industrial activity and exogenous emissions are accumulated as follows:

$$E_t^f = \sigma_t (E^{\text{a,dt}} + E^{\text{d,dt}}) + E_t^{\text{Land}} \quad (3.14)$$

where σ_t is the emission coefficient from dirty energy sources as in W. D. Nordhaus (2017) and follows:

$$\sigma_t = \sigma_0 \exp\left(\frac{g_0^\sigma}{\log(1 + \delta^\sigma)} \left((1 + \delta^\sigma)^t - 1\right)\right). \quad (3.15)$$

and E_t^{Land} are exogenous emissions as in W. D. Nordhaus (2017) that follow:

$$E_{\text{Land},t} = E_{\text{Land},0} \exp(-\delta^{\text{Land}} t). \quad (3.16)$$

Damages and resource constraint

The final output of the economy is subject to damages due to temperature increase:

$$Y_t^{\text{Net},i} = \Omega^i (T_{\text{AT},t}) (K_t^i)^\alpha (A_t^i (1 - \pi_t^i - \xi_t^i) L_t^i)^{1-\alpha-\nu} (E_t^i)^\nu \quad (3.17)$$

where the climate damages are supposed to be different for both of the regions and are considered as:

$$\Omega^i (T_{\text{AT},t}) = \psi_1^i T_t^{\text{AT}} + \psi_2^i (T_t^{\text{AT}})^2. \quad (3.18)$$

Final output net of damages is used for the consumption and investment which gives the resource constraint:

$$Y_t^{\text{Net},i} + (1 - \delta) K_t^i = C_t^i + K_{t+1}^i \quad (3.19)$$

I present the full write up of the model with the Bellman equation in Section 3.A.1.

3.4.2 Parametrization

To parametrize the model, I partially rely on the values available from the literature and partially use the World Bank, Penn World Table (PWT 10.01), and "Our world in data" (OWID) data sources from the period of 1990-2021 to discipline certain parameters.

For the conventional parameters such as capital and energy elasticity in the production function, depreciation rate of capital, pure rate of time preferences and intertemporal elasticity of substitution I take standard values from the literature:

The initial TFP level of each region is pinned down by the data on output, capital, labor, and energy for each region in 1990. Table 3.2 shows the values for the initial TFP levels as well as assumed TFP growth rates for each region.

Calibrated parameter	Symbol	Value	Source
Pure rate of time preferences	ρ	0.015	W. D. Nordhaus (2017)
Capital elasticity	α	0.3	W. D. Nordhaus (2017)
Energy elasticity	ν	0.04	Golosov et al. (2014)
Intertemporal elasticity of substitution	ψ	1.5	Cai and Lontzek (2019)
Capital depreciation rate	δ	0.1	W. D. Nordhaus (2017)

Table 3.1 Economic parameters

Advanced economy		Developing economy	
A_0^A	0.0115	A_0^D	0.00251
g^A	0.025	g^D	0.025

Table 3.2 TFP parameters.

I assume a 2.5% growth rate in the world TFP that is the same for both regions. The assumption of homogeneous growth in the world may be criticized for two opposite reasons. On the one hand, in line with the idea of catching up on growth, developing countries may exhibit higher growth rates than advanced economies Patel, Sandefur, and Subramanian (2021). On the other hand, the presence of poverty traps and middle-income traps can hinder growth and development, contributing to a slower growth rate in the developing world Kraay and McKenzie (2014). However, there is no unequivocal evidence, putting forward one of these theories. Thus for the sake of simplicity, I stick to the homogeneous growth rate in the world. This way effectively I assume no possibility for a full catch-up for developing countries. It may seem like a restrictive assumption, however, there is one more reason to make it. The assumption of no possibility for a full catch-up is consistent with the modeling setup. The model considers a social planner solution with the relative weights of the regions in the value function determined by dynamic Negishi weights. The nature of Negishi weights is to preserve the distribution of welfare across regions to exclude income effects and capture only technological effects. Keeping the welfare distribution stable is another way to assume no full catch-up for the developing world. More discussion on how the assumption of no full catch-up for developing countries can affect the results of the paper is provided in the Section 3.6.

For the CES energy aggregate, I take the elasticity of substitution between dirty and green energy as 1.11 which implies parameter $\rho^{CES} = 0.1$. The reason for this choice is

based on the recent evidence that found the elasticity of substitution between green and dirty sources tends to be higher than unity (Papageorgiou, Saam, and Schulte (2017)) with some papers finding it to be much higher than unity (Jo (2020)). I stick to the conservative approach assuming low but greater than unity elasticity having in mind that higher elasticity can make all the effects more prominent.

Another issue if the elasticity of substitution can be considered the same in both regions. There is no clear answer to that, as the nature of the dominant energy technology in advanced and developing countries is fundamentally different. The main difference is that most of the countries that I consider in the advanced group are relying on a centralized energy infrastructure while developing countries are utilizing scattered small-scale mostly traditional energy sources. This difference makes it unclear if the elasticity of substitution can be higher or lower in advanced economies in comparison to developing ones. On the one hand, due to centrally functioning energy infrastructure advanced regions can be more responsive to change in energy prices and thus be more flexible in substituting dirty energy sources with green ones. On the other hand, developing countries may benefit from the absence of any infrastructure and be able to implement green high-power energy systems from scratch. Given the inconclusiveness of the argumentation for the baseline version of the model, I assume the elasticity of substitution between energy sources to be constant for both regions. A promising further avenue of the research includes the uncertainty quantification of the decarbonization paths based on a plausible range of the elasticity of substitution.

To determine the weights of the energy CES aggregator $\kappa_{dt}^i, \kappa_{cl}^i$ I employ the approach from Golosov et al. (2014) using relative prices of fossil fuel energy to renewable energy given by:

$$\frac{p_{dt}^i}{p_{cl}^i} = \frac{\kappa_{dt}^i}{\kappa_{cl}^i} \left(\frac{E_t^{i,dt}}{E_t^{i,cl}} \right)^{\rho^{CES}-1}. \quad (3.20)$$

As proxies for energy prices, I use Levelized Cost of Electricity (LCOE) values from IEA and IRENA databases. Although there are no accurate LCOE estimates available for the starting year 1990, I produce some back-of-the-envelope estimations to get approximate reasonable values. For fossil fuel and renewable energy usage, I rely on the World Bank data on energy usage for the year 1990.

The growth rates of the energy sources as well as the initial TFP levels for the energy sources are chosen to target the fossil fuel energy and renewable energy consumption paths provided in the data by the World Bank. Specifically, the initial TFP level in the fossil fuel and renewable energy is pinned down by the consumption of the energy and labor shares in energy sectors in 1990 for each region (more details on it are in the Section 3.B.4). The growth rates of TFP in energy sectors are chosen to match the evolution of the energy consumption as shown in the Figure 3.6.

Advanced economy				Developing economy			
$A_{dt,0}^A$	0.0458	$A_{cl,0}^A$	0.0227	$A_{dt,0}^D$	0.00712	$A_{cl,0}^D$	0.0232
g_{dt}^A	0.012	g_{cl}^A	0.014	g_{dt}^D	0.01	g_{cl}^D	0.001
κ_{dt}^A	0.75	κ_{cl}^A	0.25	κ_{dt}^D	0.82	κ_{cl}^D	0.18

Table 3.3 Energy parameters.

As a baseline speed of spillovers, I take the estimate of the full technology adoption happening in 11 years which implies $\varsigma = 0.09$ following Barrett (2021). Eaton and Kortum (1999) estimated that on average it takes the technology 11 years to be fully adopted internationally. This implies that about 9% of the technological frontier is adopted annually. This estimate was later confirmed by Comin and Hobijn (2010) which estimated the length between 5 and 16 years for the technological adoption. Dechezleprêtre, Glachant, and Ménière (2013) showed that there is no difference in technological adoption for green technologies in comparison to other types of technology. Thus I use these results and set the intensity of spillovers equal for both fossil fuel and renewable energy. Relying on these estimates may be considered as an upper bound of the spillover intensity. Indeed, the estimates of technological adoption include not only spillovers, in a sense of the definition of Grossman and Helpman (1993), but also a targeted technology transfer. Excluding this intentional technological adoption can result in a lower spillover intensity estimate.

It is important to have damage function different for both regions. It is well-documented in the literature that developing countries are subject to higher damages than advanced economies (see for example OECD review). I assume the standard quadratic damages for the advanced economies as in W. D. Nordhaus (2017) and high damages for the developing region as in Weitzman (2012a). The summary of damage coefficients is given in Table 3.4.

Advanced economy				Developing economy			
W. D. Nordhaus (2017)				Weitzman (2012a)			
ψ_1^A	0.0	ψ_2^A	0.0236	ψ_1^D	0.0	ψ_2^D	0.0746

Table 3.4 Damages parameters.

The parameters that characterize the climate system come from Folini et al. (2023) with the difference that starting value for the carbon masses as well as the temperature of the atmosphere and the ocean are adjusted for 1990 as a starting year (see Section 3.B).

Exogenous processes that are present in the model, such as labor evolution, industrial emission intensity, exogenous emissions, and radiative forcing inherit functional forms from W. D. Nordhaus (2017). The emission intensity process I calibrate to match the RCP6.0 scenario (see Figure 3.4).

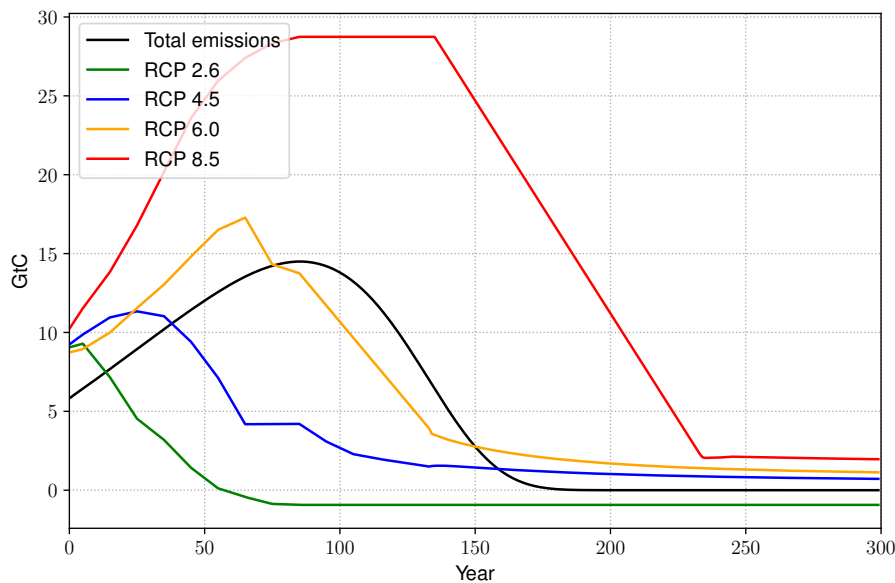


Fig. 3.4 Total industrial emissions

In the Figure 3.5 and Figure 3.6, I depict how the business-as-usual solution of the model without spillovers (in green) and with spillovers (in red) matches the data that was used for the calibration. We can see that from the data we cannot infer any information about the presence or absence of the spillovers. In both cases, the actual paths of the data are matched fairly well. This observation makes the point for the relevance of the present study. Based on the data we cannot credibly say what is the driving force for the growth in

energy sectors for developing countries. We can model it both ways. However, in line with the growth literature, it seems reasonable to assume that developing countries imitate the technology, rather than innovate themselves. Thus it may be misleading to make policy choices based on the models that assume the presence of innovation in developing countries. Section 3.5 explicitly compares the results of the model assuming its growth in every region with the model that allows for spillovers. It shows, that in the presence of spillovers, carbon taxation policy may not be necessary for developing countries.

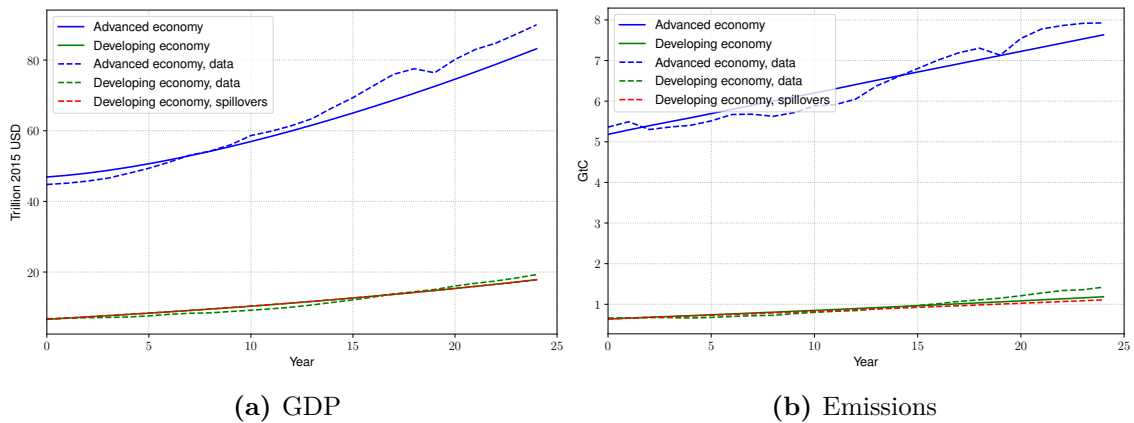


Fig. 3.5 GDP (left) and emissions (right) for advanced and developing economies, BAU scenario, computed and actual values. Year zero on the graphs corresponds to a starting year 1990.

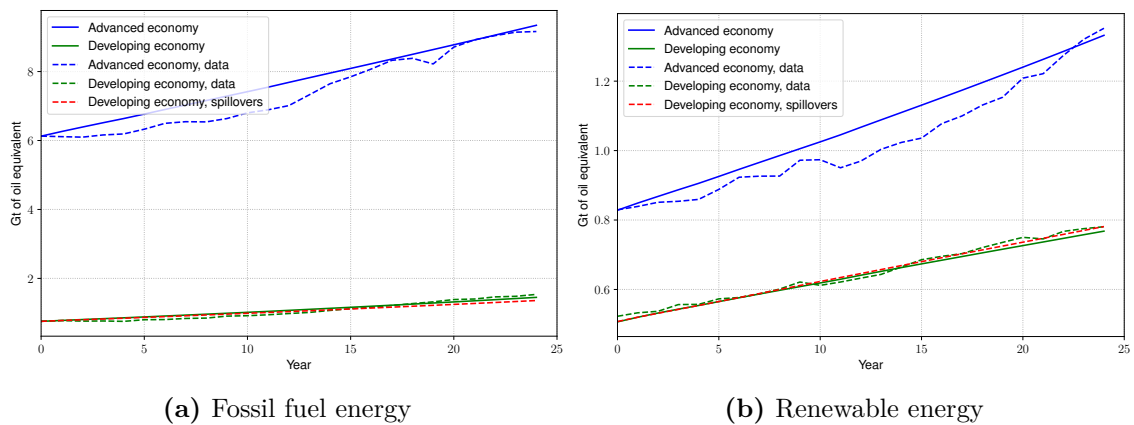


Fig. 3.6 GDP (left) and emissions (right) for advanced and developing economies, BAU scenario, computed and actual values. Year zero on the graphs corresponds to a starting year 1990.

More details on parametrization is presented in the appendix Section 3.B.

3.4.3 Solution method: Deep Equilibrium Nets

The solution to the problem is based on the deep equilibrium nets as in Azinovic et al. (2022), which is presented in great detail in Chapter 2 of the thesis. The details of the implementation of the DEQN solution to the problem from Section 3.4 can be found in Section 3.A.1.

3.5 Results

This section presents the results. To answer the research question of the paper I consider two baseline scenarios and three cases of interest.

Baseline scenarios

- 'Business-as-usual' (BAU): no carbon taxation, damages are not internalised by the social planner in both regions;
- 'Optimal': optimal carbon taxation, damages are internalised by the social planner in both of regions;

Cases of interest

- 'Second-best': carbon tax for advanced regions only, damages are internalised by the social planner in advanced region, developing region follows 'business-as-usual' scenario;
- 'Optimal' + technological spillovers: optimal carbon taxation, damages are internalised by the social planner in both of regions and the growth in energy source in developing region happens only through spillover effects;
- 'Second-best' + technological spillovers: carbon tax for advanced regions only, damages are internalised by the social planner in advanced region, developing region follows 'business-as-usual' scenario and the growth in energy source in developing region happens only through spillover effects;

The main difference between the modeling setup with and without spillovers lies in the TFP process for the energy sources. In case of no spillovers, both advanced and developing countries rely on the exogenous growth rate that is specific to the region. In the case of

spillovers, I assume, that the growth rate in the energy sector of a developing region is dependent on the growth rate of the advanced region as shown in Eq. (3.7). Figure 3.7 depicts a difference between the TFP level of both energy sources with and without the spillovers. We can see, that the presence of spillovers in the fossil fuel sector does not change the TFP path significantly. However, in the case of renewable energy sources presence or absence of spillovers plays a crucial role.

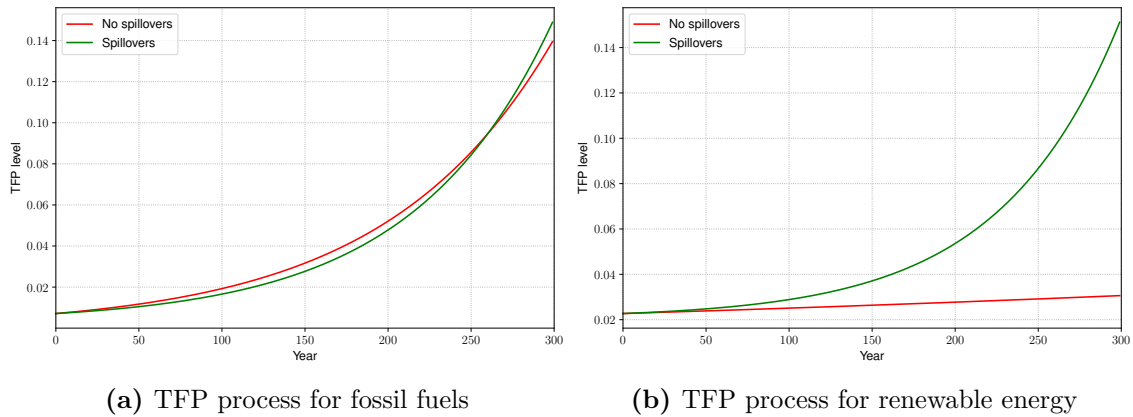


Fig. 3.7 TFP level for the fossil fuels (left) and renewable energy (right) with and without spillovers for developing economies, BAU scenario. Year zero on the graphs corresponds to a starting year 1990.

3.5.1 Results without technological spillovers

First we compare the business-as-usual case with the optimal taxation case when the social planner internalises the damages in both regions, which we can interpret as a case of optimal taxation. In this section, we do not take technological spillovers into account.

From the Figure 3.8 we can see that optimal taxation reduces damages in advanced countries from 3.5% of GDP loss to 2.5%. Similar way, damages in developing countries are reduced by an optimal intervention from almost 10% of GDP loss only to 8%. The difference in damages comes from the assumption of heterogeneity of damages affecting the regions.

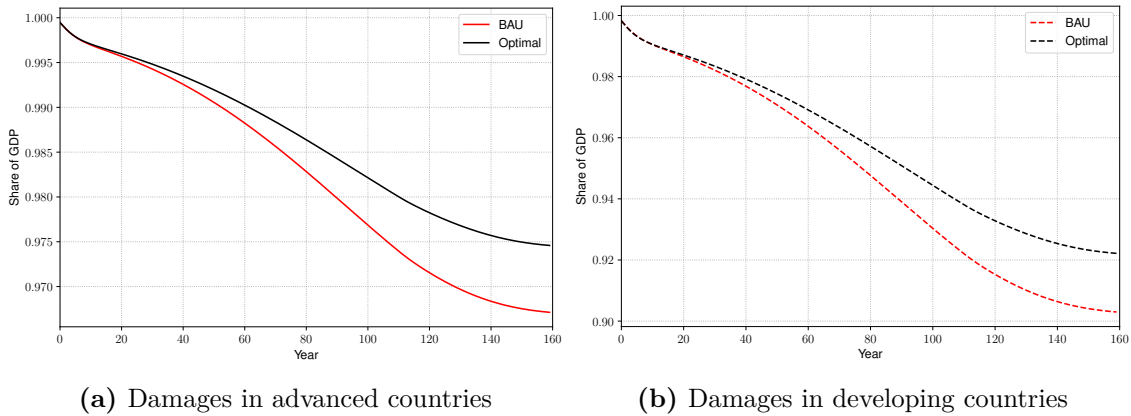


Fig. 3.8 Damages in advanced countries (left) and developing countries (right) under BAU and optimal taxation schemes. Year zero on the graphs corresponds to a starting year 1990.

Figure 3.9 shows the evolution of the dirty energy sources for both regions and Figure 3.10 depicts the results for renewable energy sources. In both cases, the effect of the 'Optimal' taxation follows the economic intuition. Thus fossil fuel usage is being reduced in the 'Optimal' case in comparison to 'BAU' and renewable energy is slightly increased due to the substitution effect. Advanced region reduces their fossil fuel usage more than developing region in line with the initial assumptions of the model, that advanced region pollutes more.

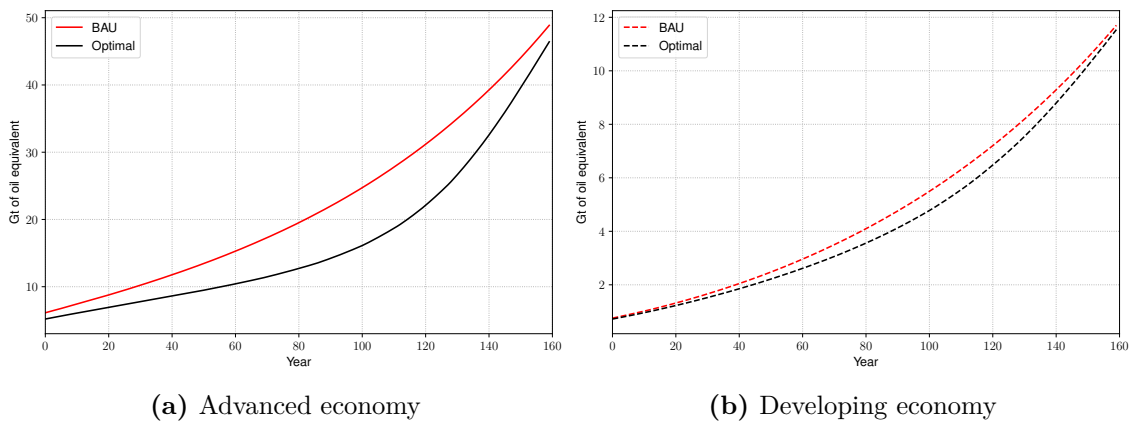


Fig. 3.9 Dirty energy in advanced economy (left) and developing economy (right) under BAU and optimal taxation schemes. Year zero on the graphs corresponds to a starting year 1990.

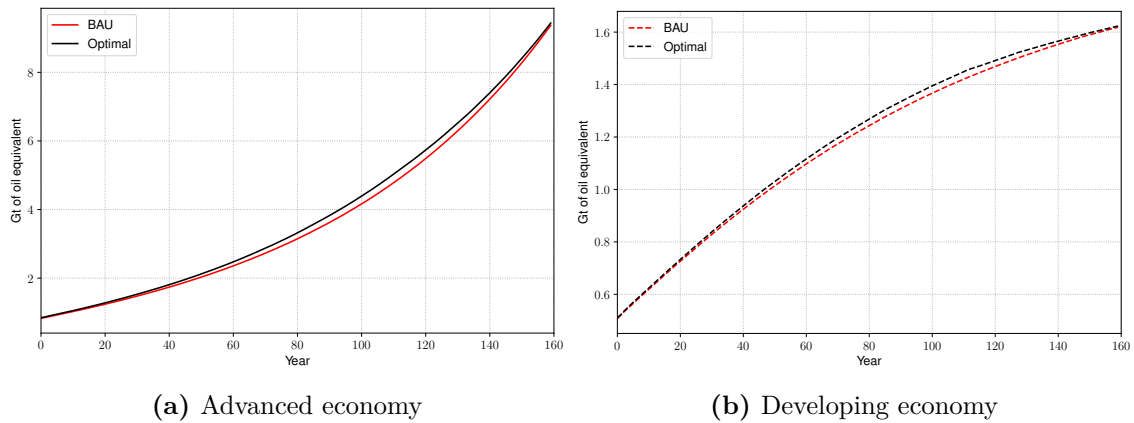


Fig. 3.10 Clean energy in advanced economy (left) and developing economy (right) under BAU and optimal taxation schemes. Year zero on the graphs corresponds to a starting year 1990.

The emissions in the Figure 3.11 predictably follow fossil fuels usage patterns. We can see that business-as-usual emissions are relatively high in comparison to the case of taxation.

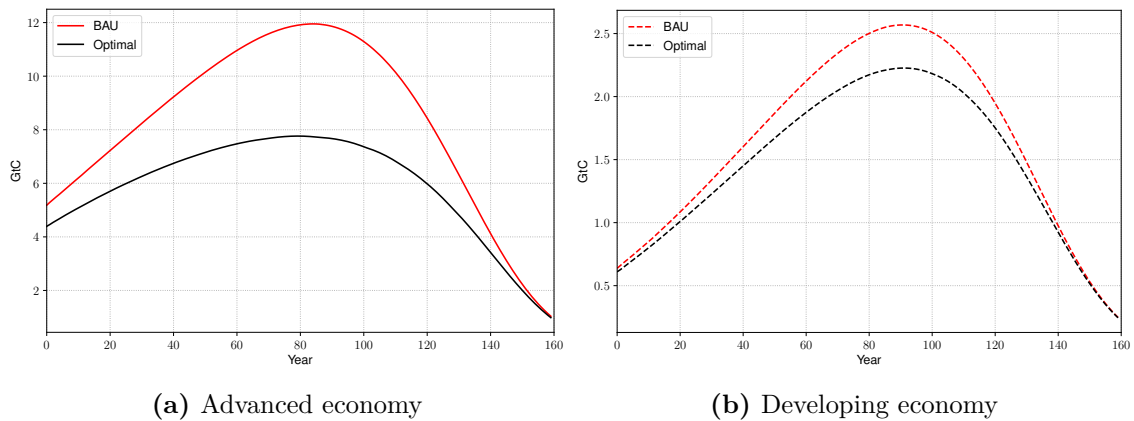


Fig. 3.11 Emissions in advanced economy (left) and developing economy (right) under BAU and optimal taxation schemes. Year zero on the graphs corresponds to a starting year 1990.

Overall, the optimal taxation scheme gives a decline in emissions of about 200GtC and $0.5C^\circ$ decrease in temperature.

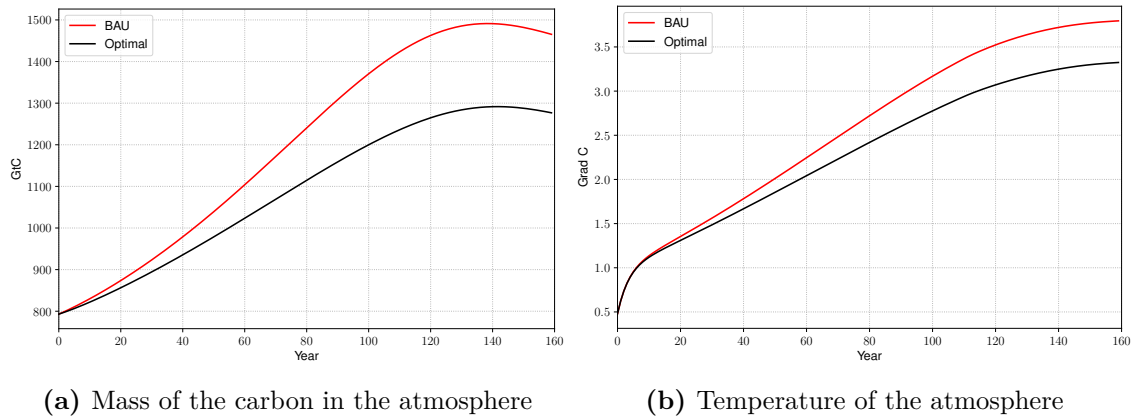


Fig. 3.12 Mass of carbon in the atmosphere (left) and temperature of the atmosphere (right) under BAU and optimal taxation schemes. Year zero on the graphs corresponds to a starting year 1990.

The value of the social cost of carbon represents the optimal carbon taxation level. In the Figure 3.13, we can see that the optimal carbon tax for developing countries equals approximately 200USD/tC in advanced regions and 90USD/tC in developing regions at the year 2040.

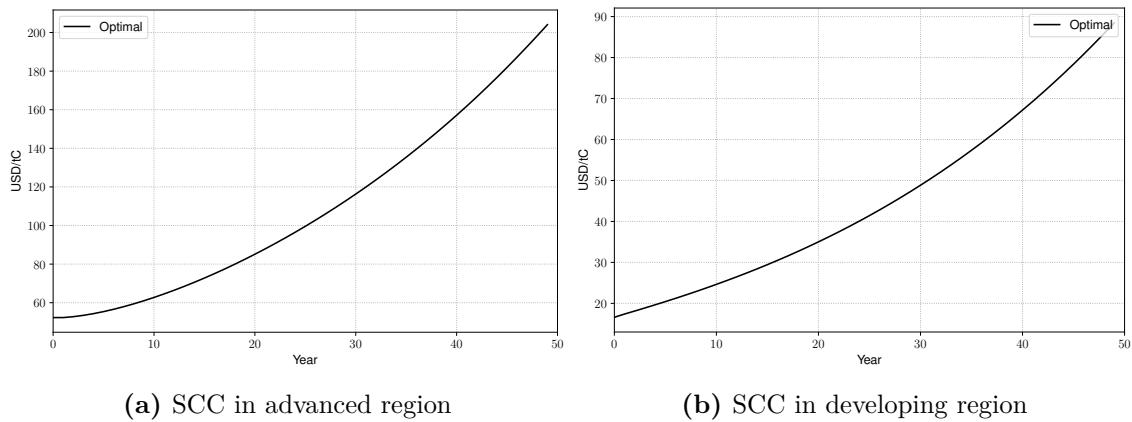


Fig. 3.13 SCC in advanced region (left) and developing region (right) under optimal taxation scheme. Year zero on the graphs corresponds to a starting year 1990.

3.5.2 Business-as-usual with technological spillovers

We consider now the business-as-usual case with technological spillovers. The technological evolution in the advanced economy remains the same as in the case without the spillovers. However, the developing economy gets the chance to catch up with the energy technologies used in the advanced economy. The only source of growth in energy technologies in developing regions are the technological spillovers.

We can see on Figure 3.14 that usage of fossil fuel energy declines moderately and renewable energy grows faster in developing economies in the presence of spillovers.

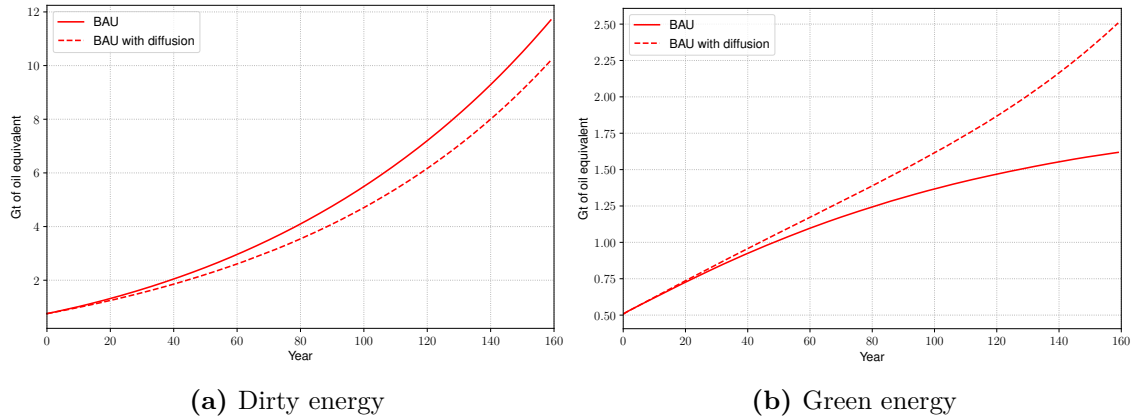


Fig. 3.14 Dirty energy (left) and green energy (right) in developing economy. Year zero on the graphs corresponds to a starting year 1990.

The reason for that is as follows: the main difference between the fossil fuel sectors in two regions is in the initial levels of TFP, but the levels are not being transferred through the spillovers. Thus, fossil fuel energy does not grow in response to the spillovers process because the growth rate of fossil fuels in advanced region is approximately the same as the respective growth rate in developing region. In fact, technology transfer in dirty energy through spillovers happens slower than in the exogenous case. At the same time green energy usage in developing countries increases dramatically due to the fact that the growth rate of TFP in renewable energy in advanced economy is much higher than in developing region. Thus the baseline level of the technological spillover in energy sector acts two folds: slowing down the TFP growth in dirty energy and accelerating the TFP growth in green energy in developing countries. Due to this twofold effect, in the case of business as usual, the presence of the technological spillovers slightly reduces the mass of carbon in the atmosphere and temperature.

It would be interesting to experiment with the elasticity of substitution between energy sources in developing countries as well as with the intensity of the spillovers process, to see if there is any plausible option to rely on technological spillovers and to improve the environmental state in business as usual case. Certainly, the contribution of the developing countries in climate change as well as in decarbonization so far is not considered significant and cannot substitute for the efforts of advanced economies. However, it would be beneficial to understand if there are certain circumstances in terms of the elasticity of

the substitution between energy sources (which we cannot influence as a policy, but we can test if it's a plausible value that can be confirmed empirically) and spillovers intensity (which we can influence as a policy) that can result in a significant reduction of the negative climate externalities in business as usual case.

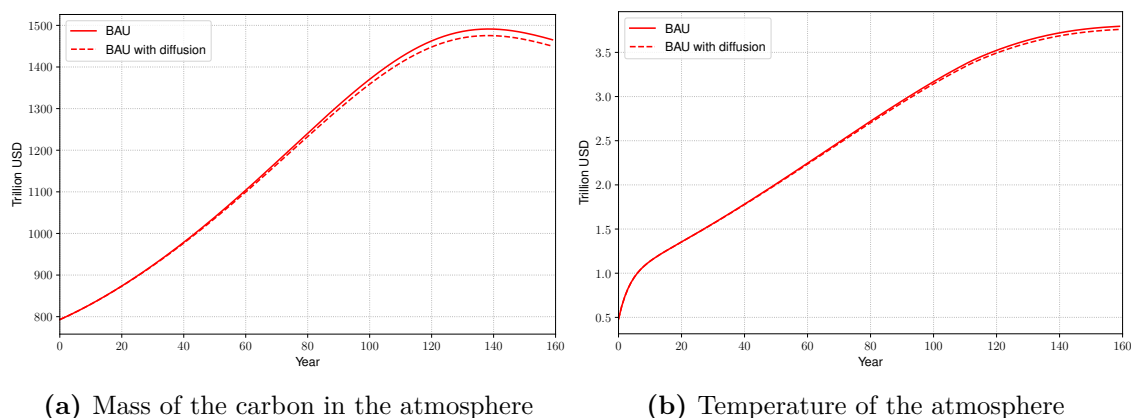


Fig. 3.15 Mass of carbon in the atmosphere (left) and temperature of the atmosphere (right). Year zero on the graphs corresponds to a starting year 1990.

3.5.3 Optimal taxation and second-best taxation with technological spillovers

As we saw in the previous section, the presence of technological spillovers in the business-as-usual case if anything makes climate indicators slightly better (under current assumptions about the elasticity of the substitution between energy inputs as well as the speed of spillovers). Now we aim at understanding if technological spillovers makes any difference for the optimal taxation case as well as for the second-best taxation case. Under the second-best taxation case I imply the case when only advanced region is subject to carbon taxation and developing region is evolving with unrestricted emissions.

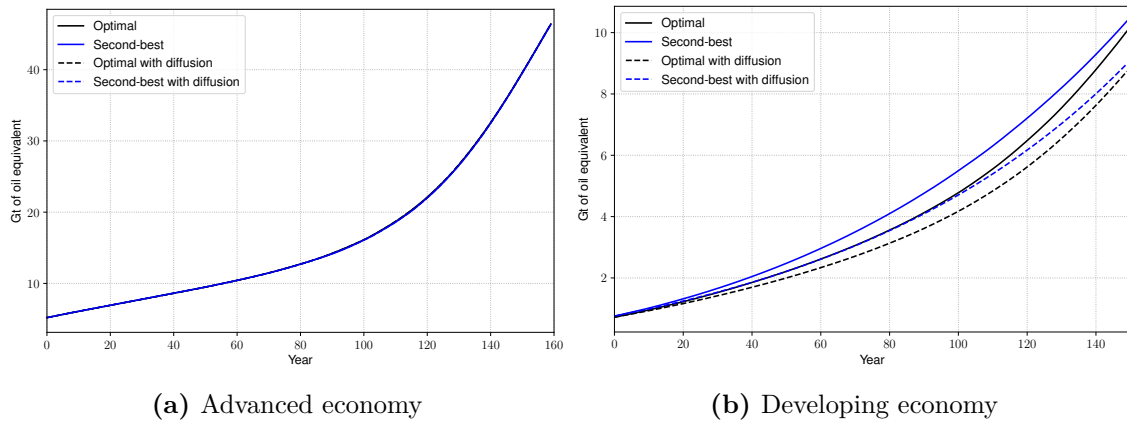


Fig. 3.16 Dirty energy in advanced (left) and developing economy (right) . Year zero on the graphs corresponds to a starting year 1990.

In the Figure 3.16 we see that the presence of the technological spillovers do not change fossil fuel usage for the advanced economy under any taxation scheme (see Figure 3.16a).

In developing countries the presence of spillovers generally decreases fossil fuel usage both in optimal and second-best cases in line with the effect of the spillovers in business-as-usual case. An interesting result that can be observed in the Figure 3.9b is that in case of spillovers and no carbon taxation in developing countries, the level of fossil fuel usage corresponds approximately to the level of fossil fuels with carbon taxation in developing countries. It means that the spillovers in renewable energy create a replacement effects in fossil fuels comparable in size with the effects of carbon taxation.

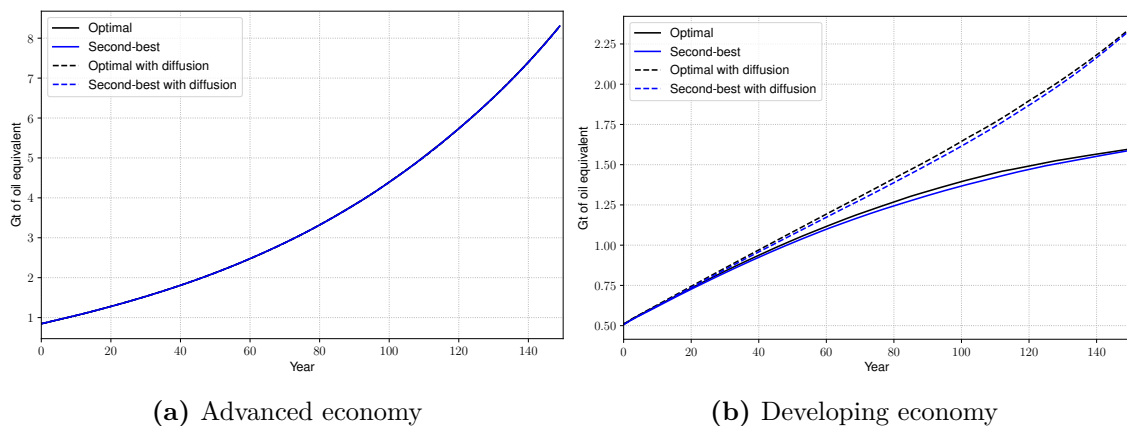


Fig. 3.17 Green energy in advanced (left) and developing economy (right). Year zero on the graphs corresponds to a starting year 1990.

Renewable energy usage, as displayed in the Figure 3.17, is substantially increased by the spillovers. In case of the renewable energy sources spillover effect is changing the growth rate of the TFP in renewable energy thus effecting significantly its productivity.

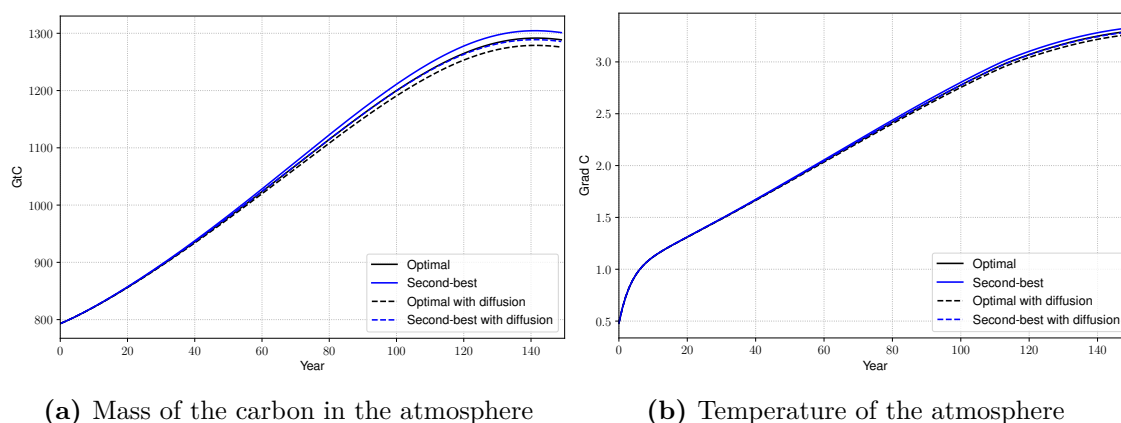


Fig. 3.18 Mass of carbon in the atmosphere (left) and temperature of the atmosphere (right). Year zero on the graphs corresponds to a starting year 1990.

In the case of taxation in an advanced economy and spillover mass of carbon in the atmosphere as well as the temperature tends to be slightly higher than in the case of optimal abatement with spillovers. From the perspective of climate change optimal mitigation with spillovers delivers the most desirable results in terms of temperature reduction.

The panel of results provides support for the policy recommendation to put effort into taxing advanced economies to provide decarbonization efforts. Developing countries being not taxed do not wipe off the gains that can be achieved by advanced economies. Allowing the developing countries to grow without the burden of environmental taxation can be a politically desirable solution and with technological spillovers the second-best taxation option becomes as good as optimal taxation without spillovers in terms of the climate impact.

3.5.4 Welfare analysis

In this section, I formally compare the welfare of the economies well as the total welfare of the social planner as consumption equivalent under different scenarios. I compare the welfare gains (losses) concerning the business-as-usual case without spillovers.

Case	Advanced region	Developing region	Total welfare
Optimal	-0.1	2.77	0.95
Second-best	-0.02	2.51	0.92
BAU with spillovers	-0.37	0.73	0.03
Optimal with spillovers	-0.01	2.74	1.0
Second-best with spillovers	-0.08	2.73	0.95

Table 3.5 Welfare values expressed in percent deviation from the BAU case without spillovers

From the Table 3.5, we can see that for developing countries the most welfare improving scenario is an optimal taxation. The reason for that can be the significant size of the damages that developing region is facing and that is not being fully covered when developing region is not internalising its damages.

The welfare gains for developing region from optimal taxation with spillovers and second-best taxation with spillovers are approximately the same. At the same time total welfare is the same in case of the optimal taxation and second-best taxation with spillovers. These two results confirm the policy recommendation that second-best taxation with spillovers is a preferable option both from the point of view of the total welfare and welfare of the developing region.

3.6 Conclusion and discussion

The green energy transition in advanced in developing countries is necessary for successful mitigation of the climate change. However, the role of technological spillovers and its interaction with carbon taxation in the decarbonization process remains unclear. Developing countries, which represent more than half of the world's population, require energy to support their economic growth, but relying on fossil fuels could jeopardize global efforts to mitigate climate change. The present paper investigates how technological spillovers between heterogeneously developed countries affect the decarbonization perspective for less developed countries. The main finding suggests that in the presence of spillovers having carbon taxation only in advanced economies becomes preferable to taxation of both and

advanced countries of spillovers are not taken into account. This highlights the importance of considering technological spillovers in the design of global climate policies.

The main result of this paper relies on two major assumptions. The first assumption concerns the way the countries were split into advanced and developing countries. In a current set-up, I assumed that advanced countries are high-income and upper-middle-income countries based on the World Bank income classification and developing countries are lower-middle-income and low-income economies. This choice was mostly driven by the empirical evidence on the innovation activity in terms of registering patents. Indeed, the set-up of the research question implies that the technology is being developed in one part of the world and adapted by the rest of the world. Both high-income and upper-middle-income countries innovate significantly, thus they were placed in the group of advanced, innovating, countries.

This split of the countries into the regions is also related to the second major assumption. By specifying the spillover process I assume the developing countries can't catch up with the advanced economies - there is always a lag in development. It is an open question whether developing countries especially the poorest ones can catch up to the level of middle-income or advanced economies. It would be possible to consider an alternative split of the world economy that puts only high-income countries in the advanced economy and the rest of the world in the developing economy. However, in this case, the context of the model presented will be significantly changed. It will be necessary to take into account that big emerging economies like China and countries of Latin America are part of the upper-middle countries and now they are driving the growth of developing regions. This would mean that innovations are not geographically anchored and spillovers can go both ways. This alternative modeling setup falls into the narrative that in general innovations around the world are produced by several big players and then spread around among other countries as well and there is a catch-up of developing countries. This alternative setup does not seem to bring additional insights to the research question of the present study, thus it was omitted.

The future avenue of research based on the built framework is twofold. First, it seems promising to conduct a global sensitivity analysis to better understand the interaction between growth rates of the energy sources in the advanced economy, technology spillovers intensity, and elasticity of substitution between energy inputs. This allows for quantita-

tively supported policy advice concerning the subsidies on innovation and technological transfer. Second, the model can be extended to include endogenous technological growth in energy as well as endogenous technological spillover intensity. This permits the exploration of directed technical mechanisms (market size effect and price effect) interacting with technological spillovers. In this case, an extension of the model with an alternative split of the world regions between advanced and developing countries as well as the possibility of catching up for the developing countries seems to be beneficial.

Appendix

3.A Model

3.A.1 Recursive formulation

$$V_t(K_t^i) = \max_{K_{t+1}^i, C_t^i, \pi_t^i, \xi_t^i} \left\{ \sum_{i \in \{a, d\}} \phi^i \frac{\left(\frac{C_t^i}{\varrho_t^i L_t}\right)^{1-1/\psi}}{1-1/\psi} \varrho_t^i L_t + e^{-\rho} V_{t+1}(K_{t+1}^i) \right\} \quad (3.A.1)$$

$$\text{s.t. } \Omega^i(T_{AT,t})(K_t^i)^\alpha \left(\varphi_t^i A_t (1 - \pi_t^i - \xi_t^i) \varrho_t^i L_t^i\right)^{1-\alpha-\nu} (E_t^i)^\nu + (1 - \delta) K_t^i - C_t^i - K_{t+1}^i = 0 \quad (\lambda_t^i) \quad (3.A.2)$$

$$1 - \pi_t^i \geq 0 \quad \perp \quad \lambda_t^{\pi^i} \geq 0 \quad (3.A.3)$$

$$1 - \xi_t^i \geq 0 \quad \perp \quad \lambda_t^{\xi^i} \geq 0 \quad (3.A.4)$$

$$E_t^i = \left(\kappa_{dt} (E_t^{i,dt})^{\rho_{CES}} + \kappa_{cl} (E_t^{i,cl})^{\rho_{CES}}\right)^{1/\rho_{CES}} \quad (3.A.5)$$

$$E_t^{i,dt} = A_{dt,t}^i \pi_t^i \varrho_t^i L_t^i \quad (3.A.6)$$

$$E_t^{i,cl} = A_{cl,t}^i \xi_t^i \varrho_t^i L_t^i \quad (3.A.7)$$

$$b_{11} M_t^{AT} + b_{21} M_t^{UO} + \sigma_t (E^{a,dt} + E^{d,dt}) + E_t^{Land} - M_{t+1}^{AT} = 0 \quad (\nu_t^{AT}) \quad (3.A.8)$$

$$b_{12} M_t^{AT} + b_{22} M_t^{UO} + b_{32} M_t^{LO} - M_{t+1}^{UO} = 0 \quad (\nu_t^{UO}) \quad (3.A.9)$$

$$b_{23} M_t^{UO} + b_{33} M_t^{LO} - M_{t+1}^{LO} = 0 \quad (\nu_t^{LO}) \quad (3.A.10)$$

$$T_t^{AT} + c_1 \left(F_{2xco2} \log_2 \left(\frac{M_t^{AT}}{M_{eq}^{AT}} \right) + F_{EX,t} \right) - c_1 \frac{F_{2xco2}}{T_{2xco2}} T_t^{AT} - c_1 c_3 (T_t^{AT} - T_t^{OC}) - T_{t+1}^{AT} = 0 \quad (\eta_t^{AT}) \quad (3.A.11)$$

$$T_t^{OC} + c_4 (T_t^{AT} - T_t^{OC}) - T_{t+1}^{OC} = 0 \quad (\eta_t^{OC}) \quad (3.A.12)$$

where $i \in \{A, D\}$, $A_t^a = \varphi_t^a A_t$, $A_t^d = \varphi_t^d A_t$, A_t is a world TFP, and $\varrho_t^a L_t^a = L_t$, $\varrho_t^d L_t^d = L_t$, where L_t is a world population. $\varphi_t^a, \varphi_t^d, \varrho_t^a, \varrho_t^d$ are exogenously given processes.

We normalize consumption, capital and energy for every economy by total labor in the economy and production TFP of the world.

$$k_t^a = \frac{K_t^a}{A_t L_t}, \quad c_t^a = \frac{C_t^a}{A_t L_t}, \quad e_t^a = \frac{E_t^a}{A_t L_t}, \quad k_{t+1}^a = \frac{K_{t+1}^a}{A_{t+1} L_{t+1}} \quad (3.A.13)$$

$$k_t^d = \frac{K_t^d}{A_t L_t}, \quad c_t^d = \frac{C_t^d}{A_t L_t}, \quad e_t^d = \frac{E_t^d}{A_t L_t}, \quad k_{t+1}^d = \frac{K_{t+1}^d}{A_{t+1} L_{t+1}} \quad (3.A.14)$$

In the objective function we divide all the terms by $A_t L_t$ and then replace $v_t = \frac{V_t}{A_t^{1-1/\psi} L_t}$.

$$\begin{aligned} \frac{V_t(K_t^a, K_t^d)}{A_t^{1-1/\psi} L_t} = & \max_{k_{t+1}^a, k_{t+1}^d, c_t^a, c_t^d, \pi_t^a, \pi_t^d, \xi_t^a, \xi_t^d} \left\{ \phi^a \frac{\left(\frac{C_t^a}{\varrho_t^a A_t L_t}\right)^{1-1/\psi} A_t^{1-1/\psi}}{1-1/\psi} \varrho_t^a \cancel{L_t} + \phi^d \frac{\left(\frac{C_t^d}{\varrho_t^d A_t L_t}\right)^{1-1/\psi} A_t^{1-1/\psi}}{1-1/\psi} \varrho_t^d \cancel{L_t} \right. \\ & \left. + \frac{e^{-\rho}}{A_t^{1-1/\psi} L_t} \frac{V_{t+1}(K_{t+1}^a, K_{t+1}^d)}{A_{t+1}^{1-1/\psi} L_{t+1}} A_{t+1}^{1-1/\psi} L_{t+1} \right\} \quad (3.A.15) \end{aligned}$$

$$v_t(k_t^a, k_t^d) = \max_{k_{t+1}^a, k_{t+1}^d, c_t^a, c_t^d, \pi_t^a, \pi_t^d, \xi_t^a, \xi_t^d} \left\{ \phi^a \frac{\left(\frac{c_t^a}{\varrho_t^a}\right)^{1-1/\psi}}{1-1/\psi} \varrho_t^a + \phi^d \frac{\left(\frac{c_t^d}{\varrho_t^d}\right)^{1-1/\psi}}{1-1/\psi} \varrho_t^d + \beta_t v_{t+1}(k_{t+1}^a, k_{t+1}^d) \right\} \quad (3.A.16)$$

We define the growth adjusted discount factor β_t as in

$$\beta_t := \exp\left(-\rho + (1-1/\psi)g_t^A + g_t^L\right). \quad (3.A.17)$$

We get a normalized problem:

$$v_t(k_t^i) = \max_{k_{t+1}^i, c_t^i, \pi_t^i, \xi_t^i} \left\{ \sum_{i \in \{a, d\}} \phi^i \frac{\left(\frac{c_t^i}{\varrho_t^i}\right)^{1-1/\psi}}{1-1/\psi} \varrho_t^i + \beta_t v_{t+1}(k_{t+1}^i) \right\} \quad (3.A.18)$$

$$\text{s.t. } \Omega^i(T_{AT,t}) (k_t^i)^\alpha \left(\varphi_t^i \varrho_t^i (1 - \pi_t^i - \xi_t^i)\right)^{1-\alpha-\nu} (e_t^i)^\nu + (1-\delta)k_t^i - c_t^i - \exp(g_t^A + g_t^L)k_{t+1}^i = 0 \quad (\lambda_t^i) \quad (3.A.19)$$

$$1 - \pi_t^i \geq 0 \quad \perp \quad \lambda_t^{\pi^i} \geq 0 \quad (3.A.20)$$

$$1 - \xi_t^i \geq 0 \quad \perp \quad \lambda_t^{\xi^i} \geq 0 \quad (3.A.21)$$

$$e_t^i = \frac{\left(\kappa_{dt} (E_t^{i,dt})^{\rho_{CES}} + \kappa_{cl} (E_t^{i,cl})^{\rho_{CES}}\right)^{1/\rho_{CES}}}{A_t L_t} \quad (3.A.22)$$

$$E_t^{i,dt} = \pi_t^i A_{dt,t}^i \varrho_t^i L_t \quad (3.A.23)$$

$$E_t^{i,cl} = \xi_t^i A_{cl,t}^i \varrho_t^i L_t \quad (3.A.24)$$

$$b_{11} M_t^{AT} + b_{21} M_t^{UO} + \sigma_t (E^{a,dt} + E^{d,dt}) + E_t^{\text{Land}} - M_{t+1}^{AT} = 0 \quad (\nu_t^{AT}) \quad (3.A.25)$$

$$b_{12}M_t^{AT} + b_{22}M_t^{UO} + b_{32}M_t^{LO} - M_{t+1}^{UO} = 0 \quad (\nu_t^{UO}) \quad (3.A.26)$$

$$b_{23}M_t^{UO} + b_{33}M_t^{LO} - M_{t+1}^{LO} = 0 \quad (\nu_t^{LO}) \quad (3.A.27)$$

$$T_t^{AT} + c_1 \left(F_{2xco2} \log_2 \left(\frac{M_t^{AT}}{M_{eq}^{AT}} \right) + F_{EX,t} \right) - c_1 \frac{F_{2xco2}}{T_{2xco2}} T_t^{AT} - c_1 c_3 (T_t^{AT} - T_t^{OC}) - T_{t+1}^{AT} = 0 \quad (\eta_t^{AT}) \quad (3.A.28)$$

$$T_t^{OC} + c_4 (T_t^{AT} - T_t^{OC}) - T_{t+1}^{OC} = 0 \quad (\eta_t^{OC}) \quad (3.A.29)$$

3.A.2 Equilibrium conditions

- Envelope theorem with respect to state variables

$$\frac{\partial v_t}{\partial k_t^i} = v_{k^i,t} = \lambda_t^i \left(\Omega^i (T_{AT,t}) \alpha (k_t^i)^{\alpha-1} (\varphi_t^i \varrho_t^i (1 - \pi_t^i - \xi_t^i))^{1-\alpha-\nu} (e_t^i)^\nu + (1 - \delta_t) \right) \quad (3.A.30)$$

$$\frac{\partial v_t}{\partial M_{AT,t}} = v_{M_{AT},t} = \nu_t^{AT} b_{11} + \nu_t^{UO} b_{12} + \eta_t^{AT} c_1 F_{2XCO2} \frac{1}{\ln 2 M_{AT,t}} \quad (3.A.31)$$

$$\frac{\partial v_t}{\partial M_{UO,t}} = v_{M_{UO},t} = \nu_t^{AT} b_{21} + \nu_t^{UO} b_{22} + \nu_t^{LO} b_{23} \quad (3.A.32)$$

$$\frac{\partial v_t}{\partial M_{LO,t}} = v_{M_{LO},t} = \nu_t^{UO} b_{32} + \nu_t^{LO} b_{33} \quad (3.A.33)$$

$$\begin{aligned} \frac{\partial v_t}{\partial T_{AT,t}} = v_{T_{AT},t} &= \sum_{i \in \{a,d\}} \lambda_t^i \Omega^{i'} (T_t^{AT}) (\varphi_t^i \varrho_t^i (1 - \pi_t^i - \xi_t^i))^{1-\alpha-\nu} (k_t^i)^\alpha (e_t^i)^\nu \\ &+ \eta_t^{AT} \left(1 - c_1 \frac{F_{2XCO2}}{T_{2XCO2}} - c_1 c_3 \right) + \eta_t^{OC} c_4 \end{aligned} \quad (3.A.34)$$

$$\frac{\partial v_t}{\partial T_{OC,t}} = v_{T_{OC},t} = \eta_t^{AT} c_1 c_3 + \eta_t^{OC} (1 - c_4). \quad (3.A.35)$$

- FOCs with respect to consumption, capital tomorrow and climate variables tomorrow

$$[c_t^i] : c_t^i = \left(\frac{\lambda_t^i}{\phi^i (\varrho_t^i)^{1-1/\psi}} \right)^{-\psi} \quad (3.A.36)$$

$$[k_{t+1}^i] : \beta_t v_{k^i,t} - \exp(g_t^A + g_t^L) \lambda_t^i = 0 \quad (3.A.37)$$

$$[M_{AT,t+1}] : \beta_t v_{M_{AT},t+1} - \nu_t^{AT} = 0 \quad (3.A.38)$$

$$[M_{UO,t+1}] : \beta_t v_{M_{UO},t+1} - \nu_t^{UO} = 0 \quad (3.A.39)$$

$$[M_{LO,t+1}] : \beta_t v_{M_{LO},t+1} - \nu_t^{LO} = 0 \quad (3.A.40)$$

$$[T_{AT,t+1}] : \beta_t v_{T_{AT},t+1} - \eta_t^{AT} = 0 \quad (3.A.41)$$

$$[T_{OC,t+1}] : \beta_t v_{T_{OC,t+1}} - \eta_t^{OC} = 0 \quad (3.A.42)$$

- Budget constraints:

$$\Omega^i(T_{AT,t}) \left(k_t^i\right)^\alpha \left(\varphi_t^i \varrho_t^i (1 - \pi_t^i - \xi_t^i)\right)^{1-\alpha-\nu} \left(e_t^i\right)^\nu + (1 - \delta) k_t^i - c_t^i - \exp\left(g_t^A + g_t^L\right) k_{t+1}^i = 0 \quad (3.A.43)$$

- KKT condition for π_t^i :

$$\Psi^{FB}\left(\lambda_t^{\pi^i}, 1 - \pi_t^i\right) = \lambda_t^{\pi^i} + \left(1 - \pi_t^i\right) - \sqrt{\left(\lambda_t^{\pi^i}\right)^2 + \left(1 - \pi_t^i\right)^2}, \quad (3.A.44)$$

where

$$\begin{aligned} \lambda_t^{\pi^i} = & \lambda_t^i \nu A_{dt,t}^i \varrho_t^i L_t \kappa_{dt} \Omega^i(T_{AT,t}) \left(k_t^i\right)^\alpha \left(e_t^i\right)^\nu \left(\varphi_t^i \varrho_t^i (1 - \pi_t^i - \xi_t^i)\right)^{1-\alpha-\nu} \left(E_t^i\right)^{-\rho} \left(E_t^{i,dt}\right)^{\rho-1} \\ & - (1 - \alpha - \nu) \varphi_t^i \varrho_t^i \left(\varphi_t^i \varrho_t^i (1 - \pi_t^i - \xi_t^i)\right)^{-\alpha-\nu} \lambda_t^i \Omega^i(T_{AT,t}) \left(k_t^i\right)^\alpha \left(e_t^i\right)^\nu + \nu_t^{AT} \sigma_t A_{dt,t}^i \varrho_t^i L_t. \end{aligned} \quad (3.A.45)$$

- KKT condition for ξ_t^i :

$$\Psi^{FB}\left(\lambda_t^{\xi^i}, 1 - \xi_t^i\right) = \lambda_t^{\xi^i} + \left(1 - \xi_t^i\right) - \sqrt{\left(\lambda_t^{\xi^i}\right)^2 + \left(1 - \xi_t^i\right)^2}, \quad (3.A.46)$$

where

$$\begin{aligned} \lambda_t^{\xi^i} = & \lambda_t^i \nu A_{cl,t}^i \varrho_t^i L_t \kappa_{cl} \Omega^i(T_{AT,t}) \left(k_t^i\right)^\alpha \left(e_t^i\right)^\nu \left(\varphi_t^i \varrho_t^i (1 - \pi_t^i - \xi_t^i)\right)^{1-\alpha-\nu} \left(E_t^i\right)^{-\rho} \left(E_t^{i,cl}\right)^{\rho-1} \\ & - (1 - \alpha - \nu) \varphi_t^i \varrho_t^i \left(\varphi_t^i \varrho_t^i (1 - \pi_t^i - \xi_t^i)\right)^{-\alpha-\nu} \lambda_t^i \Omega^i(T_{AT,t}) \left(k_t^i\right)^\alpha \left(e_t^i\right)^\nu. \end{aligned} \quad (3.A.47)$$

Calibrated parameter	Symbol	Value 1990	Source
Capital in advanced economy (trill USD 2015)	K_0^A	148.03	PWT 10.01
Capital in developing economy (trill USD 2015)	K_0^D	14.31	PWT 10.01
Mass of carbon in the atmosphere (1000 GtC)	M_0^{AT}	0.723	author's elaboration
Mass of carbon in the upper ocean (1000 GtC)	M_0^{UO}	0.555	author's elaboration
Mass of carbon in the lower ocean (1000 GtC)	M_0^{LO}	1.301	author's elaboration
Temperature of the atmosphere (C°)	T_0^{AT}	0.64	author's elaboration
Temperature of the ocean (C°)	T_0^{OC}	0.15	author's elaboration

Table 3.B1 Starting states

3.B Parametrisation

3.B.1 Initial values

3.B.2 Parametrisation of the exogenous processes for the starting year 1990

The functional forms of the exogenous variables can be found in the Section 1.B. However, the parametrisation of the exogenous processes was adjusted to the starting year 1990.

The adjusted parameters are presented in the tables below. **Population**

Calibrated parameter	Symbol	Value 1990
Annual rate of convergence	δ^L	0.012
World population at starting year [billion]	L_0	3.03
Asymptotic world population [billion]	L_∞	11.5

Table 3.B2 Annual parametrization for labor evolution

Carbon Intensity

Calibrated parameter	Symbol	Value 1990
Initial growth of carbon intensity per year	g_0^σ	-0.008
Decline rate of decarbonization per year	δ^σ	0.01
Initial carbon intensity (1000GtC)	σ_0	0.0002

Table 3.B3 Annual parametrization for carbon intensity evolution

Emissions from land

Calibrated parameter	Symbol	Value 1990
Emissions from land (1000GtC per year)	$E_{\text{Land},0}$	0.00127
Decline rate of land emissions (per year)	δ^{Land}	0.023

Table 3.B4 Annual parametrization for the emissions from land.**Exogenous radiative forcing**

Calibrated parameter	Symbol	Value 1990
Forcings of non-CO2 GHG (Wm-2)	F_0^{EX}	0.25
2100 forcings of non-CO2 GHG (Wm-2)	F_1^{EX}	1.0
Number of years before 2100	T	110

Table 3.B5 Annual parametrization for the exogenous forcing.**3.B.3 The climate system**

The functional forms of the temperature equations can be found in the Section 1.B. However, the starting values for the temperature equations were adjusted to the starting year 1990. The adjusted parameters are presented in the tables below.

Calibrated parameter	Symbol	Value 1990
Concentration in atmosphere (1000GtC)	$M_{\text{INI}}^{\text{AT}}$	0.723
Concentration in upper strata (1000GtC)	$M_{\text{INI}}^{\text{UO}}$	0.555
Concentration in lower strata (1000GtC)	$M_{\text{INI}}^{\text{LO}}$	1.301

Table 3.B6 Annual parametrization for the mass of carbon.

Calibrated parameter	Symbol	Value 1990
Atmospheric temp change (°C) from 1850	T_0^{AT}	0.64
Lower stratum temp change (°C) from 1850	T_0^{OC}	0.15

Table 3.B7 Annual parametrization for the temperature.

3.B.4 Energy sector

To get parametrisation for the energy sector I first compute the labor shares in energy sector under the assumption of profit maximisation and given energy consumption in the year 1990. The net output was defined as follows:

$$Y_0^i = \Omega^i (T_{AT,0}) (K_0^i)^\alpha (\varphi_t^i A_0 (1 - L_{dt,0} - L_{cl,0}))^{1-\alpha-\nu} \left((\kappa_{dt} (A_{dt,0}^i L_{dt,0}^i)^{\rho_{CES}} + \kappa_{cl} (A_{cl,0}^i L_{cl,0}^i)^{\rho_{CES}})^{\frac{1}{\rho_{CES}}} \right)^\nu.$$

I take the derivative of the net output with respect to labor shares in energy sector:

$$\begin{aligned} \frac{\partial Y_0^i}{\partial L_{dt,0}^i} &= -(1 - \alpha - \nu) \frac{1}{1 - L_{dt,0}^i - L_{cl,0}^i} + \nu \kappa_{dt} \frac{1}{L_{dt,0}^i} \left(\frac{E_{dt,0}^i}{E_0^i} \right)^{\rho_{CES}} \\ \frac{\partial Y_0^i}{\partial L_{cl,0}^i} &= -(1 - \alpha - \nu) \frac{1}{1 - L_{dt,0}^i - L_{cl,0}^i} + \nu \kappa_{cl} \frac{1}{L_{cl,0}^i} \left(\frac{E_{cl,0}^i}{E_0^i} \right)^{\rho_{CES}} \end{aligned}$$

This way I get the initial shares of labor in fossil fuel and renewable energy production:

$$L_{dt,0}^i = \frac{\nu \kappa_{dt} \left(\frac{E_{dt,0}^i}{E_0^i} \right)^{\rho_{CES}}}{1 - \alpha - \nu + \nu \kappa_{dt} \left(\frac{E_{dt,0}^i}{E_0^i} \right)^{\rho_{CES}} + \nu \kappa_{cl} \left(\frac{E_{cl,0}^i}{E_0^i} \right)^{\rho_{CES}}} \quad (3.B.48)$$

$$L_{cl,0}^i = \frac{\nu \kappa_{cl} \left(\frac{E_{cl,0}^i}{E_0^i} \right)^{\rho_{CES}}}{1 - \alpha - \nu + \nu \kappa_{dt} \left(\frac{E_{dt,0}^i}{E_0^i} \right)^{\rho_{CES}} + \nu \kappa_{cl} \left(\frac{E_{cl,0}^i}{E_0^i} \right)^{\rho_{CES}}} \quad (3.B.49)$$

From this we get the following initial labor shares:

Calibrated parameter	Symbol	Value
Labor share FF in advanced	$L_{dt,0}^A$	0.045
Labor share RE in advanced	$L_{cl,0}^A$	0.012
Production labor share	$1 - L_{dt,0}^A - L_{cl,0}^A$	0.942
Labor share FF in developing	$L_{dt,0}^D$	0.047
Labor share RE in developing	$L_{cl,0}^D$	0.001
Production initial labor share	$1 - L_{dt,0}^D - L_{cl,0}^D$	0.94

Table 3.B8 Energy sector initial labor share values

Based on the initial labor shares computed above I pin down the initial TFP values for each energy sector in each region reported in Table 3.3, based on the energy consumption data in 1990.

3.C Countries by income groups based on the World Bank Classification

Afghanistan	Guinea-Bissau	Somalia
Burkina Faso	Korea, Dem. People's Rep	South Sudan
Burundi	Liberia	Sudan
Central African Republic	Madagascar	Syrian Arab Republic
Chad	Malawi	Togo
Congo, Dem. Rep	Mali	Uganda
Eritrea	Mozambique	Yemen, Rep.
Ethiopia	Niger	Zambia
Gambia, The	Rwanda	
Guinea	Sierra Leone	

Table 3.C9 Low income countries: economies with GNI less than \$1,086 per capita

Angola	India	Philippines
Algeria	Indonesia	Samoa
Bangladesh	Iran, Islamic Rep	São Tomé and Príncipe
Benin	Kenya	Senegal
Bhutan	Kiribati	Solomon Islands
Bolivia	Kyrgyz Republic	Sri Lanka
Cabo Verde	Lao PDR	Tanzania
Cambodia	Lebanon	Tajikistan
Cameroon	Lesotho	Timor-Leste
Comoros	Mauritania	Tunisia
Congo, Rep.	Micronesia, Fed. Sts.	Ukraine
Côte d'Ivoire	Mongolia	Uzbekistan
Djibouti	Morocco	Vanuatu
Egypt, Arab Rep.	Myanmar	Vietnam
El Salvador	Nepal	West Bank and Gaza
Eswatini	Nicaragua	Zimbabwe
Ghana	Nigeria	
Haiti	Pakistan	
Honduras	Papua New Guinea	

Table 3.C10 Lower-middle income countries: economies with GNI between \$1,086 and \$4,255 per capita.

Albania	Fiji	Namibia
American Samoa	Gabon	North Macedonia
Argentina	Georgia	Palau
Armenia	Grenada	Paraguay
Azerbaijan	Guatemala	Peru
Belarus	Guyana	Russian Federation
Belize	Iraq	Serbia
Bosnia and Herzegovina	Jamaica	South Africa
Botswana	Jordan	St. Lucia
Brazil	Kazakhstan	St. Vincent and the Grenadines
Bulgaria	Kosovo	Suriname
China	Libya	Thailand
Colombia	Malaysia	Tonga
Costa Rica	Maldives	Türkiye
Cuba	Marshall Islands	Turkmenistan
Dominica	Mauritius	Tuvalu
Dominican Republic	Mexico	
Equatorial Guinea	Moldova	
Ecuador	Montenegro	

Table 3.C11 Upper-middle income countries: economies with GNI between \$4,256 and \$13,205 per capita

Andorra	Greece	Poland
Antigua and Barbuda	Greenland	Portugal
Aruba	Guam	Puerto Rico
Australia	Hong Kong SAR, China	Qatar
Austria	Hungary	Romania
Bahamas, The	Iceland	San Marino
Bahrain	Ireland	Saudi Arabia
Barbados	Isle of Man	Seychelles
Belgium	Israel	Singapore
Bermuda	Italy	Sint Maarten (Dutch part)
British Virgin Islands	Japan	Slovak Republic
Brunei Darussalam	Korea, Rep.	Slovenia
Canada	Kuwait	Spain
Cayman Islands	Latvia	St. Kitts and Nevis
Channel Islands	Liechtenstein	St. Martin (French part)
Chile	Lithuania	Sweden
Croatia	Luxembourg	Switzerland
Curaçao	Macao SAR, China	Taiwan, China
Cyprus	Malta	Trinidad and Tobago

Table 3.C12 High income countries: economies with GNI more than \$13,205 per capita

Bibliography

- Acemoglu, D., Aghion, P., Bursztyn, L., & Hémous, D. (2012, February). The environment and directed technical change. *American Economic Review*, *102*(1), 131–66. Retrieved from <https://www.aeaweb.org/articles?id=10.1257/aer.102.1.131> doi: 10.1257/aer.102.1.131
- Acemoglu, D., Aghion, P., & Hémous, D. (2014). The environment and directed technical change in a north—south model. *Oxford Review of Economic Policy*, *30*(3), 513–530. Retrieved 2023-09-21, from <http://www.jstor.org/stable/43664661>
- Ackerman, F., Stanton, E. A., & Bueno, R. (2010, June). Fat tails, exponents, extreme uncertainty: Simulating catastrophe in DICE. *Ecological Economics*, *69*(8), 1657–1665. doi: 10.1016/j.ecolecon.2010.03.013
- Aghion, P., & Howitt, P. W. (1997). *Endogenous growth theory*. The MIT Press.
- Allen, M. R., & Frame, D. J. (2007, October). Call Off the Quest. *Science*, *318*(5850), 582–583. doi: 10.1126/science.1149988
- Anderson, B., Borgonovo, E., Galeotti, M., & Roson, R. (2014, February). Uncertainty in Climate Change Modeling: Can Global Sensitivity Analysis Be of Help? *Risk Analysis*, *34*(2), 271–293. doi: 10.1111/risa.12117
- Andrews, T., Bodas-Salcedo, A., Gregory, J. M., Dong, Y., Armour, K. C., Paynter, D., ... Liu, C. (2022, September). On the Effect of Historical SST Patterns on Radiative Feedback. *Journal of Geophysical Research (Atmospheres)*, *127*(18), e2022JD036675. doi: 10.1029/2022JD036675
- Anthoff, D., Tol, R. S. J., & Yohe, G. W. (2009, April). Risk aversion, time preference, and the social cost of carbon. *Environmental Research Letters*, *4*(2), 024002. doi: 10.1088/1748-9326/4/2/024002
- Arellano, C., Bai, Y., & Mihalache, G. P. (2020, May). *Deadly debt crises: Covid-19 in emerging markets* (Working Paper No. 27275). National Bureau of Economic Research. Retrieved from <http://www.nber.org/papers/w27275> doi: 10.3386/w27275

- Arora, V. K., Boer, G. J., Friedlingstein, P., Eby, M., Jones, C. D., Christian, J. R., ... Wu, T. (2013, August). Carbon-Concentration and Carbon-Climate Feedbacks in CMIP5 Earth System Models. *Journal of Climate*, *26*(15), 5289-5314. doi: 10.1175/JCLI-D-12-00494.1
- Arora, V. K., Katavouta, A., Williams, R. G., Jones, C. D., Brovkin, V., Friedlingstein, P., ... Ziehn, T. (2020, August). Carbon-concentration and carbon-climate feedbacks in CMIP6 models and their comparison to CMIP5 models. *Biogeosciences*, *17*(16), 4173-4222. doi: 10.5194/bg-17-4173-2020
- Azinovic, M., Gaegauf, L., & Scheidegger, S. (2022). Deep equilibrium nets. *International Economic Review*, *63*(4), 1471-1525.
- Barnett, M. (2023). Climate change and uncertainty: An asset pricing perspective. *Management Science*.
- Barnett, M., Brock, W., & Hansen, L. P. (2020a). *How should climate change uncertainty impact social valuation and policy?* Retrieved from https://larspeterhansen.org/wp-content/uploads/2020/12/shortpaper_LPH-2.pdf
- Barnett, M., Brock, W., & Hansen, L. P. (2020b). Pricing uncertainty induced by climate change. *The Review of Financial Studies*, *33*(3), 1024-1066.
- Barrage, L. (2018). Be careful what you calibrate for: social discounting in general equilibrium. *Journal of Public Economics*, *160*, 33-49.
- Barrett, P. (2021). Can International Technological Diffusion Substitute for Coordinated Global Policies to Mitigate Climate Change? *IMF Working Papers*, *2021*(173), 1. doi: 10.5089/9781513585765.001
- Bauer, M. D., & Rudebusch, G. D. (2021). The rising cost of climate change: evidence from the bond market. *The Review of Economics and Statistics*, 1-45.
- Bellman, R. E. (1961). *Adaptive control processes: A guided tour*. Princeton University Press.
- Bergstra, J. S., Bardenet, R., Bengio, Y., & Kégl, B. (2011). Algorithms for hyperparameter optimization. In *Advances in neural information processing systems* (pp. 2546-2554).
- Beusch, L., Gudmundsson, L., & Seneviratne, S. I. (2020). Emulating earth system model temperatures with mesmer: from global mean temperature trajectories to grid-point-level realizations on land. *Earth System Dynamics*, *11*(1), 139-159. Retrieved from <https://esd.copernicus.org/articles/11/139/2020/> doi: 10.5194/esd-11-139-2020

- Blatman, G., & Sudret, B. (2010, April). An adaptive algorithm to build up sparse polynomial chaos expansions for stochastic finite element analysis. *Probabilistic Engineering Mechanics*, 25(2), 183–197. doi: 10.1016/j.probengmech.2009.10.003
- Bosetti, V., Eni, F., Mattei, E., Massetti, E., & Tavoni, M. (2007). *The WITCH Model: Structure, Baseline, Solutions*. Retrieved from <http://dx.doi.org/10.2139/ssrn.960746> (Working paper)
- Brock, W., Cai, Y., Judd, K., & Xepapadeas, A. (2018). *Climate policy under cooperation and competition between regions with spatial heat transport* (Vol. 24473) (No. March).
- Brock, W. A., Engström, G., Grass, D., & Xepapadeas, A. (2013). Energy balance climate models and general equilibrium optimal mitigation policies. *Journal of Economic Dynamics and Control*, 37(12), 2371–2396. Retrieved from <http://dx.doi.org/10.1016/j.jedc.2013.09.008> doi: 10.1016/j.jedc.2013.09.008
- Brumm, J., & Scheidegger, S. (2017). Using adaptive sparse grids to solve high-dimensional dynamic models. *Econometrica*, 85(5), 1575–1612. Retrieved from <https://onlinelibrary.wiley.com/doi/abs/10.3982/ECTA12216> doi: <https://doi.org/10.3982/ECTA12216>
- Butler, M. P., Reed, P. M., Fisher-Vanden, K., Keller, K., & Wagener, T. (2014, September). Identifying parametric controls and dependencies in integrated assessment models using global sensitivity analysis. *Environmental Modelling & Software*, 59, 10–29. doi: 10.1016/j.envsoft.2014.05.001
- Cai, Y., Brock, W., Xepapadeas, A., & Judd, K. (2019). *Climate policy under spatial heat transport: Cooperative and noncooperative regional outcomes* (Tech. Rep.). The Ohio State University. Retrieved from <https://arxiv.org/abs/1909.04009>
- Cai, Y., & Judd, K. L. (2014). Advances in numerical dynamic programming and new applications. *Handbook of computational economics*, 3.
- Cai, Y., Judd, K. L., Lenton, T. M., Lontzek, T. S., & Narita, D. (2015). Environmental tipping points significantly affect the cost-benefit assessment of climate policies. *Proceedings of the National Academy of Sciences of the United States of America*, 112(15), 4606–4611. doi: 10.1073/pnas.1503890112
- Cai, Y., Judd, K. L., & Lontzek, T. S. (2012, September). *Continuous-Time Methods for Integrated Assessment Models* (NBER Working Papers No. 18365). National Bureau of Economic Research, Inc. Retrieved from <https://ideas.repec.org/p/nbr/nberwo/18365.html>
- Cai, Y., Lenton, T. M., & Lontzek, T. S. (2016, May). Risk of multiple interacting tipping points should encourage rapid CO2 emission reduction. *Nature Climate Change*, 6(5), 520–525. doi: 10.1038/nclimate2964

- Cai, Y., & Lontzek, T. (2019). The social cost of carbon with economic and climate risks. *Journal of Political Economy*, 127(6), 2684–2734. doi: 10.1086/701890
- Calel, R., & Stainforth, D. A. (2017). On the physics of three integrated assessment models. *Bulletin of the American Meteorological Society*, 98(6), 1199–1216. doi: 10.1175/BAMS-D-16-0034.1
- Calvet, L. E., Campbell, J. Y., Gomes, F., & Sodini, P. (2021). *The cross-section of household preferences* (Tech. Rep.). National Bureau of Economic Research. Retrieved from <https://www.nber.org/papers/w28788>
- Carleton, T. A., Jina, A., Delgado, M. T., Greenstone, M., Houser, T., Hsiang, S. M., . . . others (2020). *Valuing the global mortality consequences of climate change accounting for adaptation costs and benefits* (Tech. Rep.). National Bureau of Economic Research. Retrieved from https://www.nber.org/system/files/working_papers/w27599/w27599.pdf
- Chen, H., Didisheim, A., & Scheidegger, S. (2021). *Deep Structural Estimation : With an Application to Option Pricing* (Tech. Rep.). Retrieved from <https://arxiv.org/abs/2102.09209>
- Clarke, L., Edmonds, J., Krey, V., Richels, R., Rose, S., & Tavoni, M. (2009). International climate policy architectures: Overview of the EMF 22 International Scenarios. *Energy Economics*, 31(SUPPL. 2), S64–S81. Retrieved from <http://dx.doi.org/10.1016/j.eneco.2009.10.013> doi: 10.1016/j.eneco.2009.10.013
- Climate Change 2014 Synthesis Report IPCC. (2014). Climate Change 2014 Synthesis Report Summary Chapter for Policymakers. *Ipcc*, 31.
- Comin, D., & Hobijn, B. (2010, December). An exploration of technology diffusion. *American Economic Review*, 100(5), 2031–59. Retrieved from <https://www.aeaweb.org/articles?id=10.1257/aer.100.5.2031> doi: 10.1257/aer.100.5.2031
- Constantine, P. G. (2015). *Active subspaces*. Philadelphia, PA: Society for Industrial and Applied Mathematics. Retrieved from <https://epubs.siam.org/doi/abs/10.1137/1.9781611973860> doi: 10.1137/1.9781611973860
- Crost, B., & Traeger, C. P. (2013, September). Optimal climate policy: Uncertainty versus Monte Carlo. *Economics Letters*, 120(3), 552–558. doi: 10.1016/j.econlet.2013.05.019
- Crost, B., & Traeger, C. P. (2014). Optimal CO2 mitigation under damage risk valuation. *Nature Climate Change*, 4(7), 631–636. doi: 10.1038/nclimate2249

- Danabasoglu, G., Lamarque, J. F., Bacmeister, J., Bailey, D. A., DuVivier, A. K. Â., Edwards, J., ... Strand, W. G. (2020, February). The Community Earth System Model Version 2 (CESM2). *Journal of Advances in Modeling Earth Systems*, 12(2), e01916. doi: 10.1029/2019MS001916
- Dechezleprêtre, A., Glachant, M., & Ménière, Y. (2013). What drives the international transfer of climate change mitigation technologies? empirical evidence from patent data. *Environmental and Resource Economics*, 54(2), 161–178. Retrieved from <https://doi.org/10.1007/s10640-012-9592-0> doi: 10.1007/s10640-012-9592-0
- DeGroot, M. H. (1970). *Optimal Statistical Decisions*. Wiley. doi: 10.1002/0471729000
- Denning, F., & Emmerling, J. (2017). *A note on optima with negishi weights* (Tech. Rep.). Princeton University. Retrieved from https://www.researchgate.net/publication/316620892_A_Note_on_Optima_with_Negishi_Weights
- Dietz, S., van der Ploeg, F., Rezai, A., & Venmans, F. (2021). Are economists getting climate dynamics right and does it matter? *Journal of the Association of Environmental and Resource Economists*, 8(5), 895–921. Retrieved from <https://doi.org/10.1086/713977> doi: 10.1086/713977
- Dietz, S., & Venmans, F. (2019). Cumulative carbon emissions and economic policy: In search of general principles. *Journal of Environmental Economics and Management*, 96, 108–129. Retrieved from <https://doi.org/10.1016/j.jeem.2019.04.003> doi: 10.1016/j.jeem.2019.04.003
- Duarte, V. (2018, April). *Machine Learning for Continuous-Time Economics* (SSRN Scholarly Paper No. ID 3012602). Rochester, NY: Social Science Research Network. doi: 10.2139/ssrn.3012602
- Eaton, J., & Kortum, S. (1999). International technology diffusion: Theory and measurement. *International Economic Review*, 40(3), 537–570. Retrieved 2023-09-23, from <http://www.jstor.org/stable/2648766>
- Ebrahimi Kahou, M., Fernández-Villaverde, J., Perla, J., & Sood, A. (2021, July). *Exploiting symmetry in high-dimensional dynamic programming* (Working Paper No. 28981). National Bureau of Economic Research. Retrieved from <http://www.nber.org/papers/w28981> doi: 10.3386/w28981
- Eftekhari, A., & Scheidegger, S. (2022). High-dimensional dynamic stochastic model representation. *SIAM Journal on Scientific Computing*, 44(3), C210–C236. Retrieved from <https://doi.org/10.1137/21M1392231> doi: 10.1137/21M1392231

- Eftekhari, A., Scheidegger, S., & Schenk, O. (2017). Parallelized dimensional decomposition for large-scale dynamic stochastic economic models. In *Proceedings of the platform for advanced scientific computing conference* (pp. 9:1–9:11). New York, NY, USA: ACM. Retrieved from <http://doi.acm.org/10.1145/3093172.3093234> doi: 10.1145/3093172.3093234
- Epstein, L. G., & Zin, S. E. (1989, July). Substitution, Risk Aversion, and the Temporal Behavior of Consumption and Asset Returns: A Theoretical Framework. *Econometrica*, 57(4), 937. doi: 10.2307/1913778
- Eyring, V., Bony, S., Meehl, G. A., Senior, C. A., Stevens, B., Stouffer, R. J., & Taylor, K. E. (2016). Overview of the Coupled Model Intercomparison Project Phase 6 (CMIP6) experimental design and organization. *Geoscientific Model Development*, 9, 1937-1958. doi: 10.5194/gmd-9-1937-2016
- Fay, M., Hallegatte, S., Vogt-Schilb, A., Rozenberg, J., Narloch, U., & Kerr, T. (2015). *Decarbonizing development*. The World Bank Group. Retrieved from <https://EconPapers.repec.org/RePEc:wbk:wbpubs:21842>
- Fernández-Villaverde, J., Nuño, G., Sorg-Langhans, G., & Vogler, M. (2020). *Solving High-Dimensional Dynamic Programming Problems using Deep Learning* (Tech. Rep.). National Bureau of Economic Research. Retrieved from https://maximilianvogler.github.io/My_Website/Deep_Learning.pdf
- Fitzpatrick, L. G., & Kelly, D. L. (2017). Probabilistic Stabilization Targets. *Journal of the Association of Environmental and Resource Economists*, 4(2), 611–657.
- Flamos, A. (2019). *Understanding Risks and Uncertainties in Energy and Climate Policy*. doi: 10.1007/978-3-030-03152-7
- Folini, D., Friedl, A., Kubler, F., & Scheidegger, S. (2023). *The climate in climate economics*. Retrieved from https://papers.ssrn.com/sol3/papers.cfm?abstract_id=3885021
- Fredriksen, H.-B., Smith, C. J., Modak, A., & Rugenstein, M. (2023, March). 21st Century Scenario Forcing Increases More for CMIP6 Than CMIP5 Models. *Geophysical Research Letters*, 50(6), e2023GL102916. doi: 10.1029/2023GL102916
- Fried, S., & Lagakos, D. (2023). Electricity and Firm Productivity: A General-Equilibrium Approach. *American Economic Journal: Macroeconomics*.
- Gambhir, A., Napp, T., Hawkes, A., Höglund-Isaksson, L., Winiwarter, W., Purohit, P., ... Lowe, J. (2017). The contribution of non-co2 greenhouse gas mitigation to achieving long-term temperature goals. *Energies*, 10(5). Retrieved from <https://www.mdpi.com/1996-1073/10/5/602> doi: 10.3390/en10050602

- Geoffroy, O., Saint-Martin, D., Bellon, G., Voldoire, A., Olivié, D. J., & Tytéca, S. (2013). Transient climate response in a two-layer energy-balance model. Part II: Representation of the efficacy of deep-ocean heat uptake and validation for CMIP5 AOGCMs. *Journal of Climate*, 26(6), 1859–1876. doi: 10.1175/JCLI-D-12-00196.1
- Gillingham, K., Nordhaus, W., Anthoff, D., Blanford, G., Bosetti, V., Christensen, P., ... Reilly, J. (2018, October). Modeling Uncertainty in Integrated Assessment of Climate Change: A Multimodel Comparison. *Journal of the Association of Environmental and Resource Economists*, 5(4), 791–826. doi: 10.1086/698910
- Glorot, X., & Bengio, Y. (2010, 13–15 May). Understanding the difficulty of training deep feedforward neural networks. In Y. W. Teh & M. Titterton (Eds.), *Proceedings of the thirteenth international conference on artificial intelligence and statistics* (Vol. 9, pp. 249–256). Chia Laguna Resort, Sardinia, Italy: PMLR. Retrieved from <https://proceedings.mlr.press/v9/glorot10a.html>
- Golosov, M., Hassler, J., Krusell, P., & Tsyvinski, A. (2014). Optimal Taxes on Fossil Fuel in General Equilibrium. *Econometrica*, 82(1), 41–88. doi: 10.3982/ECTA10217
- Goodfellow, I., Bengio, Y., & Courville, A. (2016). *Deep learning*. MIT Press. (<http://www.deeplearningbook.org>)
- Grossman, G., & Helpman, E. (1993). *Innovation and growth in the global economy*. MIT Press. Retrieved from <https://books.google.de/books?id=4ikgmM2vLJ0C>
- Hambel, C., Kraft, H., & Schwartz, E. (2021). Optimal carbon abatement in a stochastic equilibrium model with climate change. *European Economic Review*, 132, 103642. Retrieved from <https://doi.org/10.1016/j.euroecorev.2020.103642> doi: 10.1016/j.euroecorev.2020.103642
- Hänsel, M. C., Drupp, M. A., Johansson, D. J., Nesje, F., Azar, C., Freeman, M. C., ... Sterner, T. (2020). Climate economics support for the UN climate targets. *Nature Climate Change*, 10(8), 781–789. Retrieved from <http://dx.doi.org/10.1038/s41558-020-0833-x> doi: 10.1038/s41558-020-0833-x
- Hänsel, M. C., & Quaas, M. F. (2018). Intertemporal Distribution, Sufficiency, and the Social Cost of Carbon. *Ecological Economics*, 146(December 2017), 520–535. Retrieved from <https://doi.org/10.1016/j.ecolecon.2017.11.024> doi: 10.1016/j.ecolecon.2017.11.024
- Hare, B., Brecha, R., & Schaeffer, M. (2018). Integrated Assessment Models : what are they and how do they arrive at their conclusions? *Climate Analytics*, 1–12.
- Harenberg, D., Marelli, S., Sudret, B., & Winschel, V. (2019). Uncertainty quantification and global sensitivity analysis for economic models. *Quantitative Economics*, 10(1), 1–41. doi: 10.3982/QE866

- Hassler, J., & Krusell, P. (2012). Economics and climate change: Integrated assessment in a multi-region world. *Journal of the European Economic Association*, 10(5), 974–1000. doi: 10.1111/j.1542-4774.2012.01082.x
- Hassler, J., & Krusell, P. (2018). *Environmental macroeconomics: The case of climate change* (Vol. 4). Elsevier B.V. Retrieved from <https://doi.org/10.1016/bs.hesenv.2018.08.003> doi: 10.1016/bs.hesenv.2018.08.003
- Hassler, J., Krusell, P., & Olovsson, C. (2018). The Consequences of Uncertainty: Climate Sensitivity and Economic Sensitivity to the Climate. *Annual Review of Economics*, 10, 189–205. doi: 10.1146/annurev-economics-080217-053229
- Hassler, J., Krusell, P., Olovsson, C., & Reiter, M. (2019). *Integrated assessment in a multi-region world with multiple energy sources and endogenous technical change*. Retrieved from <https://www.frbsf.org/wp-content/uploads/sites/4/Paper-3-2019-11-8-0lovsson-1045AM-1st-paper.pdf>
- Hassler, J., Krusell, P., Olovsson, C., & Reiter, M. (2020). *On the effectiveness of climate policies*. Retrieved from <http://hassler-j.iies.su.se/PAPERS/HKOR.pdf>
- Hassler, J., Krusell, P., & Smith, A. A. (2016a). Chapter 24 - Environmental Macroeconomics. In J. B. Taylor & H. B. T. H. o. M. Uhlig (Eds.), (Vol. 2, pp. 1893–2008). Elsevier. doi: 10.1016/bs.hesmac.2016.04.007
- Hassler, J., Krusell, P., & Smith, A. A. (2016b). Environmental Macroeconomics. *Handbook of Macroeconomics*, 2, 1893–2008. doi: 10.1016/bs.hesmac.2016.04.007
- Hillebrand, E., & Hillebrand, M. (2019). Optimal climate policies in a dynamic multi-country equilibrium model. *Journal of Economic Theory*, 179, 200–239. Retrieved from <https://doi.org/10.1016/j.jet.2018.11.001> doi: 10.1016/j.jet.2018.11.001
- Hope, C. (2013, April). Critical issues for the calculation of the social cost of CO₂ : why the estimates from PAGE09 are higher than those from PAGE2002. *Climatic Change*, 117(3), 531-543. Retrieved from <https://ideas.repec.org/a/spr/climat/v117y2013i3p531-543.html> doi: 10.1007/s10584-012-0633-z
- Hornik, K., Stinchcombe, M., & White, H. (1989). Multilayer feedforward networks are universal approximators. *Neural Networks*, 2(5), 359 - 366. Retrieved from <http://www.sciencedirect.com/science/article/pii/0893608089900208> doi: [https://doi.org/10.1016/0893-6080\(89\)90020-8](https://doi.org/10.1016/0893-6080(89)90020-8)
- Howard, P. H., & Sterner, T. (2017). Few and Not So Far Between: A Meta-analysis of Climate Damage Estimates. *Environmental and Resource Economics*, 68(1), 197–225. doi: 10.1007/s10640-017-0166-z

- Hwang, I. C., Reynès, F., & Tol, R. S. (2017, May). The effect of learning on climate policy under fat-tailed risk. *Resource and Energy Economics*, *48*, 1–18. doi: 10.1016/j.reseneeco.2017.01.001
- Intergovernmental Panel on Climate Change, & Intergovernmental Panel on Climate Change. (2015). Assessing Transformation Pathways. *Climate Change 2014 Mitigation of Climate Change*, 413–510. doi: 10.1017/cbo9781107415416.012
- Iooss, B., & Prieur, C. (2019). Shapley effects for sensitivity analysis with correlated inputs: Comparisons with Sobol’ indices, numerical estimation and applications. *International Journal for Uncertainty Quantification*, *9*(5). doi: 10.1615/Int.J.UncertaintyQuantification.2019028372
- IPCC. (2021). Annex vii: Glossary [matthews, j.b.r., v. möller, r. van diemen, j.s. fuglestvedt, v. masson-delmotte, c. méndez, s. semenov, a. reisinger (eds.)] [Book Section]. In V. Masson-Delmotte et al. (Eds.), *Climate change 2021: The physical science basis. contribution of working group i to the sixth assessment report of the intergovernmental panel on climate change* (p. 2215–2256). Cambridge, United Kingdom and New York, NY, USA: Cambridge University Press. doi: 10.1017/9781009157896.022
- Jackson, L. S., Maycock, A. C., Andrews, T., Fredriksen, H. B., Smith, C. J., & Forster, P. M. (2022, August). Errors in Simple Climate Model Emulations of Past and Future Global Temperature Change. *Geophysical Research Letters*, *49*(15), e98808. doi: 10.1029/2022GL098808
- Jaynes, E. T. (1957, October). Information Theory and Statistical Mechanics. II. *Physical review*, *108*(2), 171–190. Retrieved from <http://link.aps.org/doi/10.1103/PhysRev.108.171> doi: 10.1103/PhysRev.108.171
- Jaynes, E. T. (1982). On the rationale of maximum-entropy methods [Article]. *Proceedings of the IEEE*, *70*(9), 939 – 952. Retrieved from <https://www.scopus.com/inward/record.uri?eid=2-s2.0-0020187981&doi=10.1109/2fPROC.1982.12425&partnerID=40&md5=05a97aaf44a75219955549a3d5172afb> (Cited by: 1118) doi: 10.1109/PROC.1982.12425
- Jeltsch-Thömmes, A., & Joos, F. (2020, March). Modeling the evolution of pulse-like perturbations in atmospheric carbon and carbon isotopes: the role of weathering-sedimentation imbalances. *Climate of the Past*, *16*(2), 423–451. doi: 10.5194/cp-16-423-2020
- Jensen, S., & Traeger, C. (2013). Optimally climate sensitive policy: A comprehensive evaluation of uncertainty & learning. *Department of Agricultural and Resource Economics, UC Berkeley*.

- Jensen, S., & Traeger, C. P. (2014, July). Optimal climate change mitigation under long-term growth uncertainty: Stochastic integrated assessment and analytic findings. *European Economic Review*, *69*, 104–125. doi: 10.1016/j.euroecorev.2014.01.008
- Jo, A. (2020, October). *The Elasticity of Substitution between Clean and Dirty Energy with Technological Bias* (CER-ETH Economics working paper series No. 20/344). CER-ETH - Center of Economic Research (CER-ETH) at ETH Zurich. Retrieved from <https://ideas.repec.org/p/eth/wpswif/20-344.html>
- Joos, F., Prentice, I. C., Sitch, S., Meyer, R., Hooss, G., Plattner, G.-K., ... Hasselmann, K. (2001, December). Global warming feedbacks on terrestrial carbon uptake under the Intergovernmental Panel on Climate Change (IPCC) Emission Scenarios. *Global Biogeochemical Cycles*, *15*(4), 891–907. doi: 10.1029/2000GB001375
- Joos, F., Roth, R., Fuglestedt, J. S., Peters, G. P., Enting, I. G., Bloh, W. v., ... others (2013). Carbon dioxide and climate impulse response functions for the computation of greenhouse gas metrics: a multi-model analysis. *Atmospheric Chemistry and Physics*, *13*(5), 2793–2825.
- Keeling, C. D. (1973). Industrial production of carbon dioxide from fossil fuels and limestone. *Tellus*, *25*(2), 174–198. Retrieved from <https://onlinelibrary.wiley.com/doi/abs/10.1111/j.2153-3490.1973.tb01604.x> doi: <https://doi.org/10.1111/j.2153-3490.1973.tb01604.x>
- Keller, D. P., Lenton, A., Scott, V., Vaughan, N. E., Bauer, N., Ji, D., ... Zickfeld, K. (2018). The carbon dioxide removal model intercomparison project (cdmip): rationale and experimental protocol for cmip6. *Geoscientific Model Development*, *11*(3), 1133–1160. Retrieved from <https://gmd.copernicus.org/articles/11/1133/2018/> doi: 10.5194/gmd-11-1133-2018
- Kelly, D. L., & Kolstad, C. D. (1999, February). Bayesian learning, growth, and pollution. *Journal of Economic Dynamics and Control*, *23*(4), 491–518. doi: 10.1016/S0165-1889(98)00034-7
- Kelly, D. L., & Kolstad, C. D. (2001). Solving infinite horizon growth models with an environmental sector. *Computational Economics*, *18*(2), 217–231. doi: 10.1023/A:1021018417052
- Kelly, D. L., & Tan, Z. (2015). Learning and climate feedbacks: Optimal climate insurance and fat tails. *Journal of Environmental Economics and Management*, *72*, 98–122. doi: 10.1016/j.jeem.2015.05.001
- Kingma, D. P., & Ba, J. (2014). Adam: A method for stochastic optimization. *arXiv preprint arXiv:1412.6980*.
- Knutti, R., Rugenstein, M. A. A., & Hegerl, G. C. (2017, October). Beyond equilibrium climate sensitivity. *Nature Geoscience*, *10*(10), 727–736. doi: 10.1038/ngeo3017

- Kotlikoff, L., Kubler, F., Polbin, A., & Scheidegger, S. (2021a). Making carbon taxation a generational win-win. *International Economic Review*, 62, 3-46.
- Kotlikoff, L., Kubler, F., Polbin, A., & Scheidegger, S. (2021b, 02). Pareto-improving carbon-risk taxation. *Economic Policy*, 36(107), 551-589. Retrieved from <https://doi.org/10.1093/epolic/eiab008> doi: 10.1093/epolic/eiab008
- Kotlikoff, L. J., Kubler, F., Polbin, A., & Scheidegger, S. (2021, September). *Can today's and tomorrow's world uniformly gain from carbon taxation?* (Working Paper No. 29224). National Bureau of Economic Research. Retrieved from <http://www.nber.org/papers/w29224> doi: 10.3386/w29224
- Kraay, A., & McKenzie, D. (2014, September). Do poverty traps exist? assessing the evidence. *Journal of Economic Perspectives*, 28(3), 127-48. Retrieved from <https://www.aeaweb.org/articles?id=10.1257/jep.28.3.127> doi: 10.1257/jep.28.3.127
- Krusell, P., & Smith Jr, A. A. (2018). Climate change around the world.. Retrieved from <http://www.econ.yale.edu/smith/munich2.pdf>
- Kubler, F., & Scheidegger, S. (2023). Uniformly self-justified equilibria. *Journal of Economic Theory*, 212, 105707. Retrieved from <https://www.sciencedirect.com/science/article/pii/S0022053123001035> doi: <https://doi.org/10.1016/j.jet.2023.105707>
- Känzig, D. R., & Konradt, M. (2023, May). *Climate policy and the economy: Evidence from europe's carbon pricing initiatives* (Working Paper No. 31260). National Bureau of Economic Research. Retrieved from <http://www.nber.org/papers/w31260> doi: 10.3386/w31260
- Le Quéré, C., Andrew, R. M., Friedlingstein, P., Sitch, S., Hauck, J., Pongratz, J., ... Zheng, B. (2018, December). Global Carbon Budget 2018. *Earth System Science Data*, 10(4), 2141-2194. doi: 10.5194/essd-10-2141-2018
- Leach, A. J. (2007, May). The climate change learning curve. *Journal of Economic Dynamics and Control*, 31(5), 1728–1752. doi: 10.1016/j.jedc.2006.06.001
- Le Gratiet, L., Marelli, S., & Sudret, B. (2017). Metamodel-Based Sensitivity Analysis: Polynomial Chaos Expansions and Gaussian Processes. In R. Ghanem, D. Higdon, & H. Owhadi (Eds.), *Handbook of Uncertainty Quantification* (pp. 1289–1325). Cham: Springer International Publishing. doi: 10.1007/978-3-319-12385-1_38
- Lemoine, D., & Traeger, C. (2014). Watch your step: Optimal policy in a tipping climate. *American Economic Journal: Economic Policy*, 6(1 B), 137–166. doi: 10.1257/pol.6.1.137

- Lemoine, D., & Traeger, C. P. (2016, May). Economics of tipping the climate dominoes. *Nature Climate Change*, 6(5), 514–519. doi: 10.1038/nclimate2902
- Lenton, T. M., Held, H., Kriegler, E., Hall, J. W., Lucht, W., Rahmstorf, S., & Schellnhuber, H. J. (2008). Tipping elements in the earth's climate system. *Proceedings of the national Academy of Sciences*, 105(6), 1786–1793.
- Lontzek, T. S., Cai, Y., Judd, K. L., & Lenton, T. M. (2015, may). Stochastic integrated assessment of climate tipping points indicates the need for strict climate policy. *Nature Climate Change*, 5(5), 441–444. Retrieved from <http://www.nature.com/articles/nclimate2570> doi: 10.1038/nclimate2570
- Lontzek, T. S., & Narita, D. (2011, December). Risk-Averse Mitigation Decisions in an Unpredictable Climate System. *The Scandinavian Journal of Economics*, 113(4), 937–958. doi: 10.1111/j.1467-9442.2011.01679.x
- Lontzek, T. S., Narita, D., & Wilms, O. (2016, November). Stochastic Integrated Assessment of Ecosystem Tipping Risk. *Environmental and Resource Economics*, 65(3), 573–598. doi: 10.1007/s10640-016-0054-y
- Ma, X., & Zabaras, N. (2010, may). An adaptive high-dimensional stochastic model representation technique for the solution of stochastic partial differential equations. *J. Comput. Phys.*, 229(10), 3884–3915. Retrieved from <https://doi.org/10.1016/j.jcp.2010.01.033> doi: 10.1016/j.jcp.2010.01.033
- MacDougall, A. H., Eby, M., & Weaver, A. J. (2013, December). If Anthropogenic CO₂Emissions Cease, Will Atmospheric CO₂Concentration Continue to Increase? *Journal of Climate*, 26(23), 9563–9576. doi: 10.1175/JCLI-D-12-00751.1
- Maliar, L., Maliar, S., & Winant, P. (2021). Deep learning for solving dynamic economic models. *Journal of Monetary Economics*, 122, 76–101. Retrieved from <https://www.sciencedirect.com/science/article/pii/S0304393221000799> doi: <https://doi.org/10.1016/j.jmoneco.2021.07.004>
- Marrel, A., Iooss, B., Laurent, B., & Roustant, O. (2009, March). Calculations of Sobol indices for the Gaussian process metamodel. *Reliability Engineering & System Safety*, 94(3), 742–751. doi: 10.1016/j.ress.2008.07.008
- McInerney, D., Lempert, R., & Keller, K. (2012). What are robust strategies in the face of uncertain climate threshold responses? *Climatic Change*, 112(3), 547–568. Retrieved from <https://doi.org/10.1007/s10584-011-0377-1> doi: 10.1007/s10584-011-0377-1
- Meinshausen, M., Smith, S. J., Calvin, K., Daniel, J. S., Kainuma, M. L. T., Lamarque, J. F., ... van Vuuren, D. P. P. (2011, November). The RCP greenhouse gas concentrations and their extensions from 1765 to 2300. *Climatic Change*, 109(1-2), 213–241. doi: 10.1007/s10584-011-0156-z

- Mengis, N., & Matthews, H. D. (2020). Non-co₂ forcing changes will likely decrease the remaining carbon budget for 1.5 c. *npj Climate and Atmospheric Science*, 3(1), 1–7.
- Michaelis, P., & Wirths, H. (2020). DICE-RD: an implementation of rate-related damages in the DICE model. *Environmental Economics and Policy Studies*, 22(4), 555–584. Retrieved from <https://doi.org/10.1007/s10018-020-00269-4> doi: 10.1007/s10018-020-00269-4
- Miftakhova, A. (2021a). Global sensitivity analysis for optimal climate policies: Finding what truly matters. *Economic Modelling*, 105, 105653. Retrieved from <https://www.sciencedirect.com/science/article/pii/S026499932100242X> doi: <https://doi.org/10.1016/j.econmod.2021.105653>
- Miftakhova, A. (2021b, December). Global sensitivity analysis for optimal climate policies: Finding what truly matters. *Economic Modelling*, 105, 105653. doi: 10.1016/j.econmod.2021.105653
- Miftakhova, A., Judd, K. L., Lontzek, T. S., & Schmedders, K. (2020). Statistical approximation of high-dimensional climate models. *Journal of Econometrics*, 214(1), 67–80.
- Millar, R. J., & Friedlingstein, P. (2018, May). The utility of the historical record for assessing the transient climate response to cumulative emissions. *Philosophical Transactions of the Royal Society of London Series A*, 376(2119), 20160449. doi: 10.1098/rsta.2016.0449
- Murphy, K. P. (2012). *Machine learning: A probabilistic perspective*. The MIT Press.
- Murphy, K. P. (2022). *Probabilistic machine learning: Advanced topics*. MIT Press. Retrieved from probml.ai
- Nicholls, Z. R. J., Meinshausen, M., Lewis, J., Gieseke, R., Dommenges, D., Dorheim, K., ... Xie, Z. (2020, October). Reduced Complexity Model Intercomparison Project Phase 1: introduction and evaluation of global-mean temperature response. *Geoscientific Model Development*, 13(11), 5175–5190. doi: 10.5194/gmd-13-5175-2020
- Nordhaus, W. (2013). *Integrated economic and climate modeling* (Vol. 1). Elsevier. Retrieved from <http://dx.doi.org/10.1016/B978-0-444-59568-3.00016-X> doi: 10.1016/B978-0-444-59568-3.00016-X
- Nordhaus, W. (2018). Projections and uncertainties about climate change in an era of minimal climate policies. *American Economic Journal: Economic Policy*, 10(3), 333–360. doi: 10.1257/pol.20170046
- Nordhaus, W. D. (1979). *Efficient use of energy resources*. Yale University Press, New Haven, CT.

- Nordhaus, W. D. (1997). Managing the global commons: The economics of climate change. *Environmental Values*, 6(1), 106–108.
- Nordhaus, W. D. (2008). *A Question of Balance: Weighing the Options on Global Warming Policies*. Yale University Press.
- Nordhaus, W. D. (2012). Estimates of the Social Cost of Carbon: Background and Results from the Rice-2011 Model. *SSRN Electronic Journal*, 1, 273–312. doi: 10.2139/ssrn.1945844
- Nordhaus, W. D. (2017). Revisiting the social cost of carbon. *Proceedings of the National Academy of Sciences of the United States of America*, 114(7), 1518–1523. doi: 10.1073/pnas.1609244114
- Nordhaus, W. D., & Boyer, J. (2000). *Warming the world: economic modeling of global warming*. MIT press Cambridge, MA.
- Oakley, J. E., & O'Hagan, A. (2004). Probabilistic sensitivity analysis of complex models: A Bayesian approach. *Journal of the Royal Statistical Society: Series B (Statistical Methodology)*, 66(3), 751–769. doi: 10.1111/j.1467-9868.2004.05304.x
- Owen, A. B. (2014, January). Sobol' Indices and Shapley Value. *SIAM/ASA Journal on Uncertainty Quantification*, 2(1), 245–251. doi: 10.1137/130936233
- Papageorgiou, C., Saam, M., & Schulte, P. (2017, 05). Substitution between Clean and Dirty Energy Inputs: A Macroeconomic Perspective. *The Review of Economics and Statistics*, 99(2), 281–290. Retrieved from https://doi.org/10.1162/REST_a_00592 doi: 10.1162/REST_a_00592
- Patel, D., Sandefur, J., & Subramanian, A. (2021). The new era of unconditional convergence. *Journal of Development Economics*, 152, 102687. Retrieved from <https://www.sciencedirect.com/science/article/pii/S030438782100064X> doi: <https://doi.org/10.1016/j.jdeveco.2021.102687>
- Pigou, A. C. (1920). Wealth and welfare, london, 1912. *Later editions, The Economics of Welfare*.
- Pindyck, R. S. (2013). Climate Change Policy: What Do the Models Tell Us? *Journal of Economic Literature*, 51(3), 860–872. doi: 10.1257/jel.51.3.860
- Pindyck, R. S. (2017, January). The Use and Misuse of Models for Climate Policy. *Review of Environmental Economics and Policy*, 11(1), 100–114. doi: 10.1093/leep/rew012
- Popp, D. (2004). ENTICE: Endogenous technological change in the DICE model of global warming. *Journal of Environmental Economics and Management*, 48(1), 742–768. doi: 10.1016/j.jeem.2003.09.002
- Rasmussen, C. E., & Williams, C. K. I. (2005). *Gaussian processes for machine learning (adaptive computation and machine learning)*. The MIT Press.

- Renner, P., & Scheidegger, S. (2018). Machine learning for dynamic incentive problems. *Available at SSRN 3462011*. (Working paper)
- Rickels, W., Reith, F., Keller, D., Oschlies, A., & Quaas, M. F. (2018, March). Integrated Assessment of Carbon Dioxide Removal. *Earth's Future*, 6(3), 565–582. doi: 10.1002/2017EF000724
- Ridge, S. M., & McKinley, G. A. (2021). Ocean carbon uptake under aggressive emission mitigation. *Biogeosciences*, 18(8), 2711–2725. Retrieved from <https://bg.copernicus.org/articles/18/2711/2021/> doi: 10.5194/bg-18-2711-2021
- Roe, G. H., & Baker, M. B. (2007, October). Why Is Climate Sensitivity So Unpredictable? *Science*, 318(5850), 629–632. doi: 10.1126/science.1144735
- Saltelli, A., & D’Hombres, B. (2010). Sensitivity analysis didn’t help. A practitioner’s critique of the Stern review. *Global Environmental Change*, 20(2), 298–302. doi: 10.1016/j.gloenvcha.2009.12.003
- Saltelli, A., Ratto, M., Andres, T., Campolongo, F., Cariboni, J., Gatelli, D., . . . Tarantola, S. (2008). *Global sensitivity analysis: the primer*. John Wiley & Sons.
- Scheidegger, S., & Billionis, I. (2019, April). Machine learning for high-dimensional dynamic stochastic economies. *Journal of Computational Science*, 33, 68–82. doi: 10.1016/j.jocs.2019.03.004
- Shapley, L. S. (1953). A value for n-Person games. In H. W. Kuhn & A. W. Tucker (Eds.), *Contributions to the theory of games (AM-28), volume II* (pp. 307–318). Princeton: Princeton University Press. doi: doi:10.1515/9781400881970-018
- Smith, R. C. (2014). *Uncertainty Quantification: Theory, Implementation, and Applications*. Society for Industrial and Applied Mathematics.
- Sobol, I. M. (2001, February). Global sensitivity indices for nonlinear mathematical models and their Monte Carlo estimates. *Mathematics and Computers in Simulation*, 55(1–3), 271–280. doi: 10.1016/S0378-4754(00)00270-6
- Song, E., Nelson, B. L., & Staum, J. (2016, January). Shapley Effects for Global Sensitivity Analysis: Theory and Computation. *SIAM/ASA Journal on Uncertainty Quantification*, 4(1), 1060–1083. doi: 10.1137/15M1048070
- Spear, S. E. (1988, February). Existence and local uniqueness of functional rational expectations equilibria in dynamic economic models. *Journal of Economic Theory*, 44(1), 124–155. doi: 10.1016/0022-0531(88)90099-3
- Stern, N. (2008, April). The Economics of Climate Change. *American Economic Review*, 98(2), 1–37. doi: 10.1257/aer.98.2.1
- Stern, N. H. (2007). *The economics of climate change: the stern review*. Cambridge University Press.

- Sterner, E. O., & Johansson, D. J. A. (2017, March). The effect of climate-carbon cycle feedbacks on emission metrics. *Environmental Research Letters*, *12*(3), 034019. doi: 10.1088/1748-9326/aa61dc
- Sudret, B. (2008, July). Global sensitivity analysis using polynomial chaos expansions. *Reliability Engineering & System Safety*, *93*(7), 964–979. doi: 10.1016/j.res.2007.04.002
- Sun, Y., Apley, D. W., & Staum, J. (2011). Efficient Nested Simulation for Estimating the Variance of a Conditional Expectation. *Operations Research*, *59*(4), 998–1007.
- Taylor, K. E., Stouffer, R. J., & Meehl, G. A. (2012). An Overview of CMIP5 and the Experiment Design. *Bull. Amer. Meteor. Soc.*, *93*, 485–498. doi: 10.1175/BAMS-D-11-00094.1
- Tebaldi, C., Debeire, K., Eyring, V., Fischer, E., Fyfe, J., Friedlingstein, P., . . . Ziehn, T. (2021, March). Climate model projections from the Scenario Model Intercomparison Project (ScenarioMIP) of CMIP6. *Earth System Dynamics*, *12*(1), 253–293. doi: 10.5194/esd-12-253-2021
- Thao, S., Garvik, M., Mariethoz, G., & Vrac, M. (2021). *Combining global climate models using graph cuts* (Tech. Rep.). doi: <https://doi.org/10.21203/rs.3.rs-586868/v1>
- Thompson, T. M. (2018). Modeling the climate and carbon systems to estimate the social cost of carbon. *Wiley Interdisciplinary Reviews: Climate Change*, *9*(5), 1–12. doi: 10.1002/wcc.532
- Tokarska, K. B., Stolpe, M. B., Sippel, S., Fischer, E. M., Smith, C. J., Lehner, F., & Knutti, R. (2020). Past warming trend constrains future warming in cmip6 models. *Science Advances*, *6*(12). Retrieved from <https://advances.sciencemag.org/content/6/12/eaz9549> doi: 10.1126/sciadv.aaz9549
- Traeger, C. P. (2014, September). A 4-States DICE: Quantitatively Addressing Uncertainty Effects in Climate Change. *Environmental and Resource Economics*, *59*(1), 1–37. doi: 10.1007/s10640-014-9776-x
- Traeger, C. P. (2019). *ACE – Analytic Climate Economy (with Temperature and Uncertainty)*. Retrieved from https://papers.ssrn.com/sol3/papers.cfm?abstract_id=3307622
- van der Ploeg, F. (2021, October). Carbon pricing under uncertainty. *International Tax and Public Finance*, *28*, 1122–1142. doi: <https://doi.org/10.1007/s10797-021-09686-x>
- Villa, A. T., & Valaitis, V. (2019). *Machine Learning Projection Methods for Macro-Finance Models* (Tech. Rep.). doi: 10.2139/ssrn.3209934

- Waldhoff, S., Anthoff, D., Rose, S., & Tol, R. S. J. (2014). The marginal damage costs of different greenhouse gases: An application of fund. *Economics*, *8*(1), 20140031. Retrieved 2023-09-24, from <https://doi.org/10.5018/economics-ejournal.ja.2014-31> doi: doi:10.5018/economics-ejournal.ja.2014-31
- Webster, M., Jakobovits, L., & Norton, J. (2008, July). Learning about climate change and implications for near-term policy. *Climatic Change*, *89*(1-2), 67–85. doi: 10.1007/s10584-008-9406-0
- Weil, P. (1989, November). The equity premium puzzle and the risk-free rate puzzle. *Journal of Monetary Economics*, *24*(3), 401–421. doi: 10.1016/0304-3932(89)90028-7
- Weitzman, M. L. (2012a). Ghg targets as insurance against catastrophic climate damages. *Journal of Public Economic Theory*, *14*(2), 221–244.
- Weitzman, M. L. (2012b, March). GHG Targets as Insurance Against Catastrophic Climate Damages. *Journal of Public Economic Theory*, *14*(2), 221–244. doi: 10.1111/j.1467-9779.2011.01539.x
- Weyant, J. (2017). Some contributions of integrated assessment models of global climate change. *Review of Environmental Economics and Policy*, *11*(1), 115–137. doi: 10.1093/reep/rew018
- Winter, E. (2002, January). The shapley value. In *Handbook of Game Theory with Economic Applications* (Vol. 3, pp. 2025–2054). Elsevier. doi: 10.1016/S1574-0005(02)03016-3
- Wouter Botzen, W. J., & van den Bergh, J. C. (2012). How sensitive is Nordhaus to Weitzman? Climate policy in DICE with an alternative damage function. *Economics Letters*, *117*(1), 372–374. Retrieved from <http://dx.doi.org/10.1016/j.econlet.2012.05.032> doi: 10.1016/j.econlet.2012.05.032
- Younes, A., Mara, T. A., Fajraoui, N., Lehmann, F., Belfort, B., & Beydoun, H. (2013). Use of Global Sensitivity Analysis to Help Assess Unsaturated Soil Hydraulic Parameters. *Vadose Zone Journal*, *12*(1). doi: 10.2136/vzj2011.0150
- Zaliapin, I., & Ghil, M. (2010, March). Another look at climate sensitivity. *Nonlinear Processes in Geophysics*, *17*(2), 113–122. doi: 10.5194/npg-17-113-2010
- Zelinka, M. D., Myers, T. A., McCoy, D. T., Po-Chedley, S., Caldwell, P. M., Ceppi, P., ... Taylor, K. E. (2020). Causes of Higher Climate Sensitivity in CMIP6 Models. *Geophysical Research Letters*, *47*(1), 1–12. doi: 10.1029/2019GL085782
- Zhao, Y., Basu, A., Lontzek, T. S., & Schmedders, K. (0). The social cost of carbon when we wish for full-path robustness. *Management Science*, *0*(0), null. Retrieved from <https://doi.org/10.1287/mnsc.2023.4736> doi: 10.1287/mnsc.2023.4736